Titre: Title:	Structural Behaviour of Cast-in-Place and Precast Concrete Barriers Anchored to Bridge Deck Overhangs and Subjected to Transverse Static Loading
Auteur: Author:	Matthew Namy
Date:	2012
Type:	Mémoire ou thèse / Dissertation or Thesis
Référence: Citation:	Namy, M. (2012). Structural Behaviour of Cast-in-Place and Precast Concrete Barriers Anchored to Bridge Deck Overhangs and Subjected to Transverse Static Loading [Mémoire de maîtrise, École Polytechnique de Montréal]. PolyPublie. https://publications.polymtl.ca/905/

UNIVERSITÉ DE MONTRÉAL

STRUCTURAL BEHAVIOUR OF CAST-IN-PLACE AND PRECAST CONCRETE BARRIERS ANCHORED TO BRIDGE DECK OVERHANGS AND SUBJECTED TO TRANSVERSE STATIC LOADING

MATTHEW NAMY

DÉPARTEMENT DES GÉNIES CIVIL, GÉOLOGIQUE, ET DES MINES

ÉCOLE POLYTECHNIQUE DE MONTRÉAL

MÉMOIRE PRÉSENTÉ EN VUE DE L'OBTENTION

DU DIPLÔME DE MAÎTRISE ÈS SCIENCES APPLIQUÉES

(GÉNIE CIVIL)

AOÛT 2012

UNIVERSITÉ DE MONTRÉAL

ÉCOLE POLYTECHNIQUE DE MONTRÉAL

Ce mémoire intitulé :

STRUCTURAL BEHAVIOUR OF CAST-IN-PLACE AND PRECAST CONCRETE BARRIERS ANCHORED TO BRIDGE DECK OVERHANGS AND SUBJECTED TO TRANSVERSE STATIC LOADING

Présenté par : NAMY Matthew

en vue de l'obtention du diplôme de : Maîtrise ès sciences appliquées

a été dûment accepté par le jury d'examen constitué de :

M. LÉGER Pierre, Ph. D., président

M. CHARRON Jean-Philippe, Ph. D., membre et directeur de recherche

M. MASSICOTTE Bruno, Ph. D., membre et codirecteur de recherche

M. MAILHOT Guy, M. Sc., membre

ACKNOWLEDGEMENTS

Throughout my graduate studies I relied on the help and support of my friends, family, and the academic community at Polytechnique Montreal. Without their contribution, I would never have been able to complete my master's studies.

I would first like to thank my research director, Prof. Jean-Philippe Charron, who supervised each stage of my project in exemplary manner. Prof. Charron's availability, acute attention to detail, patience, and support, all contributed to the successful completion of my studies. I would also like to thank my co-director, Prof. Bruno Massicotte. In addition to Prof. Massicotte's personal qualities, his expertise in bridge design and analysis was instrumental during both the experimental and numerical phases of this project. I enjoyed working together with Professor's Charron and Massicotte, and learned a great deal. I feel very fortunate to have had them as my research directors.

The contribution of the industrial partners, Ciment St. Laurence, Euclid Chemical, the City of Montreal, and Béton Brunet Group, was greatly appreciated. Béton Brunet, in particular, contributed an extensive investment in time, personnel, and energy as they took charge of the production and transportation of all the laboratory specimens. I am very grateful for their help.

My research project included an extensive laboratory phase, during which time I relied on the expertise and hard-work of the Polytechnique GRS laboratory team. Lab coordinators, engineers, technicians, and interns all took part in this project. In particular I would like to thank Mr. Cédric Androuët and Mr. Guillaume Cossette each for their substantial contribution to my project. I would also like to thank Joan Hingant for his help as a study abroad student from Strasbourg, France.

There was a great work environment within the Structures Group and I made many friends. As I adapted to graduate studies, Fabien Lagier was always willing to answer my questions and I relied greatly on his advice. Thanks also to Sébastien Delsol who spent many hours helping me in the lab, at Béton Brunet, and with ATENA. Clélia Desmettre was also a great help and friend.

Finally, I would like to thank my family. I could always count on their unyielding support and encouragement during my graduate studies.

`

RÉSUMÉ

Au Canada et aux États-Unis la majorité des nouveaux dispositifs de sécurités des ponts sont faits des parapets de béton coulé en place. Ce genre de parapets répond bien aux critères de performance recherchés pour la sécurité, soit maintenir sur le pont et bien rediriger les véhicules afin d'éviter qu'ils sortent de la chaussée. Cependant, les parapets sont coulés directement sur la dalle déjà durcie, ce qui restreint les déformations dues au retrait et aux variations thermiques. Ceci engendre la formation des fissures au jeune âge qui accélère la dégradation de parapets et diminue leur durabilité. De plus, la construction de parapets coulés en place constitue une étape qui ralentit la mise en service dû aux opérations de pose d'armatures et de mûrissement du béton. Ceci est particulièrement coûteux pour le remplacement de parapets sur les ponts existants. Pour rectifier ces problématiques de durabilité et de vitesse de construction, l'École Polytechnique de Montréal a mis au point des parapets préfabriqués en béton à haute performance renforcé de fibres métalliques (BHPRF). Les parapets préfabriqués ainsi développés permettent d'une part, d'augmenter la qualité de construction et d'éliminer la problématique de durabilité associée à la formation des fissures au jeune âge. D'autre part, les BHPRF utilisés ont une résistance à l'ouverture des fissures améliorée et une microstructure plus dense, ce qui ralentit la pénétration et diffusion des chlorures dans le béton. Enfin, les parapets préfabriqués permettent de réduire le temps d'installation et accélérer la réparation des ponts.

L'obtention d'une performance mécanique adéquate pour le niveau de performance 2 (PL-2) avec des parapets préfabriqués en BHPRF a été démontrée dans des projets antérieurs réalisés à l'École Polytechnique. Cependant, la performance de l'ensemble parapet et dalle de tablier en porte-à-faux n'avait pas été évaluée. Ce projet de recherche a étudié le comportement mécanique de trois ensembles parapet et dalle en porte-à-faux de 6 m de longueur soumis à un chargement statique transversal appliqué sur les parapets visant à reproduire les forces d'impacts de véhicules. Les parapets avaient les configurations suivantes : un parapet continu coulé-en-place typique des constructions faites au Québec, et deux configurations de trois parapets préfabriqués avec niche de liaisonnement avec la dalle coulée en place, une configuration sans liaison entre les parapets et une configuration avec clés de cisaillement entre les parapets. Le comportement de chacune de ces configurations ont été analysés et comparés.

`

Les résultats ont démontré que les parapets préfabriqués reliés avec une clé de cisaillement ont une rigidité et une résistance équivalente au parapet coulé en place, et dépassent les exigences de conception des normes pour les ponts construits au Canada ou aux États-Unis. Les dalles en porte-à-faux ont toutes eu un comportement semblable pendant les essais avec un réseau de fissures bien réparti. Les résultats des essais ont été reproduits avec des analyses non-linéaires par éléments finis. Une étude paramétrique a ensuite été réalisée pour évaluer les effets d'échelle, pour déterminer les endroits critiques d'impacts, et pour étudier l'effet de certaines modifications de la conception des parapets et de la dalle.

Les études paramétriques ont démontré que pour une longueur de 4 m, longueur attendue pour des parapets préfabriqués industriellement, il y un gain de résistance important pour les deux configurations de parapets préfabriqués (avec et sans clés) par rapport à des parapets préfabriqués de 2 m. Les configurations expérimentales, avec des parapets préfabriqués de 2 m de longueur, étaient aussi pénalisantes pour la performance mécanique de la structure que celle correspondant à un chargement excentré au bord des parapets préfabriqués de 4 m. Le choix de tester des parapets préfabriqués de 2 m était donc conservatrice. La conception de la structure dalle-parapet avec une dalle conçue en BHPRF offre des résultats intéressants. La dalle en BHPRF avec une résistance en flexion équivalente à celle d'une dalle conventionnelle permet une réduction de 50% de la quantité de renforcement transversal, offre un gain de résistance et de rigidité à la structure, et diminue la fissuration pour une même charge appliquée.

Ce mémoire décrit en détail ce projet de recherche : une revue de la littérature pertinente au sujet de recherché, l'étude préliminaire avec analyses par éléments finis pour établir les paramètres du montage expérimental, les plans de conception et de fabrication de chaque spécimen, l'installation et l'assemblage de chaque montage y compris l'instrumentation, les résultats et les analyses de tous les essais, et l'étude finale à l'aide des analyses non linéaires par éléments finis. Le mémoire contient deux articles soumis à des revues avec comité de lecture.

`

ABSTRACT

In Canada and the United States the majority of new longitudinal bridge barriers are made with cast-in-place concrete barriers. These barriers adequately meet the safety performance criteria to contain and redirect errant vehicles. However, the barriers are cast directly onto the hardened deck and the restrained barrier movements due to shrinkage and thermal effects cause early-age cracking. The early-age cracking accelerates barrier deterioration and decreases their durability. Furthermore, between the rebar placement, formwork assembly, and concrete curing, the installation of cast-in-place barriers is a lengthy process delaying the operational readiness of bridges. The time costs are particularly high during barrier repair and replacement work on existing bridges. In order to resolve these problems, Polytechnique Montreal has been developing a new design of precast bridge barriers made from high-performance steel fibre reinforced concrete (HPFRC). Precasting improves fabrication quality and solves the problem of early-age cracking. In addition, the HPFRC has an increased resistance to crack openings and a denser concrete microstructure, which prevents the penetration and diffusion of harmful chlorides in the concrete. Finally, well-conceived precast barriers reduces installation and repair time of the bridge barriers.

The mechanical performance of the HPFRC precast barriers was shown to exceed performance level 2 (PL-2) design criteria in recent projects carried out at Polytechnique Montreal. However, the overall performance of the precast barriers anchored to bridge deck overhangs was not been evaluated. In this research project, the mechanical behaviour of three different barrier configurations subjected to transverse static loading and anchored to identical 6 m long bridge decks with 1 m overhang lengths was evaluated. The following barrier configurations were considered: a typical cast-in-place barrier used in Quebec, and two arrangements of three precast barriers with a cast-in-place connection to the deck, in one the precast barriers were placed side-by-side independently, and in the other shear keys were added between the adjacent precast barriers. The behaviour of the three bridge decks were then analysed and compared.

The results demonstrated that the precast barriers with shear keys have a strength and rigidity equivalent to the Quebec cast-in-place barrier and exceed the design forces recommended in the Canadian and American bridge codes. The deck overhangs behaved similarly in each test with well distributed flexural cracks. Nonlinear finite element models were able to accurately simulate

`

each laboratory test and were then used to carry out a parametric study to investigate the effects of barrier length, eccentric edge loading, and design modifications.

The finite element studies demonstrated that precast barriers with 4 m lengths, the expected industrial length of the precast barriers, there is a significant increase in load-carry capacity for the two tested precast barrier configurations. The effect of using 2 m precast barriers was shown to be at least as critical to the structural performance as eccentric loads applied at the edges of 4 m precast barriers. The most promising design modification was changing the ordinary concrete slab design to HPFRC designed with an equivalent flexural resistance. The HPFRC slab allowed a 50% reduction in steel reinforcement, increased the load-carry capacity of the bridge deck, and reduced crack opening widths in the slab overhang for a given load.

This master's thesis comprehensively details this entire research project. The following sections are presented: a review of the relevant literature, the initial finite element study to determine the appropriate parameters for the laboratory tests, the design and fabrication of the test specimens, the installation and assembly of the test setup including instrumentation, the test results and analysis, and a final study using nonlinear finite element analysis. The master's thesis contains two articles as they were submitted to peer-review journals.

`

TABLE OF CONTENTS

`

`

`

`

`

LIST OF TABLES

`

`

LIST OF FIGURES

`

`

`

`

`

LIST OF ABBREVIATIONS AND SYMBOLS

Abbreviations/Symbols (Greek):

ε	Strain
ε_f	Fracture strain
ϕ	Coefficient of friction
ϕ_{br}	Material bearing strength reduction coefficient
ϕ_c	Concrete strength reduction coefficient
ϕ_s	Steel strength reduction coefficient
υ	Poissons ratio

Abbreviations/Symbols (Latin):

App	Approximately
B_r	Bearing strength in terms of force
c/c	Center-to-center
E	Young's modulus
ºC	Degrees Celsius
f_y	Steel yield stress
f'_c	Concrete compressive strength in terms of stress
f'_t	Concrete tensile strength in terms of stress
G_F	Fracture Energy
h	Drop height
Hz	Hertz
kN	Kilonewton
ksi	Kip per square inch

`

lbf	Pound-force
L_c	Critical yield line length
m	Metre
m	Mass
MPa	Megapascal
o/c	On-center spacing
PL-#	Performance Level - # (i.e. 2)
psi	Pound-force per square inch
QC	Québec
R_w	Barrier ultimate strength
TL-#	Test Level - # (i.e. 4)
v	Velocity
Vol	Volume
w_0	Critical crack opening width where tensile stresses no longer transfer across the crack opening

`

LIST OF ACRONYMS

AADT	Average Annual Daily Traffic
AASHTO	American Association of State and Highway Transportation Officials
ACI	American Concrete Institute
ASCE	American Society of Civil Engineers
ASTM	American Society for Testing and Materials
BHPRF	Béton haute performance renforcé de fibres métalliques
BEI	Barrier Exposure Index
CHBDC	Canadian Highway Bridge Design Code
CDPBS	Connection Details for Precast Bridge Systems
CSA	Canadian Standards Associations
DOT	Department of Transportation (preceded by state initials)
EHFG	Euclid High-Flow Grout
FHWA	(United States Department of Transportations') Federal Highway Administration
FRC	Fibre Reinforced Concrete
FRM	Fibre Reinforced Mortar
GM	General Motors
HPC	High Performance Concrete
HPFRC	High Performance Fibre Reinforced Concrete
HRB	Highway Research Board
HTCS	High Tension Cable System
IS	Impact Severity (kJ)
LRFD	Load Resistance Factored Design
LVDT	Linear Variable Differential Transformer

`

MASH	Manual for Assessing Safety Hardware
MSL	Multiple Service Level
MTQ	Québec Ministry of Transportation / Ministère des Transports du Québec
NCHRP	National Cooperative Highway Research Program
NHS	(United States) National Highway System
NLFE	Nonlinear Finite Element (method/analysis)
OHBDC	Ontario Highway Bridge Design Code
OIV	Occupant Impact Velocity (m/s)
PCI	Precast Concrete Institute
PL	Performance Level
PVC	PolyVinyl Chloride
RDG	Roadside Design Guide
SUT	Single-Unit Truck
TAC/ATC	Transportation Association of Canada/Association des Transports du Canada
TL	Test Level
TRB	Transportation Research Board
UHPFRC	Ultra-high performance fibre reinforced concrete
U.S.(A.)	United States (of America)

`

LIST OF APPENDICES

`

CHAPTER 1 INTRODUCTION

1.1 Problem

Throughout the United States (U.S.) and Canada, the overwhelming majority of longitudinal bridge barriers are made using reinforced concrete cast-in-place safety shaped barriers (NCHRP 574, TAC ATC 2010). The bridge barriers are meant to force errant vehicles to remain on the roadway and their two primary functions are (MASH 2009, CSA 2006):

1. To contain the vehicle on the bridge;
2. To safely redirect the vehicle back onto the roadway or bring the vehicle to a stop within an acceptable distance.

Crash testing and field experiences have demonstrated that the commonly used Jersey and F shaped safety barriers adequately meet these mechanical demands. However, in aggressive environments, they often deteriorate prematurely and require expensive repair or replacement work to maintain their structural integrity (Haluk & Attanayaka, 2004). The deterioration is due to a combination of several factors. Often there is the formation of early-age vertical cracks on the barriers, as the deck slab fully restrains the barrier movements caused by concrete shrinkage and thermal dilations (Cusson & Repette, 2000). The barriers are also often exposed to severe environmental conditions, and in colder climates they must resist freeze-thaw cycles and the chlorides present in de-icing salts. The early-age cracks are aesthetically unpleasant, but more importantly they give an immediate opening for chlorides to quickly penetrate into the concrete matrix through capillary suction and absorption (Conciatori 2005). The corrosion of the reinforcing steel reduces the structural capacity, while the pressure induced by the rust growth causes concrete spalling, delamination, and pop-out. The use of epoxy-coated reinforcement has shown premature degradation. In areas with more extreme winter climates, such as Canada, the United States, and Northern Europe, these processes can lead to premature degradation of the barriers, and necessitate expensive bridge barrier repairs and replacement (Haluk & Attanayaka, 2004).

Since 2007, Polytechnique Montréal has been developing precast high performance steel fibre reinforced concrete (HPFRC) bridge barriers as a solution to the above durability issues. The proposed precast barriers offer several advantages compared to the cast-in-place barriers

currently in use. Precasting provides a higher standard of fabrication quality associated with industrialized manufacturing, and will allow the precast barriers to reach their steady-state volume at the precast plant without restraint. The HPFRC material has exceptional durability and mechanical properties. The HPFRC matrix microstructure is much denser than ordinary concrete and the steel fibres limit crack opening widths (Rossi et al, 1987). These properties prevent the penetration and movement of chlorides into the HPFRC, and provide a high resistance to chloride induced degradation. From a mechanical perspective, the steel fibres give the concrete an improved resistance to crack openings and increased fracture energy. The improved mechanical properties of the concrete allow the removal of up to 60% of the traditional reinforcement while maintaining an equivalent mechanical strength (Niamba 2009, Duchesneau 2010), thereby reducing the potential of damage due to steel corrosion. The HPFRC precast barriers will improve the barriers resistance to degradation by eliminating early-age cracking, by slowing the speed of water and chloride ingress into the concrete matrix, and by reducing the potential for corrosion.

The improved durability of the precast barriers provides a strong incentive for their use, and the reduced construction time associated with their installation provides another. Cast-in-place concrete barriers are typically poured in alternating sequences, to reduce early-age cracking and to incorporate bridge expansion joints (TAC ATC 2011, Bisonnette and Morin 2000). For a standard single-span 30 m bridge, it is estimated that the sequenced construction (rebar cage assembly, formwork assembly, casting and curing) requires at least 18 days. However, the precast barrier systems designed at the Polytechnique Montréal (Niamba 2009, Duchesneau 2010) only require an estimated 4 days for installation (Charron et al, 2011), and the FHWA Connection Details for Precast Bridge Systems Report (CDPBS 2009) estimates a precast barrier installation time of 1 to 2 days. The faster installation (or repair) time of precast concrete barriers is a significant financial benefit, particularly in urban areas where construction costs associated with traffic delays and hazards can reach up to 30% of the total project costs (Duchesneau et al. 2011).

Two precast barrier configurations designed according to Canadian Standards Association Highway Bridge Design Code (CSA 2006) performance level 2 (PL-2) requirements, equivalent to AASHTO test level 4 (TL-4), have been tested and analysed at Polytechnique Montréal (Niamba 2009, Duchesneau 2010). The experimental programs evaluated the static and dynamic performance of the barriers alone in order to demonstrate that the barrier and connection strength

`

met the needs of a PL-2 / TL-4 barrier. However, the mechanical behaviour of the precast barriers and slab at a realistic scale and with representative boundary conditions is necessary to evaluate the precast barrier designs as they will be used on highway bridges. The precast barriers do not have the same longitudinal continuity or connection detail as their cast-in-place counterparts, and there is a risk that the load transfer mechanics between the precast barrier and the deck slab could negatively impact the behaviour of the bridge deck, particularly the overhang portion of the bridge. In order to adequately assess the performance of the precast barriers, the mechanical behaviour of the reference MTQ Type 201 cast-in-place barrier must be evaluated as well.

1.2 Objectives

The experimental study described in this master's thesis is meant to establish the performance of the precast barriers developed by Duchesneau (2010) in realistic bridge conditions. The experimental study will evaluate and compare the structural behaviour of 6 m long bridge decks with 1 m overhangs during the static loading of the bridge barriers to simulate the transverse impact forces from vehicles.

Three different barrier configurations will be tested. Test Configuration 1 will test a continuous cast-in-place MTQ Type 201 F shaped barrier and establish the reference bridge deck behaviour. Test Configuration 2 will test the precast barriers developed by Duchesneau (2010) as they were designed. Test Configuration 3 will test the same precast barriers with the addition of shear connections between barriers. The design of a simple and effective shear connection between precast barriers compatible with the precast barriers developed by Duchesneau (2010) will be necessary for Test Configuration 3. Once the experimental tests will be completed and analysed a finite element study will be carried out to broaden the experimental findings and optimize the precast barrier design.

The performance of the reference cast-in-place barrier configuration will be compared with that of the precast barrier configurations to determine their structural adequacy for use on highway bridges, evaluate the impact of using precast barriers on the durability of the bridge slab overhang, and to optimize the precast barrier design for industrial use.

1.3 Methodology

The research project was split into three distinct phases:

`

In Phase I, an appropriate setup for the experimental tests was designed. An initial qualitative finite element analysis study was carried out in order to establish the necessary bridge deck length, overhang width, and overhang support conditions. The finite element study also identified important performance indicators for instrumentation during experimental testing. Once the general parameters of the laboratory tests were established, the design of each laboratory specimen, load application details, and instrumentation plans could be finalized.

In Phase II, the fabrication, installation, experimental testing, and data analysis for the three different test configurations was performed.

In Phase III, a quantitative finite element evaluation was performed. First, the test configurations were accurately simulated. The validated numerical models were then used to correct fabrication errors and to evaluate key design parameters as a means to optimize the final design of the precast barriers.

The results from Phases II and III were used to provide recommendations for the final design of the precast barriers to be used on actual bridges.

1.4 Organization of Master's Thesis

This Master's Thesis is divided into five Chapters. Chapter 1 introduces the research topic, problem statement, objectives, methodology, and report organization. Chapter 2 provides a non-exhaustive review of the relevant literature. Chapter 3 consists of a stand-alone article on the results and analysis of the experimental portion of this project (Phases I and II) submitted for publication in the ASCE Journal for Bridge Engineering. Chapter 4 consists of a stand-alone article on the results and analysis of the numerical portion of this project (Phase III) submitted for publication in the ACI Structure Journal. Chapter 5 consists of complimentary information to both Chapter 3 and Chapter 4 that could not be presented in the articles. Chapter 6 concludes this research report by highlighting the important findings and observations and providing future recommendations concerning the project. Following the conclusion, five Appendices have been attached to comprehensively detail the design & as-built drawings (APPENDIX A), the instrumentation plans (APPENDIX B), the slab overhang design (APPENDIX C), the specimen fabrication (APPENDIX D), and the injected mortar optimization study (APPENDIX E).

`

CHAPTER 2 LITERARY REVIEW

2.1 Introduction

The safety and efficacy of highway bridge barriers has greatly improved since the advent of the automobile. The continued evolution in barrier technologies, barrier evaluations, and barrier design requirements and/or guidelines throughout North America are the driving force behind these improvements.

The first part of this non-exhaustive literary review covers traditional barrier designs, the development of barrier regulations in the United States (U.S.) and Canada, and the most current governing regulations. The second part of the review of the literature is on the proposed designs of precast concrete rigid bridge barriers with an emphasis on the connection details, structural testing, and design methods developed for the precast barrier designs.

2.2 Bridge Barriers

2.2.1 Purpose

Bridge barriers make up a primary safety feature of the bridge railing system. The barriers are installed on the edge of the roadway surface and should contain vehicles within the bridge. The Canadian Highway Bridge Design Code (CSA-S6 2006) stipulates that traffic barriers:

> *Shall be provided on both sides of highway bridges to delineate the superstructure edge and to reduce the consequences of vehicles leaving the roadway. The barrier adequacy in reducing the consequences of vehicles leaving the roadway shall be determined from crash tests.*

The CSA (2006) underlying barrier design and evaluation theory originates from the American Association of State Highway and Transportation Officials (AASHTO) Guide Specifications for Bridge Railings 1989 and the AASHTO LRFD Bridge Design Specifications 2004. The AASHTO LRFD (2004) further clarifies that the primary purposes of the barriers are to contain the vehicle and either redirect it safely back into the roadway or bring it to a controlled stop.

`

2.2.2 Barrier Types

Several types of barriers have been designed and constructed to meet the demands of the evolving vehicle fleet and to take advantage of newer technologies. The barriers are all intended to contain and redirect vehicles and to protect vehicle occupants and bystanders. However, their proper design depends largely on the geographic and demographic environment in which they will be used. Longitudinal barriers are broadly categorized as flexible, rigid, or semi-rigid (MASH 2009).

The flexible barriers are often preassembled and simply placed on the roadway surface with a pinned or bolted connection (Oregon Precast Barrier, Texas Cross-Bolt Precast Barrier, Washington State Precast Barrier). The flexible barriers are subject to large displacements up to 2.5 m during heavy impacts (TAC ATC 2010), and are most often used for temporary installations or in areas of low speed traffic without heavy trucks. The large displacement limits the usage of flexible barriers to areas with sufficient room.

Semi-rigid barriers are most-often permanently fixed to the roadway, and typically consist of high tension cable systems (HTCS), or weak-post W-beam guardrail systems. The HTCS are cheaper to install than more rigid steel guardrails and concrete barriers, and they have been shown to successfully contain and redirect vehicles during heavy impacts (Medina 2006, WSDOT 2009). However, they require too much space for deflections to be practically used on most bridges and are perceived by the public as less secure than more rigid barriers (TAC ATC 2010). Semi-rigid barriers are most often used as medium barriers to prevent cross-traffic accidents, or on low-speed, low-use bridges and roadways.

In spite of certain advantages of the flexible and semi-rigid barriers – cheaper installation, greater dissipation of impact energy, more aesthetically pleasing designs – rigid barriers are most compatible with bridge structures and better suited to resist heavy impacts. Rigid barriers are almost exclusively used on highway bridges throughout North America (TAC ATC 2010). Rigid barriers are fixed permanently to the roadway structure and experience only very small amounts of lateral deflection during vehicle impacts. The most commonly used rigid barriers are cast-in-place concrete, metal post-and-beam, or a combination of the two (Figure 2-1).

`

a) Rigid Concrete Barrier b) Metal Post-and-Beam Barrier c) Combination Barrier

Figure 2-1: Permanent Barrier Types (Photos from TAC ATC 2010)

Although both concrete and post-and-beam barrier designs have been successfully crash tested and approved for use throughout North America, a survey of state DOT's in the United States determined that concrete barriers account for over 75% of the longitudinal barrier inventory and that 44% of states do not use metal post-and-beam type barriers at all (NCHRP 574). The concrete barriers have likely gained the market since they have much lower maintenance costs (Mak 1990), and the increased flexibility of the metal barriers was not shown to improve occupant safety during impacts (NCHRP 289).

The rigid concrete barriers have been in use since the 1940's (NCHRP 244) and they have undergone extensive research and development. The safety shaped Jersey and F barriers have come to dominate the American market (Figure 2-2) and accounted for 68% of concrete barriers in use within the US as of 2006 (NCHRP 554). Their structural adequacy and vehicle impact interaction have consistently shown satisfactory performance during full-scale crash tests (Buth 1990, FHWA Bridge Rail Guide 2005).

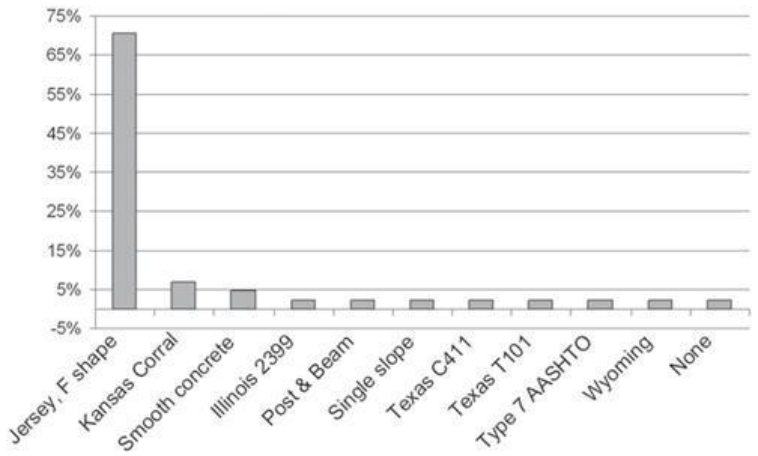

Figure 2-2: Concrete Barriers Used in the United States (NCHRP 554)

`

2.2.2.1 Safety Shaped Concrete Barriers

Research and development into rigid concrete barrier safety shapes began in the 1950's at General Motors' (GM) proving grounds in Milford Michigan (Mak et al. 1990) where the first safety shaped GM barrier was developed. The New Jersey Department of Transportation was also developing concrete safety shapes around this time and created the Jersey shaped barrier in 1959 (Kozel 2004). In an effort to improve the vehicle stability after impacts with Jersey shapes, a numerical parametric study with six different barrier shapes labelled A-F was performed. The F shaped barrier demonstrated the most improvement in the parametric study, as well as in subsequent crash testing, and has since been incorporated onto North American bridge and roadways (McDevitt 2000). The geometry of the GM, Jersey, and F shaped concrete barriers are shown in Figure 2-3.

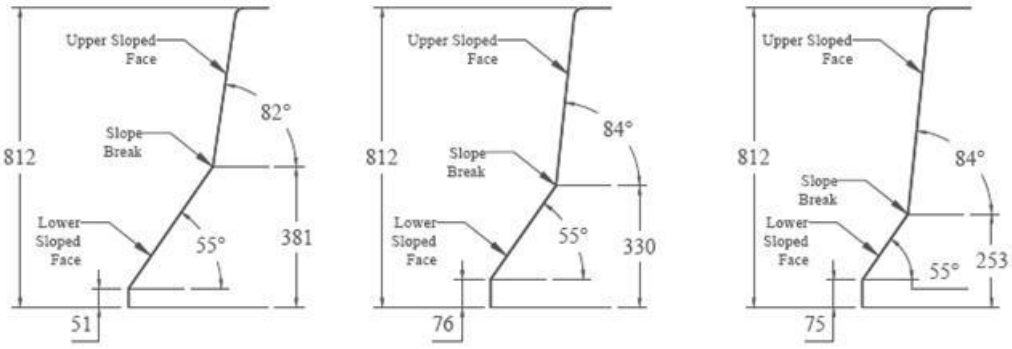

a) GM Shape b) Jersey Shape c) F Shape

Figure 2-3: Concrete Barrier Safety Shapes (McDevitt 2000)

The safety shapes were designed to minimize damage to vehicles during impacts, and the vehicle impact behaviour with concrete safety shaped barriers is described by McDevitt (2000). During the more common shallow angle impacts with passenger vehicles, the front tires will most often simply ride up the lower sloped face and redirect the vehicle back onto the roadway with minimal damage. For more severe angle impacts there is a multi-stage response. The vehicle bumper will hit and ride up the upper sloped face of the barrier providing an initial uplift and redirection, and almost immediately after, as the vehicle begins to re-align itself parallel to the barrier, the wheel will then come into contact with lower sloped face of the barrier creating additional (and substantially more) vehicle lift. The multi-stage impact behaviour is shown Figure 2-4. The upward lift during impact lowers the friction between the vehicle and roadway and therefore

`

reduces the energy necessary to redirect the vehicle. However, the lift also decreases the vehicle stability and in certain instances can lead to vehicle rollover when returning to the roadway. The impact behaviour of heavy trucks is substantially different. A heavy truck will roll towards and over the barrier until the underside of the carriage slides along the top of the barrier, preventing the roll to continue as the truck is redirected back onto the roadway (Figure 2-4).

a) Passenger Vehicle Impact b) Single Unit Truck Impact

Figure 2-4: Typical Impact Response with Safety Shape (TAC ATC 2010)

For passenger vehicle impacts the key design parameters are the angles of the two sloped faces and the height of the slope break from the road surface. The shallower the slope angle, the easier for the vehicle to roll up the barrier. The higher the slope break the longer the vehicle will ride up the lower sloped face. Shallower angles and higher slope breaks both generate more vehicle lift and roll during impacts (Mak 1990, McDevitt 2000). As can be seen in Figure 2-3, the slope angles of the three shapes are very similar but the slope break has been consistently lowered as the safety shaped barriers have been improved. The slope break of the GM barrier was too high and their use was discontinued due to vehicle instability during crash tests (McDevitt 2000). For impacts with heavy trucks the key design parameter is the barrier height. The truck carriage must come into contact with the barrier at a high enough point to prevent the truck from rolling over. The minimum height of the barriers is therefore an important design parameter and is specified in the North American codes depending on the expected level and speed of truck traffic.

Critical vehicle accelerations during impact and vehicle rollover have been isolated as major causes of fatality during run-off the road accidents of passenger vehicles (NCHRP 289). An

`

optimized safety shape will provide enough lift to reduce vehicle contact with the roadway and lower vehicle accelerations without causing the vehicle to rollover. Full-scale crash tests and numerical simulations (Buth 1990, McDevitt 2000) have demonstrated that both the Jersey and F shaped barriers adequately contain and redirect vehicles. The F shape has a slope break 77 mm lower than the Jersey shape, and has been shown to be less likely to cause vehicle rollover (Buth 1990, McDevitt 2000). However, the F shape was designed only after Jersey shaped barriers had already been installed in many regions throughout North America, and since the advantages of the F shape have not been unanimously demonstrated (Mak 1990) and the in-service performance of Jersey shaped barriers has been adequate, the Jersey barrier remains the dominant safety shaped barrier on bridges and roadways throughout North America.

2.2.2.2 Single Slope

Single slope barriers are another rigid barrier system currently in use in North America. These barriers come in two variations with either a vertical front face or a constant-sloped front face with an angle very similar to the upper sloped face of the safety shaped barriers (Figure 2-5). The single slope barriers present significant savings in terms of bridge and roadway maintenance. As opposed to safety shaped barriers, the geometry of the single slope barriers is not affected by the pavement overlay thickness. As long as the minimum barrier height is maintained new pavement can be poured directly on top of the existing roadway surface. For safety shapes however, the existing overlay must be ground down before refinishing, an expensive and time consuming process (Mak 1990). The single slope barriers also decrease the lift forces during impacts and therefore have a much lower risk of vehicle rollover.

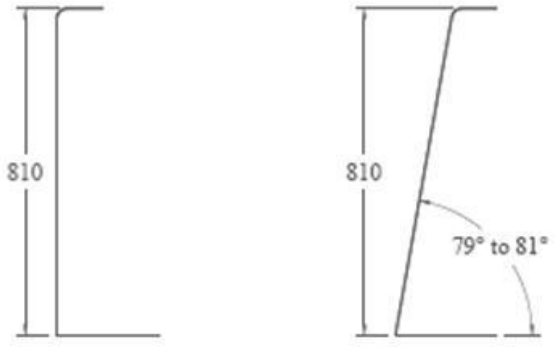

b) Vertical Face c) Constant Slope

Figure 2-5: Concrete Barrier Single Slope Shapes (TAC ATC 2010)

`

The 32 in. (812 mm) vertical face barrier was crash-tested by Buth et al. (1990) with a small vehicle, pickup truck, and single unit truck (SUT). The barrier successfully contained and redirected each vehicle, but the lateral accelerations recorded were significantly higher than those of the safety shaped barriers. For instance, the lateral acceleration recorded with the SUT impact test was 4.6 g and 2.5 g for the vertical face and F shape barriers respectively (Buth 1990). Essentially the vertical face barrier simply redirects the vehicle back away from the barrier; therefore the kinetic crash energy is absorbed primarily by vehicle crush during impact. The result is a more stable vehicle, but greater lateral accelerations associated with increased risk of occupant injury.

The constant slope barrier was therefore developed to combine the advantages of safety shaped and vertical face barriers. Mak et al. (1994) crash tested a 32 in. (812 mm) constant slope barrier with a 79° slope face with a pickup truck and SUT. The constant slope barrier demonstrated improved vehicle stability, and lateral accelerations comparable to Jersey shaped barriers. Despite the potential economic gains of using a constant slope barrier, their use represented a very small amount of the concrete barriers in use throughout the US in 2006 (Figure 2-2).

2.2.3 Considerations

The constant-sloped barriers seem to strike a good balance between minimizing vehicle accelerations and maintaining vehicle post-impact stability, and the financial savings are also considerable since the pavement overlay thickness does not affect the barrier-vehicle impact behaviour (Mak 1994). The F shaped concrete barrier is the current standard in Quebec, CA, however consideration should be given to moving towards the use of constant slope barriers.

2.3 Barrier Regulations in North America

As personal vehicles and heavy truck traffic have increased in use throughout North America, it became necessary to standardize the design and evaluation of bridge and traffic barriers. In the U.S. there are several agencies that contribute to the development and oversight of codes governing the highway system. The combined and connected publications from the Federal Highway Administration (FHWA), the AASHTO, the Transportation Research Board (TRB), the Highway Research Board (HRB), and the National Cooperative Highway Research Program (NCHRP) have created a convoluted series of regulatory documents and jurisdictional authority.

`

The following section of the literary review is an attempt to trace the development of barrier design recommendations and crash testing standards in the U.S. and Canada.

2.3.1 Chronological Development

Due to the complicated nature of vehicle barrier impacts, crash testing has been used as a barrier design and development tool since the 1930's. In the initial crash tests, vehicles were simply rolled down hills into barriers; there were neither standardized impact procedures nor evaluation criteria (FHWA Presentation 2009). In the 1950's and 1960's the personal use of automobiles became increasingly common and more extensive resources were devoted to the development of barriers. In the U.S. the first crash testing procedural guidelines were published in 1962 in HRB Circular 482. The one page document recommended using an 1819 kg sedan with an impact velocity of 97 km/h and at 7° and 25° impact angles. The idea was to reproduce the *worst practical conditions* with impact tests. Circular 482 was followed up with NCHRP Report 154. A 16 page document published in 1974 that added the small vehicle (1023 kg) crash test, and proposed evaluation criteria for the first time. NCHRP 154 also considered other components of railing systems, such as terminals, transition barriers, and crash cushions. The crash testing guidelines were modified again in 1978 when the TRB published Circular 191 to address certain flaws in NCRHP 154.

Throughout this time the American and Canadian regulatory agencies did not require crash testing for the design of bridge and roadway barriers. The design of the barriers was based on static design methods, past experience, and engineering judgment (TAC ATC 2010). In 1980 another more complete set of crash testing guidelines was published in NCHRP Report 230.

NCHRP Report 230 "Recommended Procedures for the Safety Performance Evaluation of Highway Safety Appurtenances," was a 36 page document that updated crash testing procedures and evaluations. The report added large buses and heavy trucks into the crash test vehicle matrix, and implicitly introduced the concept of different barrier performance levels. The crash tests were evaluated on the barrier structural adequacy, occupant risk, and vehicle trajectory after collision.

The NCHRP 230 report became the primary full scale vehicle crash test reference in the U.S. and Canada (MASH 2009, TAC ATC 2010). Crash tests throughout the late 1970's and early 1980's demonstrated that several of the highway and bridge barriers designed with static methods were structurally inadequate as shown in Figure 2-6, and several dramatically failed the NCHRP 230

`

crash tests (FHWA Memo 1996). As a result, the regulating agencies began implementing crash test requirements for the design and use of barriers. The FHWA first issued a policy memorandum in 1986 stating that bridge barriers on the U.S. National Highway System (NHS) had to be proven crashworthy according to the NCHRP 230 criteria. The FHWA memo contained a list of 22 barrier designs that were already considered crashworthy based on existing crash test data (these designs included both Jersey and F shape concrete barriers). The AASHTO Guide Specifications for Bridge Barriers published in 1989 also required for bridge barriers to be crash tested.

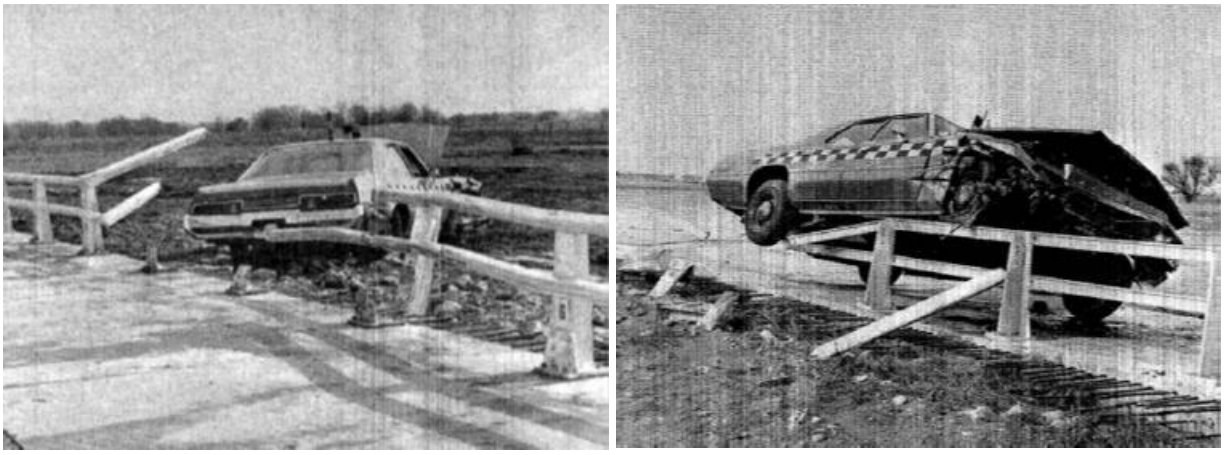

Figure 2-6: Failed Crash Test (TAC ATC 2010)

The Guide Specifications (1989) explicitly detailed the crash testing vehicle matrix and used the barrier multiple performance level concept. The multiple performance level concept was first formally introduced in NCHRP Report 239 (1981). The idea being that different site conditions – posted speed-limit, heavy truck traffic composition, barrier exposure index – merit different levels of barrier performance. Three different barrier performance level testing criteria were listed, and were different although generally compatible with the crash test matrix specified in the NCHRP 230, where the multiple performance level concept was implicitly present with the required (Level 2) and recommended supplementary crash tests (Levels 1 and 3). The AASHTO Guide Specification (1989) then provided a series of selection tables to determine the barrier performance level necessary for a given bridge. The selection tables were calculated with the cost-benefit analysis program called BCAP. The idea was to select the barrier performance level that provides an appropriate level of security with the least total cost, considering the costs of installation, maintenance, and vehicle crashes.

`

The AASHTO Guide Specifications (1989) also introduced the hierarchy concept that bridge anchors and decks should be designed to resist the ultimate moment, shear, and punching loads that can be transferred from the barrier. In other words, the barriers should fail before either the anchors or bridge deck. Static loads and loading conditions – height and surface – were specified for each barrier performance level to design the barrier anchors and bridge decks to resist the ultimate barrier capacity.

The Ontario Highway Bridge Design Code (OHBDC 1991) incorporated most of the recommendations from the AASHTO Guide Specifications (1989) and was the first Canadian regulatory authority to require crash testing and introduce the multiple performance level concept. The OHBDC also used BCAP to create selection tables for the barrier performance level, and included design loads for the anchor and bridge deck design. These concepts were endorsed nationally throughout Canada with the release of the Canadian Highway Bridge Design Code in 2000.

Modifications to the passenger vehicle fleet and more extensive experience with crash testing lead to the publication NCHRP Report 350 in 1993 as the successor to NCHRP 230. The new 64 page report used metric units for the first time and replaced the 1819 kg sedan with a 2000 kg pickup truck as the standard test vehicle. NCHRP 350 also endorsed the multiple performance level concept, but defined them in terms of barrier crash test levels (TL). NCHRP 350 categorized 6 different test levels for barrier classification.

In 1994 AASHTO also published the LRFD Bridge Design Specifications 1st Edition as an alternative to the AASHTO Standard Specifications for Highway Bridges. In the AASHTO LRFD (1994) the barrier performance level concept was continued, however the vehicle crash test matrix differed from both the Guide Specifications (1989) and NCHRP 350 (1993). In order to limit confusion regarding the different crash testing specifications listed in the various research reports and regulatory documents, the FHWA, the ultimate authority on the NHS, issued a memorandum in 1996 to clarify its position on crashworthy barriers and formally define compatibility between the different documents (Table 2-1). The FHWA 1996 memorandum stated that:

- As of august 16, 1998 all new barriers installed on the NHS had to be successfully crash tested to the NCHRP 350 criteria. Minimal TL rating for the NHS would be TL-3.

`

- Barriers successfully meeting the NCHRP 230 criteria are considered adequate and do not need to be crash tested again with NCHRP 350 requirements.
- The FHWA strongly recommended that AASHTO adopt the NCHRP 350 crash testing criteria and test levels.
- The FHWA published a list of 68 barrier designs accepted as crashworthy and their respective TL.

Table 2-1: Barrier Crash Testing Equivalencies (FHWA Memo 1996)

Bridge Railing Testing Criteria	Acceptance Equivalencies					
NCHRP Report 350	TL-1	TL-3	TL-3	TL-4	TL-5	TL-6
NCHRP Report 230	--	MSL-1,-2	--	MSL-3	--	--
AASHTO Guide Specs 1989	--	PL-1	--	PL-2	PL-3	--
AASHTO LRFD Specs 1993	--	PL-1	--	PL-2	PL-3	--

AASHTO followed the FHWA recommendation, and in the 2nd Edition of the AASHTO LRFD (1998) six barrier crash test levels as defined in the NCHRP 350 were specified. The 1998 LRFD no longer provided selection tables to select the necessary barrier test level, but indicated a general guide and left the test level selection up to the bridge governing authority.

The codes in the U.S. and Canada have continued to develop with emerging technologies and increased crash test data. However, no major innovations have developed in regards to bridge barrier design and evaluation since the 1990's. In 2009 the Manual for Assessing Safety Hardware (MASH 2009) was published by AASHTO to succeed NCHRP Report 350. The MASH (2009) document updated the crash tests vehicles to better represent the traffic fleet, added more objective crash test evaluation criteria, and addressed some flaws noted in the NCHRP 350. The AASHTO LRFD 5th Edition and the AASHTO Roadside Design Guide were published in 2010 and 2011 respectively and are the most recent American publications on the design of bridge barriers. In Canada, a more recent bridge design code was published by CSA in 2006, however there were no notable changes in the approach to bridge barrier design and evaluation from the 2000 edition.

The FHWA remains the ultimate authority to approve barrier prototypes for use on the United States NHS. The FHWA maintains a public inventory assessable online, the Bridge Rail Guide

`

(2005), with approved barriers of different type and TL. Barriers approved for use in the U.S. are considered acceptable in Canada for the equivalent PL as defined by the FHWA in Table 2-1.

2.3.2 Governing Codes

2.3.2.1 Manual for Assessing Safety Hardware (MASH) 2009

The MASH (2009) is based on the same *worst practical conditions* philosophy as the initial crash test document, HRB Circular 482. The idea is to create crash testing criteria that simulate extreme impact conditions that may occur over the lifetime of a barrier system. For instance, the small vehicle is representative of the 2nd percentile lightest and the pickup truck is representative of the 90th percentile heaviest passenger vehicle. The impact speed, 100 km/h, and impact angle, 25°, together approximate the 92.5th percentile of off-road impacts on high speed roadways. Considering these crash test parameters together, the crash tests simulate extreme impacts for the lightest and heaviest passenger vehicles on the roadway. In addition, strategic *critical impact points* are identified for each barrier type and configuration to test the weakest portion of the barriers or areas of particular impact hazards. The *critical impact points* identified for rigid concrete barriers are at barrier joints and transitions between the rigid concrete barrier and potentially more flexible roadway barriers. Consideration is still given for practicality; the crash test criteria must allow for barrier types that are financially feasible.

The MASH (2009) maintained the 6 TL's from the NCHRP Report 350, and the test level vehicle types and speed requirements are shown in Table 2-2. TL's 1-3 modify impact speed criteria, and TL's 4-6 vehicle type criteria. General descriptions of the test vehicle types and weights are listed in Table 2-3, and photos of the standard test vehicles are shown in Figure 2-7.

`

Table 2-2: Test Levels (MASH 2009)

Test Level	Test Vehicle Designation and Type	Test Conditions	
		Speed km/h (mph)	Angle (degrees)
1	1100C (Passenger Car)	50 (31)	25
	2270P (Pickup Truck)	50 (31)	25
2	1100C (Passenger Car)	70 (44)	25
	2270P (Pickup Truck)	70 (44)	25
3	1100C (Passenger Car)	100 (62)	25
	2270P (Pickup Truck)	100 (62)	25
4	1100C (Passenger Car)	100 (62)	25
	2270P (Pickup Truck)	100 (62)	25
	10000S (Single-Unit Truck)	90 (56)	15
5	1100C (Passenger Car)	100 (62)	25
	2270P (Pickup Truck)	100 (62)	25
	36000V (Tractor-Van Trailer)	80 (50)	15
6	1100C (Passenger Car)	100 (62)	25
	2270P (Pickup Truck)	100 (62)	25
	36000T (Tractor-Tank Trailer)	80 (50)	15

Table 2-3: Vehicle Gross Static Mass Upper and Lower Limits (MASH 2009)

Test Vehicle Designation and Type	Target Vehicle Weight, kg (lb.)	Acceptable Variation, kg (lb.)
1100C (Passenger Car)	1 100 (2 420)	± 25 (55)
1500A (Passenger Car)	1 500 (3 300)	± 100 (220)
2270P (Pickup Truck)	2 270 (5 000)	± 50 (110)
10000S (Single-Unit Truck)	10 000 (22000)	± 300 (660)
36000V (Tractor-Van Trailer)	36 000 (79 300)	± 500 (1 100)
36000T (Tractor-Tank Trailer)	36 000 (79 300)	± 500 (1 100)

`

a) 1100C Passenger Car

b) 2270P Pickup Truck

c) 10000S Single-Unit Truck

d) 36000V Tractor-Van Trailer

Figure 2-7: Standard Crash Test Vehicle Types (TAC ATC 2010)

A notable change in the crash test matrix between the MASH (2009) and NCHRP 350 (1993) is the SUT test for TL-4. In Report 350, the SUT had a specified weight and impact speed of only 8000 kg and 80 km/h. The modification was necessary because the TL-4 test in Report 350 had a lesser impact severity (IS), a measure of impact energy, than its TL-3 test. The MASH has fixed this logical incoherence (Figure 2-8). The IS for TL-3 has also been increased from the NCHRP Report 350.

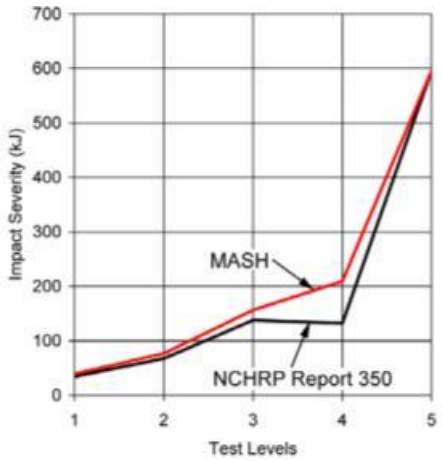

Figure 2-8: Impact Severity (TAC ATC 2010)

`

The evaluation criteria in the MASH (2009) have become more precisely defined and quantifiable. Like the NCHRP Reports 230 and 350 (1980, 1993), three criteria are used to assess a full scale impact:

1. Structural Adequacy
2. Occupant Risk
3. Post-impact Trajectory

The barrier structural adequacy refers to the containment and redirection of the crash test vehicle. The primary function of a barrier is to maintain a vehicle on the roadway. The vehicle should also remain stable and return to the roadway with a maximum of 75° pitch and roll angles. Heavy trucks may rollover on their side during a successful crash test. The reason for this discrepancy is that crash data does not indicate the strong causal link between rollover and fatality for heavy trucks as it does for passenger vehicles.

The occupant risk is considered in terms of penetration or excessive deformation of the vehicle occupant compartment, and the theoretical occupant impact velocity (OIV) and subsequent ride down acceleration. The theory is based on two concepts. The first is that penetration of barrier components into the vehicle can often prove fatal during high speed accidents and must be avoided at all costs. Likewise, if the occupant compartment deforms too severely during impact there is a much higher risk of fatalities. The extent of allowable intrusion is shown in Table 2-4, however specific limits are also provided for certain high risk components, such as the roof, windshield, and windows.

Table 2-4: Occupant Compartment Intrusion Ratings (MASH 2009)

Rating	Extent of Intrusion
Good	< 6 in. (150 mm)
Acceptable	6 in. – 9 in. (150 – 225 mm)
Marginal	9in. – 12 in. (225 – 300 mm)
Poor	> 12 in. (300 mm)

The second concept is the theoretical limits of OIV and vehicle ride down accelerations. This was introduced in NCHRP Report 230 (1980) and has been shown to be a relatively good measure of

`

impact risk. The idea is that the occupant will have an initial impact within the occupant compartment during impact, and then go through ride down accelerations. If the OIV and ride down accelerations are below a certain threshold criteria, the occupants are less likely to be critically injured. The OIV is simply the integral of the horizontal (x) and longitudinal (y) accelerations from the beginning of vehicle impact until occupant impact at time t*. And the ride down is the greatest average vehicle acceleration in the x and y directions after time t*. The acceleration is averaged over a 0.01 s time interval because accelerations that are less than 0.007 s in length are typically not injurious to occupants. Time of occupant impact, t*, is found by taking the double integral of the lateral and longitudinal accelerations and finding the smallest time for either the lateral movement to reach 0.6 m or the longitudinal movement to reach 0.3 m. The MASH (2009) provides a maximum threshold and recommended limit for both the OIV and ride down acceleration (Table 2-5). The vertical accelerations are not considered because passenger vehicles must always remain upright and therefore vertical accelerations are seen as less critical.

Table 2-5: OIV and Ride down Acceleration (MASH 2009)

Occupant Impact Velocity, m/s (ft/s)		
Component	Preferred	Maximum
Longitudinal, Lateral	9.1 (30)	12.2 (40)
Occupant Ride down Acceleration, G		
Component	Preferred	Maximum
Longitudinal, Lateral	15	20.5

The post-impact trajectory is an effort to minimize the risks of a subsequent collision between the impacting vehicle and other vehicles or objects on the roadway. Ideally, the impacting vehicle will not rebound into adjacent or opposing lanes of traffic. MASH (2009) has adopted the *exit box* criterion directly from European norms. The idea is that when the crash test vehicles remain within a conceptual exit box after barrier impact, then they are unlikely to pose a high risk of secondary collisions during actual accidents. The exit box dimensions are based off of the vehicle type and geometry (length and width). The concept and dimensions are shown in Figure 2-9.

`

Distance for Exit Box Criterion

Vehicle Type	A ft (m)	B ft (m)
Car/Pickup	$7.2 + V_W + 0.16V_L$ ($2.2 + V_W + 0.16V_L$)	32.8 (10.0)
Other Vehicles	$14.4 + V_W + 0.16V_L$ ($4.4 + V_W + 0.16V_L$)	65.6 (20.0)

V_W = Vehicle Width
V_L = Vehicle Length

a) Geometry

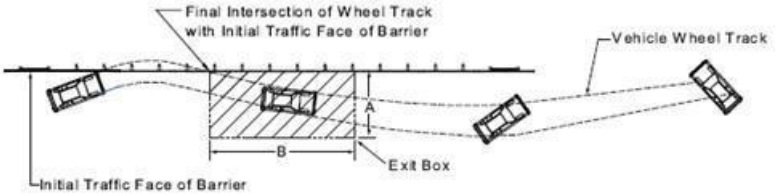

b) Concept

Figure 2-9: *Exit Box* Criterion (MASH 2009)

The MASH (2009) does not require in-service evaluation for barrier approval, but they are highly recommended. An in-service evaluation is seen as a valuable way to evaluate a barrier's performance in numerous impacts with different vehicles, speed, angles, and site-conditions. The impacts will likely not be as extreme as crash tests, but they provide the missing information. Therefore crash testing and in-service evaluations are highly complementary. However, in-service evaluations are also necessary to identify secondary problems with barrier design, such as installation difficulties, expensive maintenance, and poor durability. In-service evaluations provide valuable information; the problem is that it is difficult for a state or provincial agency to invest in an extensive in-service evaluation for an unproven barrier prototype. Therefore the amount of actual impact data collected before approval of a barrier for full use is generally very limited.

2.3.2.2 AASHTO Roadside Design Guide (RDG) 2011 and LRFD 5th Edition 2010

The AASHTO RDG (2011) and LRFD (2010) are the governing documents guiding barrier design in the United States.

The RDG (2011) gives general indications on bridge barrier purpose, performance requirements, selection guidelines, and maintenance or replacement. The RDG reiterates that longitudinal bridge barrier primary purpose is to prevent vehicles from leaving the roadway, that barriers must meet certain geometric criteria, resist static design loads as specified in the AASHTO LRFD (2010), and that all barriers on the NHS must have been crash tested to at least the TL-3 in NCHRP Report 350 (1993). Higher barrier test levels may be necessary if a barrier failure would be particularly hazardous, if the bridge height is abnormally high, and if the bridge shape is unusual. The selection of the barrier type depends on the following:

1. Necessary barrier performance

`

2. Roadway and bridge barrier compatibility
3. Cost (railings that minimize deck maintenance are desirable)
4. Past Experience (barrier in-service evaluations)
5. Aesthetics

The top consideration should always be barrier performance needs however. The RDG (2011) states that most barrier designs since 1964 are structurally adequate. However, retrofit of these older barriers should increase barrier strength and improve longitudinal continuity. The RDG (2011) explains that the FHWA is responsible for the evaluation and approval of new barrier prototypes based off crash testing but also recognizes that there is a precedent for the FHWA to approve barrier designs similar to crashworthy barriers without requiring new crash tests (FHWA 2000 Memorandum).

The AASHTO LRFD (2010) specifies six barrier test levels and crash test criteria that are still based off of NCHRP Report 350. Barrier heights, geometric requirements, and design loads are also identified with respect for the design of new barriers for crash tests, as shown in Figure 2-10. Barrier design loads are to be applied with the Extreme Event II limit state with impact load factor of 1.0. The transverse and longitudinal horizontal forces are to be applied together and separately from the vertical force. The length of application of the transverse and longitudinal, L_T and $L_{L,}$ come from the length of vehicle-barrier contact observed during crash testing. The 1.07 m (3.5 ft) is the length of the rear-tire axel of the SUT, and the 2.44 m (8.0 ft) is the length of the double axels of the design tractor-trailer truck. The length of the vertical load, L_V, comes from the length over which the weight of the vehicle rests on the barrier. In the case of the SUT and tractor-trailer trucks, this length corresponds to the vehicle carriage.

The Extreme Event II limit state is an ultimate limit state and therefore the barrier only needs to survive the application of these static loads. The LRFD (2010) provides simplified formulas to use Yield Line Analysis for the design of rigid concrete barriers with the load conditions specified in Figure 2-10. The barrier should also be checked for punching shear failure. The anchors and bridge deck overhang must also be designed for the Extreme Event II limit state, as well as the truck load in the Strength limit state. The LRFD (2010) recommends designing the anchors and deck to resist the shear and moment loads transferred from the barrier at its ultimate strength calculated using the yield line analysis. Thus, while the LRFD (2010) does not explicitly

`

mention the hierarchy concept, it is implicit since the anchors and slab overhang are designed to resist the ultimate barrier strength. It is recognized in the LRFD (2010) that since the barrier and deck overhangs are designed to survive crash tests, they are most likely overdesigned.

The AASHTO LRFD (2010) does not provide detailed selection tables for the barrier crash test level to specify for different bridge sites, it does however provide the following guidelines:

TL-1 Work zones in local streets with low traffic speed and volume

TL-2 Generally acceptable for work zones

TL-3 Acceptable for high speed roadways with low quantities of heavy vehicles

TL-4 Acceptable for the majority of highways, freeways, expressways and interstates with regular mixture of trucks and heavy vehicles

TL-5 Use justified in TL-4 areas where a high quantity of heavy trucks is expected or unfavorable bridge conditions exist

TL-6 Use justified in TL-4 areas where heavy trucks with high centre of gravity are expected or unfavourable bridge conditions exist.

LRFD defines unfavourable conditions as bridges with small bending radius, steep downgrades, and/or inclement weather.

Design Forces and Designations	Railing Test Levels						Barrier Types
	TL-1	TL-2	TL-3	TL-4	TL-5	TL-6	
F_T Transverse (kips)	13.5	27.0	54.0	54.0	124.0	175.0	
F_L Longitudinal (kips)	4.5	9.0	18.0	18.0	41.0	58.0	
F_V Vertical (kips) Down	4.5	4.5	4.5	18.0	80.0	80.0	
L_T and L_L (ft.)	4.0	4.0	4.0	3.5	8.0	8.0	
L_V (ft.)	18.0	18.0	18.0	18.0	40.0	40.0	
He (min) (in.)	18.0	20.0	24.0	32.0	42.0	56.0	
Minimum H Height of Rail (in.)	27.0	27.0	27.0	32.0	42.0	90.0	

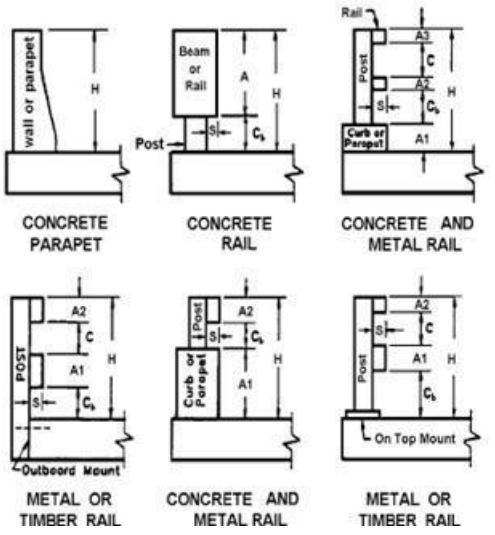

Figure 2-10: AASHTO LRFD (2010) Design Forces and Barrier Types

`

2.3.2.3 CSA (2006) Canadian Highway Bridge Design Code

In Canada, the CSA (2006) is the national code governing both the evaluation and design of bridge barriers. The treatment of barrier loading, design, and evaluation is based off of the AASHTO Guide Specifications for Bridge Barriers (1989) and AASHTO LRFD (1994) documents whose design criteria were mainly influenced by NCHRP Report 230 (1980). Provincial codes may also provide extra stipulations for barrier design and crash testing; however they have not been included in this review of the literature.

The CSA (2006) states that barriers must *delineate the superstructure edge and to reduce the consequences of vehicles leaving the roadway*, and the barriers are defined into three different performance levels as per the AASHTO (1989) and described as follows:

PL-1 Sufficient for use in low traffic volume bridges with no unusual safety hazards

PL-2 Sufficient for use on high-to-moderate traffic volume bridges on high speed roadways with normal mix of heavy truck traffic

PL-3 Sufficient for use on high-traffic volume bridges on high speed roadways with large mix of heavy truck traffic

The code commentary recognizes the equivalence between the three performance levels listed and the NCHRP 350 test levels as defined by the FHWA in Table 2-1. Like the older AASHTO documents, the CSA (2006) provides selection tables to determine what barrier performance level is necessary at different bridge sites. The selection tables were determined using the cost/benefit analysis program, BCAP, and consider the barrier clearance, traffic speed, and barrier exposure index (BEI). The BEI is itself determined using selection tables based off of the bridge AADT, roadway type, curvature, grade, and height.

General crash test guidelines – vehicle type, weight, impact speed, and impact angle – are specified for the different performance levels. However, the commentary refers the evaluation of crash tests to be done in accordance with NCHRP Report 230 (1981). It also references previously crash tested barrier types and their level of crashworthiness (both the Jersey and F shaped concrete safety shaped barriers crash tested by Buth et al. (1990) for PL-2 are referenced).

The CSA (2006) stipulates that crash tested barrier designs may be modified, but the modifications must not harmfully affect the vehicle barrier interaction during impacts. The

`

commentary provides examples of the following acceptable modifications: using materials of equivalent or superior properties or using anchors with equivalent or greater strength than crash tested anchors. The CSA (2006) commentary noted specifically that the rigidity of the barrier should remain unchanged or be increased.

For the design of anchors, and deck overhang, the CSA (2006) provides the equivalent static design loads and minimum barrier height for each PL (Table 2-6). The application details are shown in Figure 2-11. The impact loads come from the AAHSTO Guide Specifications (1989); however they were adjusted to account for the live load factor of 1.7, and the noted increase in the strength of structures under dynamic loads of 40%. There is no dynamic load allowance, and the static design loads are to be applied simultaneously to the barrier. The barrier performance should be determined from crash tests. However, the design loads can be used for the initial design of new barriers, as well as for the anchor and deck overhang reinforcement details.

Table 2-6: Equivalent Static Impact Loads (CSA 2006)

Performance level	Transverse load	Longitudinal load	Vertical load	Height
PL-1	50 kN	20 kN	10 kN	0.68 m
PL-2	100 kN	30 kN	30 kN	0.80 m
PL-3	210 kN	70 kN	90 kN	1.05 m

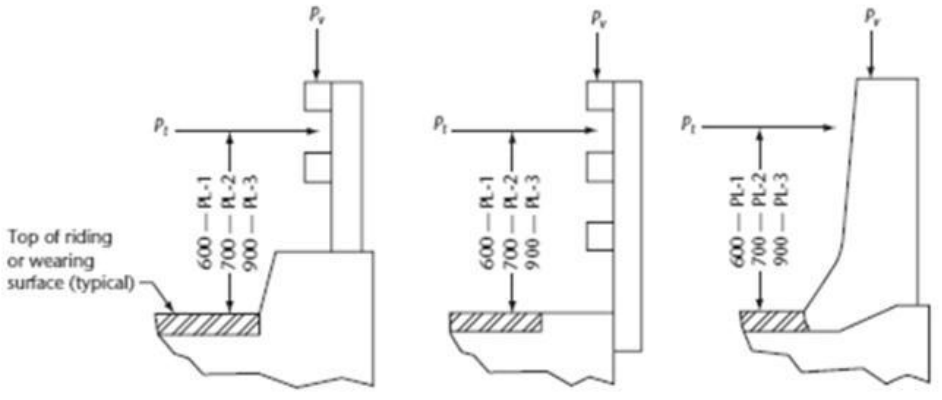

Notes:
(1) *Traffic barrier types are illustrative only and other types may be used.*
(2) *Transverse load P_t shall be applied over a barrier length of* 1200 mm *for PL-1 barriers,* 1050 mm *for PL-2 barriers, and* 2400 mm *for PL-3 barriers.*
(3) *Longitudinal load P_ℓ shall be applied at the same locations and over the same barrier lengths as P_t. For post and railing barriers, the longitudinal load shall not be distributed to more than three posts.*
(4) *Vertical load P_v shall be applied over a barrier length of* 5500 mm *for PL-1 and PL-2 barriers and* 12 000 mm *for PL-3 barriers.*
(5) *These loads shall be used for the design of traffic barrier anchorages and decks only.*

Figure 2-11: Application of Impact Design Loads (CSA 2006)

`

The code stipulates that the transverse bending moment in the deck overhang should be calculated using the greater of either the CL-W wheel loads or the barrier impact loads as specified in Table 2-6 and Figure 2-11. An acceptable refined analysis method (grid lines, finite element) or yield line analysis method should be used.

Anchors that have successfully passed crash testing are suitable for field use to the appropriate performance level. Anchors are considered to have passed crash testing if neither the anchors nor deck are significantly damaged (or need of replacement). New anchor details should be designed to resist the ultimate flexural, shear, and punching loads that can be transferred by the barrier during impact. However, their design need not exceed loads greater than specified in Table 2-6.

2.3.3 Expected Modifications to American and Canadian Codes

The publication of the MASH (2009), as well as an expected amendment in 2012 to the chapter 12 of the CSA (2006) bridge design code dealing with bridge barriers (TAC ATC 2010), implies impending modifications to the treatment of bridge barriers by the governing authorities in the U.S. and Canada.

The MASH (2009) modified the vehicle test matrix and impact conditions, notably increasing the impact severity for TL-3 and TL-4 barriers (Figure 2-8). Since the MASH is an AASHTO document and has also already been recognized as the successor to the NCHRP Report 350 (1993) by the FHWA for the crash testing of new barriers as of 2012, it is very likely that the upcoming AASHTO RDG and LRFD editions will incorporate these changes with higher equivalent static design loads for barriers, anchors, and deck overhangs.

The TAC ATC 2010 guide has shed some insight into the expected modifications to chapter 12 of the CSA (2006). Most notably, is the expected use of NCHRP 350 (1993) as the new basis for the crash testing and design load criteria. The three performance levels are expected to be converted to the six test levels as defined in NCHRP Report 350 (1993). The barrier heights are also to be changed to better comply with the crash test vehicle matrix from Report 350 (1993). Another expected change is the process of determining the necessary barrier PL/TL at a bridge site. The process is expected to be simplified, and one possibility is to use the algebraic approach currently used by the Ontario Ministry of Transportation.

`

2.3.4 Considerations

The increased impact severity for TL-3 and TL-4 in the MASH (2009) is an important point to address because certain barriers that were shown to be adequate for TL-3 and TL-4 of the NCHRP Report 350 (1993) may no longer be crashworthy for these test levels. The TRB, AASHTO, and FHWA all worked closely together in the preparation of the MASH (2009) and anticipated this problem and a two-fold approach was taken. First, all barriers crash tested to the NCHRP Report 350 (1993) criteria are still considered crashworthy for the respective test level in MASH (2009) and are not in need of new crash testing. Second, during the preparation of MASH (2009), the TRB performed crash tests with the new testing criteria on several of the most popular barriers in use in the U.S. Most of the barriers passed the MASH (2009) crash tests for their respective test level, but one notable exception was the TL-4 32 in (812 mm) Jersey shaped concrete barrier. The SUT actually rolled over the barrier and therefore was not contained (The F shaped TL-4 32 in barrier was not tested). The FHWA and AASHTO will jointly review the results and decide on whether the Jersey barrier should still be considered adequate for TL-4 designated areas. The FHWA may very well approve the continued use of the TL-4 32 in Jersey shaped concrete barrier; however, this provides another argument for bridge authorities to shift towards an increased use of constant-sloped barriers.

It is important to note that both the CSA (2006) and the RDG (2011) allow for existing crash tested barriers to be modified without further crash tests so long as detailed analytical and/or experimental data demonstrate that the modifications will not have any negative effects on the crash test behaviour of barriers. This precedent was first set by the FHWA in their May 16th 2000 Memorandum where they accepted the Colorado Type 10 bridge rail on the basis of analytical analysis and a comparison to the crash tested Wyoming TL-4 rail. This is an important method for the approval of barrier modification because the costs of crash testing are prohibitive.

The discrepancies between American and Canadian regulations must be highlighted because in general the two nations share very similar codes, highways, vehicle fleets, and barrier designs. In general, Canada has been slow to update their regulations to reflect changes in the United States. Presently, the primary references for the CSA (2006) are NCHRP Report 230 and the ASSHTO Guide Specifications for Bridge Barriers published in 1980 and 1989 respectively. The updates expected to the CSA bridge design code in 2012 are only expected to move to the crash test

`

criteria from NCHRP Report 350 published in 1993. The CAN/CSA should make more of an effort to be up-to-date, if anything, to best account for changes in the passenger vehicle fleet and heavy truck traffic. The difference in the calculation of the static equivalent design loads is another important difference. The CSA (2006) accounts for the increase in strength of materials during highly dynamic impacts of approximately 40% while the AASHTO codes do not. The approach of the CSA (2006) is more logical, albeit less conservative than AASHTO and results in factored design loads that are 40% smaller than their AASHTO counterparts. The problem with this situation is that many of the barriers in use in Canada have been designed to resist the AASHTO design loads. Therefore the hierarchy principal that barriers should fail before the anchors and deck is potentially compromised on Canadian bridges when the barriers have been designed to the higher AASHTO factored loads, and the anchors and deck overhang to the lower CSA (2006) factored loads. This is a discrepancy that should be addressed in the upcoming code modifications.

2.4 Precast Concrete Rigid Bridge Barriers

Recently there has been a lot of research and development into designing adequate precast concrete rigid bridge barriers. The impetus for this research is the potential to produce a higher quality bridge barrier with a reduction in installation time related costs. Precasting is known to improve quality because standardized fabrication processes are used and the fabrication environment is well regulated. The on-site installation time can also be significantly reduced since the barrier arrives on-site already built and only needs to be fixed to the bridge deck. The FHWA Connection Details for Precast Bridge Systems Report (CDPBS 2009) estimates a precast barrier installation time of 1 to 2 days for a standard single span bridge and Charron et al. (2011) estimates, more conservatively, 4 days for the installation of undercut connected precast barriers. This represents an enormous savings in time costs compared to typical cast-in-place barriers. Between reinforcement placement, formwork assembly, concrete casting, and curing the cast-in-place installation time for an equivalent single span bridge takes approximately 18 days (Charron et al. 2011). Another advantage of precast concrete barriers is that the shrinkage strains of the barriers are much less restrained (if not totally unrestrained) by the rigid bridge deck, and therefore shrinkage cracks are less likely to develop. The shrinkage cracks typical to cast-in-place barriers are aesthetically unpleasing and expose the steel reinforcement to more rapid migration

`

of chlorides reducing the barrier durability. It is clear that a well-conceived and well fabricated precast concrete bridge rigid barrier system can improve the bridge railing aesthetics, increase the barrier durability, and reduce time costs of installation.

The key to all precast structural elements is the design of the connection detail between the precast element and the remaining structure. Moreover, as has been previously documented, all barriers to be approved for use on the U.S. and Canadian highway bridges must be proven through full-scale crash testing. Crash testing is a cost and labor intensive process, and very few regulatory agencies have been willing to invest in the crash testing of the precast barrier designs. This subsequent review of the literature will evaluate different proposed precast barriers, their connection types, and the different structural validation methods used to establish the structural adequacy of the precast barrier and connection. Finally, a small segment will also summarise the different analysis methods available in the literature for precast barriers.

2.4.1 Connection Types

The Precast Concrete Institute (PCI) Bridge Design Manual (2010) cites two typical connection types used between precast concrete barriers and bridge decks. The first, through anchor connection, uses threaded reinforcement protruding from the bottom of the precast barrier through the entire deck and are fixed underneath using bolts and bearing plates (Figure 2-12-a). The second, undercut anchor connection, is similar except the protruding reinforcement is anchored directly into the deck using some sort of adhesive anchoring system (Figure 2-12-b). It should be noted the anchors could be undercut in the precast barrier as opposed to the deck (Charron et al. 2011). These two connection types can be more broadly categorized as bolt-down anchor connections. There exists in the literature another connection type, where a voided recess is cast into the precast barrier and injected with a cementitious material (concrete, mortar, or grout) once the barriers are placed on the deck (Figure 2-13). The injected material and reinforcement protruding into the recess connect the barrier to the injected section to the deck. This connection type will be referred to as the injected recess connection. A few examples of these connections and their typical properties will be examined in the following sub-sections.

`

2.4.1.1 Bolt-Down Anchor Connections

Bolt-down anchor connections are the most commonly designed precast barrier to deck systems found in the literature. These connections have been shown to be mechanically efficient and some designs have even been crash tested to NCHRP 350 Test Level 4 (LB Foster Precast Barrier, Clampcrete Precast Barrier). The general principal of these connections is to provide anchoring sleeves in the new bridge deck using PVC or steel with a sleeve spacing compatible with the precast barriers. The threaded rebars are then passed through the sleeves, bolted, post-tensioned, and grouted in place to secure the barrier to the deck (Figure 2-12). The through anchor design could also be compatible with existing bridge decks, however the decks would have to be cored at each anchor which would be very time consuming. The design considerations for these systems are the tensile capacity of the anchors and the concrete breakout capacity at bearing sites. Table 2-7 presents several different bolt-down anchor systems proposed and their general properties. The designs are similar, the main differences being barrier length, through-anchor or undercut anchor design, anchor spacing, anchor bar size, and anchor post-tension force. The anchor spacing is an important design consideration. The larger the spacing the faster the installation, but also the greater the tensile transfer force at each anchor during impacts.

Some concerns with the bolt-down anchor systems is the extensive use of steel bars, nuts, and bearing plates that could potentially corrode if they are not properly protected from aggressive environments. The movement of water through the seams and corrosion of bottom anchors and steel framing has been observed for these systems (FHWA CDPBS 2009). Moreover, each anchor must be aligned, post-tensioned, and grouted at an average spacing of 645 mm, all this labor could potentially reduce the gains in time-costs associated with precast elements.

`

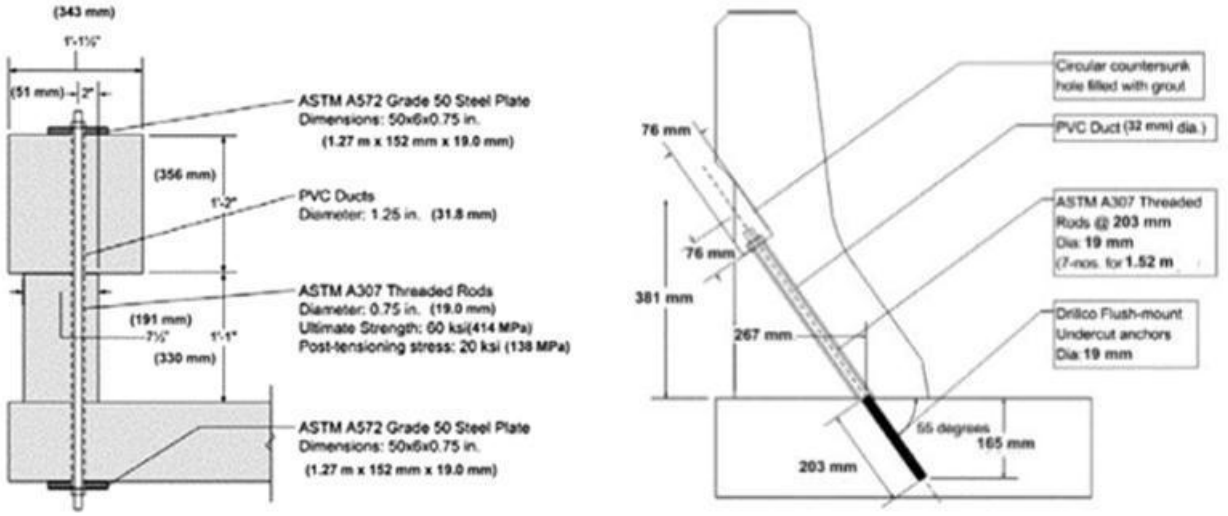

a) Mitchell 2010 Through Anchors b) Mitchell 2010 Undercut Anchors

Figure 2-12: Bolt-Down Anchor Connections (Mitchell 2010)

Table 2-7: Precast Barriers with Bolt-Down Anchor Connection

Designer	Barrier Length	Connection	Anchor Size	Anchor Spacing	Post-Tension Force
Alywan, 2007	6.10 m	Through	25.4 mm	773 mm	--
Clampcrete	--	Through	--	--	--
LB Foster	6.10 m	Undercut	25.4 mm	610 mm	--
Mitchell, 2010	1.52 m	Through	19.0 mm	203 mm	50 kN
Mitchell, 2010	1.52 m	Undercut	19.0 mm	203 mm	50 kN
Ngan, 2008	5.79 m	Through	25.0 mm	830 mm	--
Niamba, 2010[1]	2.00 m	Undercut[2]	32.0 mm	1500 mm	240 kN
Patel, 2009[3]	3.00 m	Through	25.0 mm	600 mm	79 kN

[1]70 MPa-1.5% FRC barrier considered. [2]Undercut side in Barrier. [3]Also Sennah, 2011.

2.4.1.2 Injected Recess Connections

Only three examples of the injected recess have been found in the literature (Aminmansour 2004, Duchesneau 2010, and Jeon 2011). Figure 2-13 shows two of the proposed connections. The injected recess connections have proven to be mechanically efficient, as the Aminmansour (2004) and Duchesneau (2010) barriers have both shown static and dynamic resistances exceeding the load requirements for Test Level 4 barriers (Jeon as well but only with static tests). Still none of the injected recess designs have been proven through crash testing.

`

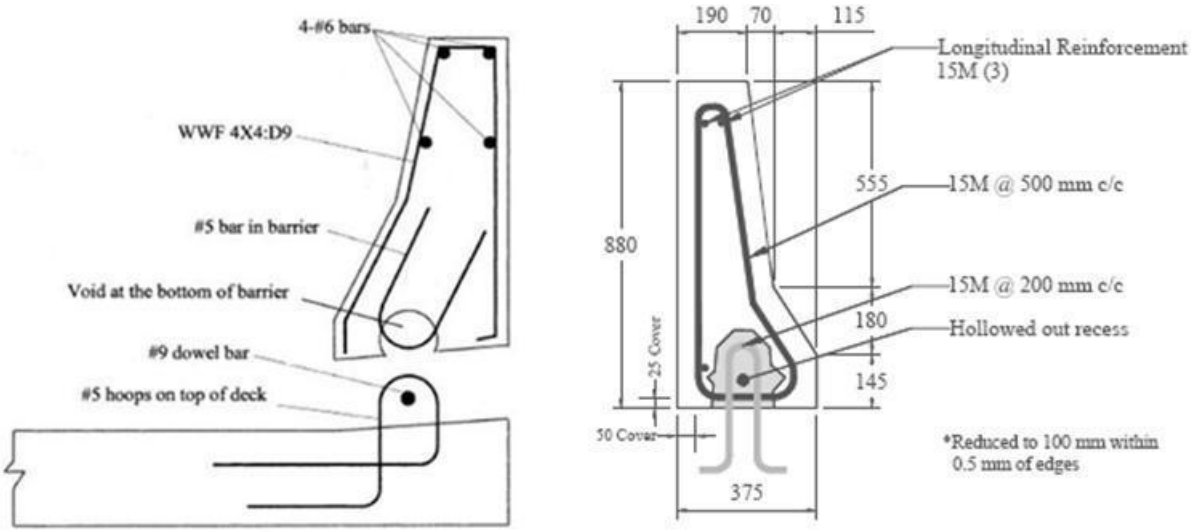

a) Aminmansour 2004 b) Duchesneau 2010

Figure 2-13: Injected Recess Connection

The advantage of this connection method is that the mechanics of force transfer from the barrier to the deck is done in a manner very similar to cast-in-place barriers, which has been proven through crash testing and extensive use throughout North America (Figure 2-2). The disadvantage is that the quality of the injection – material properties and fill – is an essential component of the structural capacity and must be adequately monitored and controlled. In the end-to-end injection method employed by Aminmansour (2004) and Duchesneau (2010), assessing the injection quality is particularly difficult because there can be no visual inspection of the recess. In the design proposed by Jeon (2011), shown in Figure 2-14, the cementitious material is poured into slits blocked out in the barrier that sit directly above the recess. This is perhaps an improved injection detail because it uses the force of gravity and the recess injection can be visually inspected.

`

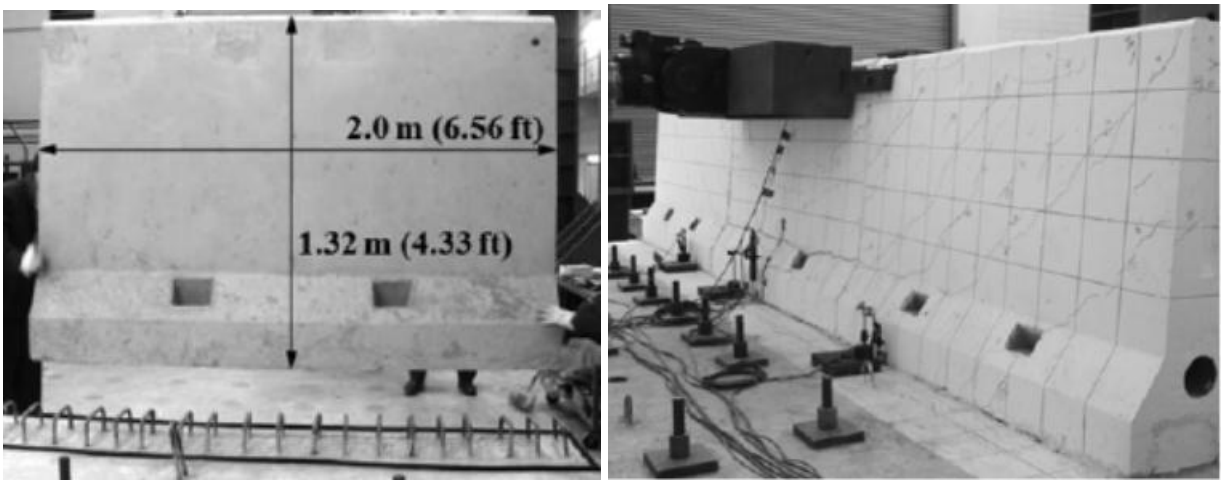

Figure 2-14: Precast Barrier Jeon (2011)

The Aminmansour (2004) design is the only recess that has hooped anchor bars entering the recess from both the barrier and the deck. Once in place a longitudinal bar is inserted between the hoops. This is an interesting detail because it confines the fill material between the opposing hoop anchors which is essentially working as continuous reinforced cylinder under multiple point loads (Figure 2-15). Aminmansour (2004) tested two series precast barriers, Series I with a 300 mm hoop bar spacing and regular grout material, and Series II with 229 mm hoop bar spacing and a fibre reinforced grout material. Series I can be seen as a weaker recess design and Series II stronger. The results of form Aminmansour (2004) showed that increasing the recess capacity moved the failure area from the recess to the slab overhang (Figure 2-16), but both designs still had a similar ultimate strength, 269 kN and 277 kN respectively, and the weak recess exhibited significant energy dissipation as the dowel bar deformed and the crack opened (Figure 2-16).

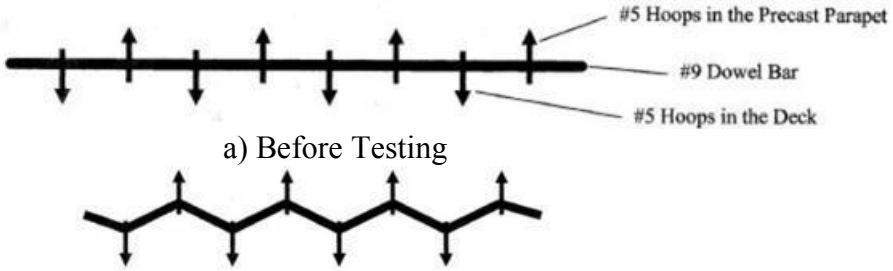

a) Before Testing

b) After Testing

Figure 2-15: Dowell Bar and Recess Reinforcement (Aminmansour, 2004)

`

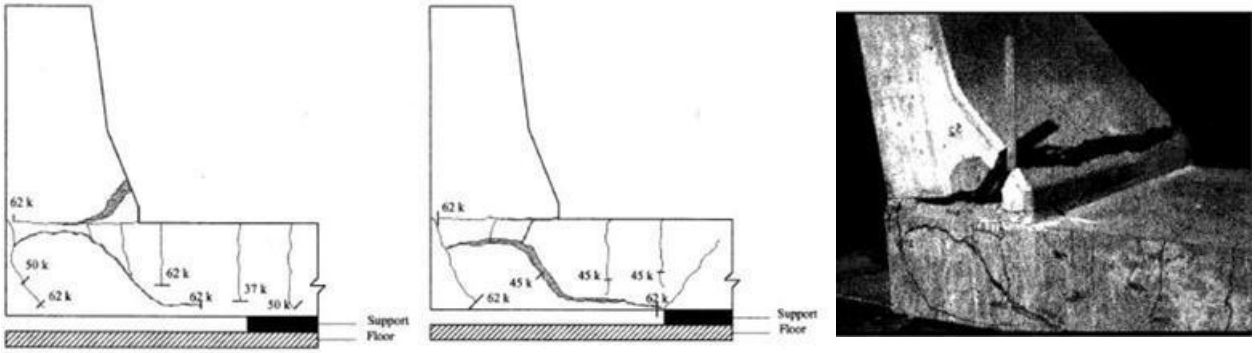

a) Series I Failure Schematic b) Series II Failure Schematic c) Series I Failure Photo

Figure 2-16: Aminmansour (2004) Static Test Results

2.4.1.3 Longitudinal Barrier Continuity

Several of the precast barrier designs, including the Clampcrete and LB Foster TL-4 crash tested barriers, have included a connection between precast barriers to provide a certain longitudinal continuity and to transfer the lateral impact force from one precast barrier to another (Jeon 2011, Ngan 2008, Patel, 2009). The barrier connection is most often a simple mechanical shear key (Figure 2-17), however some designs provide more robust shear and moment continuity (Figure 2-18).

The mechanical shear keys are typically simpler and more efficient designs. For instance, as shown in Figure 2-17, the LB Foster precast barrier uses a steel plate simply inserted into slits cast into the barriers, and the Jeon (2011) design cast a mechanical joint into the barrier shape. The experimental phase for Jeon (2011) highlighted that the dry joint was did not provide enough of a connection and an epoxy was added to improve the connection performance, increasing labor costs and perhaps transferring some bending as well. The shear and moment connection designed by Patel (2009) shown in Figure 2-18 uses a male/female connection between HSS and S beams cast into the barriers using shear studs. Once the barriers are placed the entire shear area is filled with grout. The Clampcrete design also shown in Figure 2-18 is perhaps more efficient. Steel dowels are fitted into metal couplers at the barrier edges to provide continuity to the longitudinal rebar. The dowel effect and the rebar continuity should transfer both shear and moment forces.

`

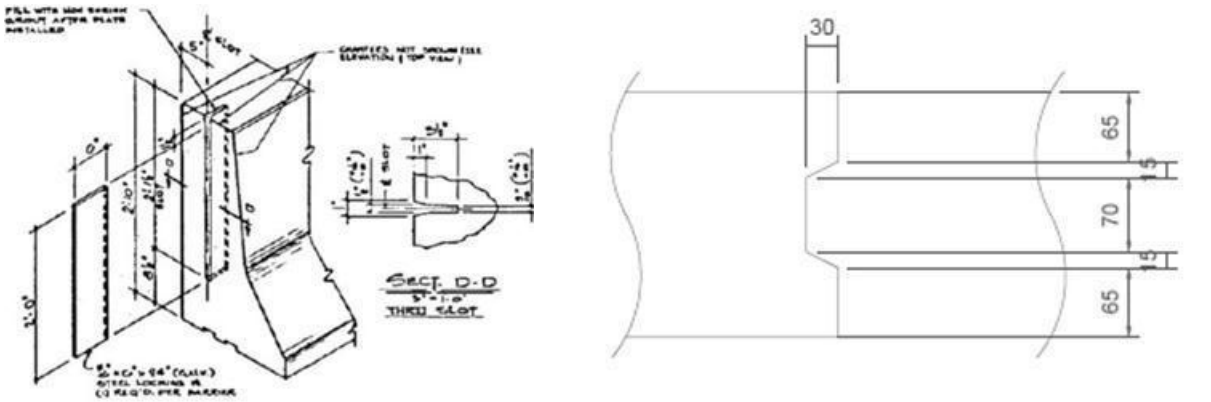

a) LB Foster (FHWA Bridge Rail Guide 2005) b) Jeon (2011)

Figure 2-17: Longitudinal Connections, Mechanical Shear Keys

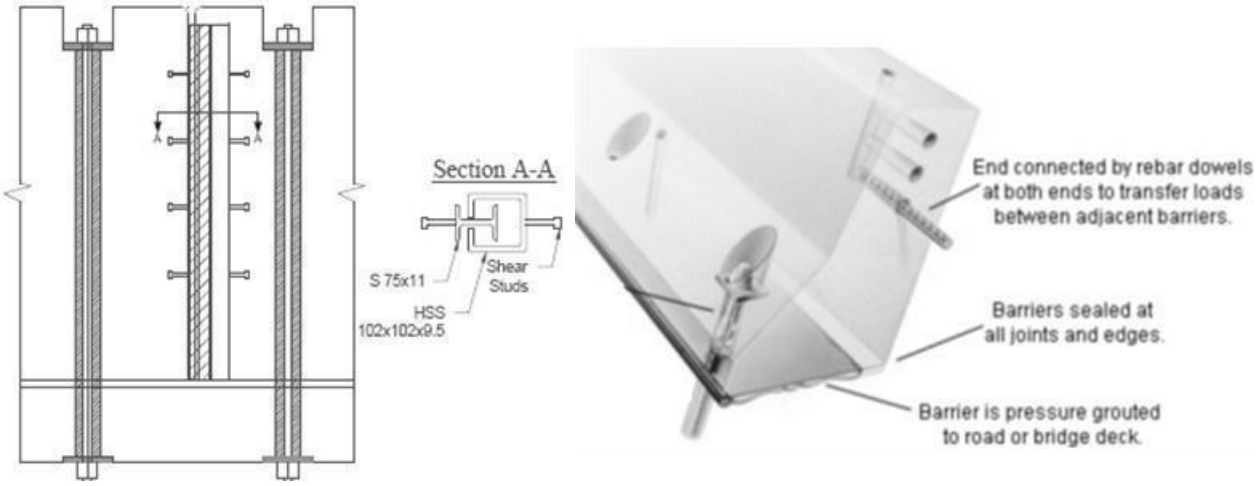

a) Patel (2009) or Sennah (2011) b) Clampcrete (FHWA CDPBS 2009)

Figure 2-18: Longitudinal Connections, Shear and Moment

Only the work of Jeon (2011) has evaluated the influence of the longitudinal connection on barrier performance, as the connection detail was improved during the experimental testing phase. The addition of the epoxy at the shear key increased the ultimate strength from 250 kN to 290 kN. This implies that a longitudinal connection is an important design component of precast barriers; however, this does not localize the effect of the shear key but only the improvement of adding epoxy to the dry joint. Moreover, it should be noted that Jeon (2011) was testing a TL-5 barrier and therefore the static load was applied over a 2.44 m length exceeding that of the 2.0 m precast barrier. Therefore the loading apparatus itself engaged the exterior barriers making it more difficult to evaluate the performance of the shear connection used.

`

In general, the longitudinal connection should be simple, effective, and durable. The connection proposed in the LB Foster system is very simple, but there is a risk that the eventually the steel plate could corrode and damage the barriers due to rust growth. The Patel (2009) connection is likely very mechanically effective but it requires costly materials and is more labor intensive and could also potentially have durability problems. The Jeon (2011) and Clampcrete designs seem to best combine simplicity, efficiency, and durability.

2.4.2 Structural Validation Methods

As has been stated previously, both the Canadian and American codes require full-scale crash testing before a barrier can be approved for use. This requirement is often necessary due to the complicated vehicle-barrier behaviour during impacts and is a means to guarantee both adequate barrier strength and vehicle impact response. However, the costs of full scale crash tests are prohibitive and in some ways an impediment to improving barrier designs. Table 2-8 lists the research projects on precast barriers cited in this review. It can be seen that in spite of the large resources devoted to the development of precast barrier systems, only two have actually been crash tested. As a means of avoiding crash tests, researchers have often restricted themselves to using a crash tested safety shape and then attempted to prove the structural adequacy of the new barrier systems using static and/or dynamic tests (Table 2-8). The idea is that if static or dynamic strength is shown to be sufficient to resist the impact energy associated with a barrier test level, and if the rigidity and shape are identical to the crash proven barrier, then it can safely be assumed that the new barrier would also be crash worthy. Certain local authorities, such as the New York Department of Transportation (FHWA CDPBS 2009), have accepted this design philosophy for approving the use of barriers within their jurisdiction. This section of the review will evaluate the primary methods used by researchers to demonstrate that their new precast barrier designs are crashworthy. In general either static tests, dynamic tests, numerical simulations, or some combination are used.

The MASH (2009) does address the use of structural analysis, static tests, dynamic tests, and computer simulations in the design of new barrier systems in Appendix D, however none of these methods are deemed adequate to assess the crash test performance of a new barrier design. The applications and limitations for each of these design techniques according to the MASH (2009) are paraphrased in Table 2-9.

`

Table 2-8: Precast Barrier Structural Adequacy Evaluation

Designer	Barrier Design Level	Static Strength	Dynamic Strength	Crash Test Level	Structural Adequacy
Alywan, 2007	TL-3	262 kN	--	--	TL-3
Aminmansour, 2004[1]	--	277 kN	365 kN	--	PL-2 / TL-4
Clampcrete	--	--	--	PL-2 / TL-4	PL-2 / TL-4
Duchesneau, 2011[2]	PL-2 / TL-4		> 215 kN[3]	--	PL-2 / TL-4
Jeon, 2011	PL-3 / TL-5	360 kN	--	--	PL-2 / TL-4
LB Foster	--	--	--	PL-2 / TL-4	PL-2 / TL-4
Mitchell, 2006 and 2010	TL-3	116 kN	170 kN[3]	--	TL-3
	TL-3	--	271 kN[3]	--	TL-3
Ngan, 2008	PL-2 / TL-4	250 kN	--	--	PL-2 / TL-4
Niamba, 2010[2]	PL-2 / TL-4	350 kN	> 215 kN[3]	--	PL-2 / TL-4
Sennah, 2011	PL-3 / TL-5	175 kN	--	--	PL-3 / TL-5

[1]Series II considered. [2]70 MPa-1.5% FRC barrier considered. [3]Max impact force.

Table 2-9: Barrier Design Technique (MASH 2009 Paraphrased)

Technique	Application	Limitations
Structural Analysis	Preliminary design of bridge barrier	Barrier-vehicle impact behaviour unknown and occupant risk impossible to assess.
Static Tests	Validation of structural analysis and force-displacement behaviour	Dynamic behaviour remains unknown, and occupant risk impossible to assess.
Dynamic Tests (Pendulum)	Dynamic strength of bridge barrier and anchor systems	Only transversal impact and cannot evaluate extent of vehicle crush.
Computer Simulations	Parametric studies and design optimization	Models need to be validated using crash tests and are influenced by small details.

2.4.2.1 Static Tests

Static tests are generally used in the design of new precast barriers (Table 2-8) and allow researchers to establish the structural capacity of the barrier, anchors, deck, and to evaluate the effect of certain important design modifications. There is no standardized ASTM static test for

`

barriers and therefore every research institution must develop their own testing setup (Figure 2-19). Some of the key testing parameters to consider are the length, boundary condition (deck overhang or no), and loading surface.

The static tests are considered to validate the system design when the factored equivalent static design forces from the AASHTO LRFD (2010) or CSA (2006) are met for the appropriate barrier TL or PL. In the case of the AASHTO LRFD (2010) loads, this may be overly conservative since the increase in material strength is not accounted for. The strength of materials is approximately 40% higher due to high strain rate effects associated with vehicle impacts (CSA 2006), and it is likely that the barrier's ultimate strength will be higher during dynamic tests than static tests. This physical phenomenon is apparent in the study of Aminmansour (2004) and Mitchell (2006), see Table 2-8. The MASH (2009) warns that although static testing will cause failure at the lowest load level, this may not be the lowest energy mode. The literature does not suggest that this would be a concern for rigid concrete barriers (Aminmansour 2004, Mitchell 2006, Niamba 2009, Duchesneau 2010).

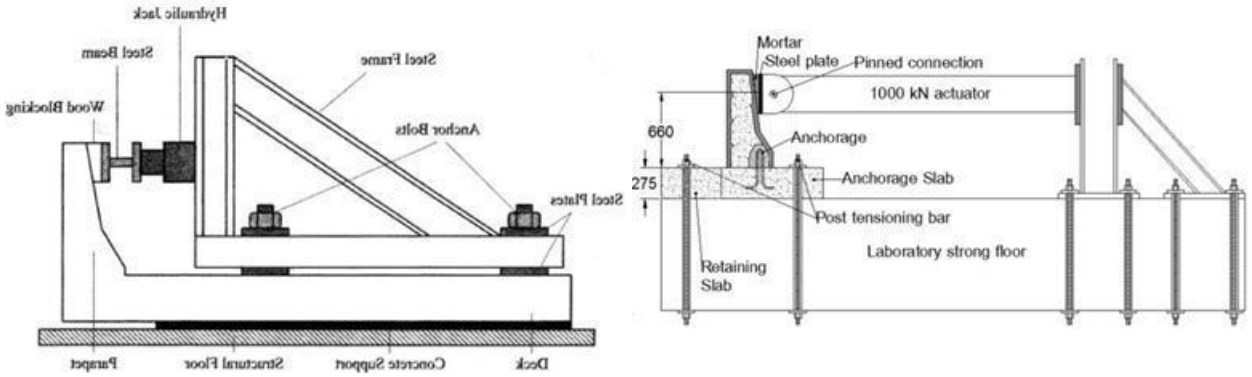

a) Aminmansour (2004) b) Duchesneau (2010)

Figure 2-19: Static Test Setups

2.4.2.2 Dynamic Testing

Certain research projects have also created dynamic tests to establish the structural capacity of the precast barrier designs. The dynamic tests have the advantage that they can recreate realistic crash load histories (Figure 2-20) and indeed prove the dynamic capacity of the barrier systems. Though they require much more extensive preparation and instrumentation than static tests.

The most typical setup is the pendulum or drop mass tests shown in Figure 2-20 (Aminmansour 2004, Mitchell 2010). In the pendulum test, the impact severity is calibrated by varying the drop

`

height and suspended mass. If the impact between mass and barrier occurs at the lowest point, the kinetic impact energy ($\frac{1}{2}mv^2$) can be reasonably assumed to equal the potential energy (mgh) before releasing the mass. The time history of the mass accelerations monitored with accelerometers are used to determine the load history and dynamic strength of the barriers. For these tests it is important that the crush package (mass nose) is calibrated to have a similar crush behaviour as a vehicle to accurately reproduce the loading signal.

The test setup used at Polytechnique Montréal by Niamba (2009) and Duchesneau (2010) is an interesting and novel dynamic test. This impact setup used a hydraulic actuator to provide a controlled dynamic impulse onto the barrier specimen (Figure 2-21). The impulse signal was a smoothened load history recorded during the impact test of a Toyota Echo with a 20° impact angle and 110 km/h impact velocity published by Jiang et al. (2004). This testing method presents a more controlled method of applying the vehicle crash signal and there is no longer need for a calibrated crush package since the load history is controlled by the actuator. The instrumentation is also simplified since the actuator will also monitor the load history and accelerometers are no longer necessary.

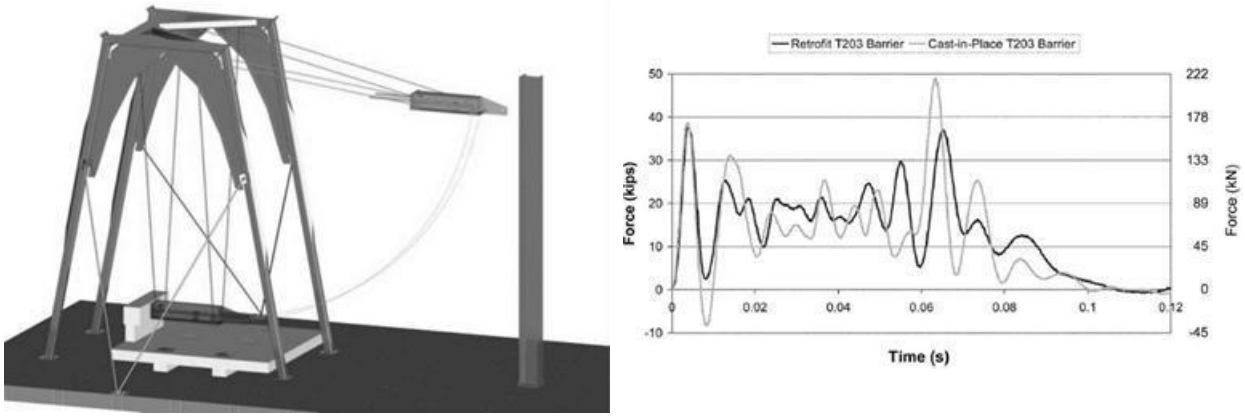

a) Test Setup (Mitchell 2006) b) Load History (Mitchell 2010)

Figure 2-20: Pendulum Test

`

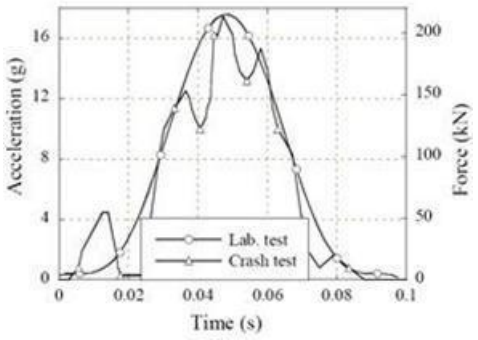

a) Application of Dynamic Force (Duchesneau 2010) b) Load History (Niamba 2009)

Figure 2-21: Dynamic Test Setup Niamba (2009) and Duchesneau (2010)

2.4.3 Analysis Methods

An appropriate structural analysis of a precast barrier is one of the most important steps to detail and optimize a new barrier design. Presently, yield line analysis is the main method used to determine the ultimate strength of reinforced concrete cast-in-place barriers. Hirsch (1978) derived the yield line formulas initially proposed in the AASHTO Guide Specifications for Bridge Barriers (1989) and still used today in the AASHTO LRFD (2010). Jeon (2011) has derived new yield line equations based upon the failure planes observed during the static loading of TL-5 barriers. Yield line analysis has been shown to provide a good estimate of the barrier ultimate flexural strength for cast-in-place barriers. However, strut-and-tie analysis is perhaps better suited for the design of precast barriers. Strut-and-tie analysis considers shear, flexure, and torsion for reinforced concrete structures in a unified design approach and can be used to design disturbed structural regions such as impact areas and the load transfer between barrier and slab. Aminmansour (2004) did an extensive analysis of the force movement during static loading of barriers and provided valuable insights into an optimized strut-and-tie model. This portion of the review of the literature will examine the different design methods proposed by Hirsh (1978), Jeon (2011), and Aminmansour (2004).

2.4.3.1 Yield Line Analysis

Yield line analysis is an ultimate strength method and is based on the following assumptions:

- Flexural strength controls the barrier failure;
- The reinforced concrete barrier is ductile enough for yield planes to develop;

`

- The steel is fully yielded along the rupture line and the resisting moment is evenly distributed along the rupture line;
- The reinforced concrete sections rotate around the yield lines as rigid bodies.

Though equilibrium concepts can be used, yield line analysis is typically developed using the principle of virtual work. The ultimate strength is calculated by setting the external work done by the applied forces equal to the internal work done by the resisting mechanism. This method is an upper-bound solution and inherently non-conservative. Therefore a minimization process using partial differentiation to identify parameters leading to minimum energy conditions (angles and yield line lengths) and also evaluating other potential failure planes must be carried out to approach the actual ultimate strength. The proposed yield lines derived by Hirsch (1978) and Jeon (2011) for continuous barriers are shown in Figure 2-22.

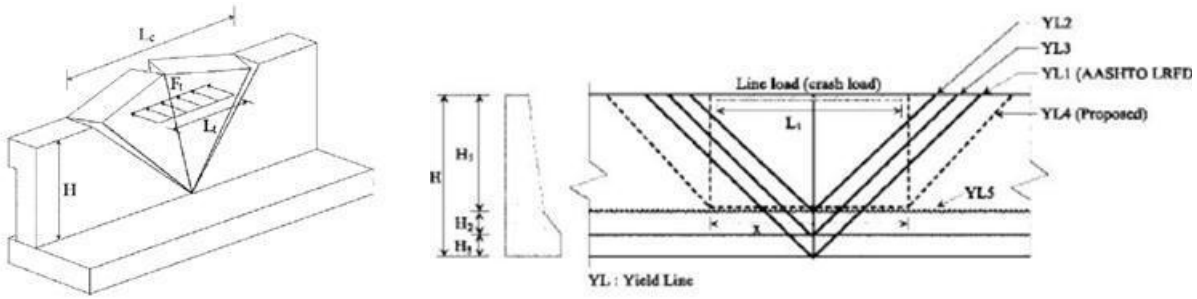

a) Hirsch (1978), AASHTO LRFD (2010) Yield Lines

b) Jeon (2011) Yield Lines

Figure 2-22: Yield Lines for Rigid Concrete Barriers

The solution by Hirsch (1978) for the yield line pattern in Figure 2-22-a is

$$R_w = \left(\frac{2}{2L_c - L_t}\right)\left(8M_b + 8M_w + \frac{M_c L_c^2}{H}\right) \qquad \text{Equation 2-1}$$

$$L_c = \frac{L_t}{2} + \sqrt{\left(\frac{L_t}{2}\right)^2 + H\left(\frac{M_b + M_w}{M_c}\right)} \qquad \text{Equation 2-2}$$

and the solution by Jeon (2011) for yield line pattern 4 (YL4) in Figure 2-22-b is:

`

$$R_w = 4\sqrt{\frac{2M_{c1}M_{w1}}{H_1}} + \frac{M_{c1}L_t}{H_1}$$ Equation 2-3

$$L_c = 2\sqrt{\frac{2M_{w1}H_1}{M_{c1}}} + L_t$$ Equation 2-4

where R_w is the ultimate strength of the barrier, L_c is the critical yield line length, and M_c and M_w are the barrier flexural strength per unit length about the longitudinal and vertical axes respectively (M_b is the additional flexural strength per unit length at the top of the barrier analysed by Hirsch (1978) in Figure 2-22a). The subscript 1 in Jeon's equations refers to the height of the upper sloped face of the barrier H_1, because the proposed yield lines occur only over that portion of the barrier (Figure 2-22b). Jeon (2011) compared the computed ultimate strength using the Hirsch (1978) formulas and the proposed Jeon (2011) formulas to the results from tests performed on the TL-5 barriers. In Table 2-10 Jeon's (2011) equations were more accurate. Jeon (2011) used the failure planes observed to derive the yield line equations and that his barriers did include a joint at the edge of the precast barriers (Figure 2-17b) that likely affected the barrier continuity and may have affected the development of the failure planes.

Table 2-10: Yield Line Analysis Jeon (2011)

Specimen No.	Test Strength	Hirsch (1978)	Jeon (2011)
3	360 kN	558 kN	397 kN
4	330 kN	454 kN	322 kN

Jeon (2011) applied the yield line analysis method to help provide insight into a proper design for discontinuous precast barriers (no longitudinal connection), and isolated four potential failure planes (Figure 2-23). The critical impact load for the barrier is governed by the edge impact case (Figure 2-23a) and the maximum applied load, P, was calculated by Jeon (2011) as:

$$P_{centric} = 2\sqrt{\frac{M_c M_w}{H}}$$ for case A, Equation 2-5

$$P_{eccentered} = \frac{L}{H}M_c$$ for case B Equation 2-6

`

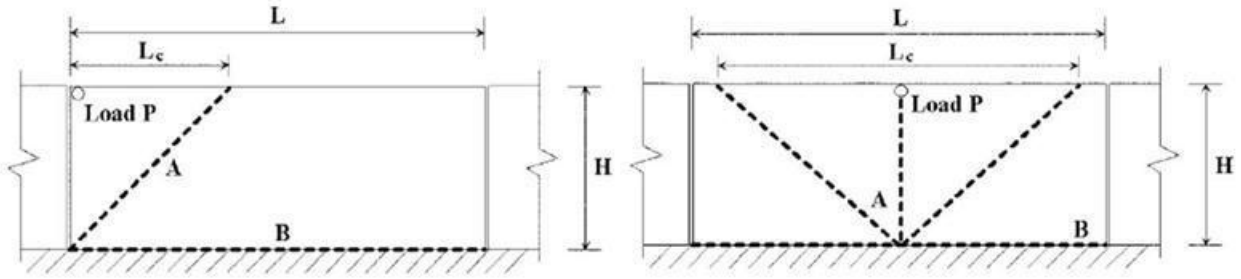

a) Crash at Joint (Edge) of Barrier b) Crash in General Part (Centre) of Barrier

Figure 2-23: Failure Modes of Precast Barriers without Longitudinal Connection (Jeon 2011)

The controlling factor governing whether the failure mode is on the diagonal, case A, or horizontal, case B, is shown to be the geometric length to height ratio of the precast barrier. Ideally, the case B failure will occur because the failure will cross the entire barrier section and is a more efficient failure mode (Jeon 2011). Assuming that M_c is equal to $\frac{M_w}{H}$ (a reasonable assumption for Jersey and F shaped barriers), the diagonal yield failure will occur for edge impacts as long as L > 2H, and for general impacts when L > $4\sqrt{2}H$.

2.4.3.2 Strut-and-Tie Analysis

Strut-and-tie analysis of reinforced concrete is based on the truss analogy. The cracked reinforced concrete section is analysed as an analogous truss of struts, ties, and nodes that resist the applied forces (Figure 2-24). The compressive struts represent concrete stress fields that are primarily in compression. Tension ties are members of the analogous truss in tension. Steel reinforcement generally transfers the tensile loads, but tensile stress fields do form in concrete until they exceed the concrete tensile strength. The nodes are the areas where the forces meet. It is important to verify the bearing capacity of the concrete struts and the anchorage of the steel ties at nodes. The positioning of the steel reinforcement will control the load redistribution once the concrete cracks. A well designed strut-and-tie model will position the steel to optimize the internal resistance and therefore minimize the quantity of steel reinforcement necessary.

`

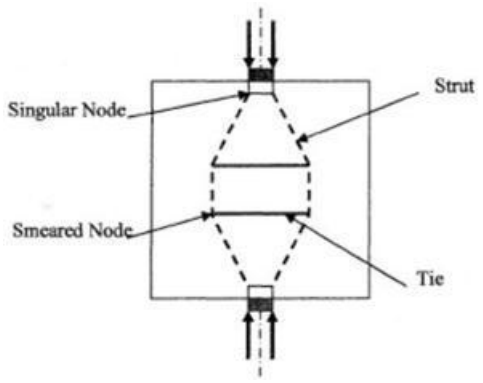

Figure 2-24: Strut-and-Tie Model (Aminmansour 2004)

Figure 2-25-a shows the initial strut-and-tie model of Aminmansour (2004) for the Series II precast barriers. Strut D represents the barrier transverse reinforcement and node N_5 the dowel bar in the injected recess (Figure 2-13a). A concrete tie was necessary to balance the forces at node N_6, which is not an ideal design because of the weak tensile capacity of the concrete. Once the concrete tie fails, truss members A, I, and H become zero force members and the internal load path is redistributed as shown in Figure 2-25b. It should be noted that since Aminmansour (2004) wanted to evaluate the strength of the precast barriers and connection, the slab had been designed to resist twice the load. In spite of this, the ultimate strength of the Series II barriers, where failure occurred in the slab (Figure 2-16b), of 277 kN compared to Series I, where failure occurred in the barrier (Figure 2-16a), of 267 kN represents only a 3% increase in strength. The lack of strength gain is due to the opening of the shear crack in the slab once concrete tie I fails. To improve the performance of the precast barrier, Aminmansour (2004) considered changing the shape of the anchor bars to develop a steel tie crossing the diagonal tensile crack. The proposed anchors are superimposed over the deformed slab and the corresponding strut-and-tie model are shown in Figure 2-26. Aminmansour (2004) noted the importance of hooking the legs of the anchor bar back towards the slab overhang edge in order to develop compressive struts at end of the slab (Figure 2-26-b). The improved anchor detail is a cost-effective way of improving the structural performance without additional reinforcement, and is a good demonstration of how the strut-and-tie modeling can optimize the design of disturbed regions.

`

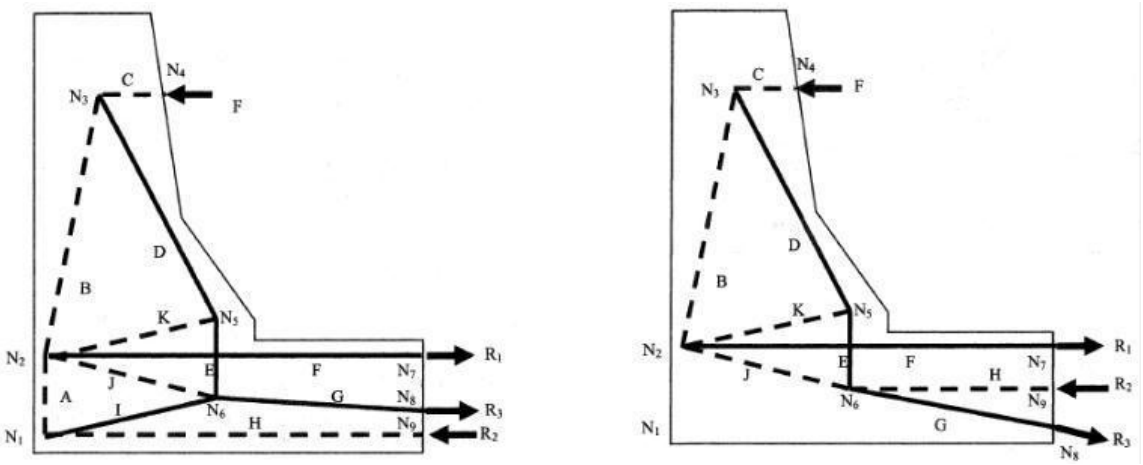

a) Model with Concrete Strut* b) Model without Concrete Strut*

*Struts dashed and ties solid

Figure 2-25: Aminmansour (2004) Strut-and-Tie Model Series II Precast Barriers

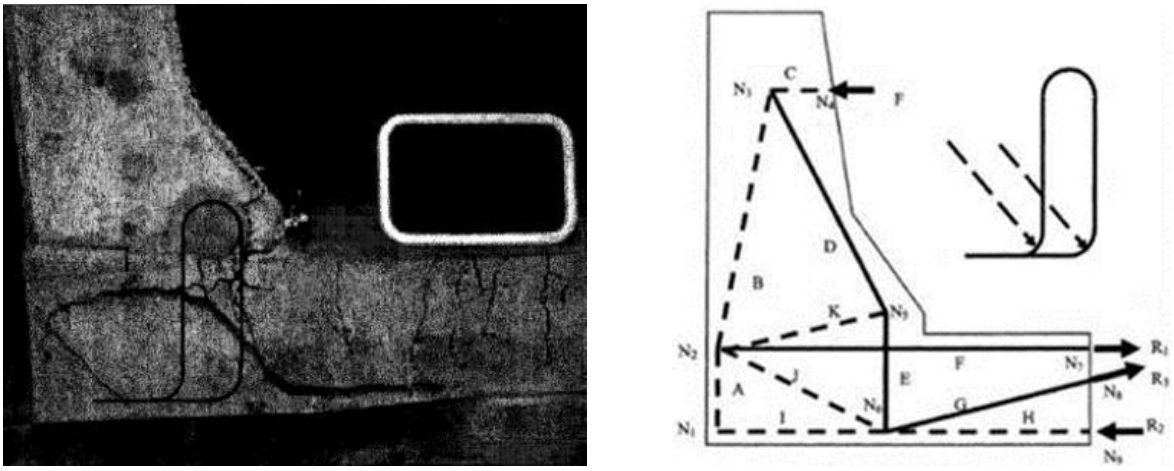

a) Proposed Anchor Superimposed on Specimen b) Corresponding Strut-and-Tie Model

Figure 2-26: Aminmansour (2004) Improved Barrier-Deck Connection Detail

2.4.4 Considerations

The review of the precast barrier systems proposed in the literature brings up several considerations for the future design and approval of new precast barrier prototypes.

The mechanical performance of both bolt-down and injected recess connections have been extensively proven through static and dynamic testing throughout the literature. When comparing the two connection types, the injected recess stands out as a superior connection detail. The connection is more similar to the well proven cast-in-place barrier connection and is less labor intensive. The injected recess also seems less costly because there is no need for expensive high

`

strength steel threaded bars, nuts, and anchor plates, and the reduced amount of steel components also lowers the risk of durability problems. The only disadvantage of this method is the questions surrounding the quality of the injection. However, combining the designs of Aminmansour (2004) and Jeon (2011) should resolve this potential issue. The mechanical connection of the hooped anchors and dowel provide substantial ductility to the recess in spite of a weaker injection material (Aminmansour 2004) and the Jeon (2011) injection method simplifies the process and provides a visual inspection of the finished injection.

It is notable that most of the precast anchor designs have longitudinal connection details between barriers. Jeon (2011) is the only researcher to have demonstrated the impact of using an improved connection detail; however, the Jeon (2011) connections were not adequately tested since the loading apparatus directly activated all three precast barriers at one time. Because longitudinal connections increase installation time and material costs, a more thorough examination of their impact remains necessary.

Crash testing has been shown to be a necessary requirement to ensure that barrier designs are structurally adequate and that the post-impact behaviour of the vehicle is acceptable. However, looking through the literature it is clear that few institutions possess the resources needed to implement full-scale crash tests (Table 2-8). The crash testing requirement should not become an impediment to improving the bridge barriers. The approach adopted by the NY DoT merits note. The NY DoT has allowed barrier designs to be modified so long as the crash tested geometry remains unchanged and either static or dynamic testing establish the barrier structural adequacy and rigidity (CDPBS 2009). It is a reasonable assumption since the concrete bridge barriers deflect very little during impacts, that modifying the design will not affect the impact dynamics so long as the strength remains sufficient and impact geometry unchanged. If the governing codes – CSA 2006, MASH 2009, AASHTO 2010, and RDG 2011 – were to more officially sanction this design method, it would facilitate the validation of new and improved barrier prototypes.

In the MASH (2009) Appendix D, they do evaluate some of the methods used to establish barrier structural adequacy. The reader is warned that static load methods may underestimate the energy mode of failure. Several researchers have tested both the ultimate static and dynamic capacity of concrete bridge barriers and have consistently found that dynamic loading causes a similar failure mode at an elevated ultimate strength for rigid cast-in-place barriers. Indeed the research of

`

Aminmansour (2004) and Mitchell (2006) show an increase of 32% and 47% in barrier ultimate strength during dynamic loading of their respective precast barrier designs. There are two proposed mechanisms for the increase in strength of concrete at high strain rates (Brara & Klepaczko, 2007). The first is the effect of free water within the concrete porous structure which adds a viscous behaviour and slightly increases ultimate strain and strength of concrete. The second is that during short impulses the micro cracks do not have the time to localize and find the path of least resistance to opening. They therefore pass through as opposed to around stiffer aggregate materials and increase the concrete strength. The research implies that static loading of either bolt-down or injected recess precast barrier types would not underestimate the energy mode of failure. In light of the increased costs in time, equipment, and energy, static testing should be sufficient to establish the structural adequacy of a precast barrier with one of these types of connections.

The analysis methods used to evaluate and optimize the precast barrier designs are very helpful in the design of new types of precast barriers. The proposed yield line analysis equations from Jeon (2011) have been shown to provide an adequate estimate of the ultimate strength of the barriers (Table 2-10). Moreover, the analysis of the potential failure planes for precast barriers without connections has shed light on the effect of the barrier length to height ratio. Jeon (2011) showed that a diagonal yield line will develop for edge impacts so long as L > 2H, and for general impacts when L > $4\sqrt{2}H$ if $M_c \approx \frac{M_w}{H}$ (for the standard MTQ Type 201 F-shaped barrier used in Quebec M_c = 127 kN-m/m and $\frac{M_w}{H}$ = 124.2 kN-m/m). This means that for a precast barrier based off of the MTQ Type 201 barrier that is 820 mm in height, a length of 1.76 m is required to ensure diagonal rupture line at edge impacts and 4.98 m is required to ensure diagonal rupture line across the entire barrier. A 5 m precast length may be too long due to practical considerations, but it is important to keep this in mind.

The strut-and-tie analysis by Aminmansour (2004) highlights the importance of using anchor bars that cross the potential shear crack in the slab overhang underneath the barrier. The anchors proposed by Aminmansour (2004) are similar to those used in the Duchesneau (2010) precast barrier, however both legs hook back towards the far edge of the slab cantilever. This is an important design consideration because it will help develop the compressive strut in the concrete at this location, and could potentially improve the Duchesneau (2010) barrier design.

`

2.5 Conclusions

The review of the literature concerning barrier types, regulations, and precast designs brings up certain conclusions for this research project.

- The F shaped safety barrier is the current standard in Quebec and therefore continued research into the development of a new type of precast barrier should use the MTQ Type 201 F shaped barrier as the reference prototype;
- Design modifications of a currently used and crash tested bridge barrier may be approved for use on the American and Canadian highway network if the structural adequacy of the modified barrier is adequately demonstrated;
- The injected recess connection type between precast barrier and deck stands out as the most complete connection method;
- The effect of including longitudinal connections between barriers still has not been adequately examined in the literature;
- An acceptable static strength is sufficient to establish the structural adequacy for precast concrete bridge barriers, and it can be assumed that the dynamic strength is 30-45% greater;
- The Duchesneau (2010) precast concrete barrier design, based off of the MTQ Type 201 barrier, is ideal for continued research. It is based off of a crashworthy barrier, it uses the injected recess connection, and it has already been mechanically proven using both static and dynamic testing.

`

CHAPTER 3 ARTICLE 1: "STRUCTURAL BEHAVIOUR OF CAST-IN-PLACE AND PRECAST CONCRETE BARRIERS SUBJECTED TO TRANSVERSE STATIC LOADING AND ANCHORED TO BRIDGE DECK OVERHANGS."

Abstract

In this study, experimental testing was performed on cast-in-place and precast barriers subjected to quasi-static loading and anchored to 6 m long bridge decks with a 1 m overhang. The three selected bridge barrier configurations include an ordinary concrete cast-in-place barrier, and two high performance fibre reinforced concrete (HPFRC) precast barriers, one with and one without barrier-to-barrier connections. An experimental setup dedicated to testing the large-scale barrier-deck slab overhang specimens to failure was designed. The structural behaviour of the three barrier configurations were analysed and compared. The tests demonstrated that all three test configurations exceeded the design criteria in the CSA (2006) and AASHTO LRFD (2010), that the durability of the slab overhang is not adversely affected when using precast barriers, and that the shear key designed to connect the precast barriers provides adequate barrier longitudinal continuity.

3.1 Introduction

Throughout North America, reinforced concrete bridge barriers are used to force errant vehicles to remain on the roadway. The bridge barriers two primary functions are to contain errant vehicles and adequately redirect them back onto the roadway (MASH 2009, CSA 2006). Crash testing and field experience has demonstrated that the commonly used Jersey and F shaped safety barriers meet these performance demands. However, in severe environmental conditions, they often deteriorate prematurely and require expensive repair or replacement work to maintain their structural integrity. Barrier cracks usually form at an early-age as the deck slab restrains barrier shrinkage and thermal dilations after casting (Cusson & Repette, 2000). The early-age cracks are aesthetically unpleasant, but more importantly they give an immediate opening for water and chlorides to quickly penetrate into the concrete matrix. Barriers are also often exposed to severe environmental conditions, and in cold regions they must resist freeze-thaw cycles and chlorides

present in de-icing salts. The vertical cracks due to restrained barrier movement have been shown to accelerate barrier degradation necessitating costly maintenance and repair work (Haluk et al, 2004).

An extensive research project carried out at Polytechnique Montreal is aimed at developing precast high performance fibre reinforced concrete (HPFRC) bridge barriers as a solution to the above durability issues. The proposed precast barriers offer several advantages compared to the cast-in-place method. Precasting provides a higher standard of fabrication quality, and eliminates early-age cracking due to restrained barrier movement since the HPFRC is free to reach its steady-state volume at the precast plant. In addition, the HPFRC material has superior durability and mechanical properties because the steel fibres limit crack openings and increase fracture energy (Desmettre and Charron, 2012). Finally, installation of precast barriers could enable significant time savings. Charron et al. (2011) estimates 4 days for the installation of precast barriers on a standard 30 m long single span bridge. This is a significant reduction compared to cast-in-place barriers that take up to 18 days, especially during repair of existing bridge barriers where traffic disruption implies a significant project cost. The improved durability of the precast barriers and the reduced time costs anticipated with faster installation provide a strong financial incentive for their use.

Two different precast barriers were designed, optimized, and tested with different types of high and ultra-high performance steel fibre reinforced concrete's in preceding projects (Niamba 2009; Duchesneau et al. 2011). The designs were based on a Quebec Ministry of Transportation (MTQ) Type 201 F shaped barrier shown in Figure 3-2a (MTQ 2010). The MTQ Type 201 barrier is used in Quebec for PL-2 (AASHTO TL-4 equivalent) category barriers. The proposed precast barriers have less steel reinforcement and reduced sections compared to the MTQ 201 barrier. The precast barriers differ from one another primarily in their respective barrier to slab connection. Niamba used steel couplers embedded into the precast concrete barrier, which would then be post-tensioned with steel rods anchored unto the underside of the bridge deck. The Duchesneau et al (2011). design left a hollowed out recess into the base of the precast barrier, which would then be positioned above the anchor bars cast into the bridge slab and injected with an appropriate cementitious material to secure the barrier to the slab (Figure 3-2b). The connection design of Duchesneau et al (2011). was selected for this project, because of its simplicity, efficiency, and similarity to the well-established cast-in-place barrier slab connection.

`

Using precast barriers limits the length to transfer impact loads from the barrier to the slab and increases the stress concentrations in the anchor bars and slab reinforcement. to attenuate this effect, the length of the bridge barrier can be increased or a longitudinal connection between barriers can be added to increase the effective load-transfer length. The experimental study described in this paper compares the performance of a continuous 6 m cast-in-place barrier against two different HPFRC precast barrier configurations – each using three adjacent 2 m barriers, however one with and one without barrier-to-barrier shear connections. The barriers in all three configurations are supported on a slab overhang selected to be representative of realistic bridge deck connection and load transfer conditions. The principal objectives for this study were to evaluate the effect of using precast barriers on the structural behaviour and durability of the bridge deck overhang during equivalent static loading and to design a simple and effective longitudinal shear connection between barriers.

3.2 Experimental Program

3.2.1 Design Criteria

The precast barriers were designed for the PL-2 barrier performance level criteria according to Canadian regulations (CSA 2006), or the TL-4 barrier test level in AAHSTO (2010). The minimum transverse, longitudinal, and vertical factored static loads to be resisted by the anchors and slab are shown in Table 3-1.

Table 3-1: AASHTO 2010 and CSA 2006 Design Criteria for TL-4/PL-2 Barriers

Force Direction	AASHTO 2010 TL-4	CSA 2006 PL-2
Transverse	240 kN	170 kN
Longitudinal	80 kN	51 kN
Vertical	80 kN	51 kN

The AASHTO and CSA design loads were both calculated as static equivalent loads of the maximum crash test forces for the respective performance (test) level. However, the CSA considers the 40% increase in structural resistance observed during dynamic vehicle impacts when calculating the static equivalent loads while the AASHTO does not. This explains the 40%

`

difference between the AASHTO and CSA transverse impact load. The minimum transversal resistance necessary for the PL-2 / TL-4 barriers is obtained by dividing the design force by the performance factor, considered as 0.75 for concrete barriers, which gives 320 kN and 227 kN for the AASHTO (2010) and CSA (2006), respectively.

3.2.2 Preliminary Nonlinear Finite Element Evaluation

A preliminary evaluation with NLFE software, ATENA 3D 4.1.4a (Cervenka 2011), was done to establish the details of the experimental configuration. The initial study evaluated the boundary and loading conditions (model length, overhang span, slab support type, truck wheel loads) and the barrier configuration (the length of the loaded barrier and the connection between precast barriers). The full report of this study can be found in Namy (2012).

The study indicated that a significant bridge deck model length was necessary to limit size effects, and a 6 m long specimen was selected as a reasonable compromise between the necessary length and practical limitations for a controlled laboratory experiment. Consideration of slab overhang span of 0.9 up to 1.8 m indicated that a 1.0 m slab overhang length was a critical length and is representative of typical bridges. A 1.0 metre wide concrete support block was selected to recreate the rigid slab and beam interface typical of stiff prestressed concrete bridge beams. Decreased torsional or flexural restraining conditions, more representative of actual bridge deck and exterior beam restraints, were shown to be less critical than the selected rigid conditions.

The barrier continuity was the independent variable between laboratory tests because the NLFE study highlighted the significance of barrier continuity on the load transfer length and structural performance. The three barrier configurations described in Table 3-2 were tested.

Table 3-2: Laboratory Test Configurations

Laboratory Test	Barrier Type	Longitudinal Continuity
Configuration 1	One 6-m long cast-in-place (reference) barrier	Full
Configuration 2	Three 2-m long precast barriers	None
Configuration 3	Three 2-m long precast barriers with shear key connection	Partial

`

3.2.3 Design of Laboratory Specimens

Figure 3-1 presents the basic configuration of the laboratory tests and the instrumentation installed on the specimens.

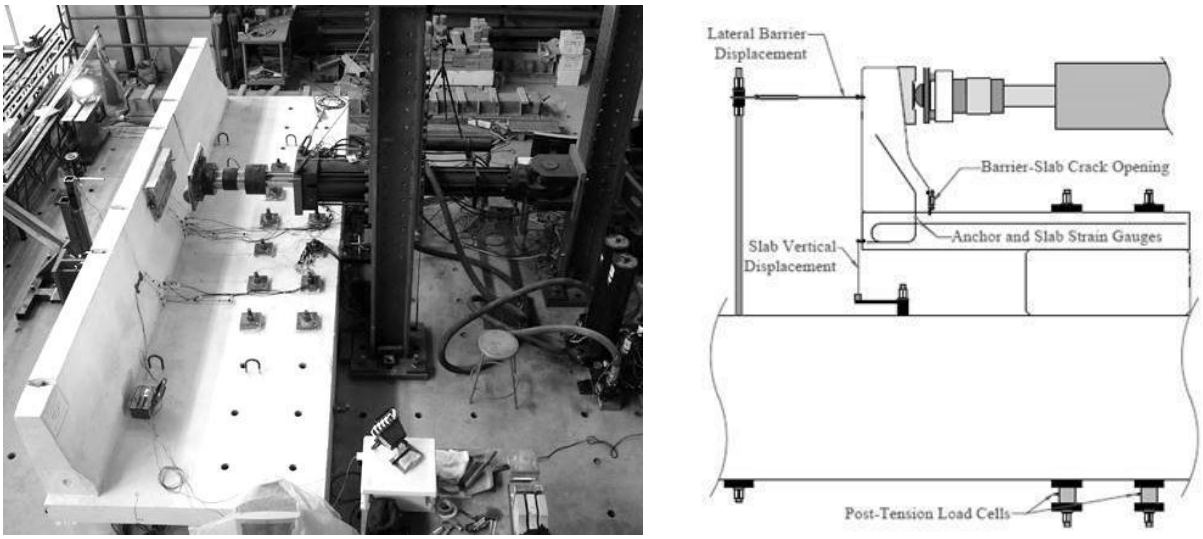

a) Overhead View b) Instrumentation, Elevation View

Figure 3-1: Experimental Setup

The support block had to be robust and maintain its integrity for all three lab tests, and therefore a HPFRC 70 MPa concrete mix with 1.5%-Vol fibres (30 mm length and 0.5 mm diameter) was used for its fabrication. The three deck slabs were fabricated using the match-cast technique with the support block to ensure a proper connection. High strength post-tensioned bars clamped the deck slab to the support block to laboratory strong floor.

The three slabs were identical and their reinforcement details were determined for a 1.0 m long deck slab cantilever according to the CSA (2006) and MTQ (2010) specifications. The slabs were each 225 mm in depth and 2 m wide. The top transverse reinforcement consisted of 20M bars every 150 mm c/c and the bottom transverse reinforcement of 15M bars every 150 mm c/c with 60 mm and 35 mm of top and bottom cover, respectively. Hooked ends (180º) were added to the transversal slab reinforcement to avoid local shear failure in the disturbed area of load transfer below the barrier. Longitudinal top and bottom reinforcement consisted of 15 M bars at 300 mm c/c.

The MTQ Type 201 F shaped barrier design and anchorage method (MTQ 2010) were used for the cast-in-place option, and the anchorage system developed by Duchesneau et al. (2011) was

`

used for the precast barriers. The precast barriers were also F shaped, but made from HPFRC 70 MPa with 1.5%-Vol fibres. The precast barriers had a transverse section reduced by 10% from the Type 201 barrier, and 60% less steel reinforcement was used (15M at 500 mm c/c as opposed to 200 mm c/c).

An effective shear key was a crucial design component for Test Configuration 3 (Table 3-2). It consisted of a trapezoidal recess boxed out from the ends of the barriers (Figure 3-2c). The recess descends from the top to the bottom of the barrier forming a hexagonal void when the precast barriers are placed side-by-side. This design was easily integrated into the assembly of the precast barriers, and the shear keys can be filled with the same material and at the same time as the recess between the barrier and slab.

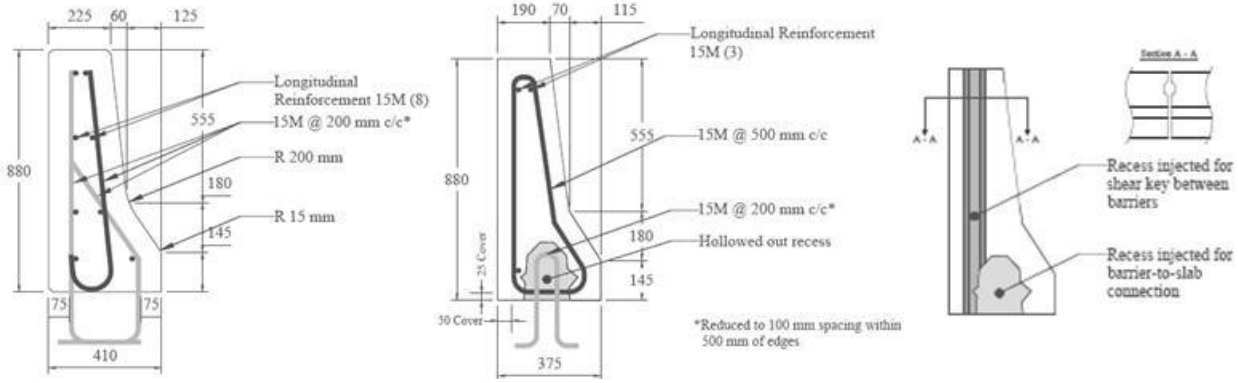

a) MTQ Type 201 Cast-in-place Barrier

b) Precast Barrier developed by Duchesneau et al (2011)

c) Shear Key

Figure 3-2: Barrier Sections

3.2.4 Experimental Conditions

Table 3-3 lists the mechanical properties of the concretes in each specimen. Grade 400W steel was used for all reinforcement throughout the project. Due to the large production scale and potentially other factors, such as a different cement quarry source, unexpectedly large amounts of air were found in the HPFRC's used for the precast barriers. The precast barriers' compressive and tensile strength (f'_c and f_t) were significantly lower than their design values.

During the pour of the cast-in-place MTQ Type 201 barrier, the formwork was not rigid enough and deformed due to the pumping energy and static concrete pressure. The barrier ended up having a transverse section width approximately 10% larger than designed. The effect of the

`

enlarged barrier section and unexpected concrete properties are examined in Section 3.3.4 of this article.

Table 3-3: Specimen Concrete Mechanical Properties

Specimen	Cast-in-place Barrier & Slabs[1]	Support Block	Precast Barriers[2]	Precast Barrier[3]	Injected Mortar[1]
Material (MPa)	HPC 35	HPFRC 70	HPFRC 70	HPFRC 70	FRM 50
f'_c (MPa)	54.4	70.1	47.8	59.2	50.2
f_t (MPa)	3.0[4]	5.7	3.1	3.0	3.3
E_c (MPa)	36300	24380	25800	35800	22700
υ	0.24	--	0.24	0.28	0.21

[1.] Average [2.] Test configuration 2 [3.] Test configuration 3 [4.] Calculated from CSA (2006)

3.2.5 Experimental Setup

The slab overhang and bridge barrier were anchored to the support block and laboratory strong floor with 12 to 16 high strength steel bars tensioned at 350 kN (Figure 3-1). For the precast barrier installation, the barrier/barrier and barrier/slab joints were all sealed and the hollowed out recess and shear recess (Configuration 3 only) were injected with a fibre reinforced mortar (FRM-1% Vol Fibre). The FRM mix contained steel fibres (10 mm length and 0.2 mm diameter), a shrinkage reducing admixture, and a water-reducing admixture. The added components were to ensure the mix had the proper fresh and hardened state properties for injection and strength.

The applied quasi static load was displacement controlled with a 1000 kN capacity hydraulic actuator at a rate of 0.6 mm/min. Once the structure reached its ultimate capacity, the displacement speed was increased to 1.2 mm/min. The actuator was pinned at its extremity and supported by a counterweight swing. The swing mechanism counterbalanced the weight of the actuator, reducing forces perpendicular to the actuator piston during loading.

A loading plate made from ultra-high performance fibre reinforced concrete (UHPFRC) was fastened to the barrier using drop-in anchors to precisely control the load application height, 700 mm from slab grade (CSA 2006), and surface, 350x700 mm^2 (AASHTO 1989). The contact between the actuator and UHPFRC load plate was done with a high-performance (f_y = 800 MPa) half steel cylinder with a 76.2 mm radius of curvature and a thin steel plate (f_y = 400 MPa) was used to increase the bearing resistance at load transfer.

`

To quantify the structural behaviour during loading, each bridge deck had several displacement potentiometers, strain gauges, and load cells instrumented at a 5 Hz reading frequency (Figure 3-1).

3.3 Results and Analysis

3.3.1 Strength, Failure, and Ductility

Table 3-4 summarises the results for the three different bridge deck configurations. In Figure 3-3 the applied load is plotted against the lateral barrier displacement and the vertical slab displacement. The minimal static strength from the CSA (2006) is indicated with a dotted line. During each test, the structure was inspected at 50 kN intervals of strength increase and at peak strength to evaluate the damage on the slab and barrier. Drops in applied load seen in the graphs at these intervals are due to the relaxation of the structure during the inspections.

The reference Test Configuration 1, with a cast-in-place barrier, remained linear-elastic until an applied load of 70 kN. After, the stiffness began to diminish as cracks coalesced within the slab overhang. The post-cracking rigidity remained constant between 150 kN and 460 kN, and then began to decrease. The structure entered the yielding phase at 500 kN, and shear cracks were also observed on the back side of the barrier at this load. The peak load was reached at 527 kN. The structure then began losing strength and failed dramatically in punching shear. The failure was very fragile as the load dropped suddenly to 240 kN. The ratio of lateral barrier displacement at 250 kN yield strength to peak strength was 1.4.

Test Configuration 2, with discontinuous precast barriers, remained linear-elastic until an applied load of 90 kN. The initial and post-cracking rigidity were very similar to Configuration 1 until the structure began yielding at 220 kN. The failure mode was in flexure due to the overturning transverse moment. The failure was ductile, and the ratio of lateral barrier displacement at 250 kN yield strength to peak strength was 1.9.

Test Configuration 3, with shear connections between precast barriers, remained linear-elastic until an applied load of 90 kN. The initial and post-cracking rigidities were also very similar to Configuration 1 until the structure began yielding at 375 kN. The onset of yielding coincided with the formation of shear cracks in the two exterior barriers adjacent to the loaded barrier. The shear cracks were controlled only with steel fibres, and by 400 kN the shear cracks reached the

`

back face of the exterior barriers and began opening. As the cracks opened the connection between the barriers was lost, restricting the load transfer length between barrier and slab to the 2 m length of the loaded precast barrier itself. The structure reached a peak force of 404 kN before failing in flexure in much the same way as Configuration 2. The failure was ductile and the displacement at 250 kN yield strength to peak strength displacement ratio was 2.7.

Table 3-4: Experimental Results Summary

Configuration	1 (reference)	2	3
Linear-elastic, kN	0 – 70	0 – 90	0 – 90
Yield onset, kN	500	220	375
Peak load, kN	527	296	404
Failure mode	Punching Shear	Flexure	Shear and Flexure

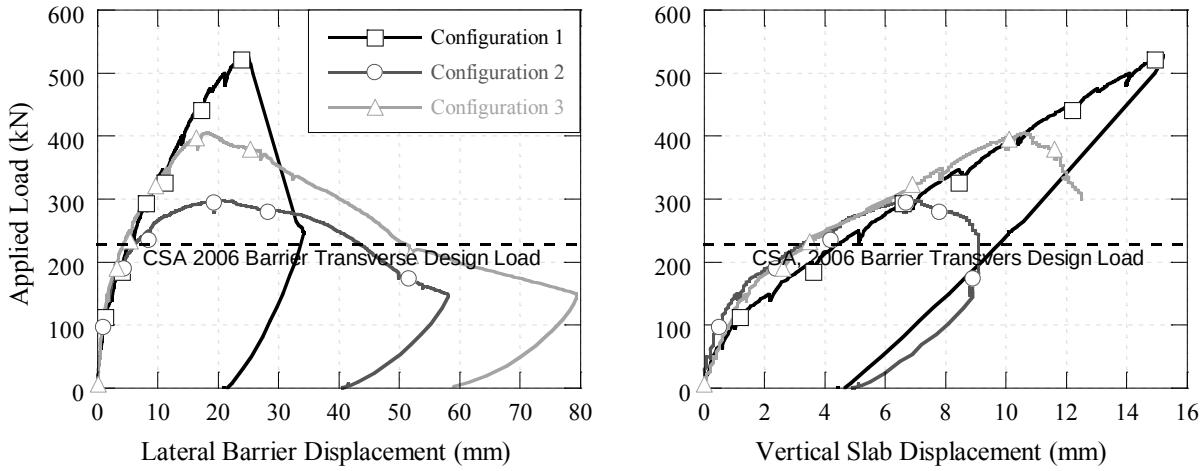

Figure 3-3: Lateral Barrier and Vertical Slab Displacements

3.3.2 Slab Barrier Interaction

In Figure 3-4 the applied load is plotted against the opening width at the edge of the barrier-slab interface.

The opening was caused by the formation and growth of a crack at the cold-joint, and is controlled by the tensile and cohesive properties of the contact surface and the anchor bars crossing the crack plane. The opening at peak load was 2.5 mm for Configurations 1 and 3 and 5 mm for Configuration 2. For Configuration 1, the opening width decreased as the structure failed,

`

whereas the opening grew to nearly 20 mm in Configurations 2 and 3. The difference in post-peak behaviour is related to the failure mode of the respective configurations.

The barrier-slab interface was also closely monitored during each test. The crack opening at the interface was first observed in Configuration 1 at 250 kN over a 1.5 m length beneath the load application, and the crack grew to 5 m in length by 300 kN. In Configuration 2 the crack opening was first observed at 200 kN over the 2 m length of the loaded precast barrier. The crack width grew in magnitude as the test went on, however the crack length was logically confined to the loaded barrier. In Configuration 3 the crack opening was visible over a 2.5 m length at 250 kN, and by 350 kN was visible over entire barrier-slab 6 m length. The opening continued to increase until peak load and then grew mainly between the loaded barrier and slab, as in Configuration 2.

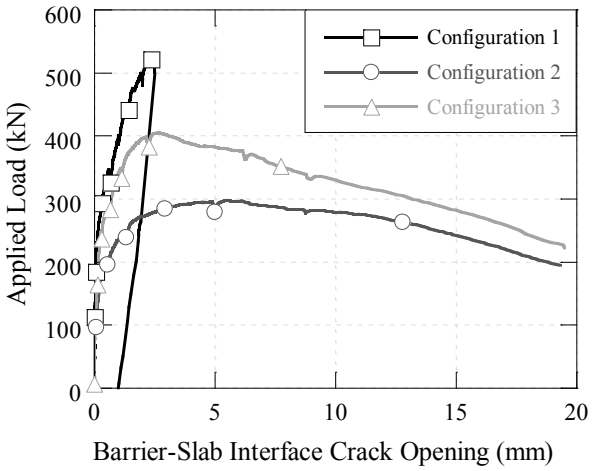

Figure 3-4: Barrier-Slab Interface Crack Opening Width

3.3.3 Cracking Pattern

Figure 3-5 provides a virtual reconstruction of the damage in each structure at 250 kN and ultimate load.

The crack formation and growth within the slabs was very similar for all three test configurations. The first visual cracking occurred in the slab overhang at 150 kN. Between 150 and 250 kN cracks formed and developed, running longitudinally in the overhang region (perpendicular to loading) and reached the edges around 250 kN or 300 kN. They then began to join one another and form a webbed crack pattern.

`

The crack patterns in the barriers varied depending on the test configuration. In Configuration 1, vertical cracks first formed on the back face of the cast-in-place barrier at 250 kN due to longitudinal curvature. The front face of the barrier started cracking around 300 kN, and by 350 kN the front face of the barrier was cracked along diagonal rupture lines due to the double curvature (longitudinal and transverse) of the barrier. At 500 kN shear cracks became visible on the back side of the barrier, followed by the rupture cracks at 527 kN.

In Test Configuration 2, the precast barriers did not exhibit any damage due to longitudinal curvature throughout the test. At 250 kN, a longitudinal crack was found on the front face of the loaded precast barrier (at barrier slope break) due to the transverse overturning moment. The longitudinal crack ran the length of the barrier and continued to grow during yielding.

In Test Configuration 3, shear keys transferred the load from the loaded precast barrier to the exterior barriers. At 300 kN very small cracks were noticeable in the FRM at the two edges of the injected recess and at the top face of both shear keys. The cracks in the shear keys spread into the two exterior precast barriers at 350 kN and progressed to the back edge of the two exterior barriers by 400 kN. Also at 400 kN, the first signs of damage were visible on the loaded barrier as cracks opened on the back face due to longitudinal curvature. During structural yielding, a longitudinal crack became visible on the front face of the loaded barrier.

`

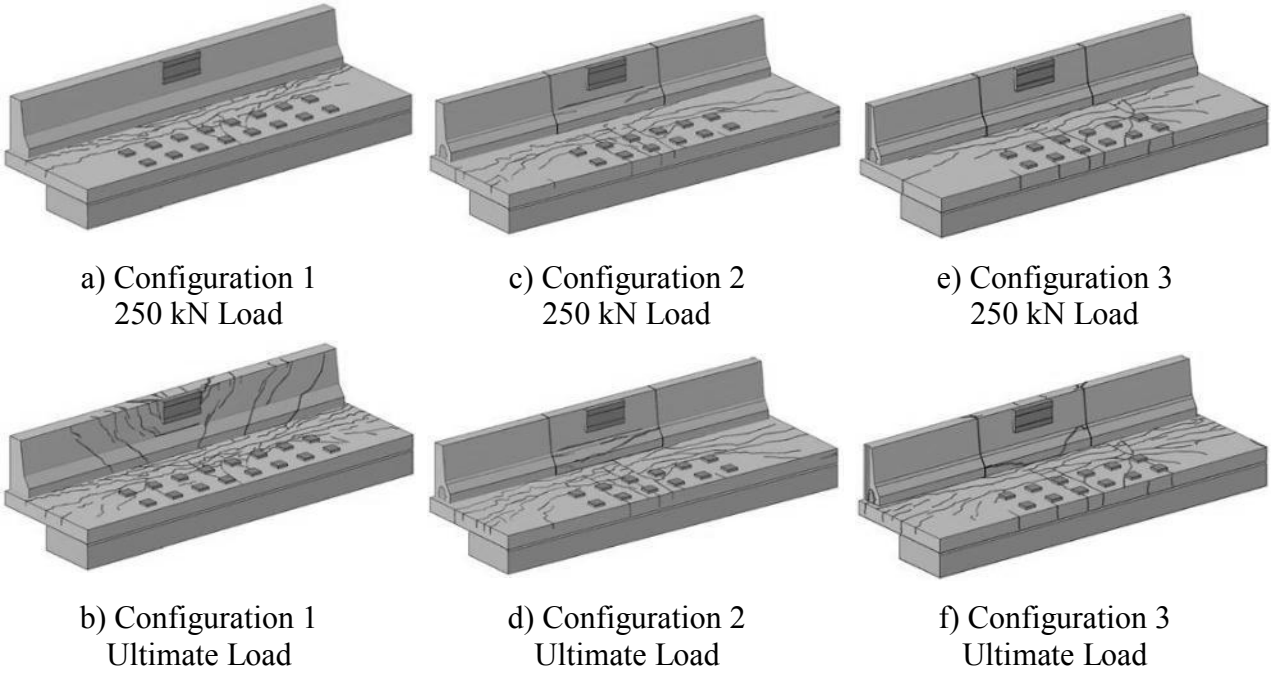

a) Configuration 1
250 kN Load

c) Configuration 2
250 kN Load

e) Configuration 3
250 kN Load

b) Configuration 1
Ultimate Load

d) Configuration 2
Ultimate Load

f) Configuration 3
Ultimate Load

Figure 3-5: Structural Damage at 250 kN and Ultimate Load

3.3.4 Strain in Reinforcing Bars

The anchor and slab reinforcement strain were measured locally at centre section with strain gauges installed directly on the vertical leg of an anchor bar – tensile strain caused by the moment couple between barrier and slab – and on the upper-row of a slab reinforcing bar – tensile strain caused by negative moment in the slab overhang (Figure 3-1). In Figure 3-6 the applied load is plotted against anchor strain and slab reinforcement strain for each configuration.

The measured strains in each test were similar at a given load until the onset of yielding in Configurations 2 and 3 at 250 kN and 400 kN respectively. The slight delay observed between structural and strain yielding (see Table 3-4) is likely due to the positioning of the strain gauges, which did not perfectly reflect the critical zones.

In Test Configuration 1 the post-cracking rate of strain change with respect to load remained generally constant for the entire test, and the anchor and slab reinforcement strain surpassed 2000 με. The strains measured in the anchor and slab reinforcement behaved similarly. In Test Configurations 2 and 3 the anchor strain reached 3300 με and 2200 με, respectively, which indicate that the anchor bars were yielding.

`

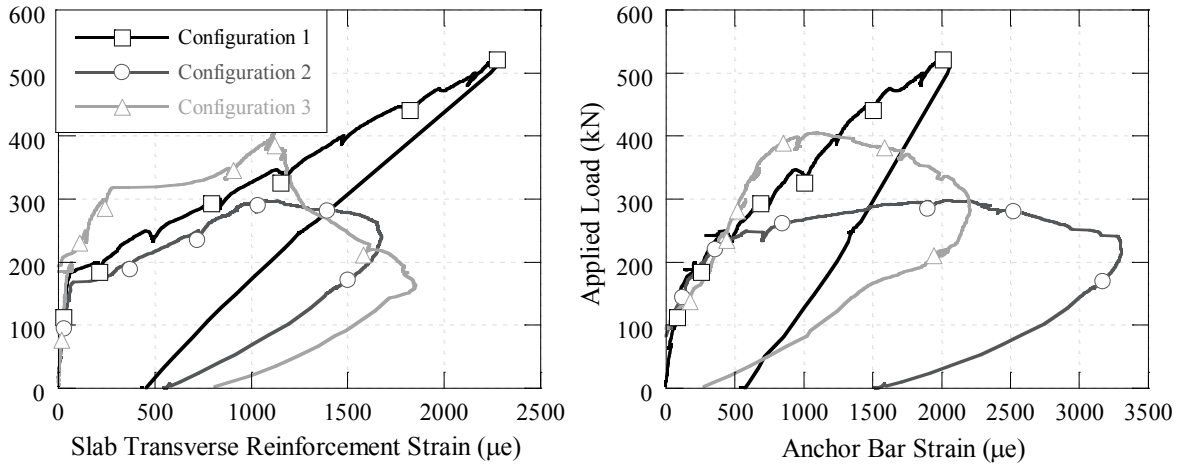

Figure 3-6: Slab Transverse Reinforcement and Anchor Bar Strain

3.3.5 Numerical Correction to Fabrication Errors

As discussed in Section 3.2.4, problems encountered during specimen fabrication modified the geometric and mechanical properties of certain specimens from the design specifications. A numerical correction was performed with finite element software to account for the construction errors.

Table 3-5 below summarises the fabrication errors and their effect on the structural behaviour. The fabrication problems were advantageous to the structural behaviour of the cast-in-place barrier configuration, and were disadvantageous to both precast barrier configurations. Figure 3-7a shows the accurate reproduction of the as-built force displacement behaviour of each Configurations using NLFE, and Figure 3-7b shows the force displacement behaviour after numerically correcting the fabrication errors. The correction lowers the stiffness and ultimate strength for Configuration 1 and does the opposite for Configurations 2 and 3.

Table 3-5: Fabrication Problems and Consequences

Configuration	Problem	Design	As-Built	Implication
1 Cast-in-place	Increased Section	MTQ 201	+10 %	Increased resistance & stiffness
1 Cast-in-place	Barrier Concrete	35 MPa	59 MPa	Increased resistance & stiffness
2 Precast	Barrier HPFRC	70 MPa	48 MPa	Decreased resistance & stiffness
3 Precast with connection	Barrier HPFRC	70 MPa	59 MPa	Decreased resistance & stiffness

`

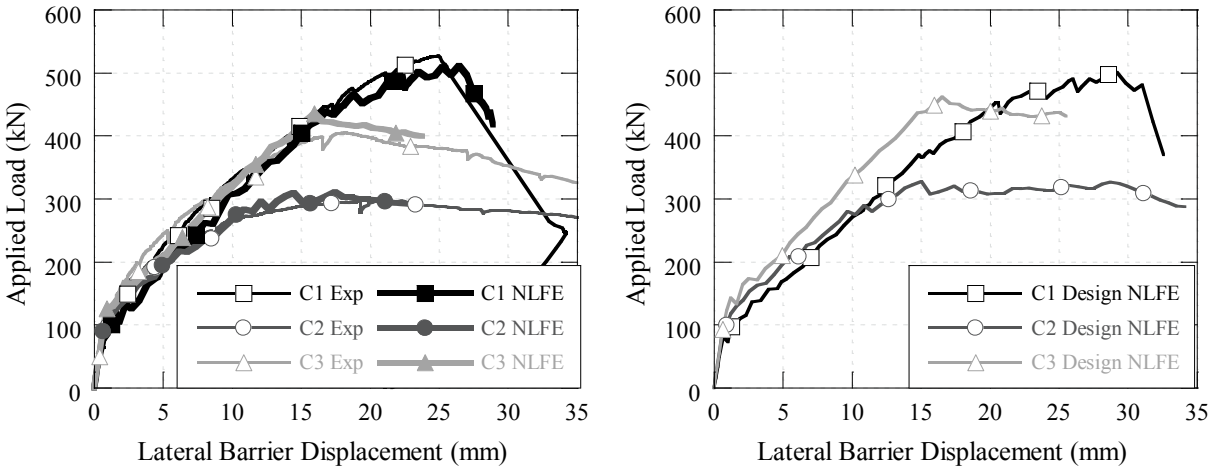

a) Experimental and NLFE Reproduction b) NLFE Correction to Fabrication Errors

Figure 3-7: Lateral Barrier Displacement, Experimental and NLFE Models

3.4 Discussion

This discussion focuses on the experimental results; however, it is important to consider the fabrication errors and the implications of the numerical correction presented in Figure 3-7b. The structural performance of the bridge decks with different barrier configurations imply several considerations for the behaviour, design, and use of precast bridge barriers.

The design criteria for the transverse static equivalent loads presented in Section 3.2.1 were 320 kN and 227 kN for the AASHTO 2010 and CSA 2006, respectively. Configurations 1 and 3 each exceeded these design criteria. Configuration 2 with an ultimate strength of 296 kN only met the CSA (2006) requirements. However, as noted previously, a 30-40% increase in barrier strength is expected during dynamic loading (Aminmansour 2004, CSA 2006, Mitchell et al. 2006). Furthermore the static strength of NLFE correction for Configuration 2 is 328 kN and meets the AASHTO (2010) requirements. Therefore the static-strengths of the three design configurations can be considered to meet the design criteria from the Canadian and American bridge codes.

The results clearly indicate that the continuous barrier configurations used almost the entire 6 m length to transfer the applied load from the barrier to the slab. In Configurations 1 and 3, the crack opening at the barrier-slab interface ran nearly the entire 6 m length, whereas the opening was confined to 2 m for Configuration 2. The difference in the length of load transfer explains the reduced load carrying capacity for Configuration 2, and Configuration 3 once the shear connections failed. The structural behaviour of Test Configuration 3 was almost identical, or even

`

superior, to Configuration 1 until the connections began failing at 375 kN (Figure 3-3) or 460 kN in the numerically corrected NLFE model (Figure 3-7b). The length of barrier to slab load transfer means that an effective connection between precast barriers is necessary to provide adequate barrier longitudinal continuity and optimize the mechanical performance of the bridge deck. In light of this point, the remaining discussion will focus on the results for Test Configurations 1 and 3.

Test Configuration 1 had a punching failure in the barrier characterized with a sudden loss of load-carry capacity (Figure 3-3). Test Configuration 3 had a two-phase failure. The initial failure occurred in shear in the barriers adjacent to the loaded barrier near the connections, the load path was then redistributed and the failure mode shifted to flexure as the anchors became critical. Considering that the strength of both Test Configurations 1 and 3 far exceed the PL-2/TL-4 requirements, the failure mode of Test Configuration 3 is considerably more ductile and preferable from a structural design viewpoint since more energy is dissipated during failure. The failure of both configurations occurs in the barriers, which follows the hierarchy concept implicit in the CSA (2006) and AASHTO (2010). The hierarchy concept is that the anchors and slab should be designed to resist the ultimate strength of the barrier. The shear connections controlled the ultimate strength for Test Configuration 3, and therefore should not be designed to exceed the capacity of the anchors or slab.

A secondary research objective was to evaluate if the mechanics of bridge decks using precast barriers instead of cast-in-place barriers might be detrimental to overall durability, and particularly that of the slab overhang. The slab overhang behaviour – displacement, crack growth, and crack openings – was similar for all three test configurations (Figure 3-5). Initial cracking within the overhang is inevitable because of the much smaller lever arm for the internal resisting moment between the slab and the F shaped barriers. The results indicate that the slab durability will not be adversely affected using precast bridge barriers. The crack opening at the barrier-slab interface also affects the bridge deck durability. This interface is a potential site for water ingress and corrosion of anchor reinforcement. The barrier-slab interface behaviour of Configurations 1 and 3 superposed until the applied load reached 310 kN during testing, which represents a very rare and extreme impact condition for these bridge barriers (MASH 2009, Jiang et al 2004), and service-life impacts are not expected to reach this force level. Therefore, precast barriers with connections do not have an increased risk of water penetration at the barrier-slab interface.

`

The quasi-static loading behaviour and failure mode for rigid concrete bridge barriers has been shown to be representative of dynamic loading as well (Aminmansour 2004, Charron et al. 2011, Mitchell et al. 2006). Therefore comparing the static behaviour of precast barrier Configuration 3 against that of the crash tested cast-in-place barrier Configuration 1 provides insight into the potential crash test performance for the precast barriers. The force displacement (vertical and horizontal) relationship of the two configurations was very similar until the applied load exceeded 375 kN during testing. Considering that the frontal geometry of the barriers is identical and that 375 kN exceeds the expected impact force, it is logical that the vehicle-barrier impact behaviour should be very similar during crash tests. There was also no visually discernible relative displacement between precast barriers of Test Configuration 3 until the shear cracks in the exterior barriers began opening at 400 kN of applied load in the tests. Thus, the edges of the precast barriers are highly unlikely to cause vehicle snag during a crash test. The results indicate that the precast barriers with lateral shear connections would have the same vehicle-barrier crash test performance as the MTQ Type 201 cast-in-place barriers.

The numerical study performed to address the fabrication errors suggests that the design behaviour of Configuration 3 would have nearly an equivalent strength and stiffness, and superior energy dissipating capacity as Configuration 1 (Figure 3-7b). This correction was performed using NLFE models that very accurately simulated the experimental results with the as-built properties.

Furthermore, a numerical study performed to address the size effect of the precast barrier length performed in Namy (2012) suggests that many of the differences observed in this experimental program would be less discernible when 4 m precast barriers are used. The strength performance of the three Test Configurations would be largely equivalent, within 10%, as well as the structural stiffness and cracking behaviour. The importance of adding shear keys to connect the precast barriers would therefore be diminished. The keys help maintain a uniform displacement between precast barrier edges up to a static load of 400 kN, which could be key to successfully crash testing of the precast barriers.

3.5 Conclusions

The objectives for this research project were to evaluate the structural performance and durability of the bridge deck overhang during quasi-static loading with cast-in-place and precast barrier

`

configurations, and to design a simple and effective shear connection compatible with the precast barriers. The following conclusions can be drawn from the analysis of the experimental and numerical results:

- The ultimate strength of all three bridge deck configurations with cast-in-place and precast barriers built to the design specifications exceed the design criteria specified in the CSA 2006 and AASHTO 2010;
- Longitudinal barrier continuity is necessary to provide an appropriate barrier to slab load transfer length and maximize the structural performance of the bridge deck;
- The shear keys, forming a hexagonal recess at the ends of the precast barriers, filled with a cementitious composite during installation provide adequate longitudinal continuity;
- The bridge deck using precast barriers with shear keys had an ideal failure mode and maintained a preferable failure hierarchy (CSA 2006, AASHTO 2010) ;
- Durability of the bridge deck should not be adversely affected when using precast barriers with adequate longitudinal continuity;
- The bridge deck behaviour during static loads indicate that the vehicle-barrier interaction during crash testing would be very similar with either the MTQ Type 201 cast-in-place barrier or the precast barrier developed by Duchesneau et al. (2011) with shear keys.
- The numerical correction demonstrates that the precast barriers installed with lateral shear connections provide comparable mechanical performance to the cast-in-place barrier reference configuration.

The precast barrier developed by Duchesneau et al. (2011) with shear keys are made of a more durable concrete material and present a similar strength, displacement behaviour, and geometry to the MTQ Type 201 F shaped barrier. In consequence, these precast barriers meet the stipulations of the CSA (2006) for modifying existing barrier designs. It is very likely that precast barriers with shear connections would successfully pass PL2 / TL 4 crash tests. The industrial use of these precast barriers should be strongly considered given the improved durability of the HPFRC barrier, the advantages of precasting, and the mechanical performance.

`

3.6 References

AASHTO. (1989) Guide Specifications for Bridge Railings. American Association of State and Highway Transportation Officials. Washington, D.C., U.S.A.

AASHTO. (2010) Load Resistance Factor Design (LRFD) Bridge Design Specifications. American Association of State and Highway Transportation Officials. Washington, D.C., U.S.A.

Aminmansour, M. (2004). Performance characteristics of precast and reinforced concrete bridge barriers subjected to static and impact loads. Ph.D. Thesis. The Pennsylvania State University, Altoona, PA, U.S.A.

Charron, J-P., Niamba, E., Massicotte, B. (2011). Static and dynamic behaviour of high- and ultrahigh-performance fibre-reinforced concrete precast bridge parapets. ASCE Journal of Bridge Engineering, Vol 16, Issue 3, pp. 413-421.

CSA-S6-06. (2006) Canadian Highway Bridge Design Code (CHBDC). CSA International. Toronto, Canada.

Cervenka, V., Jendele, L., and Cervenka, J. 2011. ATENA Program documentation. Cervenka Consulting Ltd. Prague, Czech Republic.

Cusson, D., Repette, W. (2000). Early-Age Cracking in Reconstructed Concrete Bridge Barrier Walls. ACI Materials Journal, Vol 97, No 4, pp. 438-446.

Desmettre, C., Charron, J-P. (2012). Water permeability of reinforced concrete with and without fibre subjected to static and constant tensile loading. Cement and Concrete Research, Vol 42, Issue 7, pp. 945-952.

Duchesneau, F., Charron, J-P., Massicotte, B. (2011). Monolithic and hybrid precast bridge barriers in high and ultra-high performance fibre reinforced concretes. Canadian Journal of Civil Engineering, Vol 38, No 8, pp. 859-869.

Haluk, A., Attanayaka, U. (2004). Causes and cures for cracking of concrete barriers (Research Report No RC-1448). Wayne State University, Detroit, MI, U.S.A.

Jiang, T., Grzebieta, R.H., Zhaor, X.L. (2004). Predicting impact loads of a car crashing into a concrete roadside safety barrier. International Journal of Crashworthiness, Vol 9, No 1, pp. 45-63.

`

MASH. (2009). Manual for Assessing Safety Hardware. American Association of State Highway and Transportation Officials. Washington, D.C., U.S.A.

MTQ Normes, Tome III (2010). Normes – Ouvrages d'Art Tome III. Ministère des Transport du Québec. Québec, QC, CA.

Mitchell, G., Tolnai, M., Gokani, V., Picòn, R., Yang, S., Klingner, R.E. (2006). Design of Retrofit Vehicular Barriers using Mechanical Anchors (Report No 4823-1F). University of Texas at Austin, TX, U.S.A.

Namy, M. (2012). Structural behaviour of cast-in-place and precast concrete barriers anchored to bridge deck overhangs and subjected to transverse static loading. M.Sc. Thesis. Polytechnique Montréal, Montréal, CA.

Niamba, É. (2009). Development of precast bridge barriers using high performance fibre reinforced concrete's (Développement de barrières préfabriqués en bétons renforcés de fibres pour les ponts). M.Sc. Thesis. Polytechnique Montréal, Montréal, CA.

`

CHAPTER 4 ARTICLE 2: "NUMERICAL STUDY OF CAST-IN-PLACE AND PRECAST CONCRETE BARRIERS FOR BRIDGE DECKS."

Abstract

Nonlinear Finite element (NLFE) calculations were performed to reproduce the mechanical behaviour of concrete barriers anchored to bridge deck overhangs and submitted to static transverse loading by Namy (2012). The behaviour of the three different barrier configurations – a normal concrete cast-in-place barrier, high performance fibre reinforced concrete (HPFRC) precast barriers, and HPFRC precast barriers with barrier-to-barrier connections – anchored to slab overhangs were accurately simulated with the NLFE models. The validated NLFE models were then used to investigate the impact of the fibre orientation in the HPFRC precast barriers, the effect of the precast barrier length, the eccentric load application, and the utilisation of a HPFRC slab overhang. The fibre orientation of the HPFRC precast barriers was shown to be well oriented to resist the applied overturning moment but not the shear loads at the barrier-to-barrier connections. The effect of using smaller 2 m model precast barriers instead of the 4 m expected industrial length significantly reduced the structural load-carry capacity. The precast barrier length was as critical to the structural performance as the application of an eccentric load. The HPFRC slab allowed the reduction of crack spacing and crack opening widths, and increased the rigidity and load-carry capacity of the bridge deck overhang.

4.1 Introduction

Bridge barriers are used to protect vehicle occupants during off-road bridge accidents. Their primary functions are to contain vehicles, and redirect them back onto the roadway or stop them within an acceptable distance (MASH 2009, CSA 2006). Cast-in-place concrete barriers have proven through crash-testing and in-field evaluations that they meet these structural requirements. However, they are prone to early-age cracking due to a combination of shrinkage and thermal dilations (Cusson & Repette, 2000). The early-age cracks immediately expose barriers to water ingress increasing the risk of corrosion from chlorides and damage from freeze-thaw cycles, and have been observed to accelerate the deterioration processes requiring premature and expensive bridge repairs (Haluk & Attanayaka, 2004).

`

Polytechnique Montreal has been developing precast bridge barriers to solve the durability problems encountered with cast-in-place reinforced concrete bridge barriers. The proposed barriers are precast with a high performance steel fibre reinforced concrete (HPFRC). Precasting provides a higher standard of fabrication quality, and will not restrain early-age barrier movement. The HPFRC also offers enhanced durability and mechanical properties. The matrix microstructure is denser than normal concrete and the steel fibres limit crack opening widths (Desmettre and Charron, 2012). In addition, the reduced installation time of the precast barriers provides important savings to time related costs.

Many precast barriers have been developed and introduced in the literature (Aminmansour 2004; Duchesneau 2010; Jeon et al., 2011; Mitchell et al., 2006; Niamba 2009), however the large-scale performance of the bridge deck overhang has not been adequately evaluated and compared with their cast-in-place barrier counterparts. Jeon (2011) tested 6 m bridge deck overhangs; however, the research objective was to formulate yield line formulas to calculate the ultimate strength of precast barriers. The governing American and Canadian bridge codes (AASHTO LRFD 2010, CSA 2006) both implicitly provide a failure hierarchy as the slab overhang and anchors are designed to resist the ultimate barrier strength. It is therefore necessary to evaluate the performance of the entire deck overhang structure at a large-scale to identify how barrier continuity or precast barrier lengths affect the failure hierarchy. An evaluation of the slab overhang damage during barrier loading is also important to optimize the slab design, the barrier-slab connection, and ultimately improve the durability of the slab overhang.

This study presents a numerical investigation of the experimental tests performed in Namy (2012) comparing the structural behaviour of bridge deck overhangs during static loading with cast-in-place and precast barriers. The experimental behaviour was reproduced numerically using nonlinear finite element (NLFE) analysis software. The numerical models were then used to gather more information about the bridge deck overhang behaviour and optimize the design of the barriers and slab.

4.2 Research Significance

The overall behaviour of bridge deck overhangs has not been adequately investigated in the literature, particularly when precast barriers and utilisation of fibre reinforced concrete is considered. The barrier continuity – barrier length and barrier-to-barrier connections –

`

significantly affect the structural behaviour. This study evaluates these design parameters, with NLFE models validated on full-size bridge decks tested in laboratory, and quantifies their effect to propose design recommendations.

4.3 Experimental Program

The experiments in Namy (2012) consisted of a 6.2 m long by 2.0 m wide slab with 1 m overhang. The slab was representative of short bridge deck overhangs, and was clamped onto a 1 m wide, 6.2 m long, and 0.4 m high concrete block representing a torsionally stiff girder. The slab and block were anchored to the laboratory strong floor with post-tensioned high strength steel bars tensioned to 350 kN. The barriers were loaded in the transverse direction at the structure mid-length (centre) in quasi-static controlled displacement. The load was applied 700 mm above the slab (CSA 2006). Figure 4-1a provides an overhead view of the general laboratory configuration. Figure 4-1b shows an elevation view of the instrumentation used to quantify the structural response during loading. The testing program is described in Table 4-1.

The barrier configuration was the variable under study. The MTQ Type 201 (MTQ 2004) cast-in-place barrier was used for Test Configuration 1 (Figure 4-2a), and the precast barriers developed by Duchesneau (2010) for Test Configurations 2 and 3 (Figure 4-2b). The barriers were all F shaped and designed for performance level 2 (PL-2), equivalent to AASHTO test level 4 (TL-4), stipulating a minimal factored design strength resisting the static transversal load of 227 kN (CSA 2006). The precast barriers were fabricated with a 70 MPa HPFRC with 1.5%-Vol steel fibres 30 mm length and 0.5 mm diameter. A shear key was added between precast barriers to increase longitudinal barrier continuity in Test Configuration 3 (Figure 4-2c). A fibre reinforced mortar (FRM) was used for the injected recesses.

Table 4-1: Laboratory Test Configurations

Laboratory Test	Barrier Type	Continuity
Configuration 1	One 6 m long cast-in-place barrier	Yes
Configuration 2	Three 2 m long discontinuous precast barriers	No
Configuration 3	Three 2 m long precast barriers with shear key connections	Yes

`

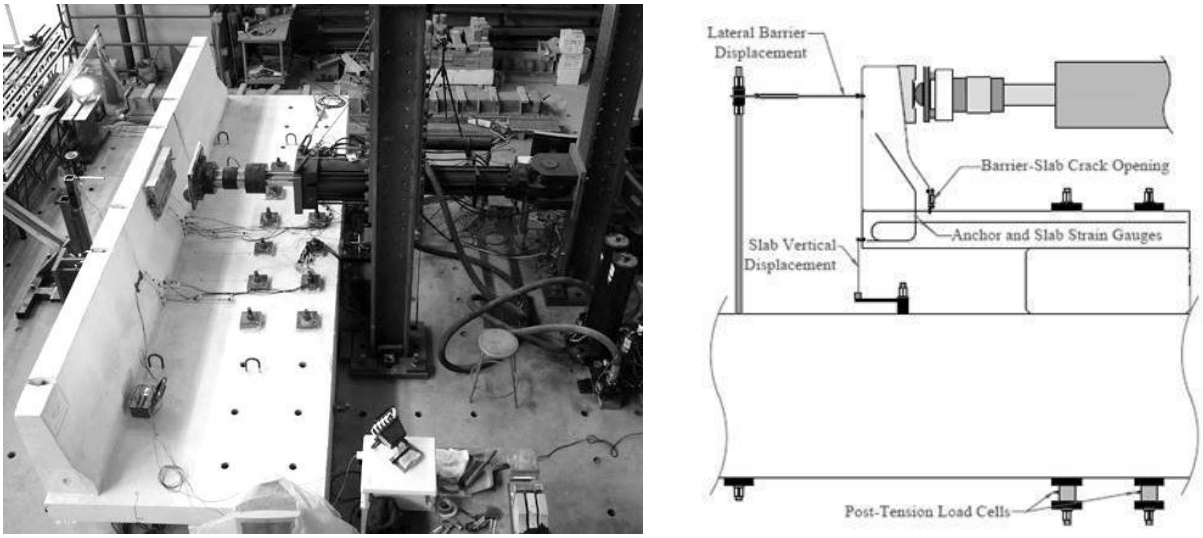

a) Overhead View b) Instrumentation, Elevation View

Figure 4-1: Experimental Setup

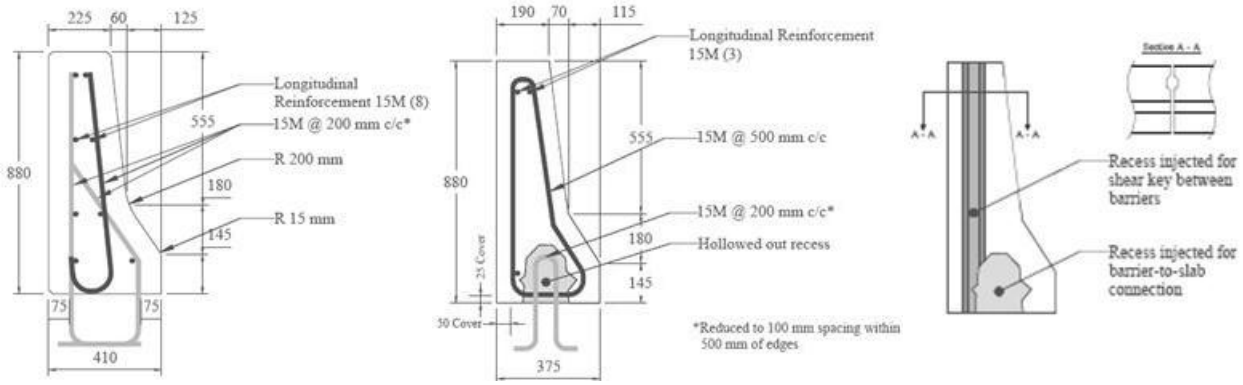

*Dimensions shown in mm (1 mm = 1/25.4 in)

a) MTQ Type 201 Cast-in-Place Barrier b) Precast Barrier developed by Duchesneau et al (2011) c) Shear Key

Figure 4-2: Barrier Configurations

4.4 Numerical Modeling

4.4.1 3D Finite Element Analysis Program

NLFE software, ATENA 3D (Cervenka et al. 2011), designed specifically for non-linear analysis of reinforced concrete structures, was used in this project. The *Nonlinear Cementitious* formulation can simulate the tensile and compressive behaviour of concrete, crack closure, and high confinement. Rankine failure criterion is used to determine the onset of fracture, $\sigma \leq f_t$, and crack band theory relates fracture energy, G_F, with fracture strain, ε_f, and crack opening width.

`

The software provides a *USER* formulation for concretes with very high fracture energy, such as a HPFRC's, and the experimentally defined strain-softening curve can be introduced into the material model. The concrete compressive hardening and softening behaviour is computed using the Menètrey-Willam (1995) failure surfaces. Strain decomposition is used to analyse the nonlinear fracture and compression strains separately.

4.4.2 3D Models

The finite elements used and their general properties are listed in Table 4-2. A labeled 3D representation of a numerical model is shown in Figure 4-3. More in-depth information about the 3D models is provided in Namy (2012).

A controlled displacement step was used to load the bridge decks, and the full Newton-Raphson iterative method to solve the structural response. The post-tensioning and loading equipment were physically entered into the numerical models in addition to the barrier(s), deck, and support block. The support and loading conditions were identical for all three models. The Bigaj (1999) bond-slip law was used to model reinforcement slip for the anchor bars where development length was inadequate. Brick finite elements were used where the structural geometry was compatible, otherwise tetrahedral elements were used. The mesh density varied depending on the structural component and was refined in areas of significant anticipated damage. Gap elements were used to model the behaviour of material interfaces. The gap element contact properties (Figure 4-3) were based off experimental data from Lessard (2009).

To properly model the structural response, the internal stresses due to restrained shrinkage and self-weight had to be accounted for. The ACI 209 (1992) formulas approximate 320 με shrinkage strain for the concrete type and ambient conditions during the 4 month delay between fabrication and testing. The shrinkage effects in the slabs and MTQ Type 201 barrier were not negligible, because of the reinforcement quantity and support conditions. ATENA's construction case feature was used to apply the shrinkage in a realistic sequence. The slab and support block were modeled in the first construction case in which the slab shrinkage and self-weight were considered. The barriers were incorporated into the NLFE model in the second construction case such that the slab shrinkage occurs before barrier installation onto the slab. The shrinkage of the cast-in-place barrier was considered, whereas the shrinkage of the precast barriers was not

`

modeled because they were not significantly reinforced and the shrinkage freely occurred before they were anchored to the slab.

Table 4-2: Finite Element Properties

Finite Element	Structural Component	Nodes	Integration Points	Interpolation Functions
3D Solid Brick	Block, Slab, Steel Plate	8	8	Linear
3D Solid Tetrahedral	Barriers, Bearing Plates, Load Bar and Plate	4	1	Linear
3D Truss Element	Reinforcement / Post-Tension Bars	2	1	Linear
3D Gap Elements	Interfaces and Joints	6 or 8	2	Linear

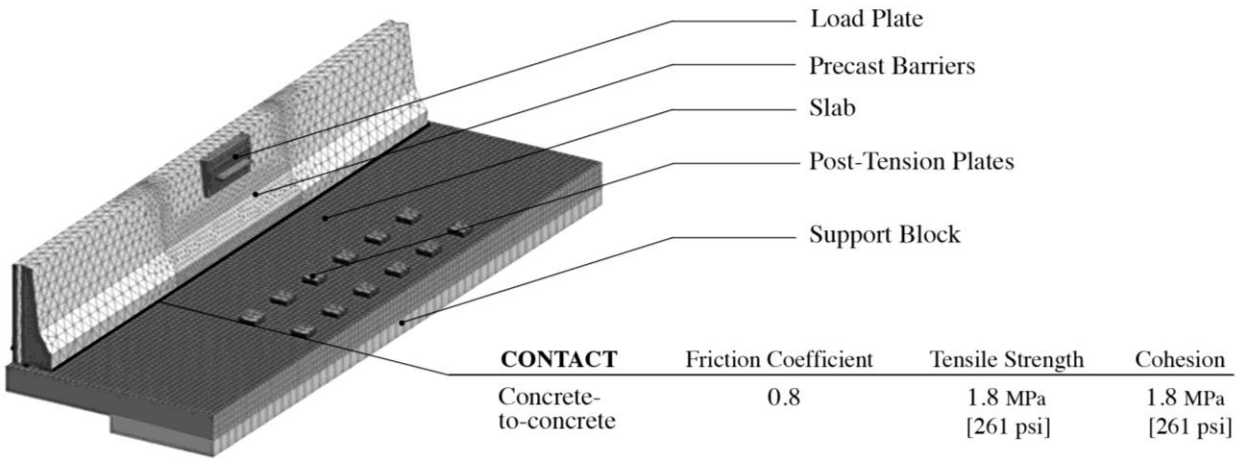

Figure 4-3: Numerical Model, Test Configuration 3 Precast Barriers with Connections

4.4.3 Model Input Properties

The mechanical properties of the concrete specimens were experimentally determined and are shown in Table 4-3. The fracture energy (G_F) suggested by the software user guide (Cervenka et al. 2011) and Hordijks (2009) strain-softening formula were used to compute the exponential softening form and critical crack opening width, w_0, for the normal concrete. The HPFRC and FRM both have very large fracture energy, and therefore the strain-softening behaviour of these materials was determined with tensile tests. The USER formulation was verified by using

`

ATENA to accurately reproduce the tensile tests (Delsol 2012). The uniaxial tensile behaviour for the different concrete's is shown in Figure 4-4.

Table 4-3: ATENA Fracture-Plastic Cementitious Material Properties

Concrete	E, MPa	υ	f_t, MPa	f'_c. MPa	G_F, N/mm
HPC[1]	34800	0.233	3.23	-52.2	0.074
HPFRC[1]	30000	0.259	3.03	-53.5	See Figure 4-4
FRM[1]	22800	0.210	3.14	-50.2	

[1]Average value used for above material properties

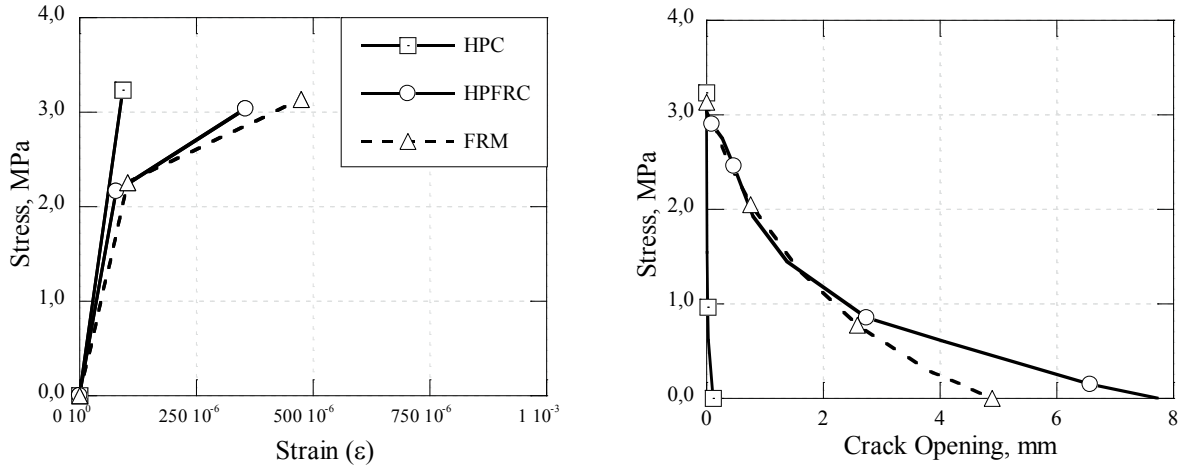

a) Pre-Peak Behaviour b) Post-Peak Behaviour

Figure 4-4: Measured Material Tensile Behaviour

4.4.4 Model Validation

The force-displacement relationships and cracking behaviour from the experimental and numerical results are compared in Figure 4-5 and Figure 4-6. The instrumentation shown in Figure 4-1b indicates that the lateral barrier displacement in Figure 4-5a and crack opening at the slab barrier interface in Figure 4-5b were recorded in line with the load application (actuator centre line). In the figures, C1, C2, and C3 refer to Test Configurations 1, 2, and 3, respectively, and Exp or Num are used to differentiate between experimental and numerical results. The results demonstrate that each deck overhang configuration exceeded the design strength of 227 kN required by the CSA (2006).

`

The close agreement between experimental and numerical stiffness, ultimate strength, cracking, and failure mode indicate that the NLFE software and modeling assumptions accurately simulate the reinforced concrete bridge deck overhang behaviour. The numerical results for Configuration 3 overestimate the ultimate strength observed experimentally. The increase in numerical strength is likely due to the fibre orientation of the HPFRC with respect to the failure plane, and is examined in Section 4.5.1.

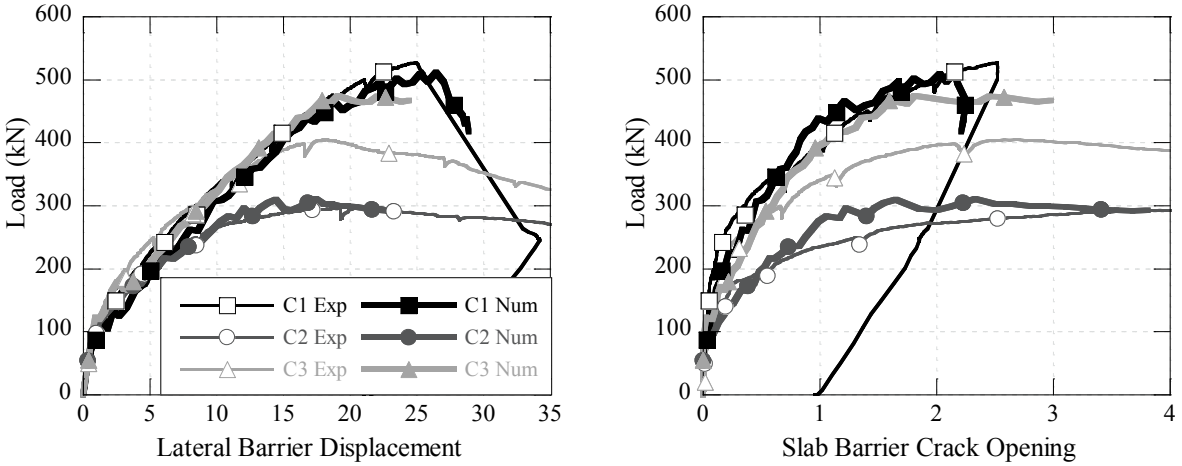

a) Lateral Barrier Displacement a) Slab Barrier Crack Opening

Figure 4-5: Experimental and Numerical Results

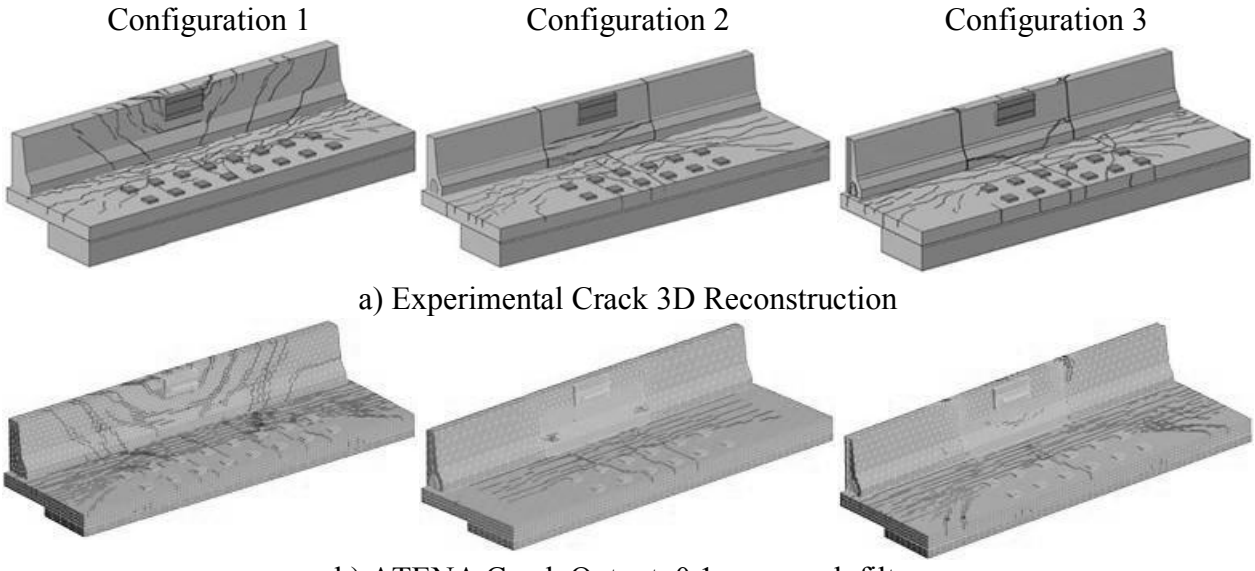

a) Experimental Crack 3D Reconstruction

b) ATENA Crack Output, 0.1 mm crack filter

Figure 4-6: Experimental and Numerical Cracking Pattern at Ultimate

4.5 Results and Discussions of Numerical Studies

The following parametric studies were performed to better understand the experimental behaviour and to evaluate modifications to the barrier or deck designs and the testing configuration.

4.5.1 Precast Barrier Fibre Orientation

The experimental behaviour of Configuration 3 began yielding when shear cracks formed at the barrier-to-barrier shear key connections on the exterior barrier side. The cracks were first noticed at the 350 kN inspection, and reached the back face of barriers by 400 kN, Figure 4-7a). The shear cracks opened quickly once peak strength was reached at 404 kN (Figure 4-7b), and the longitudinal continuity between barriers was lost. In the numerical validation model shown in Figure 4-5, the shear cracks form and grow only at a peak strength of 474 kN. The discrepancy between the experimental and numerical results is likely due to the fibre orientation.

In fibre reinforced concretes (FRC), the fibres can only limit crack opening widths and increase fracture energy when they are adequately oriented across the crack plane. If the fibres are aligned parallel to the crack, then the FRC will behave similarly to normal concrete in tension. The crack opening law for the numerical models was determined with concrete specimens poured specifically with a favorable fibre orientation. The precast barriers were poured from the back side with the front (loaded) face down. This pouring technique most likely oriented the fibres in the vertical and longitudinal direction of the barrier, favorable to resist the applied overturning moment, but not to resist the shear cracks that formed at the lateral connections.

Numerical simulations were performed with the post-peak behaviour of the HPFRC reduced only in the exterior barriers to simulate an unfavorable fibre orientation to resist shear forces in this specific area. One simulation used the 70 MPa HPFRC with a 50% post-peak efficiency and another with 15% post-peak efficiency (i.e. 50% or 15% of the HPFRC post-peak crack opening width for a given tensile stress, see Figure 4-8a). The results of the parametric studies are shown in Figure 4-8b. The model with a 15% post-peak efficiency in the exterior barriers best simulates the experimental results.

The FRC plays an important role in the precast barriers because it leads to a 10% reduction in the barrier cross-sectional surface area and a 60% reduction in steel reinforcement (Figure 4-2).

`

However, the parametric study indicates that the fibres were not well aligned to resist the shear failure observed experimentally near the barrier-to-barrier connections. Even though a 15% HPFRC efficiency dissipates a significantly greater amount of energy during fracture (Figure 4-8a), other fabrication methods for the precast barriers could be investigated to provide a more 3-D fibre orientation throughout the barriers, and even to favor a higher shear strength near the barrier connections (Figure 4-7). Pouring the barriers from the top, as is traditionally done for cast-in-place barriers, or from end-to-end are two options that could potentially improve the fibre alignment with respect to shear.

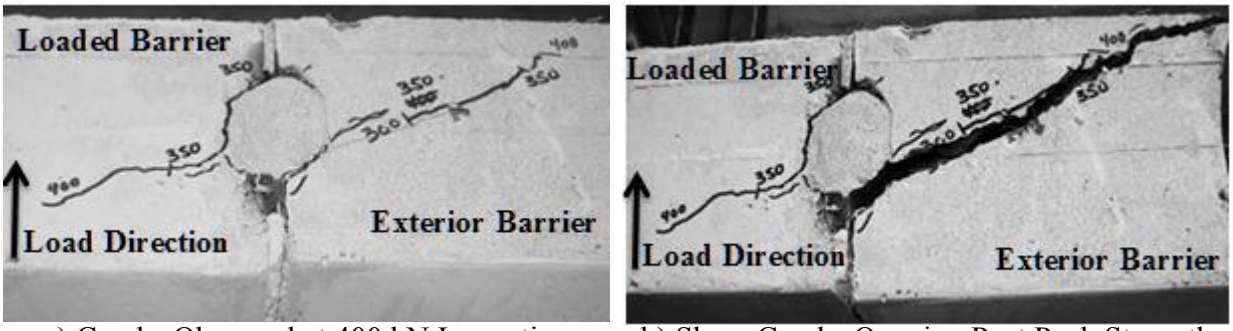

a) Cracks Observed at 400 kN Inspection b) Shear Cracks Opening Post Peak Strength

Figure 4-7: Shear Crack Development Experimental Observations

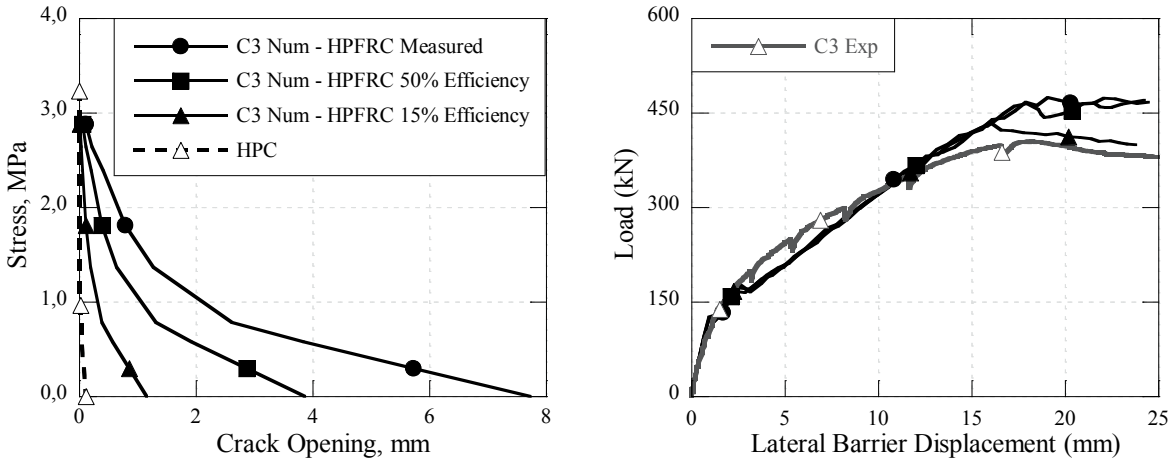

a) Post-Peak Behaviour for Exterior Barrier b) Results

Figure 4-8: Fibre Orientation, Configuration 3

`

4.5.2 Effect of the Precast Barrier Length

The length of the precast barriers in the laboratory tests were limited to 2 m for practical purposes; however, the actual length of the precast barriers designed for industrial use is expected to be 4 m. The increased length of the precast barriers would likely increase the peak strength of the precast barrier test configurations and could possibly reduce the differences observed experimentally between all three test configurations.

Numerical simulations were performed to simulate Test Configurations 2 and 3 when the loaded precast barrier was 4 m instead of 2 m. The total bridge deck overhang length was maintained, and therefore the length of the exterior barriers was shortened in the numerical models from 2 m to 1 m.

The results for the barrier length effect study are shown in Figure 4-9. The increase in loaded precast barrier length increases the ultimate strength for Configuration 2 from 310 kN to 484 kN and for Configuration 3 from 435 kN to 506 kN. The failure mode was not affected by the increase in precast barrier length.

In Test Configuration 2, the precast barriers were not connected and therefore the length of the barrier plays a very important role in the structural performance of the deck overhang. This is apparent in the results of the parametric study with a significant force increase of 56%. The results indicate that the 4 m precast barriers without connections have an equivalent performance to continuous cast-in-place barriers (Figure 4-5a). In Test Configuration 3, the precast barriers had a shear connection between one another and therefore the increased length does not have as much of an impact (16% strength increase). The peak strength of both 4 m precast barrier configurations is very similar (±5%). This is because the shear keys fail before the peak strength is reached and the same failure mode controls the two configurations. The reduced length in the NLFE model of the exterior barriers (1 m only) may have also reduced their contribution to the structural resistance for Test Configuration 3.

`

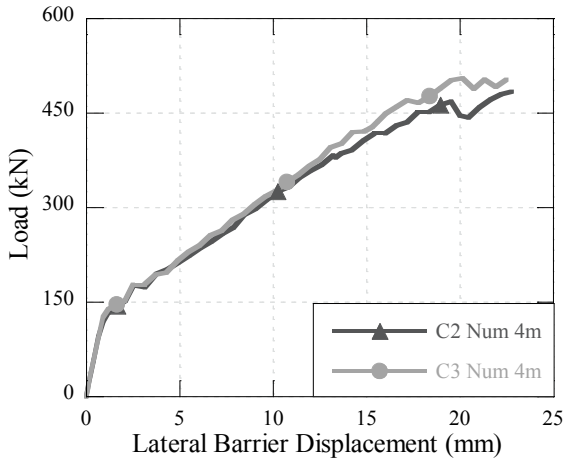

Figure 4-9: Barrier Length, Configurations 2 and 3

4.5.3 Eccentric Load Application

In the experimental setup, the precast barriers were loaded at their mid-length (centre span) and not their edges, their critical impact points. This choice is explained because the barriers were built at a reduced model length of 2 m and loading them at the edges would have been too severe of a penalty. Therefore, a parametric study was carried out on the 4 m precast barriers loaded closer to their edge to determine the performance of the precast barriers during eccentric loading.

The NLFE simulations used to evaluate the 4 m precast barrier in Section 4.5.2 were modified to evaluate their performance when the static transverse load was applied at the barrier edge.

The results for the critical impact point study are shown in Figure 4-10 and Figure 4-11. In Configuration 2, the peak strength of the edge loaded barrier is 338 kN, a 30% reduction from the centrally loaded 4 m precast barriers (Figure 4-10a). The failure mode moves from flexure due to the overturning moment only, to flexure due to longitudinal bending in the barrier in addition to the overturning moment (Figure 4-11). This is an expected failure path for barrier edge loads (AASHTO 1989, Jeon 2011). The peak strength of Configuration 3 edge loaded barriers is 419 kN, a 17% reduction from the centrally loaded 4 m barriers (Figure 4-10a). The structure initially fails at the peak strength (419 kN) in shear at the barrier connection. After the continuity has been lost, the same dual flexure failure controls the post-peak strength as in the Configuration 2 edge load study.

`

The results clearly demonstrate that the edge load is a more critical impact point for the two precast barrier test configurations (Figure 4-10a). Still, both Configurations exceed the 227 kN design requirements for PL-2 barriers (CSA 2006). For Test Configuration 2, the 4 m edge load is more resistant (14%) than the experimentally tested configuration of 2 m, and for Test Configuration 3, 4 m edge load model has an equivalent resistance to the experimentally tested configuration of 2 m (Figure 4-10b). Thus, selecting 2 m barriers for the experimental configurations reproduced a more critical case for the precast barriers without connection and was equivalent to the critical case for those with connections.

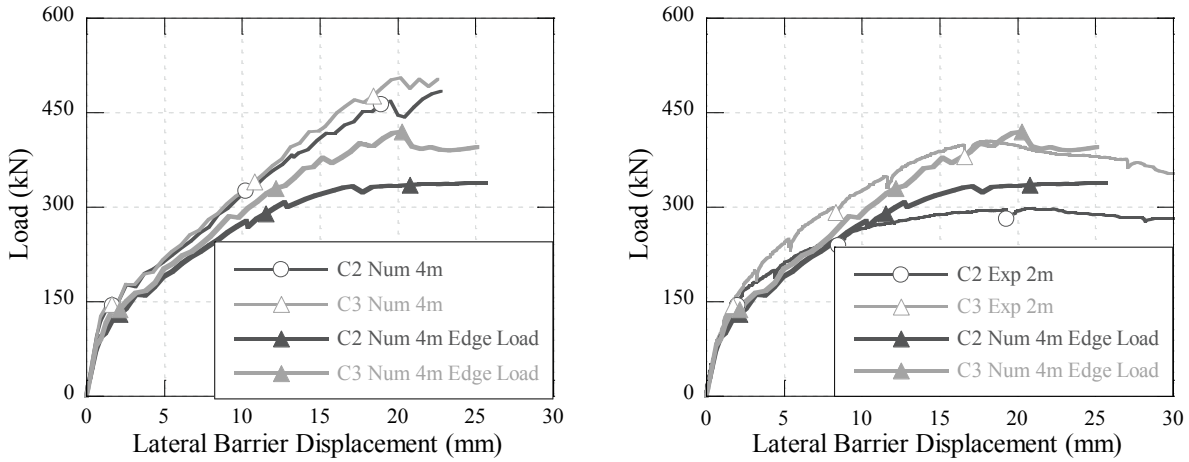

a) Comparison with Barrier Length Study b) Comparison with Experimental Study

Figure 4-10: Eccentric Load, Configurations 2 and 3

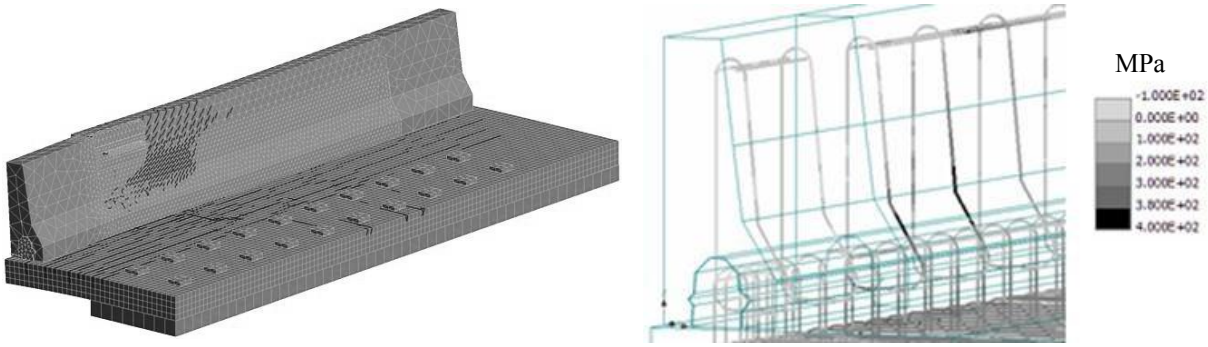

a) Deformed Shape x 5, 0.1 mm Crack Filter b) Stresses, Black indicates Yielding

Figure 4-11: Eccentric Load Failure, Configuration 2

`

4.5.4 HPFRC Slab Overhang Behaviour

The slab overhang was always the first structural component to damage during testing, and by 250 kN a significant amount of flexural cracking was always observed in the overhang slabs. The cracking is detrimental to the durability of the slab overhang, however it is difficult to prevent because the barrier has a significantly larger lever arm than the slab to resist the same applied moment. The advantages conferred when using FRC's – smaller crack opening widths and smaller crack spacing – could improve the durability of the slab overhangs.

A numerical study was performed to evaluate if the utilisation of a slab overhang designed with a 50 MPa HPFRC to obtain an equivalent flexural strength would reduce crack opening widths under service loads. The flexural strength of the HPFRC slab overhang was initially computed using a simple analysis method for FRC. The analysis method is similar to reinforced concrete analysis, except the tensile strength of the concrete is not ignored and an equivalent concrete tensile stress block is assumed to act across the entire tensile face of the concrete section. The equivalent concrete stress at ultimate is considered to be the residual FRC concrete strength at 1 mm crack width (estimated as 0.75 f_t). The modification to the slab design is shown in Figure 4-12. The spacing of the transverse reinforcement was increased from 150 mm to 300 mm, a 50% reduction of steel reinforcement, and the design strength of the modified HPFRC slab is 105 kN-m/m instead of 100 kN-m/m for the HPC slab.

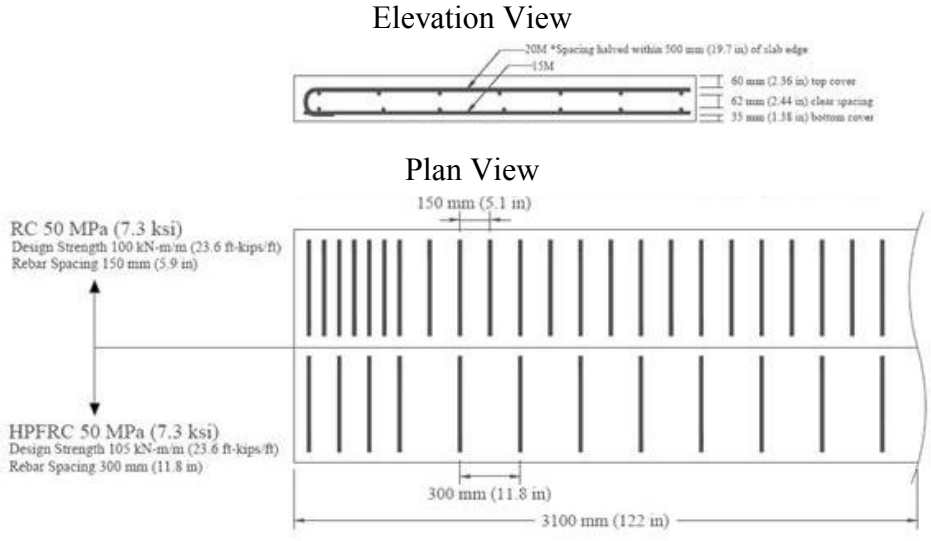

Figure 4-12: RC and HPFRC Slab Design

`

The results of the HPFRC slab behaviour study are shown in Figure 4-13 and Figure 4-14. The results indicate that replacing the HPC slab with an equivalent strength HPFRC for the slab significantly increases the structural rigidity and the ultimate strength of the bridge deck overhang (Figure 4-13a). The results also clearly show that the slab is less damaged at a given load (Figure 4-14). This behaviour is consistent with experimental data from Moffat (2001) comparing equivalent strength FRC and reinforced concrete prisms. Figure 4-14 shows the crack damage in the numerical model at 300 kN and 520 kN of applied load. At 300 kN of applied load, there are no cracks discernible with a 0.1 mm crack filter (Figure 4-14a), and the largest cracks in the slab at this load are 0.05 mm in width. The cracking in the slab observed and recorded during the experimental test exceeded 0.1 mm in width by an applied load of 150 kN. The crack spacing at 520 kN is reduced in comparison to the Configuration 1 experimental model (Figure 4-6).

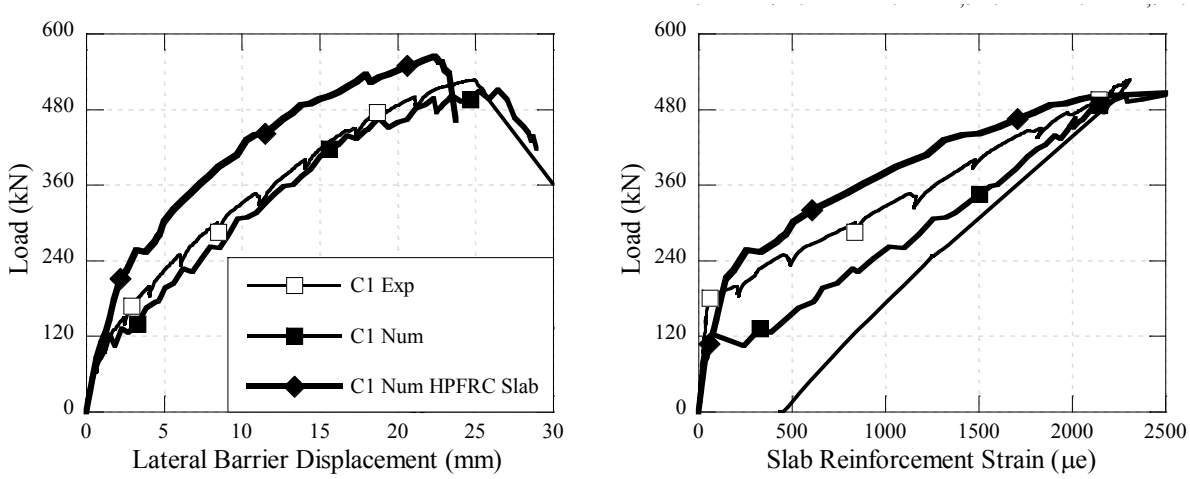

.a) Lateral Barrier Displacement b) Slab Transverse Reinforcement Strain

Figure 4-13: HPFRC Slab, Configuration 1

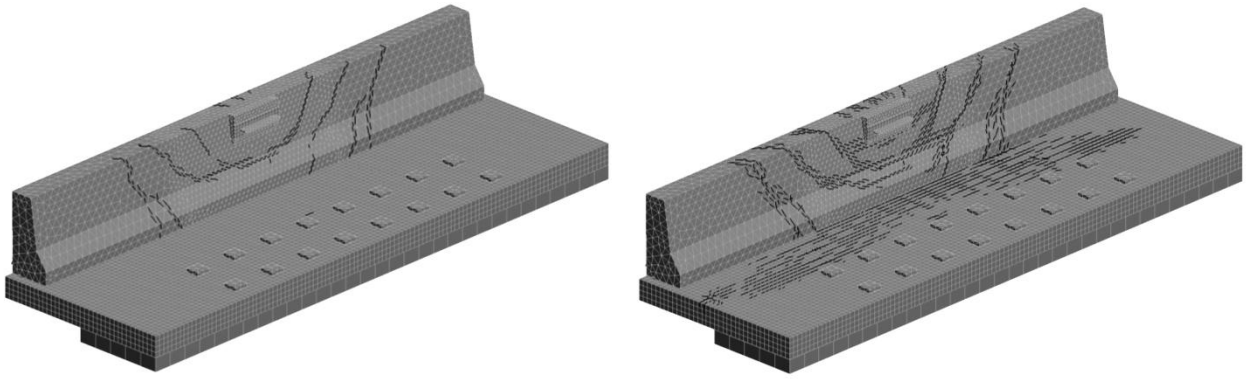

a) Numerical Model 300 kN Applied Load b) Numerical Model 520 kN Applied Load

Figure 4-14: HPFRC Slab Study, Numerical Cracking 0.1 mm Crack Filter

The gain in structural stiffness observed with the equivalent HPFRC slab is surprising because of the large reduction in slab transversal reinforcement. However, it is representative of the contribution of the FRC to the tensile resistance of the slab. The fibres bridging the cracks limit the opening widths. At a crack width of 0.05 mm for instance (max crack width in HPFRC slab at 300 kN applied load), the FRC maintains nearly all of its tensile capacity, whereas a HPC is approaching the critical crack opening width at which there are no longer any crack bridging stresses (Figure 4-13b). The slab was designed to have an equivalent strength and the slab reinforcement begins yielding at the same applied load (Figure 4-13b).

The increase in ultimate strengths shown in Figure 4-13a is related to the failure that takes place in the barrier due to punching shear, and seems independent of the slab. The numerical results indicate that the barrier punching strength is essentially superposed onto the initial strength of the uncracked structure. This is logical because the initial structural rigidity is controlled by the slab behaviour, cracking begins in the slab overhang, and the post-cracking stiffness of the structure remains unchanged.

4.6 Conclusion

The NLFE models created for this study accurately reproduced the experimental results – stiffness, crack damage, and failure mode – from Namy (2012). The results demonstrate that all three bridge deck configurations with cast-in-place and precast barriers exceed the design criteria specified in the CSA (2006) bridge design code. The validated models were then used to perform several parametric studies. The studies and general findings are listed below:

`

Fibre orientation study:

- The NLFE model accurately reproduced the experimental results for the precast barrier configuration with shear connections when the exterior HPFRC barriers were modeled with a 15% post-peak tensile efficiency.
- The reduced HPFRC post-peak efficiency is likely due to an unfavorable fibre orientation with respect to the observed shear failure. New fabrication methods may improve barrier shear strength.

Precast barrier length effect study:

- The increased length of the loaded precast barrier from 2 m to 4 m, the expected length for use on bridges, significantly enhances the load-carry capacity. 4 m precast barriers with or without shear connections present nearly an equivalent load-carry capacity to the reference cast-in-place barrier.

Eccentric load application study:

- The 4 m precast barriers were loaded flush at their edge. Edge loading decreased the load-carry capacity of the barriers with respect to centred loading; however, 4 m precast barriers subjected to eccentric loads still surpass the CSA (2006) and AASHTO (2010) design requirements.
- For precast barriers without connections, the length effect of using 2 m precast barriers was more critical to the structural behaviour than edge loading. For precast barriers with connections, the length effect of using 2 m precast barriers was as critical to the structural behaviour as edge loading.

HPFRC slab study:

- The slab overhang was modeled with an equivalent strength HPFRC that led to a 50% reduction of steel reinforcement. Utilisation of this material increases the structural stiffness and reduces damage to the slab overhang during service loads. It also increases the ultimate strength of the structure. Thus, equivalent strength HPFRC slabs are of great interest for bridge deck applications.

`

4.7 References

AASHTO. (1989) Guide Specifications for Bridge Railings. American Association of State and Highway Transportation Officials. Washington, D.C., U.S.A.

ACI Committee 209. *Prediction of Creep, Shrinkage, and Temperature Effects in Concrete Structures,* ACI Manual of Concrete Practice. Detroit, Michigan, 1992, pp. 209R-1-209R-47.

Aminmansour, M. (2004). Performance characteristics of precast and reinforced concrete bridge barriers subjected to static and impact loads. Ph.D. Thesis. The Pennsylvania State University, Altoona, PA, U.S.A.

Beaurivage, F. (2009). Study of the influence of structural parametres on the behavioural laws of fibre reinforced concrete's for structural design (Étude de l'influence des paramètres structuraux sur les lois de comportement des bétons fibrés pour la conception de structures). Montréal: Polytechnique Montréal.

CEB-FIB. 2000. Bond of reinforcement in concrete, State-of-art report. International Federation for Structural Concrete (FIB), Lausanne, Switzerland. Bulletin 10.

CSA-S6-06. 2006. Canadian Highway Bridge Design Code (CHBDC). CSA International. Toronto, Canada.

Cervenka, V., Jendele, L., and Cervenka, J. 2011. ATENA Program documentation. Cervenka Consulting Ltd. Prague, Czech Republic.

Cusson, D., Repette, W. (2000). Early-Age Cracking in Reconstructed Concrete Bridge Barrier Walls. ACI Materials Journal, Vol 97, No 4, pp. 438-446.

Delsol, S. (2012). Evaluation of the orientation coefficient in steel fibre reinforced concrete's (Évaluation du coefficient d'orientation dans les bétons renforcés de fibres métalliques). M.Sc. Thesis. Polytechnique Montréal, Montréal.

Desmettre, C., Charron, J-P. (2012). Water permeability of reinforced concrete with and without fibre subjected to static and constant tensile loading. Cement and Concrete Research, Vol 42, Issue 7, pp. 945-952.

Duchesneau, F. 2010. Design of monolithic and hybrid precast barriers using high and ultra-high performance concrete's (Conception de barrière préfabriqué hybrides et monolithiques en

`

utilisant des bétons à haute et ultra-haute performance). M.Sc. Thesis. Polytechnique Montréal, Montréal.

Haluk, A., Attanayaka, U. (2004). Causes and cures for cracking of concrete barriers (Research Report No RC-1448). Wayne State University, Detroit, MI, U.S.A.

Hordijk, D.A. 1991. Local approach to fatigue of concrete. Ph.D. Thesis. Delft University of Technology, Delft, Netherlands.

Jeon, S-J., Choi, M-S., Kim, Y-J. 2011. Failure Mode and Ultimate Strength of Precast Concrete Barrier. ACI Structural Journal: January-February 2011, Vol 108, No 1, pp. 99-107.

Lessard, M.-C. (2009). Design of pre-slabs for bridge decks with innovative concrete's (Conception de pré-dalles en bétons innovants pour les ponts). Montréal: Polytechnique Montréal, mémoire de maîtrise.

Menétrey, Ph. Willam, K.J. (1995). Triaxial Failure Criterion for Concrete and its Generalization. ACI Structural Journal, V. 92, No. 3, pp. 311-318.

Ministry of Transportation of Quebec (MTQ). 2004. Structural Design Manual – Volume 1 (Manuel de Conception des Structures – Volume I). Ministère des Transport du Québec, Québec.

Moffat, K. 2001. Analysis of bridge slabes with reduced reinforcement using steel fibre reinforced concrete's (Analyse de dalles de pont avec armature réduite et béton de fibres métalliques). M.Sc. Thesis. Polytechnique Montréal, Montréal.

Namy, M. 2012. Structural behaviour of cast-in-place and precast concrete barriers anchored to bridge deck overhangs and subjected to transverse static loading. M.Sc. Thesis. Polytechnique Montréal, Montréal.

Niamba, É. 2009. Development of precast bridge barriers using fibre reinfroced concrete's (Développement de barrières préfabriqués en bétons renforcés de fibres pour les ponts). M.Sc. Thesis. Polytechnique Montréal, Montréal.

`

CHAPTER 5 COMPLIMENTARY INFORMATION AND GENERAL DISCUSSION

The progress of this research project can be divided into three distinct phases. There was the preliminary finite element study to evaluate the general bridge deck overhang behaviour and identify the key design parameters for evaluation. Then there was the experimental phase, which included the specimen design, the testing configuration, the laboratory tests and the results analysis. Finally there was the subsequent numerical study to reproduce the experimental tests results, and evaluate other design parameters that could not be performed experimentally. Chapter 3 and Chapter 4 summarise the principal information from these three phases, while this Chapter provides all the complimentary information that could not be detailed previously.

5.1 Preliminary Finite Element Evaluation

The initial parametric study done using ATENA (Cervenka 2009) was meant to establish the behaviour of the bridge deck and barrier structure during static loading to isolate key design parameters and to define the experimental conditions. The study provided an order of magnitude of the structural performance and resistance; however, it was meant primarily as a qualitative evaluation. In light of this and the large scale of the numerical models, a simplified barrier geometry and coarse mesh was permitted as a means to reduce simulation time.

The barrier used for this study had a simplified geometry. However, the cross-sectional area, base width, reinforcement ratio, and concrete cover were all equivalent to those from the MTQ Type 201 cast-in-place barrier, and the material used was a HPFRC 50 MPa with 1 %-volume of fibre reinforcement in lieu of the traditional 50 MPa concrete.[1] A 225 mm thick normal strength concrete (35 MPa) slab was used with a 1.8 m overhang and 20M bars at 125 mm c/c spacing. The 1.8 m overhang length was selected because it is the longest bridge overhang that can be

[1]Afterwards a corrected model with a traditional 50 MPa concrete was examined to observe more realistic cracking pattern in the cast-in-place barrier, but the general structural behavior of the model remained similar. Because the study was qualitative the findings with the HPFRC were considered to be valid.

designed with simplified analysis methods of the CSA (2006). The design aids from the MTQ *Design Guide* (2004) were used to design the steel reinforcement.

The concrete was modeled using the *Nonlinear Cementitious* fracture-plastic concrete formulation. All reinforcement was modeled discretely as truss elements with an elastic-perfectly plastic bilinear material law using the nominal yield stress of 400 MPa. A bond-slip relationship was not considered for this initial analysis. The slab was fixed in all directions at its far edge. A coarse mesh of 150 mm was used for the barrier and 56 mm for the slab. The slab mesh density was significantly higher than the barrier because a minimum of 4 rows of mesh elements were necessary to model the slab bending and reinforcement yielding. The loading was applied in the middle of the barrier via a high performance steel (f_y = 800 MPa) plate with surface area of 350x700 (AASHTO 1989), and a load application height of 700 mm (CSA 2006). The loading was displacement controlled. Figure 5-1 provides a schematic of the base model used for this study.

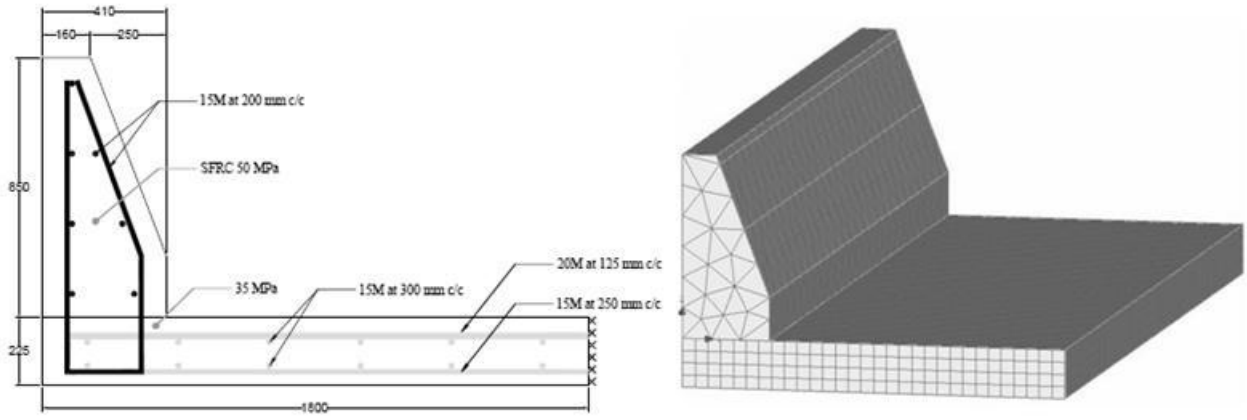

Figure 5-1: Simplified Finite Element Model for Lab Configuration Study

The base model reached a load-carry capacity of 540 kN before the slab and anchor reinforcement yielded, and the barrier was not significantly damaged during the load application. The effects of the following modifications to the base model were analysed, and the findings are summarised in Table 5-1:

- Length of the bridge deck and barrier structure
- Discontinuous precast barriers of 4 m length
- Lateral connections added between discontinuous precast barriers of 4 m length
- Cantilever overhang length

`

- Addition of inner deck-span
- Addition CL-625 truck wheel loads in addition to transversal impact force
- Centred and non-centred load application
- Boundary conditions representative of steel or concrete beams

Table 5-1: Initial Parametric Study and Findings

Condition	Force (% Change)[1]	Results
Model length 4 m	540 kN (0%)	Reference – Slab resists load along entire length. Yielding in anchor and slab reinforcement. Slab critical.
Model length 12 m	1206 kN (0%)	Increased deck length significantly increases structure resistance. Yielding of reinforcement concentrated over 4 m length. General behaviour similar to reference study.
Precast, length 12 m	670 kN (-44%)	Discontinuity in barrier restricts load transfer length to precast barrier length, and concentrates stresses in slab. Slab and anchor reinforcement become more critical. Cracking in slab concentrated in front of the loaded barrier.
Precast w/ connection, length 12 m	1152 kN (-5%)	Structure behaviour very similar to continuous configuration. Highlights interest in shear connection between precast barriers.
0.9 m Slab Overhang, length 12 m	1049 kN (-13%)	Reduced overhang length stiffens structure. Higher stress level in transversal slab reinforcement at support. Reinforcement adjusted according to MTQ *Design Guide* (2004) reducing slab resistance.
Added inner deck span, length 4 m	534 kN (-1%)	Additional deck span has insignificant influence on structural behaviour and performance.
CL625 Wheel Loads, length 4 m	500 kN (-7%)	Wheel loads do little to change structure response. Applied loads remain critical. Wheel loads solicit slab near edge support, while applied barrier load increases stress at slab-barrier junction.
Ecc. load, Precast, length 12 m	603 kN (-50%)	Eccentric load application on precast railings is critical, significantly lowering structural capacity.
Ecc. Load Precast w/connection, length 12 m	1106 kN (-8%)	Eccentric load application is much less critical in precast configuration with connections.

[1.] Percent change relative to trial with same length, 4 m or 12 m to provide a more equitable comparison

`

The simulations with precast barriers highlighted the influence of adding a connection to transmit the transverse loads between barriers. When no connection is present, the load transfer from the barrier to the slab is limited to the precast length, and therefore the anchor bars and the slab reinforcement experience significantly higher stress levels for a given load. Introducing shear connections between barrier segments proved to limit this effect, and the structural capacity essentially became equivalent to that of a continuous cast-in-place configuration. Thus, the shear connection between barriers was established as a key design condition for investigation in the experimental program.

The implication of this parameter on the experimental program was very important. First, to test the efficacy of any proposed shear connections, the length of the experimental tests would have to be able to accommodate at least three precast barriers (connection on each end of loaded barrier). Second, the length of the precast barriers would also be a very important parameter, because similar to adding a shear connection between barriers, an increased barrier length would also attenuate the concentration of load transfer. However, an increased length would also have a significant impact on the size of the experimental setup. The precast barriers selected for investigation in this project (Duchesneau 2010) were previously designed at a length of 2 m, however the length of the barriers for actual use could potentially be 4 m or even 6 m. For practical considerations in respect to fabrication, transportation, and manipulation of the experimental specimens, it was decided that 2 m barriers would be used, limiting the experimental setup to a total length of 6 m. The implications of the barrier length on the numerical findings was later considered in a numerical study.

The simulation with a reduced slab overhang length, 0.9 m instead of 1.8 m, did not significantly affect the structural behaviour. This is logical because the steel reinforcement within the overhang was adjusted with respect to the cantilever length in accordance with the MTQ *Design Guide* (2004) and, furthermore, because the applied moment from the transversal load is constant throughout the overhang. Therefore, a commonly used slab overhang length in Canada of 1 m was selected for the experimental tests. The simulation including an inner deck span in addition to the overhang span had no effect on the structural behaviour and therefore the deck slab was limited to the overhang and supported portions.

`

In the CSA (2006), the specified impact loads (transverse, vertical, and longitudinal forces) for the design are to be applied simultaneously to the barrier. The transverse and longitudinal components correspond to the vehicle deceleration during impacts, and the vertical force to the vehicle weight. Considering the structural stiffness of the barrier and deck in the longitudinal direction, the longitudinal force component was never considered. The heaviest vehicle considered for impact for PL-2 bridges is the 8000 kg Single Unit Truck (NCHRP 350), however, the condition with CL-625 truck wheel loads was examined to be conservative. The incorporation of CL-625 wheel loads applied simultaneously with the transverse impact force only marginally affected the load-carry capacity of the structure (7% decrease). This observation is logical because the wheel loads are critical to the supported edge of the slab, while the transverse impact force is critical at the barrier-slab junction. The vertical barrier load specified in the CSA (2006) was therefore not considered necessary to incorporate into the experimental setup.

The CSA (2006) also specifies that the barriers must be able to resist impact loads at all sections. Thus the effect of eccentric barrier impacts was also studied. Simulations with an eccentric load did reduce the structural resistance, particularly for precast railings without shear connection (50% loss of load-carry capacity compared to monolithic barrier). However, the resistance still exceeded the requirements of the governing codes (AASHTO 2004, CSA 2006), and the centric loading condition was seen as a more principal aspect of research for this project. Therefore, the consideration of eccentric loads would be the subject of numerical analysis and future studies.

The initial finite element evaluation formed the basis of the experimental setup and test parameters. Three 6 m long bridge deck-and-barrier configurations were tested in the laboratory. One configuration had a cast-in-place barrier, to establish a performance reference, and two configurations used precast barriers. The difference between the two precast configurations was the incorporation, or not, of a lateral shear connection between barriers. The slab only consisted of the overhang and supported portions. The overhang was 1 m in length. Only the transverse impact load was applied in the centre of each configuration.

5.2 Design of Experimental Specimens

Once the experimental program was determined the next phase of the project was to design and fabricate the laboratory specimens.

`

5.2.1 Support Block Design

Only one support block was used throughout the laboratory tests to save on time, energy, and expenses. The support block had to be able to resist stresses from transportation, post-tensioning, and the laboratory tests; to be representative of a typical prestressed concrete beam; and to be compatible with the experimental setup. Considering the strength requirements, the support block was built with a HPFRC 70 MPa (see Table 5-4 for mix design) with a high percentage of reinforcement for a continuously supported block. A 1 m width was selected to correspond to that of a NEBT prestressed bridge beam top flange encountered in Quebec. A 0.4 m height was selected to give ample room for the vertical slab deflection, and to provide access to the underside of the slab (once cantilevered) to install the necessary instrumentation. The access height was particularly important for the installation of strain gauges on the underside of the slab overhang. The chamfers at each corner of the block were meant to minimize the build-up of stress concentrations in the slab as it would rotate about the support block during loading. 65 mm post-tension ducts were poured into the block in two rows every 500 mm in order to be compatible with the anchoring pattern on the laboratory strong floor. The design drawings for the support block can be consulted in APPENDIX A.

5.2.2 Slab Design

The slabs were designed to be representative of the cantilevered portion of a bridge slab in Quebec with a 1 m non-supported overhang length. The slab thickness of 225 mm and the preliminary slab reinforcement were selected using the MTQ *Structure Design Manual* (MTQ, 2004). The design aids specified a minimum of 1780 mm^2/m of transversal reinforcement for the negative moment for a 1.0 m slab overhang. Thus, 20M bars at 150 mm c/c spacing (2000 mm^2/m) were selected for the negative moment reinforcement in the slab overhang. A clear cover of 60 mm and 35 mm were specified for top and bottom transverse reinforcement respectively. The maximum allowable longitudinal slab reinforcement was selected and corresponded to 15M bars at 300 mm c/c.

A secondary design was performed to make sure that the slab overhang met design criteria in the governing design code for bridges in Canada, CSA (2006). The slab thickness must provide enough room to meet the minimum cover specified for the top and bottom rows of transversal reinforcement, as well as the clear spacing of 55 mm between longitudinal reinforcement. The

`

minimum cover specified in Clause 8.11.2 is more conservative than the 60 mm and 35 mm clear cover allowed by the MTQ for top and bottom reinforcement respectively. The MTQ imposes less minimum concrete cover because their bridge decks are additionally sealed with an impervious membrane as well as an asphalt layer. The MTQ values were maintained because they are a more realistic representation of bridge slabs in Québec. The slab thickness of 225 mm was adequate and was maintained for the slab design.

According to Clause 5.7.1.7 (CSA 2006), the slab overhang for decks supported by prestressed concrete beams must be designed to resist the negative transverse moments caused either by the CL-625 wheel loads (Clause 3.8.3.2) in the bridge overhang or by the transversal barrier impact load (Clause 3.8.8.1 and Clause 12.4.3.5) applied independently. The transverse bending moments induced by CL-625 wheel loads can be determined with the simplified methods detailed in Clause 5.7.1.6 (CSA 2006). The negative transverse moment induced by impact loads must be calculated using either a refined analysis method or yield line theory. The factored bending moments, axial forces, and transfer lengths specified in Table C5.4 in the CSA Commentary (2006), which were derived from a FE analysis were used. The simplified method of analysis in Clause 5.7.1.2.1 (CSA 2006) must be used to find the longitudinal moment in the slab for an overhang span length of more than 3 metres. Because this method is not particularly applicable to the experimental setup though, and the maximum longitudinal reinforcement allowable in the MTQ *Structure Design Manual* (2004) was selected, the longitudinal reinforcement was assumed to exceed the code requirements. Table 5-2 below summarises the design checks performed for the slab as designed with the MTQ *Structure Design Manual* (2004). The calculations are detailed in APPENDIX D of this document.

`

Table 5-2: Slab Overhang Design Summary

Component	Interior	Exterior[2]
ϕM_R	100 kN-m/m	177 kN-m/m
αM_{ULS}	73 kN-m/m	137 kN-m/m
ϕN_R	1200 kN/m	1920 kN/m
αN_{ULS}	100 kN/m	142 kN/m
$\alpha M_{ULS}/\phi M_R + \alpha N_{ULS}/\phi N_R$	0.82	0.85
V_R, Transverse	279 kN/m	387 kN/m
αV_{ULS}, Transverse	100 kN/m	142 kN/m

The slab overhang design met all the design checks imposed by the governing CSA (2006) and was designed in accordance with the MTQ *Structure Design Manual* (2004). However, there was still concern of inadequate development length of the transverse reinforcement for the negative moment in the slab. Figure 5-2 indicates that the preliminary numerical simulations and experimental results of Benmokrane et al. (2010) demonstrated a strong risk of localized shear failure in the slab at the load transfer region of the slab beneath the bridge barrier.

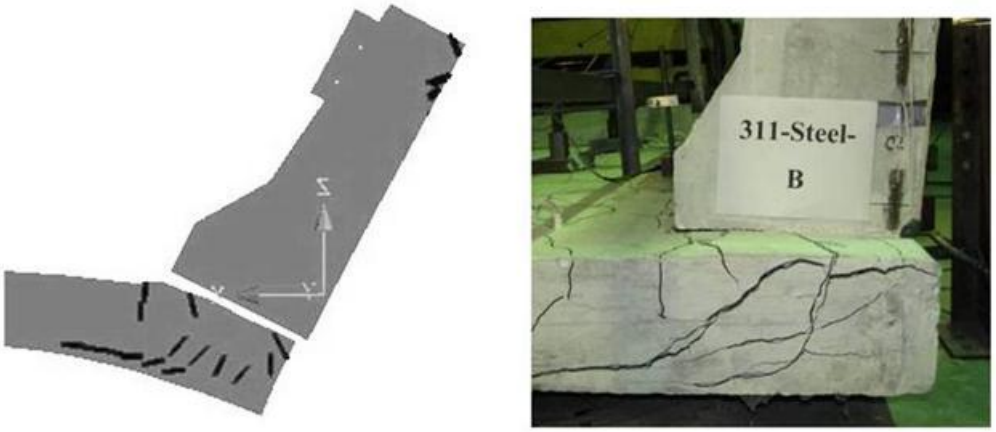

a) Numerical Model b) Benmokrane et al.(2010)

Figure 5-2: Local Shear Failure in Slab Overhang

One of the causes of this local shear failure in the slab was the inadequate development length of the transverse reinforcement at this region. The slab reinforcement proposed in the MTQ

[2]The exterior portion of the slab overhang is defined as portion within distance S_c, 1 m, of longitudinal slab edges. Due to the reduced size of the experimental setup, the exterior slab reinforcement was limited to 0.5 m on both sides.

Structure Design Manual (2004) uses straight reinforcing bars for the negative moment reinforcement. A strut-and-tie model of this disturbed region of the slab (Figure 5-3) indicates that the development length of the tie (top row of transverse reinforcement) needs to be reduced as much as possible to prevent a local shear failure. To better anchor the reinforcing bars at this region, hooks were added to the ends of the top row of transverse reinforcement, effectively decreasing the development length from 383 mm to 231 mm, a 40% reduction (See APPENDIX D for L_d calculation). The reinforcement detail in this region is an important design detail and was examined in the numerical parametric study of the project.

a) Standard Reinforcement Detail b) Modified Reinforcement Detail

Figure 5-3: Strut-and-Tie Model of Slab at Disturbed Load Transfer Region

Figure 5-4 shows the final slab design for the Test Configuration 1. The only difference between slabs designed for Test Configurations 2 and 3 was the configuration of the anchors cast into them, which depended on the barriers used. The design and as-built drawings for each slab specimen can be found in APPENDIX A.

`

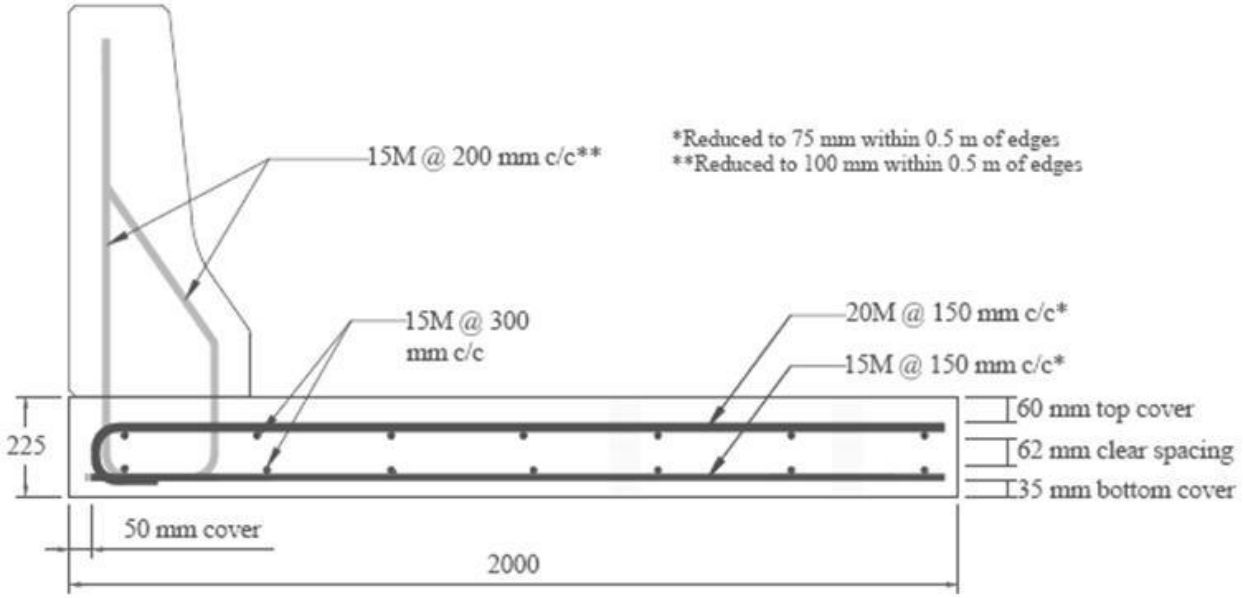

Figure 5-4: Final Slab Design Lab Trial

5.2.3 Barrier Designs

The cast-in-place barrier used to establish a reference performance of the bridge was a 35 MPa MTQ Type 201 bridge barrier which can be found in the MTQ *Structure Design Manual* (2004). This barrier has an F-shaped geometry, a barrier safety shape commonly used throughout North America, Europe, and Australia (MASH 2010, TAC ACT 2010, Jiang et al. 2004).

The precast barrier design for the laboratory test was taken directly from Duchesneau (2010) without any modifications. The barriers from Duchesneau (2010) are 2 m in length and made from HPFRC 70 MPa. The geometry is similar to that of the MTQ Type 201 barrier except that the section width is reduced by 9% at the base and 16% at the top. The steel reinforcement is also optimized with a 60% reduction of transverse reinforcement and 63% reduction of longitudinal reinforcement. These reductions to the section area and reinforcing steel are possible because of the tensile behaviour of the HPFRC 70 MPa concrete. The longitudinal barrier sections of the cast-in-place and precast barriers are shown in Figure 3-2. The design and as-built drawings for each barrier specimen can be found in APPENDIX A of this document.

The precast barriers with shear connections were similar to those designed by Duchesneau (2010), except for the trapezoidal recess added to each end of the barriers. The recesses were

injected with mortar once the barriers were installed on the deck and the mortar worked to transfer shear forces between railings. The shear key is described in Section 3.2.3. Figure 5-5 below shows photos of the shear key, during installation and after injection with a FRM.

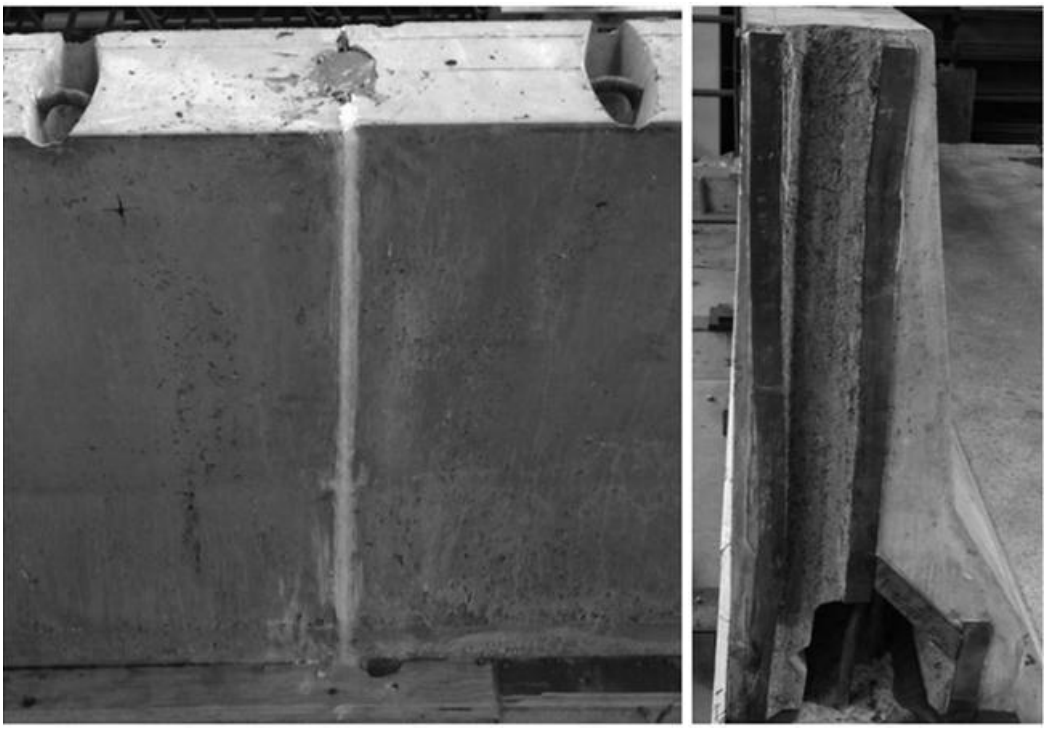

a) Plan View b) Elevation View

Figure 5-5: Shear Key

5.2.4 Loading Plate

A loading plate was fabricated to distribute the actuator load to the barrier over a controlled surface. To withstand the bearing forces, the loading plate was made from 120 MPa UHPFRC. The dimensions of the loading surface, 350 by 700 mm, are specified as an impact dimension in AASHTO (1989) for PL-2 barriers, and were selected to maintain continuity between this project and those of Duchesneau (2010) and Niamba (2009). The loading plate was anchored directly to the barrier with drop in bolts. The loading plate design is shown in Figure 5-6. After the first two configurations were tested, small cracks were detected on the back face of the loading plate. Thus a second was fabricated for the remaining test configuration as a precautionary measure. The mechanical properties of the two loading plates are given in Table 5-3.

`

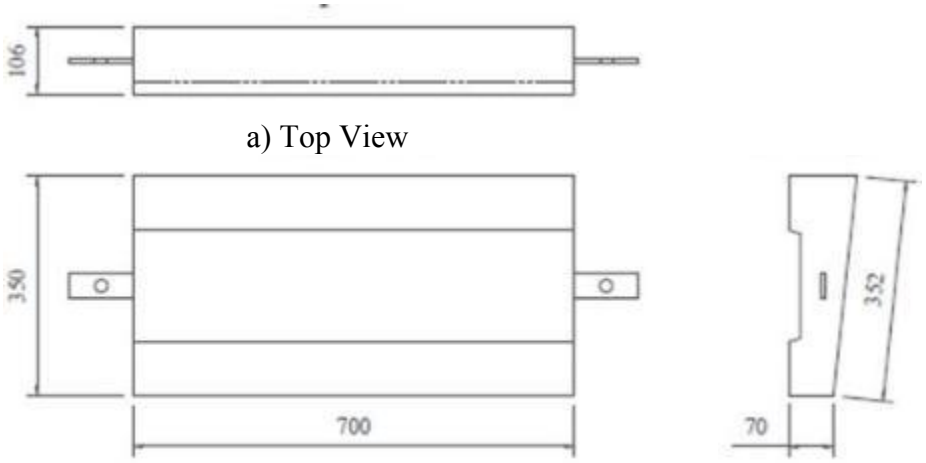

a) Top View

b) Front View

c) Side View

Figure 5-6: Loading Plate Design

Table 5-3: Loading Plate Mechanical Properties

Property	Configurations 1, 2	Configuration 3
f'_c (MPa)	105.2	114.5
f_t (MPa)[1]	9.7	11.0
E_c (MPa)	40600	39700
ν	0.25	--

[1.] Tensile strength determined with direct tension tests.

5.2.5 Concrete Composition

Table 5-4 gives the different concrete compositions used for fabrication of the 35 MPa concrete slabs and cast-in-place barrier, the HPFRC support block, and the HPFRC precast barriers.

Table 5-4: Concrete Composition*

	35 MPa Concrete	70 MPa HPFRC	
	Barrier & Slabs	Support Block	Precast Barriers
Cement, kg/m^3	360.0	650.0	625.0
Water, kg/m^3	160.0	195.0	218.8
Sand, kg/m^3	753.0	827.3	842.4
Gravel, kg/m^3	1066.0	649.0	601.7
Super-plasticizer, kg/m^3	3.1	44.4	12.1
Viscosity Modifier, kg/m^3	--	2.2	--
Air-entraining Admixture, kg/m^3	0.14	--	--
Steel Fibres, kg/m^3	--	120	120
Fibre Length, mm / Diameter, mm	--	30 / 0.5	30 / 0.5
Water / Binder Ratio, (-)	0.44	0.30	0.34

*For injected mortar and UHPFRC composition's APPENDIX E

5.3 Fabrication of Experimental Specimens

The fabrication of the laboratory specimens was done at the Sallaberry-de-Valleyfield (Québec) precast plant of Béton Brunet Group, an industrial partner for this research project. The details of each specimen pour, date, times, fresh concrete properties, and commentary, were all recorded in the Fabrication Log attached in APPENDIX D.

5.3.1 Support Block

The support block was built outdoors on an elevated steel platform. The steel platform was used directly as a form for the bottom side of the block, and wooden formwork was built-up along the sides. The fabrication of the support block was relatively straightforward, however the spacing and verticality of the post-tension ducts were very important. PVC tubes were used for the duct reservations, and they were fitted into steel inserts welded onto the platform at the exact centre-to-centre spacing, 500 mm (Figure 5-7).

Figure 5-7: Block Formwork

Figure 5-8 shows that angled steel sections were fixed on-top of the formwork with inserts fitted into the top portion of the PVC pipes. The verticality of the pipes was then adjusted before securing the steel angles to the formwork. This procedure was an effective method to maintain the spacing and verticality of the PVC pipes, as well as to resist any movement during the concrete pour. A similar design was used for the post-tension ducts in the slabs. The finishing of the block surface was also of particular importance. The slabs were anchored to the block and post-tensioned, any unevenness or asperities in the finished surface could potentially cause a stress build-up in the slabs during post-tensioning. The HPFRC used for the fabrication was completely self-leveling and compacting, which helped the surface finish. However the steel braces and inserts in the PVC pipes limited trowel access to the particularly important areas around the post-tension ducts. Furthermore, because the specimen was poured outdoors at the onset of winter, the support block was steam cured until a resistance of 50 MPa was reached. The steam curing, or perhaps temperature gradient after the steam was cut-off, seemed to have an effect on the finished surface as well, which was very flaky with several air bubbles. To improve the finishing, the entire surface was passed over with a concrete grinder.

`

Figure 5-8: Block and Steel Bracing for Post-Tensioning Ducts

5.3.2 Slab Fabrication

The slabs were each poured match-cast with the support block, meaning the support block was used directly as part of the formwork for the slabs. The remaining forms were built-up around the support block. A greasing agent was applied to the block and wooden forms before pouring the slabs in order to more easily break down the forms and remove the slabs.

Once the formwork was built-up for the slab, the PVC pipes were placed to create the post-tensioning ducts in the slab. The same steel bracing configuration was used to maintain the exact spacing and adequate verticality for the reservations as for the support block (Figure 5-9).

After the PVC pipes were fixed in, the slab reinforcement was put together directly within the forms. Plastic chairs were used to maintain the appropriate cover for the transversal reinforcement and clear spacing between the longitudinal reinforcement. The anchor bars for the cast-in-place barriers had several longitudinal reinforcing bars tied into them, essentially making a cage. This gave the anchors enough rigidity to remain in place and avoid external support during the slab pours. However, the anchors for the precast barriers had no longitudinal bars and therefore had to be supported externally.

To place the anchors for the slabs, a rectangular steel bar, 12 mm thick by 50 mm in height, was supported at the two ends of the slab, and temporary wooden supports were added before the

`

anchors were tied in. The bar was positioned to be at the centre-line of the anchors and so that the anchors could be placed on top of the bar and sit at the proper height, at which point only the longitudinal position of the bars had to be adjusted. The anchors were then tied in to the slab reinforcement where possible (Figure 5-9).

As seen in Figure 5-9, the slabs had a significant quantity of reinforcement. The placement of the reinforcement was followed from design as-strictly as possible, but there were some placement conflicts between the PVC post-tension ducts and the transverse reinforcement, as well as between the transversal reinforcement and the anchor bars. The PVC reservations always had priority because they had to be compatible with the laboratory strong floor. Thus, the transverse rebar would be moved over next to the PVC tubes at any conflicts. It also happened that the anchors would occasionally have to be moved in order to tie into the slab reinforcement. The anchor bars were placed after the slab reinforcement, it was only their positioning that could be modified. Conflicts in the placement of slab and anchor bars were most often encountered in the precast configuration, the anchor bars were skewed at a 45° angle. This was especially true within 0.5 m of the slab edges where both the transversal and anchor reinforcement were doubled. The final position of all the anchor bars was recorded and can be found on the As-Built drawings in APPENDIX A.

The concrete used for the slabs was a self-leveling and self-compacting design mix. The concrete truck poured the concrete as close to the slab centre as-possible, and the concrete was manually pushed to the far and near edges of the slab. The slabs were cast in the winter and as such were protected in a canopy. The canopy was used to protect the slabs from the elements and to insulate the slabs from the cold. However, as can be seen in Figure 5-10, the canopy also limited the truck access to the slab.

`

Figure 5-9: Slab Reinforcement and Anchor Support

Figure 5-10: Truck Assess for Slab Casting

`

The slab pours were done outdoors in the middle of winter, and as soon as the top surface of the slab was finished, the slab was covered with insulated tarps and then steam cured. 12 cylinders were poured with every slab specimen and placed in the same curing and storage conditions. The steam curing was only stopped once the slabs had met their design strength of 35 MPa. The curing was then lowered gradually in order to reduce the thermal shock.

The slabs used for the precast barrier configuration had a special surface treatment in the region where contact with the precast barriers was expected (barrier-slab interface region). Immediately after pouring, the zone was sprayed abundantly with a concrete surface retarder from Euclid Chemical (Formula S for horizontal surfaces). The next day the steam curing was temporarily stopped, and a high pressure water hose was used to remove the surface mortar and expose the aggregate in this area of the slab. In Figure 5-11 the exposed surface can be compared against the finished surface of the slab. The goal was to increase the friction and cohesion of the barrier-slab interface. This was seen as less critical for the cast-in-place barrier because the concrete was poured directly onto the slab, and for the cast-in-place configuration this area of the slab was simply left unfinished.

Figure 5-11: Exposed Aggregate Surface on Slabs

`

5.3.3 Cast-in-Place Barrier, MTQ Type 201

The cast-in-place barrier was built on-top of the slab as soon as the slab steam curing was stopped. The slab remained in its formwork while the barrier was built on top of it. The remaining rebar for the barrier was tied into the existing reinforcement cage built before the slab was poured (anchors and longitudinal reinforcement). The wooden formwork was built-up indoors and then placed on the slab. Once the formwork was fixed into place, the barrier was ready for concrete placement. The MTQ 35 MPa concrete mix was used for the cast-in-place barrier (same mix as for the slabs).

There was a delay of 10 days between the slab casting and barrier casting. The slab had been steam cured and had gained the majority of its resistance before the barrier pour. Therefore, in order to minimize the differential shrinkage between these two components, the slab surface was kept humid until the barrier pour to reduce restrained shrinkage cracks in cast-in-place barrier.

The forms were fixed to the slab on each end, and on the back and front sides. On the ends the forms were closed off using plywood and then supported with 2x6 boards. The backside of the formwork was attached to the slab using 2x6 boards screwed in at both ends. The front was fixed using four 2x8 ties screwed into the far end of the slab formwork and braced with 2x4 boards. The top of the forms were also connected using four 2x4 boards nailed to both the front and back side. Figure 5-12 shows photos of the barrier formwork assembly and fixation before the concrete placement. The formwork seemed to be very solidly supported and well-fixed to the slab.

The barrier was poured from the top, and was supported by the slab, support block, and elevated steel platform. Thus, in order to pour the barrier, a height of 2 m above ground level had to be reached. This clearance height was too high for the concrete truck available at the precast plant. An industrial concrete pump had to be used (Figure 5-13). The concrete static pressure combined with the increased pouring energy from the concrete pump were superior to the formwork resistance. The forms began to deform along their length, and particularly in the centre (fixation at the ends was the most rigid). Some concrete also began to flow in-between the joint of the formwork and slab on both the front and back sides. To limit the deflection of the formwork, several clamps were placed on the top of the barrier and tightened to reduce the relative displacement of the two sides of the formwork. However, the forms deformed and the pour was stopped once all the rebar had been covered for fear that they might collapse completely. The

`

result of this was a barrier section that was larger than the design section of the MTQ Type 201 barrier. The as-built average width of the barrier was 248 mm at the crest and 450 mm at the base, a 10% increase from design width (Figure 5-14).The as-built average height was 860 mm, 20 mm shorter than design (2% decrease). In Figure 5-15 the slight curvature of the barrier front face due to the increased deformation at the centre section can be seen as well as the concrete that spilled out along barrier-slab interface.

The effect of an increased sectional area relative to design caused the as-built barrier to be more rigid and resistant than the design barrier. This is an important point to take note of because it means the reference configuration used for this study had an improved structural performance. In order to avoid deformation of the formwork, the front and back faces of the barrier forms should have been connected with two threaded steel rods every 300 mm along the 6 m length.

Figure 5-12: Formwork Assembly and Fixation, Cast-in-place Barrier

`

Figure 5-13: Barrier Pour with Industrial Pump

Figure 5-14: Barrier As-Built Section

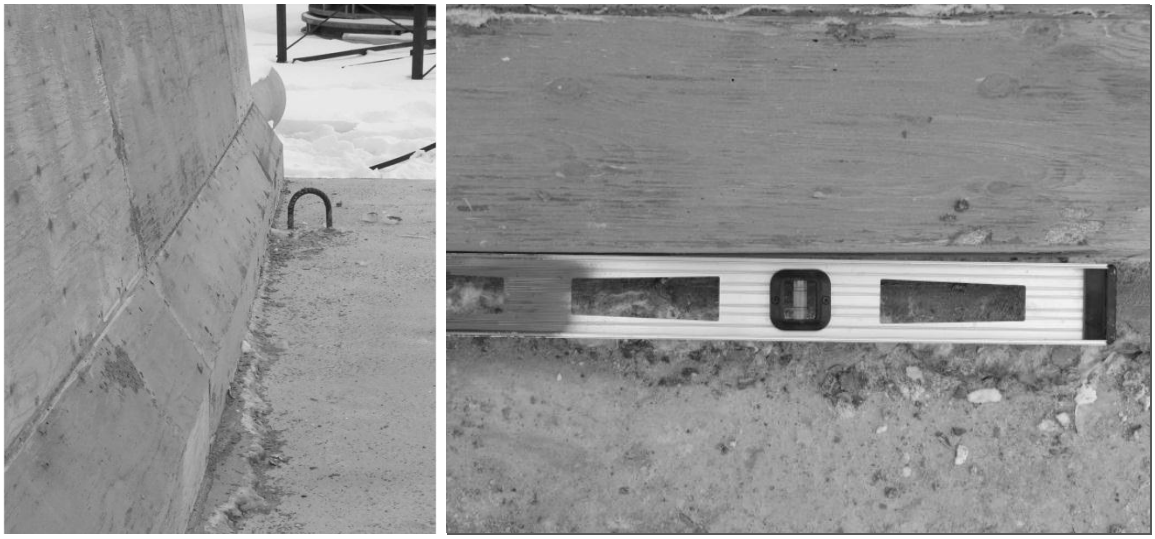

Figure 5-15: Barrier Joint Spill and Curvature

`

5.3.4 Precast Barriers

The precast barriers with and without shear connections were fabricated with the same methodology. The difference between the two configurations was limited to the forms of the barriers. One set blocked out the trapezoidal recesses at each end, which was used to incorporate a shear connection between barriers; and the other did not. The barriers were cast with 70 MPa HPFRC, which required a special mixing and pouring procedure. Six barriers were cast in two pours, one for the standard precast barriers and another for those with shear keys. The curing and form stripping procedure detailed in Duchesneau (2010) were followed.

The steel forms were supported on 4x4 blocks to improve the quality of the steam cure. Most of the form surfaces were simply cleaned and oiled. However, the surfaces that would be in contact with the injected mortar – recesses between barrier-and-slab as well as barrier lateral extremities – were coated with a EUCON Formula F surface retarder. The steel reinforcement was placed in the forms using plastic chairs and tied together. Holes were cut into the hollowed out recess between the barrier and slab to place the steel stirrups. The holes were sealed with a combination of extruded polystyrene (styrofoam) and duct tape. Once the forms surfaces were coated, the rebar placement was verified and the holes were sealed, the precast barriers were ready for casting (Figure 5-16). The preparation for the precast barriers was quick and easy.

Figure 5-16: Precast Barrier Pour Preparation

The 70 MPa HPFRC was mixed in a specific procedure to reproduce that used in the Structures Laboratory at Polytechnique Montreal where the concrete design was formulated. First the dry materials were loaded into the concrete truck. The sand and gravel were loaded at the mixing plant; however the cement could only be introduced manually. The cement at Béton Brunet was

`

incompatible with the admixtures in the HPFRC mix, and Holcim St. Laurence GU_{bSF} cement was shipped to the factory by big bag. Figure 5-17 indicates that the cement was then loaded into the truck with the aid of an overhead crane. Once the cement was added, the truck headed back to the mixing plant to load the water and admixtures. However, only 50% of the super-plasticizer was added at this time. The concrete truck proceeded to the casting area, and once there, the steel fibres were introduced into the mix by hand. The remaining quantity of super-plasticizer was also be added to the mix at this time. Once the 70 MPa HPFRC concrete was mixed the flow slump and air content were verified to ensure that the mix was adequate. The two-phased addition of the super-plasticizer was done to maintain an optimal concrete workability regardless of the delays inherent to the mixing process (adding 370 kg of steel fibres by hand and quality control checks).

Once the quality was assured, the concrete was cast into the forms and placed with the aid of an external vibrator and trowels (Figure 5-17). Internal vibrators are not compatible with FRC because the vibrators cause local segregation of the fibres. For similar reasons, only the flat surface of the trowels was used to move and compact the concrete. After pouring the concrete, the back sides of the barriers were finished and then a moistened polyethylene plastic was placed tightly over the exposed surface to maintain the finish.

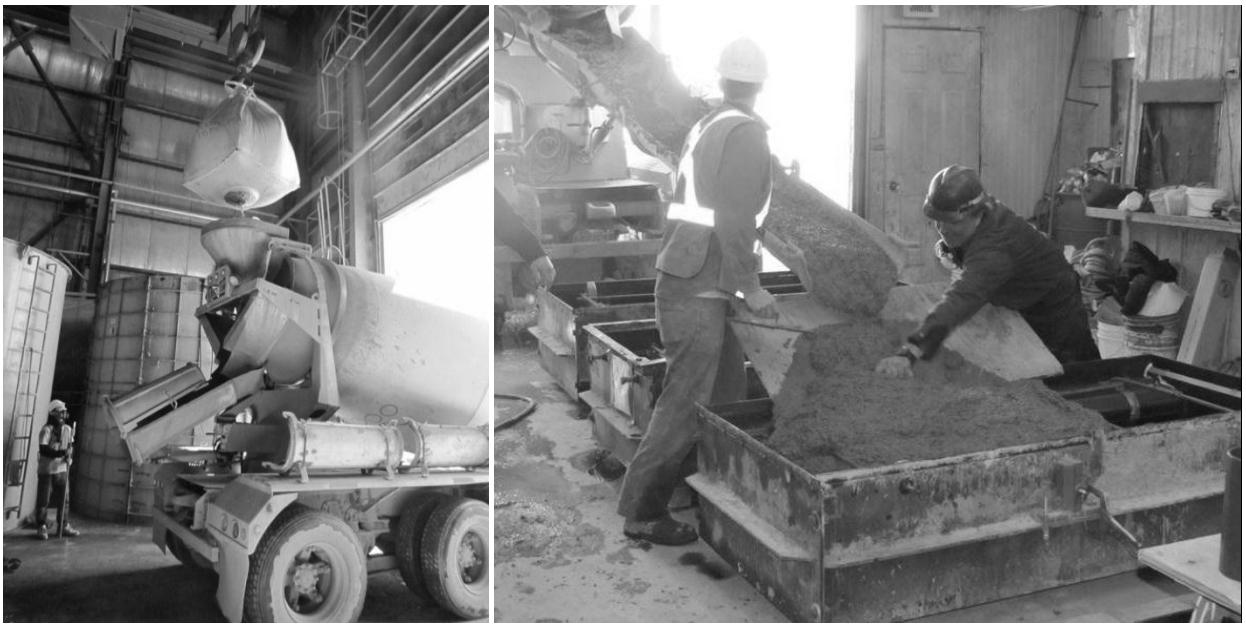

a) Loading Cement b) Casting

Figure 5-17: Precast Barrier Fabrication

`

The barriers were left alone throughout the night to allow the hydration process to start. The following morning the plastic seals were removed and steam curing began. The steam cure was stopped once the barriers reached a compressive strength of 25 MPa, at which point the formwork could safely be removed. Once the forms were broken down, a high pressure water hose was used to remove the surface mortar and expose the aggregate of the surfaces treated with the surface retarder. After which, the steam cure continued until the design strength was reached or a period of 7 days had passed, whichever came first.

During the casting of each set of specimens concrete was taken during the pour to cast 12 102 mm (4 in) cylinders as well as 4 concrete dog bone coupons for direct tensile tests (Delsol 2012). The tensile tests were used to define the HPFRC tensile stress-strain law for numerical modeling.

During the fabrication of the barriers, problems were encountered with the 70 MPa HPFRC used. The concrete had been previously formulated and verified at the Structures Lab at Polytechnique Montreal, and the fresh-state and hardened state properties of the concrete were very regular. The laboratory version of the HPFRC had a low air content between 1 and 2% as expected since no air entraining admixture was added to the concrete. However, when the concrete was mixed in the factory at an industrialized scale, the air content reached levels upwards of 10%. The air content increased dramatically after the introduction of the fibres and remaining super-plasticizer, during which time the concrete truck mixed the concrete at full capacity. It is believed that an unfortunate chemical reaction between the cement, the fibre glue, and the polycarboxylate super-plasticizer caused the high air content. It is possible that the cement fabricator changed their quarry source, or the fibre manufacturer changed the glue contents, both of which could cause the chemical incompatibility between the HPFRC components. The first attempt to cast the precast barriers had to be abandoned because the measured air content of 12% was too high. An increase by 10-11% of the air content from the design value would certainly diminish the resistance of the HPFRC to an unacceptable degree.

The HPFRC mix was changed to the mix design from Niamba (2009), which is a perfectly adequate mix from a mechanical perspective, but less workable and harder to pour and finish. Also, following consultation with experts from Euclid Chemical, a new product was brought to the pours that could potentially reduce air content within a concrete mix called EUCON Air Out.

`

The new mix design and EUCON Air Out made it possible to proceed with the barrier fabrication; however, it should be noted that the air content was always quite high, 8% for the Duchesneau barriers (no use of EUCON Air Out) and 5% for the barriers with shear keys (EUCON Air Out used). Table 3-3, the compressive and tensile strengths of the 70 MPa HPFRC concretes were lower than anticipated, and this is likely due to the increased air content. The general rule is that the compressive strength loses 3 to 5 MPa for every percent of air entrained. This is the case for a well dispersed network of air-bubbles within the cement matrix that would be created with an air entraining agent. The dispersion and shape of the air within these mixes is unknown, so the air content could have been even more detrimental to the concrete strength. Contrary to the fabrication defaults of the reference cast-in-place barrier, the reduced mechanical properties of the precast barrier HPFRC were unfavorable to the structural performance of the precast barrier test configurations.

As stated earlier, the new HPFRC mix had a reduced workability and an adequate compaction of the barriers was more difficult to ensure. During the pours, an external vibrator was used and the concrete was compacted manually with trowels. Still, there were several compaction voids on the front faces of the barriers. It is unlikely that the compaction voids had any effect mechanical performance of the barriers, but it was still not ideal for laboratory tests. The faces of the precast barriers were later patched up with plaster to improve their aesthetics. Figure 5-18 shows photos of a precast barrier before and after being patched up.

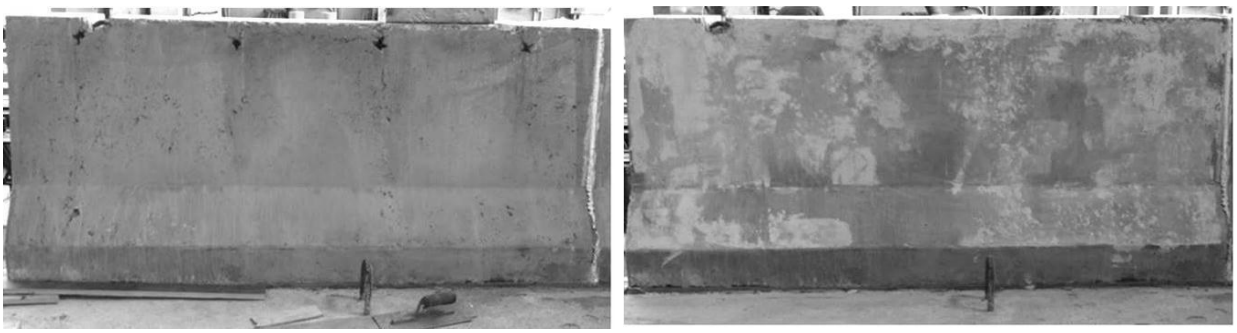

a) Before Patch Up b) After Patch Up

Figure 5-18: Precast Barriers Before and After Patch Up

5.3.5 Specimen Properties

Table 5-5 below and Table 3-3 from Section 3.2.4 give the fresh state material properties and hardened state mechanical properties of the specimens fabricated. As can be seen the average

`

compressive and tensile strengths of the 70 MPa HPFRC concrete used for the precast barriers is 53.5 MPa and 3.1 MPa respectively. Thus the concrete was much weaker than that used in the initial design of these barriers by Duchesneau (2010) with a compressive strength of 74 MPa (-28%) and tensile strength of 4.2 MPa (-26%).

Table 5-5: Specimen Fresh State Properties

Property	Cast-in-place Barrier & Slabs	Support Block	Precast Barriers[1]	Precast Barriers[2]	Injected Mortar	Loading Plates
Air Content, %	6.1	1.1	7.2	5.0	--	2.2
Slump Flow, mm	600	770	430	325	810	700
Temperature, °C	20.2	20.7	17.7	24.8	17.9	--
Density, kg/m^3	--	2425	--	2150	--	2530

[1.] Test Configuration 2. [2.] Test Configuration 3 (with shear key)

5.4 Experimental Setup and Procedure

The experimental scale for this project was quite large and an acute attention to the detail of the laboratory configuration, load application, installation, and assembly was very important. The primary objectives were to make sure that no laboratory personnel were injured, that no equipment was damaged, and that each test provided informative and exploitable results.

5.4.1 Laboratory Configuration

The laboratory setup consisted globally of the loading components: hydraulic actuator, supporting system, and loading apparatus; the specimens for each test: support block, slab, and barrier(s); and the anchoring system: post-tensioning bars, bearing plates, and lock nuts. The general setup was inspired by the projects of Duchesneau (2010) and Niamba (2009); however the details had to be modified in order to accommodate the larger scale and differing support conditions.

The loading equipment used was an MTS 1000 kN capacity hydraulic actuator. The challenge of the experimental setup was to adequately support the actuator during each test and apply the load to the barrier in a manner consistent with the previous experiments of Duchesneau (2010) and Niamba (2009). It was important to verify the response of the actuator during loading to make sure that 1 – the actuator would not be damaged by any lateral forces induced during loading (forces perpendicular to the actuator's strong axis), and 2 – that the displacements of the barrier

`

and cantilever slab would be compatible with the allowable movement of the actuator (within tolerances of semi-pinned connections and available piston stroke).

In the preliminary loading design taken from Duchesneau (2010) and Niamba (2009), the actuator was supported by a rigid column at the supported end with a semi-pinned connection, +/- 8°, and the loading end was simply supported with the piston and loading apparatus cantilevered from this support. The loading apparatus consisted of a fully pinned joint attached directly to the actuator load cell and a steel frame with an UHPFRC ram to apply the load onto the tested barrier (Figure 5-20). The loading ram had the specific 350x700 mm^2 surface as specified in AASHTO (1989) for PL-2 impacts. This design was well suited for previous tests where a 2 m barrier was anchored to a fixed, continuously supported slab and only the barrier was moving during loading. However, the slab overhang in the current setup was expected to displace and rotate during loading, significantly increasing the structure's flexibility. The increased flexibility of the structure presented certain incompatibilities with the preliminary loading design. One potential risk was that both articulated ends of actuator could activate forming a mechanism and the pinned connection nearest to the loaded end would displace vertically (Figure 5-19). Another that the contact between the UHPFRC ram and barrier could degrade as the barrier rotates relative to the ram (Figure 5-19). The reality would be some combination of both of these incompatibilities. To prevent either from occurring, two design changes were implemented. First, the pinned connection on the load end was removed. Second, instead of using the loading ram to control the surface area of load transfer, a loading plate was anchored directly to the barrier to control the surface of load transfer, and a rounded high performance steel profile, 75 mm radius or curvature, was used to apply the load (Figure 5-20).

In this configuration the friction forces and local deformation at the load application would have activated the pinned connection at the supported end and the loading forces would be resisted internally throughout the actuator's strong axis. However, the actuator would have been supported on one end by the loaded specimen. Not only creating lateral forces in the actuator piston due to its self-weight, but more importantly, the actuator support conditions would become dependent on the structural capacity of the loaded specimens. The actuator would have been vulnerable to a fragile failure within the structure, in which case it would be supported only with a semi-pinned connection at the far end. This was an unacceptable possibility, and a counter weight was installed to support the loading end of the actuator at all times during the tests.

`

The counter weight system consisted of a 3.5 m high steel frame built around the actuator with a pulley system on the top of the frame. 10 mm steel cables were used to connect the actuator to the suspended weight, and also to descend the weight all the way to laboratory basement (the cables passed through the post-tensioning ducts in the strong floor). A weight of nearly 1000 kg was necessary to balance the actuator, and it was built on top of a wooden platform loaded with laboratory materials, typically 40 kg bags of cement and 20 kg bags of steel fibres. The suspended weight was calibrated one bag at a time until the loaded end of the actuator was free standing and horizontally level. Figure 5-21 shows photos of the steel frame, cables, pulleys, and suspended weight. The counter weight eliminated the risks inherent to a brittle failure during loading, and removed the lateral forces due to gravity on the loaded end; thus effectively ensuring the protection of the MTS 1000 kN hydraulic actuator.

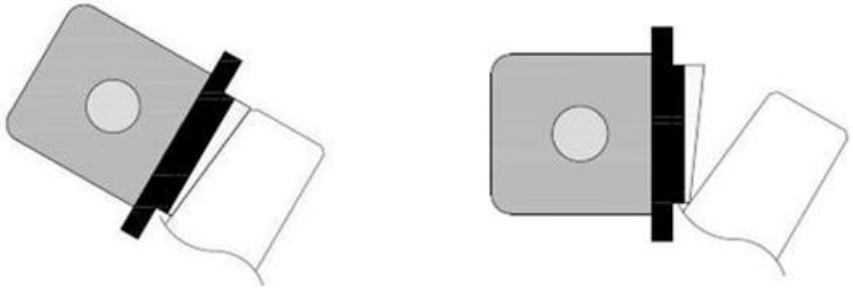

a) Loading Mechanism b) Loss of Loading Contact

Figure 5-19: Preliminary Loading Problems

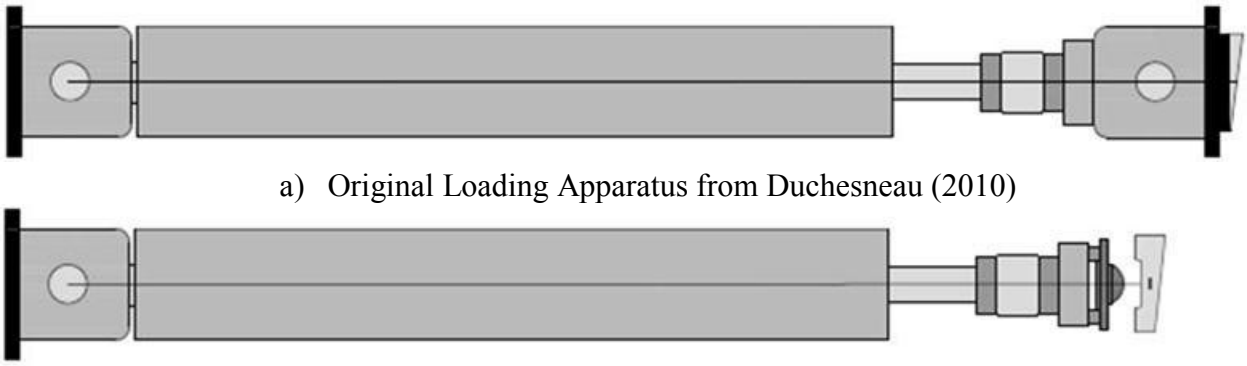

a) Original Loading Apparatus from Duchesneau (2010)

b) Modified Loading Apparatus

Figure 5-20: Loading Modification

`

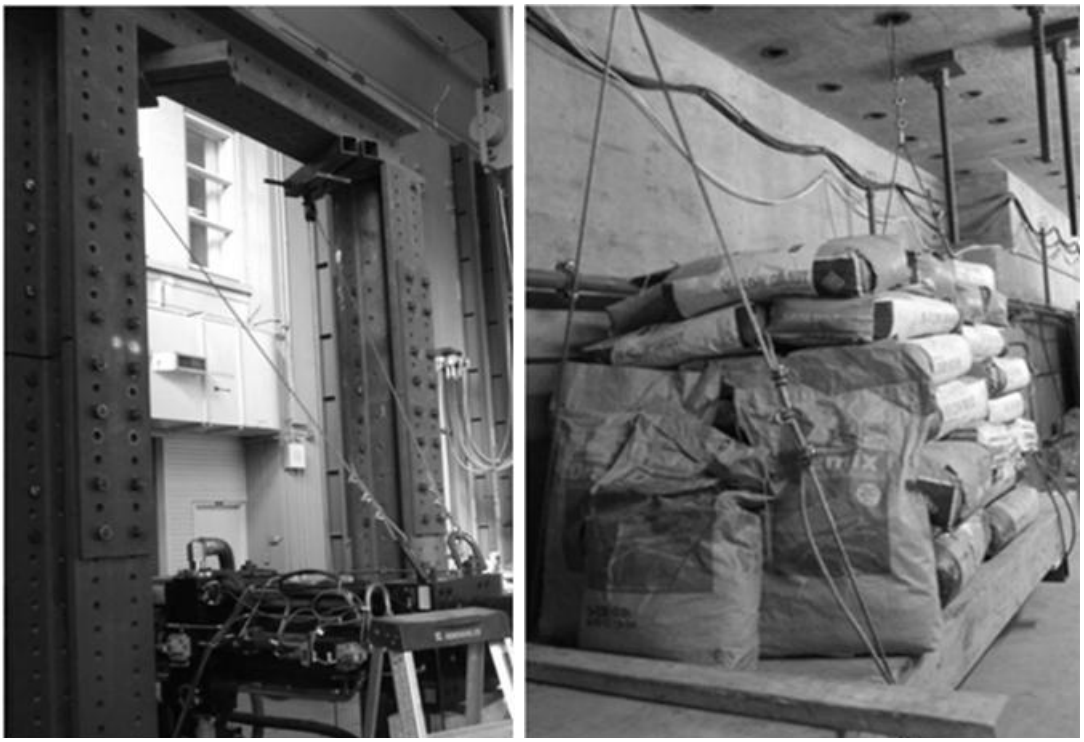

a) Frame, Cables, and Pulleys b) Suspended Weight in Lab Basement

Figure 5-21: Counter Weight System

The specifics of the load application still remained to be finalized; specifically the bearing resistance of the UHPFRC load transfer plate, and the allowable relative rotation between the rounded steel loading ram and the load transfer plate. The rounded steel ram was assembled with existing pieces from other projects at the lab.

Initially it was assumed that the UHPFRC load transfer plate would easily resist the bearing force of the loading ram. However, a check was carried out before testing. The CDH (2004) does not have any bearing formulas between rounded surfaces, and so the following formula from section [10.13] of the CSA S16.01 (2003) was used:

$$B_r = 0.00026\,\emptyset_{br}\frac{R_1}{1-{R_1}/{R_2}}\,L\,{f_y}^2, \text{where:} \qquad \text{Equation 5-1}$$

- ϕ_{br} is 0.67
- R_1, radius of the rounded steel member, is 75 mm
- R_2, radius of the load transfer plate is infinite

`

- L, length of load transfer, is estimated conservatively at 470 mm
- f_y of the UHPFRC is 105 MPa.

The resulting bearing force was only 68 kN signaling a big deficiency in the load setup. To compensate for this a 12.5 mm standard steel plate was placed between the loading ram and UHPFRC plate. Using the same formula, the bearing capacity of the steel plate was 980 kN. Still however, the bearing between the steel plate and the UHPFRC had to be checked, and the following formula from the CSA-A23.4 (2004) section [10.8] was used:

$$B_r = 0.85\,\emptyset_c f_c A_1, \text{where:} \qquad \text{Equation 5-2}$$

- A_1, the bearing area was calculated as 495 x 25 mm^2

The bearing between the two plates was 718 kN, which was at the very upper limit of what was expected, and this was considered adequate considering that material reduction coefficient was being used on what was a very small and well controlled concrete batch. The load transfer plate was also inspected after each laboratory test.

The rounded steel member was fixed onto a larger steel plate to connect it to the hydraulic actuator. It was possible that this plate and the load transfer plate could interfere with one another if there was sufficient relative rotation between the two. Figure 5-22 indicates the allowable relative rotation was finalized at 19° with the addition of an additional 12.5 mm plate between the rounded member and its backing. A 19° relative rotation was more than sufficient. Figure 5-23 shows the final load laboratory configuration schematically.

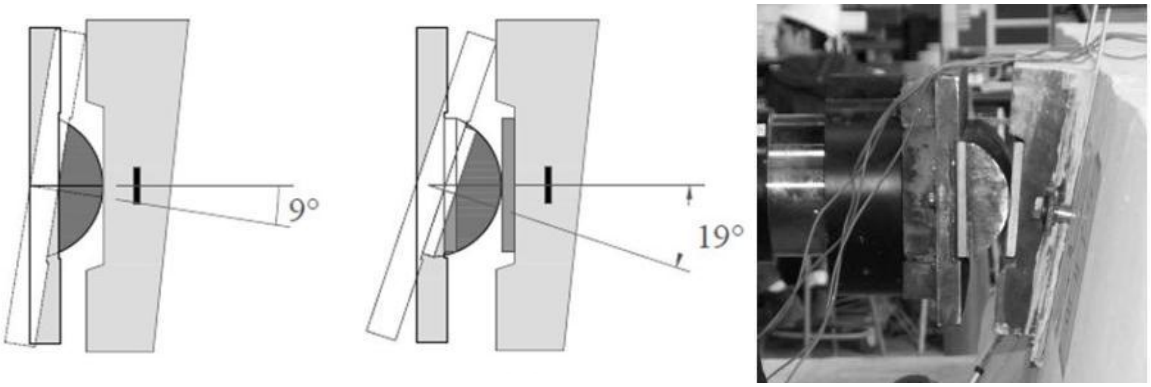

a) Initial Detail b) Final Detail c) Photo

Figure 5-22: Load Application Detail

`

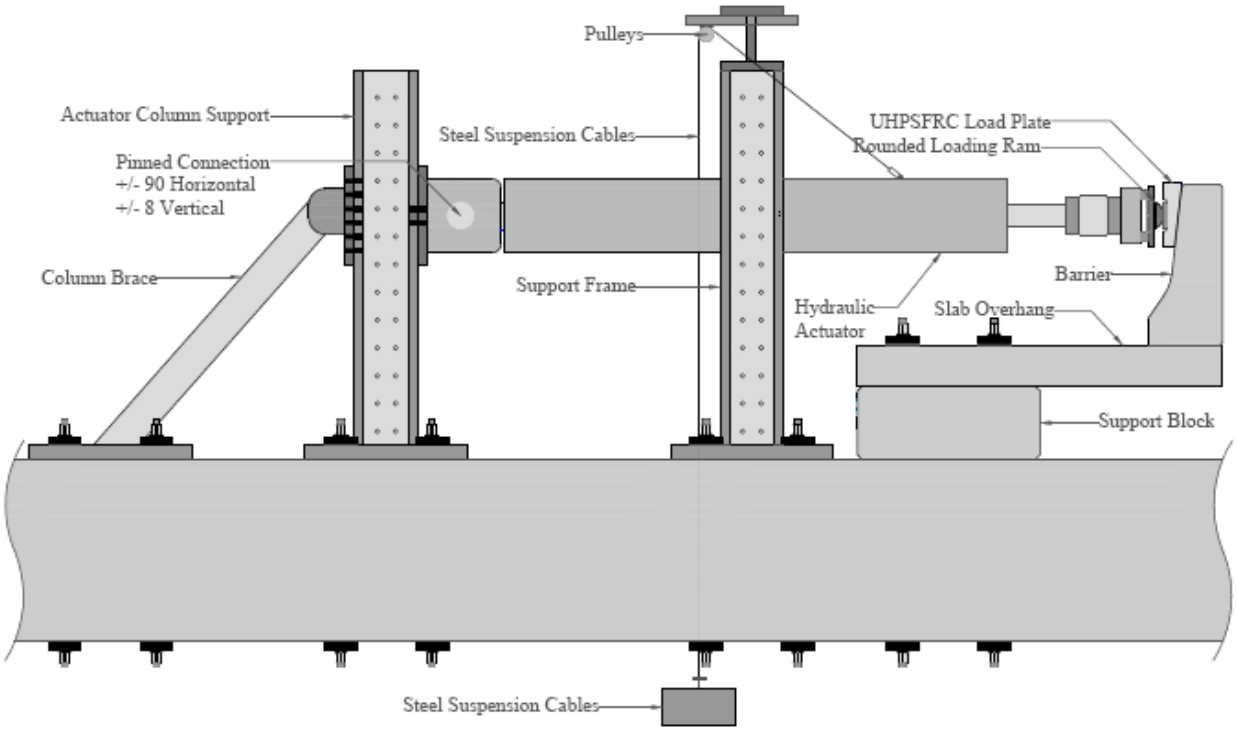

Figure 5-23: Final Laboratory Configuration

5.4.2 Installation and Assembly

For all three tests it was important to properly anchor the slab and support block to the laboratory strong-floor. The anchoring process was relatively straightforward. Post-tensioning ducts had been blocked out of the support block and slabs to match the existing pattern on the laboratory strong floor, holes at a 500 mm centre-to-centre spacing. The specimens were then positioned in place. The cantilever portion of the slab was temporarily supported, and leveled, using a 100 kN capacity hydraulic jack and a 102x102x12 mm HSS section was used to distribute the supporting surface. Once in place the post-tensioning bars were placed and stressed.

For the post-tensioning, 3.7 m long 36 mm diameter Dywidag threadbars were used with 178x191x41 mm^3 bearing plates. To avoid local cracking in the slab at the application of the post-tension forces, a thin layer of Ultracal, gypsum cement, was poured between the bearing plates and slab. The cement layer served to both level the surface and create a much improved contact between the plates and slab. Figure 5-24 shows the Ultracal layer as well as the molding used to place the plates. Dywidag bars have a cold rolled deformed pattern similar to a thread with a specified ultimate strength f_{pu} of 1030 MPa corresponding to 1048 kN, and a maximum

`

lock off stress of $0.7f_{pu}$ corresponding to 734 kN. However, the laboratory policy limits the lock off stress to $0.5f_{pu}$ equivalent to 524 kN, to guarantee the longevity of the bars.

Figure 5-24: ULTRACAL Layer and Placement Mold

The necessary post-tension lock off force for the bars was established through a numerical study at 350 kN for two rows of 8 bars centred on the specimen (total of 16 bars at 350 kN post-tension force total). During the post-tensioning two bars were always instrumented. It was noticed that there was often a significant loss between the maximum jacking force and remaining lock off force. The post-tensioning was applied in the laboratory basement from the bottom end of the bars. This meant that the jacking equipment had to be manually supported and gravity would not work to assure the vertical alignment of all the components. Thus the alignment of the bearing plates, hydraulic jack, load-transfer frame, and anchor nut all had to be verified visually and adjusted manually before jacking. It is likely that the losses occurred when these elements were skewed and the bar or anchor nuts shifted after lock off. Figure 5-25 shows a schematic of the post-tensioning equipment. The effective post-tension length of 1.7 m may also have contributed to the post-tension losses. The short post-tension distance means a smaller bar elongation (ΔL) was necessary to stress the bar, and conversely that any losses in elongation resulted in an amplified loss of prestressing force.

`

To minimize prestressing force losses, particular attention was paid to the alignment of all the jacking equipment, and a jacking force of 450 kN was reached before locking off in order to attenuate the effect of any prestressing losses. Finally, the solidity of the anchored bars was verified manually. These measures were used to ensure an adequate anchorage of the slab and beam specimens to the laboratory strong floor. During each test, the horizontal and vertical movement of the slab and beam were both measured and the results indicated that the specimens were well-anchored. However, it should be noted that with the exception of the two bars instrumented with load cells, there was no way to be sure of the final post tension force in the other Dywidag bars.

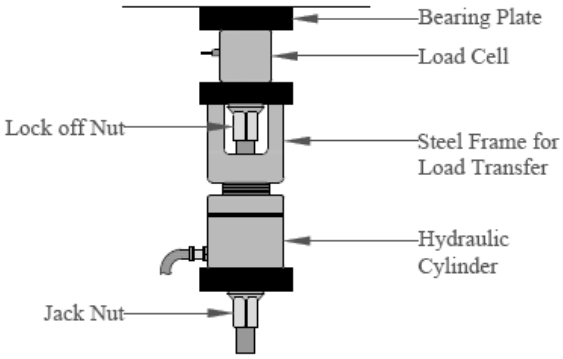

Figure 5-25: Post Tensioning Equipment

For the cast-in-place barrier configuration, the slab and barrier were fixed together before post-tensioning (anchoring); whereas the precast barriers were only installed once the slab was anchored in place.

The precast barriers were installed in much the same way as detailed in Duchesneau (2010). Before placing the barriers, a 5 mm layer of fresh mortar mix was spread over the barrier-slab contact. The contact zone was framed off with wooden forms fixed to the slab. This mortar bed was added to make sure the barrier was in full contact with the slab and to increase the contact properties (tension, cohesion, and friction) between the barriers and slab. Figure 5-26 shows the contact region with the fresh mortar layer just before placing a precast barrier.

`

Figure 5-26: Mortar Bed for Precast Barriers

In Figure 5-26 the soft rubber strips around the hollowed out recess can also be seen. These strips were glued to the specimen in the hope that they would help seal the joint between adjacent barrier.

After placing the barriers, the next step was the injection of the hollowed out sections of the barriers with the FRM. This step fixed the precast barriers to the slab, and a sufficient injection was absolutely critical to the performance of both precast configurations. To make sure of the injection quality, an optimization study on the fresh and hardened state properties of the mortar and an evaluation of the injection method were carried out. Both phases are detailed in Section

`

5.5 of this report. All three barriers with a total length of 6 m were injected at the same time from one end of the specimen to the other. To maintain pumping pressure, and to avoid important losses of mortar, all the joints had to be sealed off. The rubber strips added around the hollowed out sections at the barrier joints were meant to provide a seal, but in addition these joints were filled with expandable spray foam (soft insulation) and then completely sealed off with silicone. All the joints between the barriers and slab and the ends of the hollowed out recess were closed off with wooden boards and sealed with silicone. The pump used was a ChemGrout 50 mm displacement based air powered pump, with a maximum pressure of 2.76 MPa. The pump was fixed directly into the hollowed out recess with a steel pipe and sealed with duct tape. A photo of the joint preparation is shown in Figure, as well as the connection between the pump and recess.

a) Pump Connection b) Barrier-Slab Joint Seal

Figure 5-27: Mortar Injection Feed (left) and Joint Sealing (right)

The vertical pressure exerted by the mortar during the injection could be quite significant. Duchesneau (2010) had even experienced vertical uplift of the barrier specimens during this step. To protect against any vertical displacement of the precast barriers; the vertical movement of the barriers was restrained during the injection. Two 102x102x12 mm HSS sections were placed on the top of the barrier with wooden bearing boards at each end (HSS sections simply supported). As can be seen in Figure 5-28, a steel chain was then wrapped around each HSS and post-tensioned. Supports were aligned with the bearing boards under the slab overhang to make sure the slab was not damaged by the post-tensioning of the chains.

`

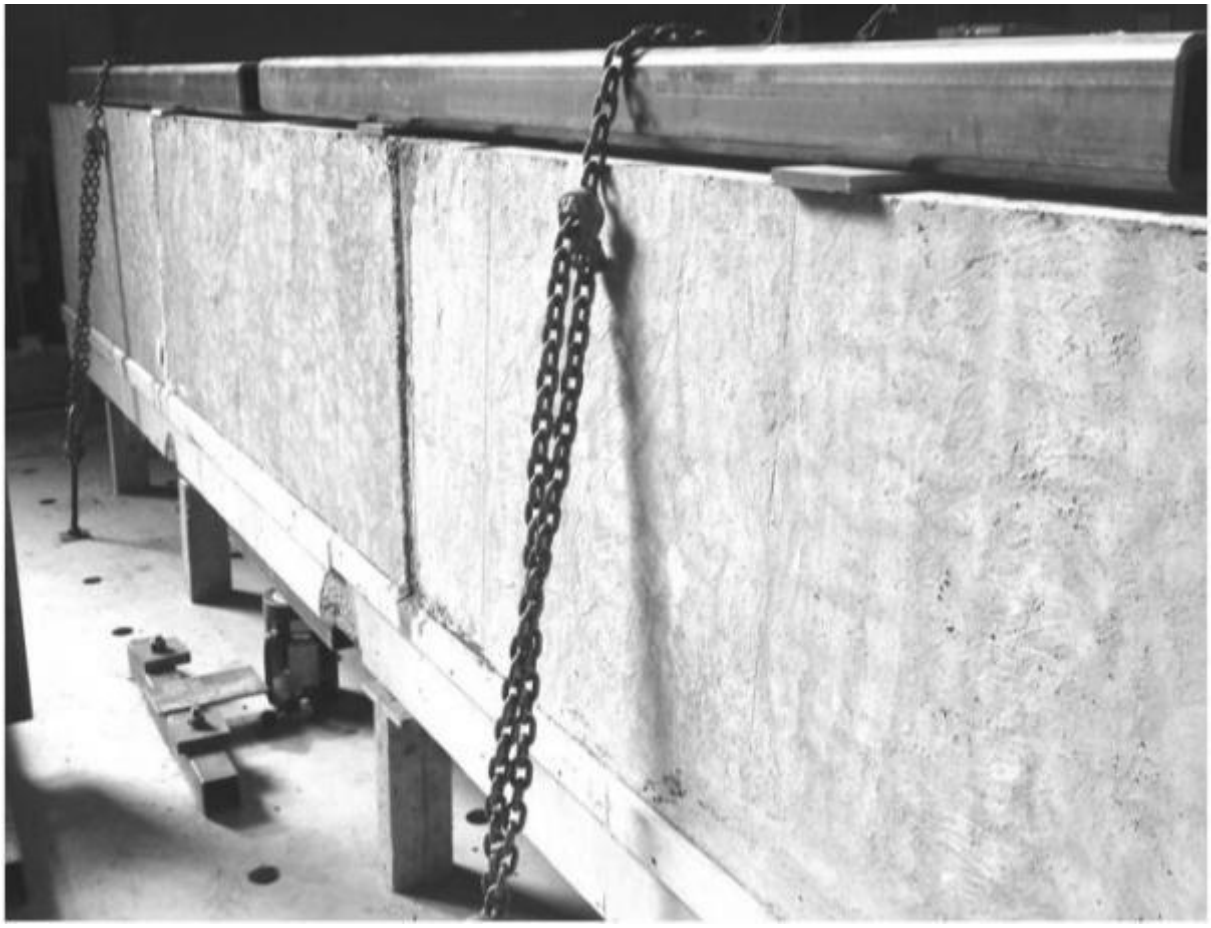

Figure 5-28: Temporary Vertical Restraint of Barriers

Figure 5-29: Ends of Hollow Recess after Injection

Photos of the ends of the injected recess are shown in Figure 5-29. The photos demonstrate the quality of the injections, the hollowed recess was completely filled at each end. The circular disturbances were due only to the injection intake, and air outtake pipes at the two ends. There was no indication that there were any air voids or pockets in the injected recess for either of the precast configurations.

For the precast configuration with connection, the same mortar was used to fill up the hexagonal recess between barriers. Figure 5-30 indicates that the seals between barriers began blowing out during the injection of the hollow recess between the barrier and slab, thus the voids in the shear keys were simply filled manually from the top opening on the following day. It should be noted, that with more functional seals there would have been no problem filling the shear keys at the same time as the hollow section of the barriers. Figure 5-30 also shows a photo of the finished shear key.

After the installation of the specimens they were all coated with a thin layer of latex based white paint cut at 50% with water. At this point each configuration was ready for instrumentation.

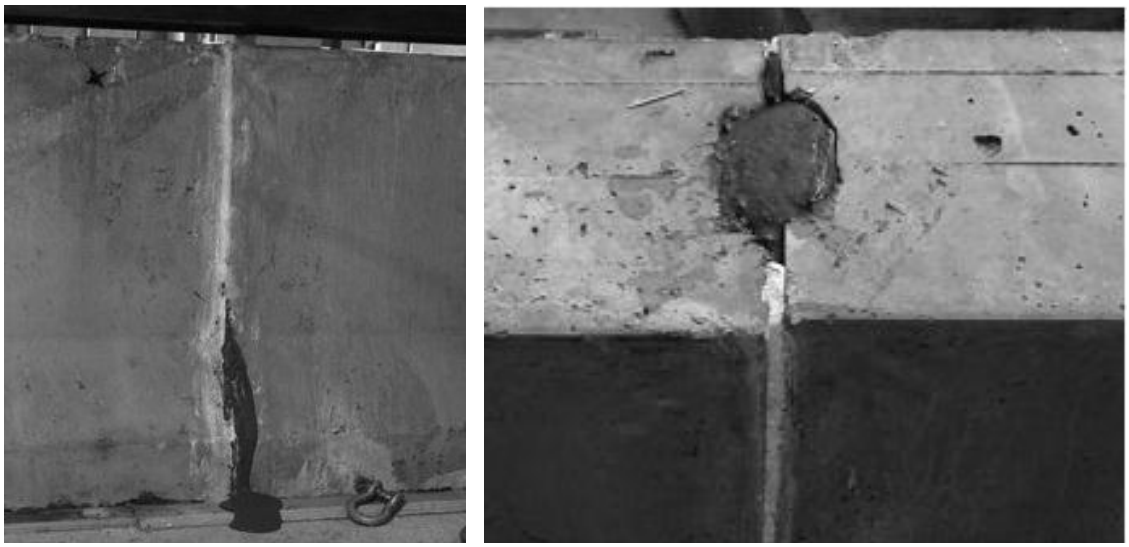

a) Joint Blowout b) Finished Shear Key

Figure 5-30: Joint Blowout and Shear Key

5.4.3 Instrumentation

To quantify the structural behaviour of each tested structure and to monitor the laboratory configuration itself, several potentiometers, strain gages and load cells were installed on the specimens before each test. An acquisition rate of 5 Hz was used for all the instrumentation

`

equipment. The complete instrumentation schematics and schedules for all three laboratory configurations are shown in APPENDIX B of this document.

The lateral displacement of the barrier directly behind the load application, and the vertical displacement of the slab provided important information about the structural rigidity and capacity. The lateral displacement was measured with a linear displacement transducer with pivot heads mounted on each end (pinned ends), and the vertical displacement with a cable-extension transducer. The typical installations used for both of these sensors are shown in Figure 5-31.

The linear displacement transducers with pivot heads were also used to measure the crack opening widths in the slab overhang and barrier front face; and the barrier uplift relative to the slab (barrier-slab crack opening width). These measures were all taken at the specimen mid-length (aligned with the actuator piston) and at a 1 m offset. The pivot heads were very useful because the pivots were fitted through 5 mm threaded rods, and the threaded rods could easily be fixed directly onto the specimen. The threaded rod placement also gave the precise location of where on the specimens the transducers measurements were taken from. Therefore, the precise length over which the crack opening measurements were taken was known, and the crack opening could be converted to strain. Figure 5-32 shows a typical installation of the transducers used to measure crack opening and relative barrier-to-slab uplift.

Two concrete strain gages were installed on the bottom face of the slab overhang directly opposite to the measures of the crack opening on the top face. Again, one strain gage was centred on the slab, and the other was offset 1 m.

Strain gages were glued onto one transversal reinforcing bar and one anchor bar – in a portion of the bar within the slab – for each test. Because the bars were not in pure tension, each bar was instrumented with a strain gauge on the tensile and compressive sides. The average reading between the two recorded measurements was used in order to better approximate the strain at the neutral axis of the bar, in addition to providing redundancy in case one of the gauges came unglued. The reinforcing bars selected for instrumentation were those at the centre section directly aligned with the actuator piston and load. The positioning of the gauges was selected to be representative of the highest strains within the bars.

Figure 5-33 shows how the longitudinal deformation of the barriers was measured over a length of 1.85 and 0.75 metres using linear transducers. The springs within the transducers were

`

compressed (counter-torqued) using rubber bands and then the actuating rod of the transducers was tied to a very stiff fishing cord, which was extended over the distance of the reading. Spacers were placed every 150 mm to maintain the same offset between the fishing cord and barrier throughout the measurement length. The rubber bands were not calibrated for these measurements, and the accuracy is not as high as the other measurements; however, these readings were used to gain qualitative insights into the longitudinal barrier deformation. For Test Configurations 2 and 3, a strain gauge was added to the front side of the barriers in order to compare the compressed and extended strains of the barrier as well as to read the barrier longitudinal curvature.

Finally, the instrumentation was also used to verify the laboratory configuration itself. Linear transducers were used to monitor the vertical and lateral movements of both the slab and support block throughout each test. This confirmed that there were no (or very little) rigid body movements (lateral sliding or vertical uplift) of the structure during loading. Two anchor bars were also connected to load cells. The load cells were used to quantify the post-tension force within these two bars and then to monitor the evolution during the tests.

The instrumentation for each configuration was very similar; however, some additional sensors were added to the tests with precast barriers. The lateral displacement at the ends of the loaded barrier and an adjacent barrier were taken in order to compare the relative barrier displacements between Configurations 2 and 3, without and with shear connections. There were also a couple of linear transducers with the actuator rods extended directly into the injected barrier recess and supported on the barrier (Appendix B Figure 4). The goal of these sensors was to determine at approximately what point the injected mortar and barrier begin separating from one another.

`

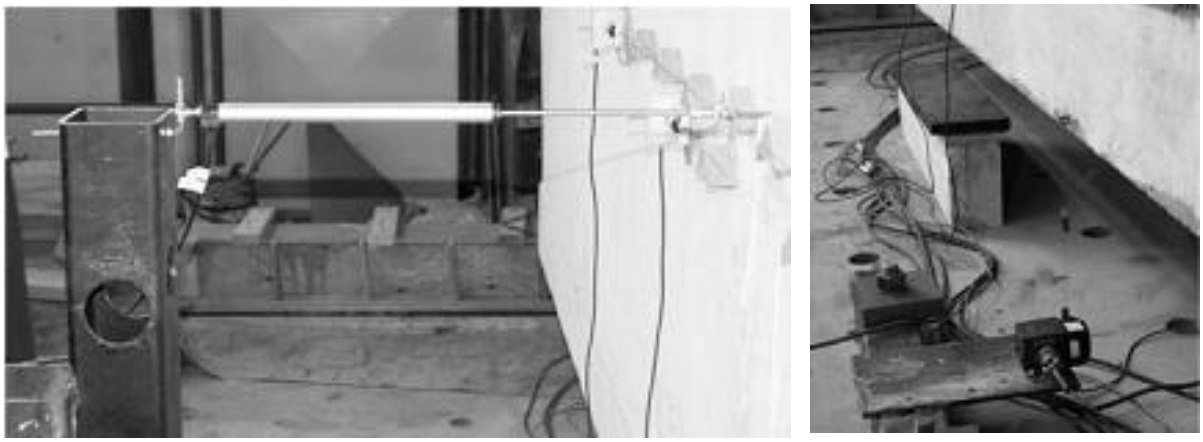

a) Lateral Displacement b) Vertical Displacement

Figure 5-31: Barrier Lateral and Slab Vertical Displacement Sensors

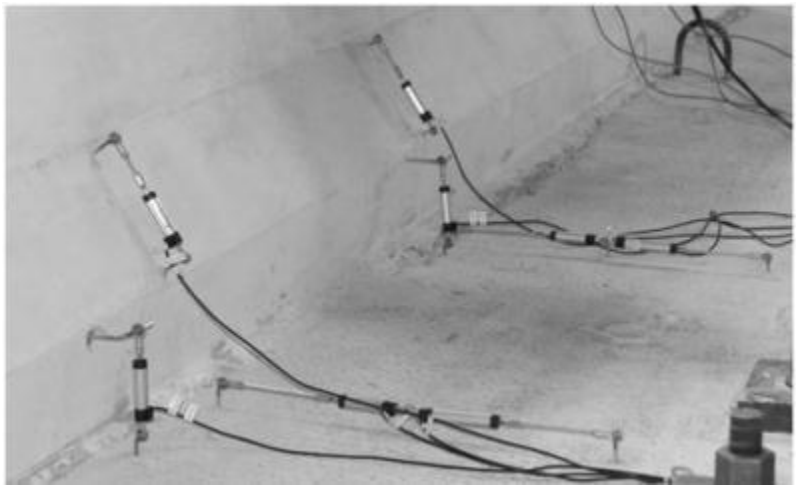

Figure 5-32: Barrier and Slab Crack Opening and Relative Uplift Sensors

Figure 5-33: Barrier Longitudinal Deformation Sensors

5.4.4 Load Application

Once the instrumentation setup was completed, the barriers were ready to be loaded. Before applying the load the UHPFRC loading surface was marked longitudinally at a height of 700 mm from the slab grade. This way the height of the loading ram would be adjusted such that the load was applied exactly at the 700 mm design height (CSA 2006). The steel plate added to the increase the bearing resistance had to be held manually. The plate was held while a small pre-load, between 3 kN and 5 kN, was placed on the barrier, securing all the elements in place. The contact between the rounded loading ram and the steel plate was then verified. A flashlight was placed underneath the load contact facing upwards and any passages of light indicated a gap. Because the actuator was pinned at the column end in both directions, it was adjusted to improve the load contact if necessary. After inspecting and approving the load contact, the loading procedure of the test began.

For each test, the barrier was loaded at 0.6 mm/min and the load was stopped at increments of 50 kN to inspect the specimens for damage. Once the structure yielded, the speed of loading was increased to 1.2 mm/min. Each laboratory test was terminated once the load had receded back to 150 kN or a complete fragile failure was imminent.

5.5 Mortar Injection Study

For Test Configurations 2 and 3, the injection of the hollow recess between the barrier and slab was the most important step of the installation process. The connection between these two components is dependent on the quality of the injection and the mechanical properties of the injected material. In order to ensure that this step was successfully implemented, a full study was dedicated to the injection method, and the fresh and hardened state properties of the FRM used for injection.

5.5.1 Injection Method

The injection method used for Duchesneau (2010), consisted of injecting the FRM mix with a displacement pump from one end of the barrier to the other. The two ends were completely sealed off with the exception of the mortar entry, fitted directly to the pump with a steel pipe, and an air outlet at the far end. The pump was placed above the hollowed section and the pipe was angled downwards (Figure 5-34), in order to use gravity to reduce the pumping resistance. The air exit,

`

extends diagonally upwards from the hollow recess as well. This was to make sure the injected mortar would only leave the hollowed section after the entire height of the recess would be filled. This injection method worked well for Duchesneau (2010), and the same method was adopted in this project.

However, the length of injection was increased by 300%, from 2 m to 6 m. The increased injection length meant a new balance would have to be found between the pumping pressure and mortar properties (initial flow rate, thixotropy, and structural buildup).

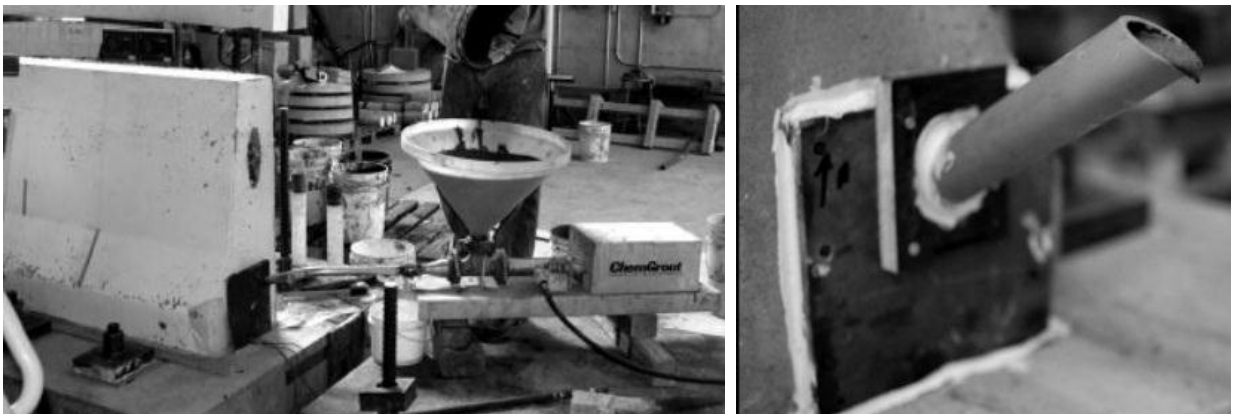

a) Pump Access b) Air Outlet

Figure 5-34: Mortar Injection, Pump Access and Air Outlet from Duchesneau (2010)

5.5.2 Mortar Mix Fresh State Properties

The initial mortar mix design was taken directly from Duchesneau (2010). The FRM used the EHFG ready-mix from Euclid Chemical which was combined with steel fibres (L = 10 mm, ϕ = 0.2 mm) and Conex (a shrinkage reducing admixture). The steel fibres were added in order to increase the rupture energy of the mortar, and the Conex was added to improve the barrier and injected mortar contact (less shrinkage). 25% of the water was added as ice in order to reduce the initial heat produced by hydration. Duchesneau's FRM mix design is shown in Table 5-6.

Preliminary tests on Duchesneau's mix indicated that the fresh state properties of the FRM mix were not suitable for a 6 m long injection. The flow rate of the initial mix was not high enough, and the structural buildup was too rapid. The self-leveling/self-compacting behaviour of the FRM was not assured for the entire injection. Following the advice of specialists from Euclid Chemical, a small increase in water content and the addition of Eucon 727 (set retarder and water

`

reducing admixture) were introduced to improve the rheological properties without significantly diminishing the mechanical behaviour of the FRM.

To test the effects of these two variables on the rheological properties of the fresh mortar, several tests were carried out on mixes with varying quantities water and Eucon 727. The temperature of the mix was taken 15 and 60 minutes after the onset of hydration to monitor the increase in heat due to hydration. Small cone and mini cone flow tests (ASTM C1437, 2007) were also performed 15 and 60 minutes after hydration in order to determine the evolution of the initial mortar flow rate and structural buildup. Finally, inclined plane tests (Khayat 2010) were performed immediately after mixing and subsequently every 20 minutes. The inclined plane provided an estimate of the static yield stress – the necessary shear to initiate flow – and was used to evaluate the evolution of the structural buildup of the FRM with time. The time interval of 60 minutes was selected because it was considered a conservative estimate of the time between hydration onset and the end of injection for the actual laboratory tests. This study was done to find an optimal amount of water and Eucon 727 to add to the original FRM mix. These two components could not be increased excessively because they both seemed to reduce the mechanical properties of the hardened FRM.

After this initial optimization study, subsequent tests were done to evaluate the influence of each component added to the EHFG ready-mix (Conex, fibres, ice, Eucon 727) on the rheological properties. In order to do this, each component was added independently to the EHFG mix and compared against a control EHFG mix without any additives. The same tests were carried out on the fresh mortar as before. The goal of this subsequent study was to determine if any modification in the proportions of the added mix components could improve the flow rate and reduce the initial structural buildup of the mortar mix.

These studies demonstrated that an increase in water content from 3.5 L to 3.65 L and an addition of 0.017 kg of Eucon 727 per bag of EHFG improved the initial flow rate of the mortar mix and reduced the structural buildup of the mortar. It was also observed that a higher proportion of ice content improved both the initial flow rate and decreased the speed of structural buildup. A final optimization study was performed to determine an optimal ice to water ratio. A 40% ice to water ratio was selected for the final FRM mixture.

`

The results of the FRM mortar optimization studies are fully explained in APPENDIX E, and the mix design is detailed in Table 5-6.

Table 5-6: FRM Mix Designs

Mix[1]	EHFG, kg	Conex, kg	Fibres, kg	Water, kg	Ice, kg	Eucon 727, kg
Duchesneau	22.7	0.33	1.014	2.190	1.460	0.000
Optimized	22.7	0.33	1.014	2.625	0.875	0.017

[1.] Mix designs are normalized to one bag of EHFG or 22.7 kg

5.5.3 Final Verification – FRM Injection and Mechanical Properties

After optimizing the FRM mix design, a final verification of the injection method and mortar mechanical properties was performed. The hollow recess of the Test Configurations 2 and 3 was modeled at scale using wooden forms (Figure 5-35).

The model recess was then injected with the optimized FRM. 250 L of FRM was necessary for the injection, accounting for potential losses and characterization specimens. This quantity exceeded the capacity of the largest concrete mixer in the structures laboratory and required the simultaneous use of three mixers; a pneumatic mixer and a portable electric mixer were used concurrently with the primary cement mixer in the structures laboratory. The pneumatic mixer was attached to the mortar pump and had a latch that, when opened, fed directly into the pump hopper (intake). The procedure of injection was therefore to produce all the FRM and bring it to the pump before beginning the injection. Once all the necessary FRM was produced the injection began. The mortar was always loaded into the pneumatic mixer before the pump to remix the FRM immediately prior to injection. During the fabrication process, the mortar remained stationary until loaded into the pneumatic mixer. For this reason the mortar was covered with plastic to reduce evaporation and mortar set, and also agitated again before injection to lower the viscosity of the previously stationary mortar through shear rejuvenation.

The model injection was very successful, and, as can be seen in Figure 5-35, the quality of the injection was impeccable. The last wooden board on the top of the model recess was left open until the final portion of the injection, in order to visually inspect the mortar flow. The observations proved that the FRM remained self-leveling and self-compacting throughout the

`

injection. During the model injection, both 100 mm cylinders and 50 mm cubes were cast to test the mortar compressive strength. Table 5-7 compares the compressive strength of the Duchesneau and optimized FRM mixes. The optimized mix is less resistant, which was expected because of the increased water/binder ratio and the addition of the water reducing admixture. However, the 7 day compressive strength still exceeded the 45 MPa minimal strength established by Duchesneau (2010).

The results of the mortar injection study confirmed that an adequate FRM mix and method had been found for the successful injection of the 6 m precast barrier hollow recess.

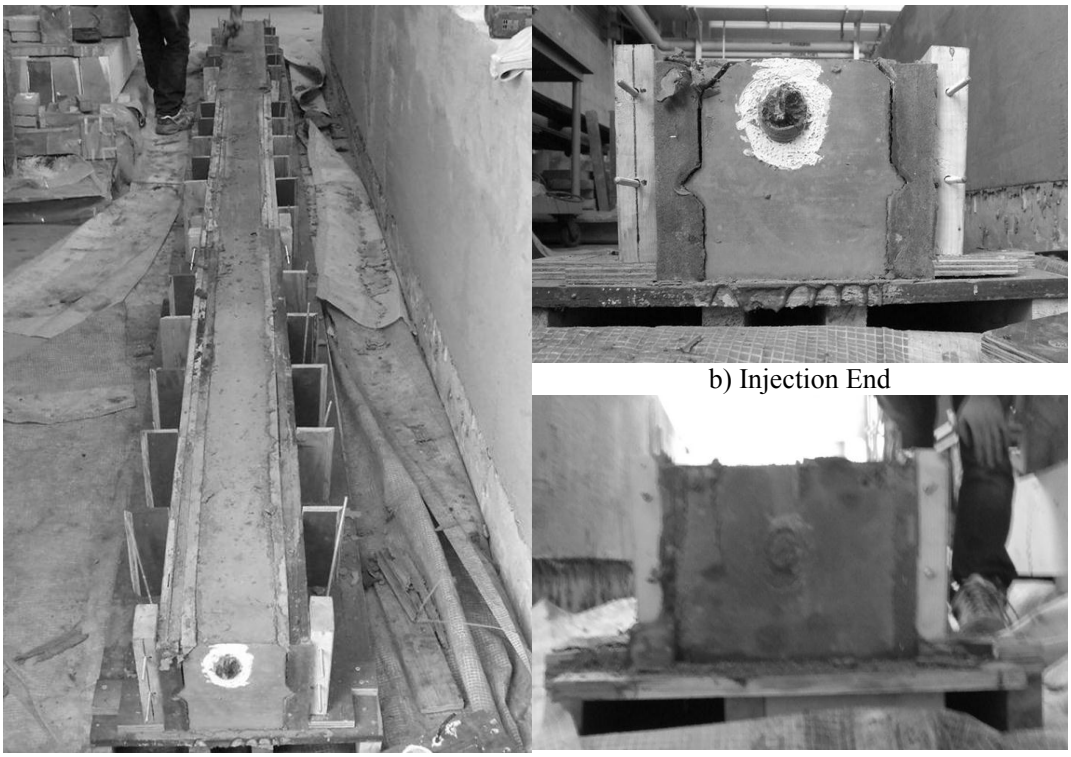

a) Overhead View

b) Injection End

c) Far End

Figure 5-35: Model Injection

Table 5-7: FRM Mix Compressive Strength

Age	Duchesneau	This Project	Difference
3	50.6 MPa	40.4 MPa	- 20.2 %
7	63.0 MPa	53.3 MPa	- 15.4 %
28	84.3 MPa	65.3 MPa	- 22.5 %

`

5.6 Complimentary Experimental Results

The results presented in this section are complimentary providing an improved comprehension of the data already presented in Chapter 3.

5.6.1 Barrier Longitudinal Strain

The LVDT's shown in Figure 5-33 measured the longitudinal tensile strain of the barriers' back face over 1.9 m and 0.8 m lengths. The longitudinal barrier strains recorded did not have the same precision as the other recorded displacements and deformations throughout the structure. However, analyzing the results of the longitudinal barrier strains are still indicative of each structures' behaviour during loading. In Figure 5-36, the strains are plotted against the applied load, and Table 5-8 compares the maximal barrier longitudinal strain for each test at intervals of 100 kN.

The increase in post-peak strain recorded over 1.9 m for Configuration 1 was due to the displacement associated with the shear failure and are not representative of the actual barrier longitudinal strain. The strain recorded over 0.8 m is always greater at a given load than the 1.9 m recording, this is logical because of the local barrier deformation at the load application. Apart from the post-peak behaviour of the curves, the longitudinal tensile strains measured on the barrier back face of the test configurations were relatively equivalent at a given load.

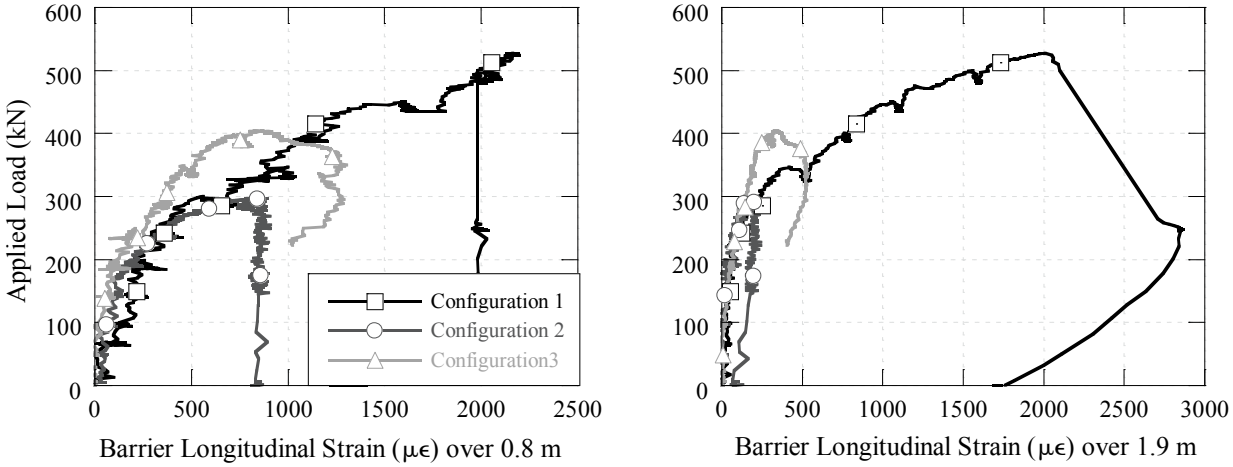

Figure 5-36: Applied Load vs. Barrier Longitudinal Strain

`

Table 5-8: Barrier Maximal Longitudinal Strain at Given Load

Load	Configuration 1 Strain, με	Configuration 2 Strain, με	Configuration 3 Strain, με
100	129	79	39
200	209	230	127
300	683	610	347
400	1181	--	804
500	2027	--	--
Peak	2170 at 527 kN	610 at 296 kN	870 at 405 kN
Cracking Force[1]	360 at 250 kN	--	800 at 400 kN

[1] Cracking force due to longitudinal curvature in barrier

The substantial longitudinal strain of the cast-in-place barrier indicates that an important component of the barrier deformation came from the longitudinal curvature. The peak strain in the cast-in-place barrier of 2170 με, taken over a 0.8 m length, means that the top rows of longitudinal reinforcement were likely yielded. The change in slope in the load vs. strain curve around 450 kN for Configuration 1 is also an indication of this (Figure 5-36). The concrete cracking and tensile stresses due to the barrier curvature certainly reduced the shear resistance of the concrete and thus the peak load as well.

The loaded precast barrier in Test Configuration 2 was 2 m in length and had no connections with the adjacent barriers. It can be seen in Figure 5-36 and Table 5-8 that, as the structure goes through its hardening phase between 200 and 300 kN, the longitudinal strain of the barrier increases significantly from 230 to 610 με. Once the structure began softening however, the longitudinal strain was completely unaffected and became constant. This behaviour implies that in the hardening regime the anchors initially yielded in the centre of the barrier and moved outwards until the anchors yielded over the entire 2 m length of the precast barrier. It is logical that during this phase the longitudinal strain of the barrier significantly increased, because the connection of the barrier to the slab is moving further away from the load. Once all the anchors yielded however, the failure mechanism essentially became a rigid body rotation of the barrier about the slab, which also explains why the longitudinal strain abruptly stopped in the softening phase.

`

In Test Configuration 3, the loaded precast barrier was connected to the adjacent barriers with shear keys. The connection between barriers had two noticeable effects when compared to Configuration 2.

The first effect was on the longitudinal strain read over a 1.9 m length. The information in Figure 5-36 was reorganised and zoomed in on in Figure 5-37 and Figure 5-38. Figure 5-37 demonstrates that there is almost a factor of 2 between the barrier strain read over 1.9 m at a given displacement between Configurations 2 and 3. Figure 5-38 demonstrates that in Configuration 2 the barrier strain is mainly localized behind the loading plate from the beginning of the test, whereas in Configuration 3 the localization only began after 240 kN. These differences are indicative of the longer load transfer width between the barrier and slab available for Configuration 3 with shear connections, which allowed tensile strain in the barrier over a greater length. The divergence between longitudinal strains read over 0.9 m and 1.8 m for Test Configuration 3 was likely due to a combination of the connection type (shear only) and the degradation of the connections as the applied load increased.

The second effect was the continued growth in barrier longitudinal strain at the beginning of structural softening. As the applied load decreased from 405 kN to 350 kN, the strains increased significantly (Figure 5-38). Thus the shear keys were degrading quickly after the peak load. This confirms that some load transfer between barriers was still occurring in this range of loading as the loaded barrier was not only rotating about the slab in a rigid-body type movement. The relative uplift between the barrier and slab offset 1 m from the load (measured in the exterior barrier) was also increasing in this softening range. This supports the argument that loads were still being transferred between the barriers in Test Configuration 3.

`

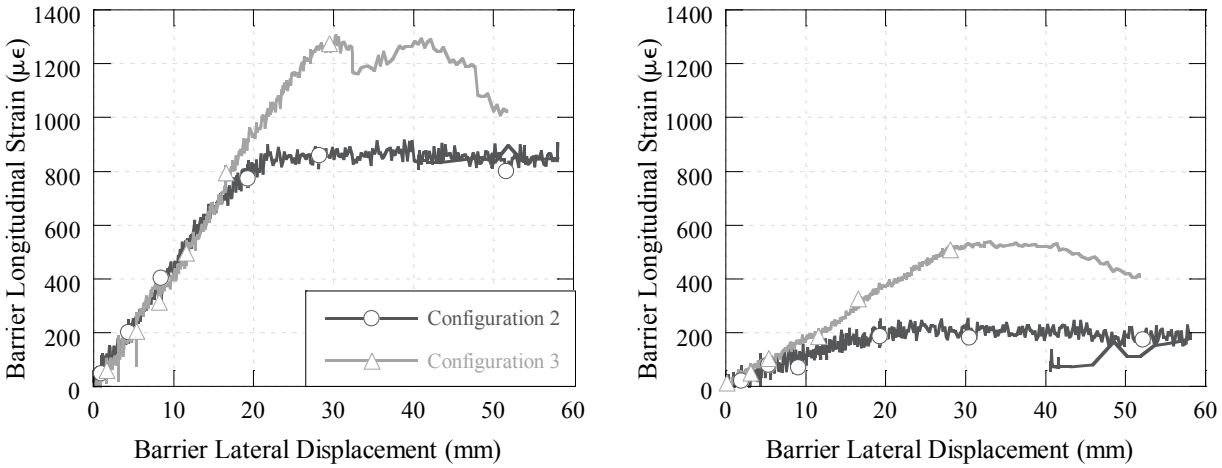

a) 0.8 m Strain Reading Length b) 1.9 m Strain Reading Length

Figure 5-37: Barrier Longitudinal Strain vs. Barrier Lateral Displacement

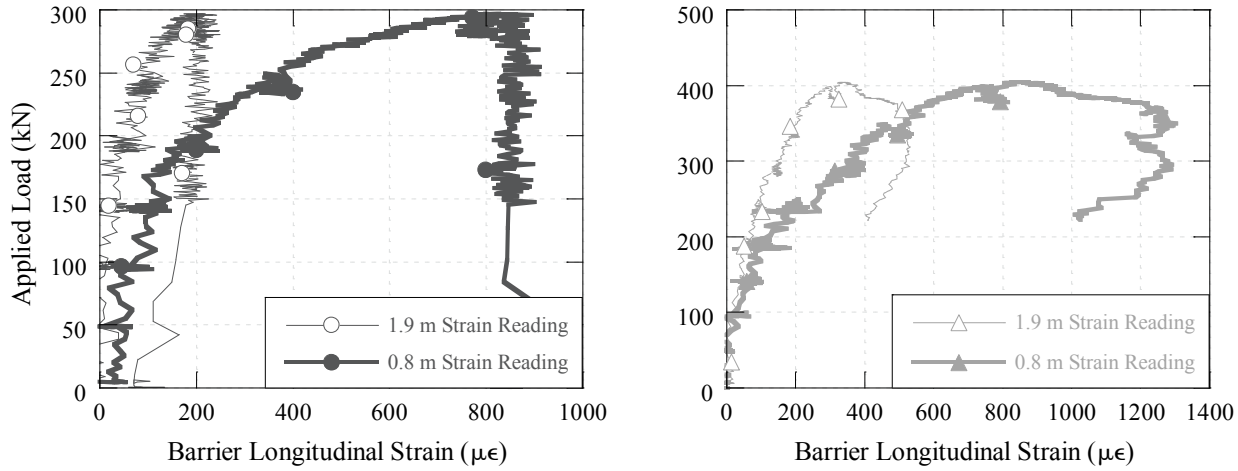

a) Test Configuration 2 b) Test Configuration 3

Figure 5-38: Applied Load vs. Barrier Longitudinal Strain

5.6.2 Relative Barrier Displacement (Precast Barriers)

For Test Configurations 2 and 3 with precast barriers, the lateral barrier displacement was measured at the edges of both the loaded and exterior barriers to determine the relative displacement between them. Figure 5-39 shows the instrumentation location. Unfortunately, the portion of the exterior barrier instrumented sheared off in Test Configuration 3, thus the measure of relative displacement was not meaningful. However, visual inspections were carried out during the lab test as well, and up to a load of 400 kN no relative displacement between the barriers was observed (Figure 5-40).

`

The graphs in Figure 5-41 show the displacements recorded for both the loaded and exterior barriers in Configurations 2 and 3. The relative displacement remained very small until a load of 170 kN was reached in Test Configuration 2. It should be noted that there was some torsion noticed in the structure during the test, and the relative opening between loaded and external barriers on the opposite (non-instrumented) end was visually more noticeable. This is apparent in Figure 5-42 comparing the relative displacement of the two joints at an applied load of 200 kN for Configuration 2.

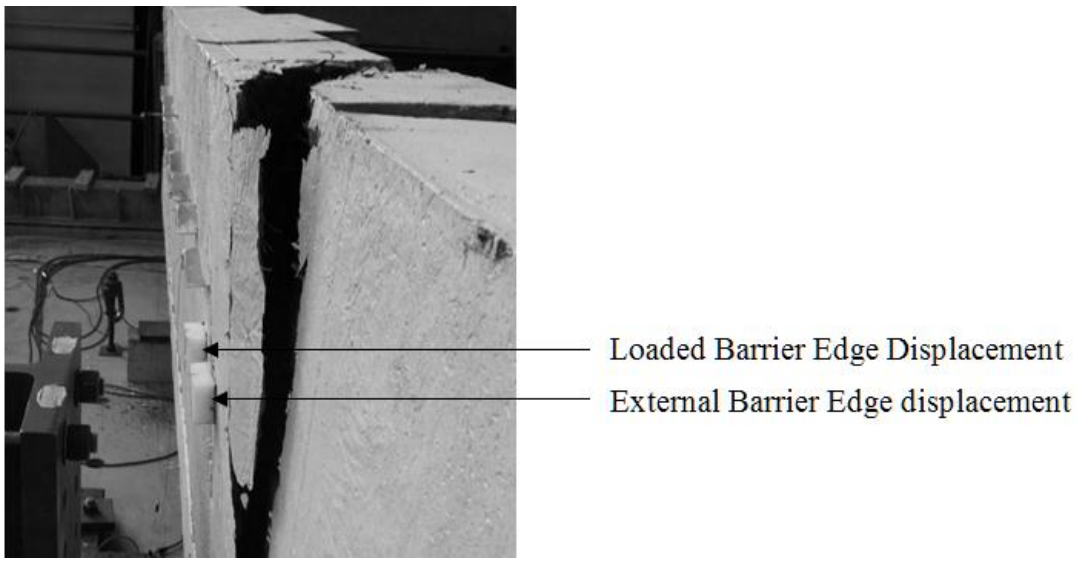

Figure 5-39: Instrumentation Location for Barrier Edges for Relative Lateral Displacements

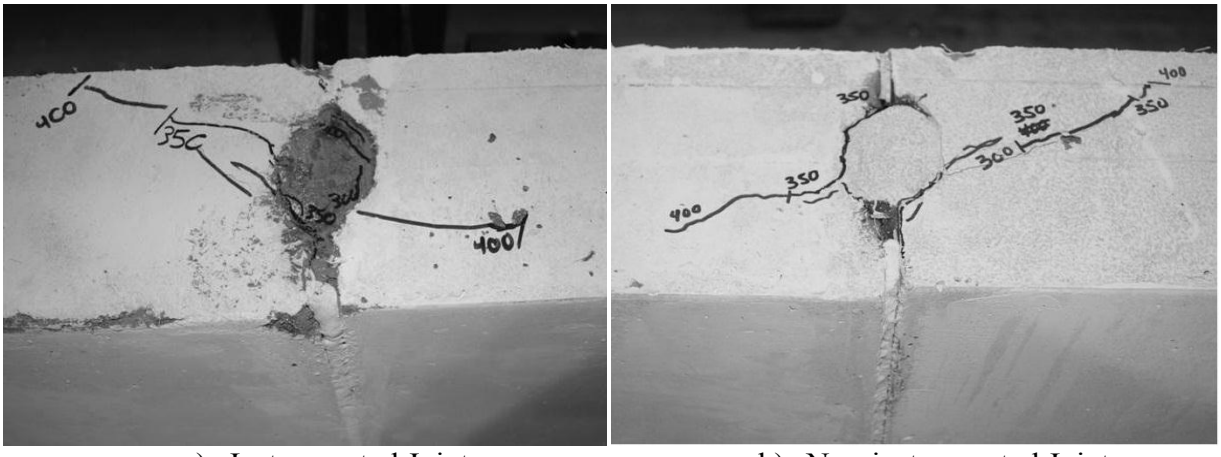

a) Instrumented Joint b) Non-instrumented Joint

Figure 5-40: Barrier-to-Barrier Joints at 400 kN for Test 3

`

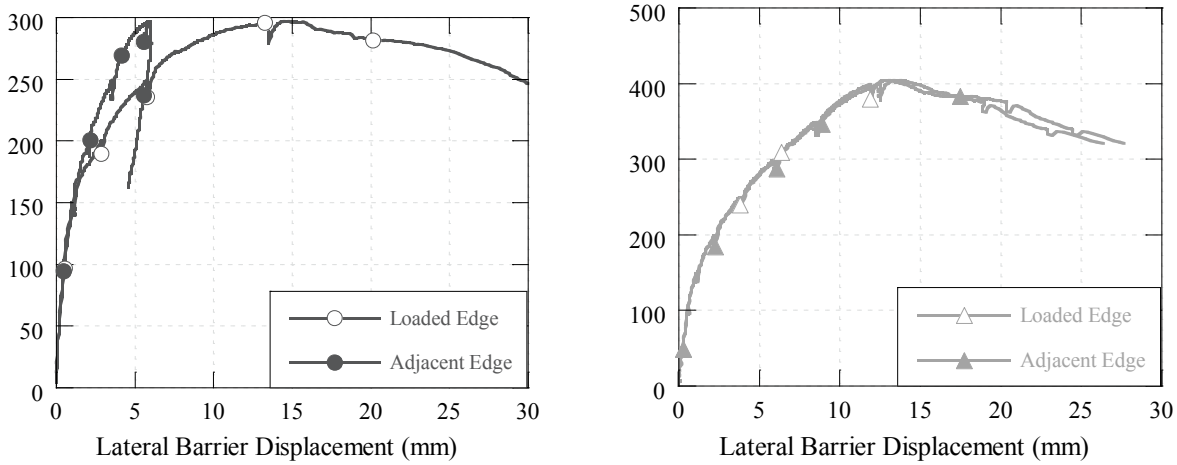

a) Test Configuration 2 b) Test Configuration 3

Figure 5-41: Relative Displacement Between Loaded and External Barriers

a) Non-instrumented Joint b) Instrumented Joint

Figure 5-42: Test Configuration 2 Relative Barrier Displacement at 200 kN Applied Load

In Configuration 2, the recorded relative edge displacements between the loaded and exterior barriers began diverging at an applied load 170 kN, and were noticed visually starting 180 kN. Considering that there was no mechanical connection between these barriers, it means that either the deformations in the injected FRM initially caused the external barriers to displace with the loaded barrier, or that during the injection some of the FRM entered the joint and provided a certain degree of adherence (friction and cohesion) between the barriers. It is likely that both of these processes occurred concurrently and worked together to limit the relative barrier displacements up to 170 kN.

The visual inspections during testing of Configuration 3 showed that the shear key was extremely effective at transferring the lateral displacements between barriers. It was only after the peak force, when the shear cracks in the external barriers coalesced and began opening, that there was any relative displacement. Figure 5-40 shows an overhead view of a barrier joints at an applied load of 400 kN. The shear cracks were highlighted, while they remained closed almost no relative displacement could be discerned. Figure 5-40 indicates that shear cracks in the barriers were observed between 300 and 400 kN, which corresponds precisely to the hardening phase of the structure. It is reasonable to believe that if the shear forces were better resisted, for example with a higher performance FRC, an optimized reinforcement detail at the barrier ends, or an improved fibre orientation, then Test Configuration 3 would have continued to behave in a manner very similar to Test Configuration 1 with the cast-in-place barrier.

5.6.3 Slab Overhang Transverse Strain

The slab overhang for each laboratory test was instrumented to measure the crack opening widths on the top face and compressive strain on the bottom face at slab mid-length and at a 1 m offset. Figure 5-43 shows the instrumentation and the sectional strain profile. The data collected by these sensors provide valuable comparative data for analysis. Figure 5-44 shows graphs comparing the slab compressive strain against the applied load. The compressive strains indicate that cracking began in the slab overhang at a load of 150 kN in Configuration 1 and 200 kN in Configurations 2 and 3, this is corroborated by visual data at the location of strain gauges and crack opening width sensors (Figure 3-5). The rates of strain change with respect to the applied load were very similar until Configurations 2 and 3 began yielding. The compressive strain at the centre section for Test Configurations 2 and 3 were indicative of slab yielding at applied loads of

`

290 kN and 370 kN respectively. The yielding behaviour is not apparent in the offset section for Configuration 2.

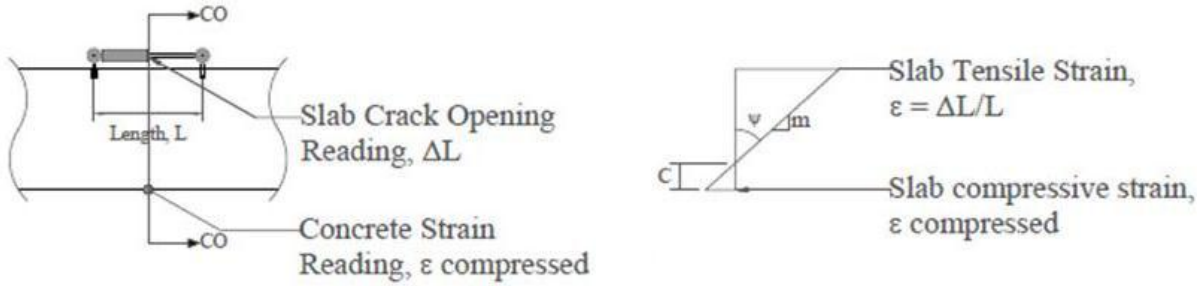

a) Slab Overhang Section CO - CO

Figure 5-43: Slab Overhang Instrumentation

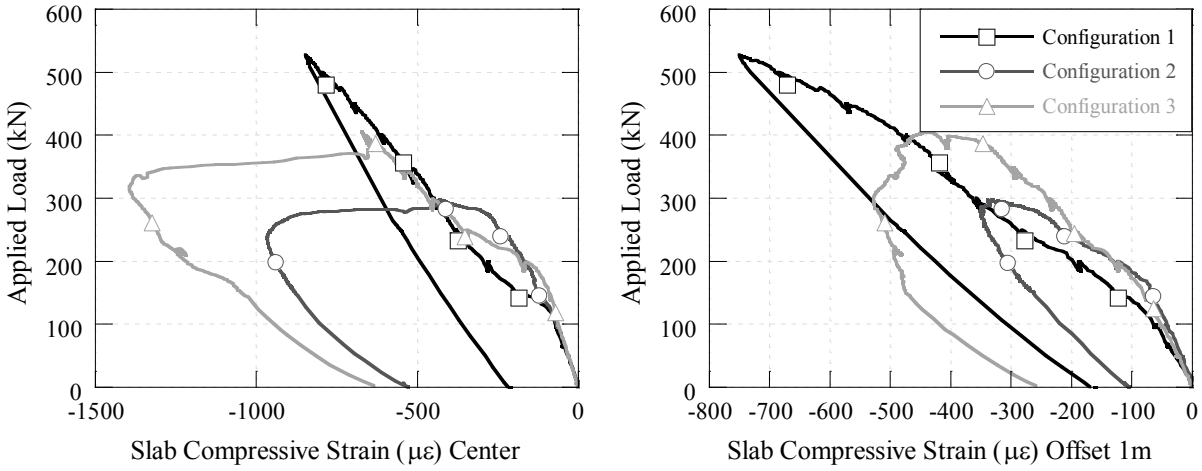

Figure 5-44: Slab Overhang Compressive Strain

The section analysis within the slab overhang demonstrated that globally the slab overhang was solicited in a similar manner for each of the three testing configurations (Figure 5-44). The two notable differences are one, the load at which the overhang begins to damage, and two, the yielding behaviour in Test Configurations 2 and 3 that is not present in Configuration 1.

The cracking of the slab overhang in Test Configuration 1 with the cast-in-place barrier is consistent with all the other observations and recorded data. In the curve comparing the vertical slab displacement against the applied load in Figure 3-3, the vertical displacement was higher in Configuration 1 between 150 kN and 300 kN than in Configurations 2 and 3. The vertical displacement of the slab was primarily controlled by the curvature within the slab overhang region. Figure 5-45 shows the damage visually observed in Configurations 1 and 3 at 150 kN (the

`

transverse cracks in both specimens were present before loading due to shrinkage, transportation, and post-tensioning pre-stresses). A longitudinal crack runs almost 4.5 m in length along the slab overhang for test 1, whereas in test 3 only a 1 m longitudinal crack was observed, which did not yet run under the crack opening instrumentation. It is important to note that the crack opening instrumentation in the slab overhang can be seen on the 3D damage reconstruction.

The cause of the earlier cracking load of the slab overhang for the cast-in-place configuration is difficult to clearly identify. It may be explained by a weaker concrete composition, more significant slab damage prior to loading, the different barrier base width, or even the more significant weight of the cast-in-place barrier. Another possibility is that the confinement in the slab beneath the barrier due to the restrained shrinkage actually induces an initial negative moment in the overhang due to Poissons effect. The increased cracking of the overhang in this load range is important, because it is a load that a bridge barrier would likely be exposed to throughout its life-cycle. However, it is also possible that the lower cracking force of the slab overhang is due to a particularity of the slab itself rather than intrinsic difference between the cast-in-place and precast barrier configurations.

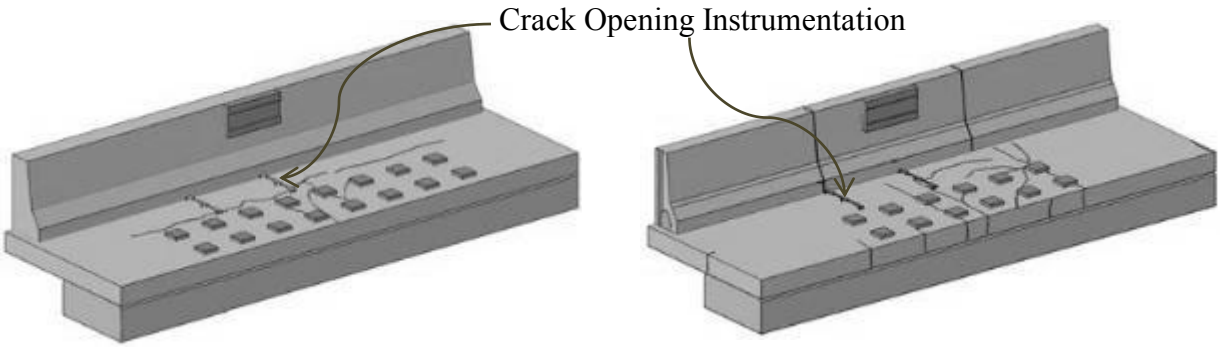

a) Configuration 1 at 150 kN b) Configuration 3 at 150 kN

Figure 5-45: Structure Damage at 150 kN

The yielding behaviour within the slab overhang apparent in the recorded compressive strain at the centre section is indicative of a fundamental difference between the 3 configurations (Figure 5-44). The slab overhang for the cast-in-place configuration is only beginning to yield at an applied load of 527 kN, whereas the compressive strain at the centre section indicates yielding at 300 and 400 kN for Configurations 2 and 3 respectively. The earlier yielding is once again specific to the load transfer length between the barrier and slab. It is interesting that the yielding evident in the centre section of slab for Test Configuration 2 was not recorded at all in the offset

`

of 1 m. The yielding of the slab overhang for the precast specimens is therefore highly local. Comparing the compressive strain between Configurations 1 and 3 again highlights the importance of the shear key between precast barriers. The compressive strain behaviour in Configuration 3 is very similar to that of Configuration 1 until a load of 350 kN was achieved. This load corresponds precisely to the coalescence of shear cracks in the exterior barriers at the barrier-to-barrier connection (Figure 5-40). The logical conclusion is that the higher the load for which the shear key between barriers is functional, the longer the precast barrier configuration will behave similarly to the cast-in-place configuration.

5.7 Complimentary Numerical Modeling

The following section provides complementary information to the numerical models and results presented in Chapter 4. The results of other parametric studies are also detailed and analysed.

5.7.1 Model Information

The material formulations and the mesh dimensions used in the ATENA models are detailed in Table 5-9 and Table 5-10.

Classical material formulations are used with the exception of the *Nonlinear Cementitious* formulation used to model the concrete behaviour. The mesh was refined in areas of significant fracture damage observed during the experimental tests for each respective configuration. For the numerical reproduction of Test Configurations 2 and 3, the tensile behaviour of the HPFRC was experimentally determined and entered into the *Nonlinear Cementitious (USER)* formulation. Numerical modeling with ATENA in the past has demonstrated that best results are obtained for the USER formulation when the minimum mesh dimension and the physical crack band are set equal to one another in the areas of expected fracture (Beaurivage 2009, Niamba 2009, Duchesneau 2010). The crack band (disturbed width during crack localization) for the HPFRC with a max aggregate size of 10 mm and fibre length of 30 mm was estimated at 35 mm. The mesh was most densely refined on the central portion of the barrier around the load application for Configuration 1; on the front face of the loaded barrier for Configuration 2; and on the two exterior barriers in the vicinity of shear transfer as well as on the front face of the loaded barrier for Configuration 3. Figure 5-46 show the surface mesh used for the simulations of Test Configuration 1 and 2 (see Figure 4-3 for Test Configuration 3).

`

Table 5-9: ATENA Material Formulations

Model Elements	Material Formulation	Details
Concrete Barrier and Slab	Nonlinear Cementitious	Fracture-Plastic model using Rankine failure criterion and smeared crack formulation
Steel bar and plates	Von Mises Plasticity	Bilinear stress-strain behaviour. Elastic limit defines onset of plastic flow, no hardening.
Reinforcement	Reinforcement	Uniaxial truss element with bilinear stress-strain law.
Post-tension bars	Reinforcement	Uniaxial truss element with bilinear stress-strain law, contact only at anchor points.
Support Block	Elastic Isotropic	Elastic and isotropic material behaviour.
Reinforcement Bond	Bigaj (1999)	Stress-slip model based off of concrete strength, bond quality, and rebar dimension.

Table 5-10: Mesh Dimensions

Structural Component	Test Configuration	Material	General Mesh Dimension, mm	Refined Mesh Dimension, mm
Slabs	1, 2, and 3	HPC	56	--
Cast-in-Place Barrier	1	HPC	100	55
Precast Barriers	2 and 3	HPFRC	100	35
Injected Sections	2 and 3	FRM	50	35

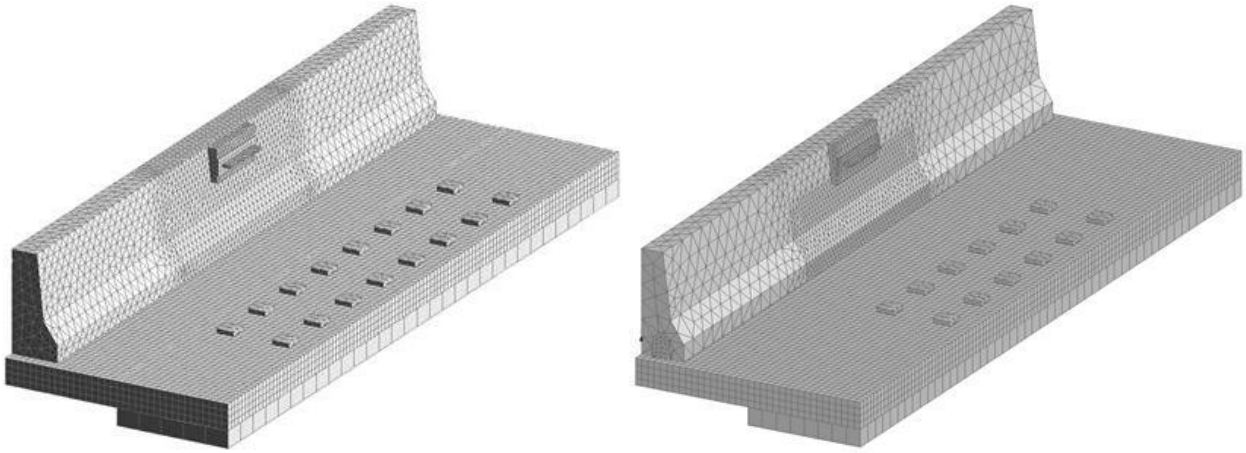

a) Test Configuration 1 b) Test Configuration 2

Figure 5-46: Test Configurations 2 and 3 Models Surface Mesh

`

5.7.1.1 Load and Support Conditions

The loading configuration was an important aspect of the numerical models. Experimentally, the load was applied by the steel actuator with a high-performance rounded steel ram, and a thin steel bearing plate / UHPFRC bearing plate were used to distribute the load onto the barrier. In the numerical model, the steel and UPHFRC load transfer plates were physically modeled with their experimentally determined material properties. The actuator and loading ram were modeled with an overly rigid bar in order to reproduce an accurate loading rigidity. The experimental and numerical loading conditions are shown in Figure 5-47. A gap contact element (Table 5-11) was added between the loading bar and steel plate to allow the bar to rotate relative to the plate during loading (the actual geometry of the loading ram was not used for calculation reasons). The properties were determined through a trial-and-error process to provide for the rotation and maintain numerical stability. Gap contacts were also added between the UHPFRC plate and barrier as well as the steel post-tensioning plates and the slab. These contacts were used to limit the transfer of shear stresses at these interfaces and prevent the UHPFRC or steel plates from externally reinforcing the concrete. The contact properties are given in Table 5-11 as mortar-to-concrete since a layer of mortar was poured at the joint between the plates and barrier or slab.

The support conditions were imposed on the support block. The bottom face of the block, which in reality was in contact with the laboratory strong floor, was fixed in the vertical and longitudinal directions, and the transversal movement of the block was controlled with a surface spring, k = 833 kN/mm, to match experimental results.

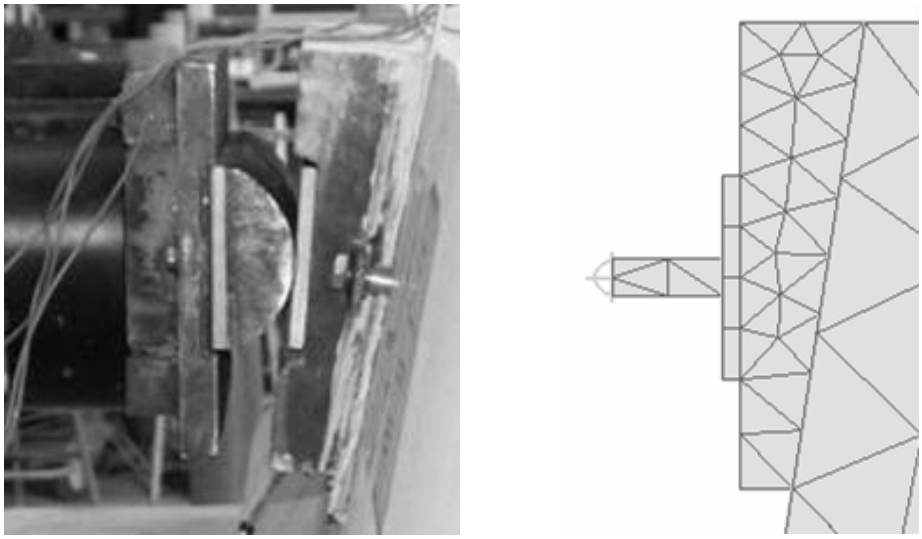

a) Actual Load Configuration b) Numerical Load Configuration

`

Figure 5-47: Load Application

Table 5-11: Gap Element Contacts

Contact	ϕ	Tension (MPa)	Cohesion (MPa)
Load bar to Steel Plate	1.0	0.0	0.2
Mortar to Concrete	0.8	0.1	0.5
Barrier to Barrier[1]	0.6	0.0	0.17

[1] Only used for Configuration 2 models to account for barrier friction

5.7.1.2 Loading Steps

Reproducing the initial state of each configuration, particularly the effects of shrinkage strain, was necessary to accurately model the structural rigidity, strength, and failure mode. Table 5-12 and Table 5-13 detail the numerical steps before displacement loading.

In Test Configuration 1, the barrier was cast directly on top of the hardened slab and the shrinkage was fully restrained. In Test Configurations 2 and 3, the barriers were precast and the shrinkage was not restrained by the slab. In addition the precast barriers had 60% less steel reinforcement than the cast-in-place barrier. For these reasons, it was not necessary to model the barrier shrinkage for Configurations 2 and 3. The ATENA construction cases feature was used to apply the slab shrinkage before the barriers were included in the numerical model. It should be noted however, that it proved impossible to apply the slab shrinkage without the support block, and therefore the slab shrinkage was restrained by the support block. Only 17% of the post-tension force was applied until the slab shrinkage was complete. This, in addition to the contact elements added between post-tension plates and slab, helped to limit incidental slab damage during shrinkage loading. The slab overhang and barrier stresses before displacement load application are shown in Figure 5-48 (tensile stresses are positive). The barrier tensile stress in Configuration 1 is much higher than for Configurations 2 and 3 because of the restrained shrinkage. Moreover, the barrier has cracked which has relieved stress on the concrete surface.

`

Table 5-12: Test Configuration 1 Model, Pre-Loading Steps

Step	Construction Cases	ATENA Load Cases	Load
1	1 – Block and Slab	S[1], 17 % Post-tension[2]	60 kN Post-tension
2	1 – Block and Slab	S, Body Force	Block and Slab weight
3	1 – Block and Slab	S, Shrinkage	150 με slab shrinkage
4	1 – Block and Slab	S, Shrinkage	150 με slab shrinkage
5	2 – Block, Slab, and Barrier	S, Body Force	Barrier weight
6	2 – Block, Slab, and Barrier	S, Shrinkage	150 με barrier shrinkage
7	2 – Block, Slab, and Barrier	S, Shrinkage	150 με barrier shrinkage
8	2 – Block, Slab, and Barrier	S, 83 % Post-tension[2]	290 kN Post-tension
9	3 – All	S, Prescribed Deformation	0.15 mm displacement

[1] Support Conditions, [2] Post-tension applied in steps to reduce slab restraint during shrinkage

Table 5-13: Test Configurations 2 and 3 Models, Pre-Loading Steps

Step	Construction Cases	ATENA Load Cases	Load
1	1 – Block and Slab	S[1], 17 % Post-tension[2]	60 kN Post-tension
2	1 – Block and Slab	S, Body Force	Block and Slab weight
3	1 – Block and Slab	S, Shrinkage	150 με slab shrinkage
4	1 – Block and Slab	S, Shrinkage	150 με slab shrinkage
5	2 – All	S, Body Force	Barrier weight
6	2 – All	S, 83 % Post-tension[2]	290 kN Post-tension
7	2 – All	S, Prescribed Deformation	0.15 mm displacement

[1] Support Conditions, [2] Post-tension applied in steps to reduce slab restraint during shrinkage

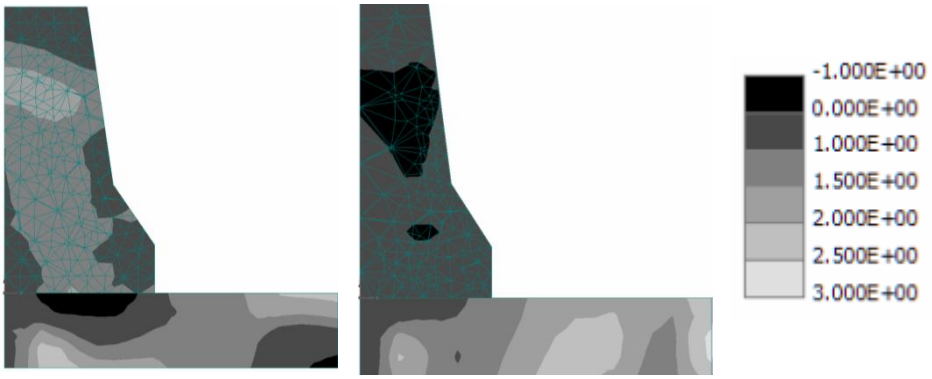

a) Configuration 1 b) Configurations 2 and 3 c) Scale (MPa)

Figure 5-48: Numerical Models, Pre-Loading Stresses, Centre Section

5.7.1.3 Numerical Model Validations

The numerical simulations were generally able to reproduce the experimental data very well. Figure 5-49, Figure 5-50, and Figure 5-51 provide comparison between experimental and numerical for complementary results for Test Configurations 1, 2, and 3, respectively. Other results are described in Chapter 3 and Chapter 4.

The vertical barrier (bending) displacement is underestimated for Test Configurations 1 and 3 starting at around 275 kN of applied load. This is likely because the slab mesh was limited to 4 rows of mesh elements due to computational limitations. The FE software manual (Cervenka 2011) recommends at least 6 rows to well reproduce bending behaviour. The slab strain and anchor strain are often overestimated in the numerical models. It should be noted that the strain recorded is a function of the discrete location of the concrete cracks, the strain rates are generally parallel between the experimental and numerical models.

`

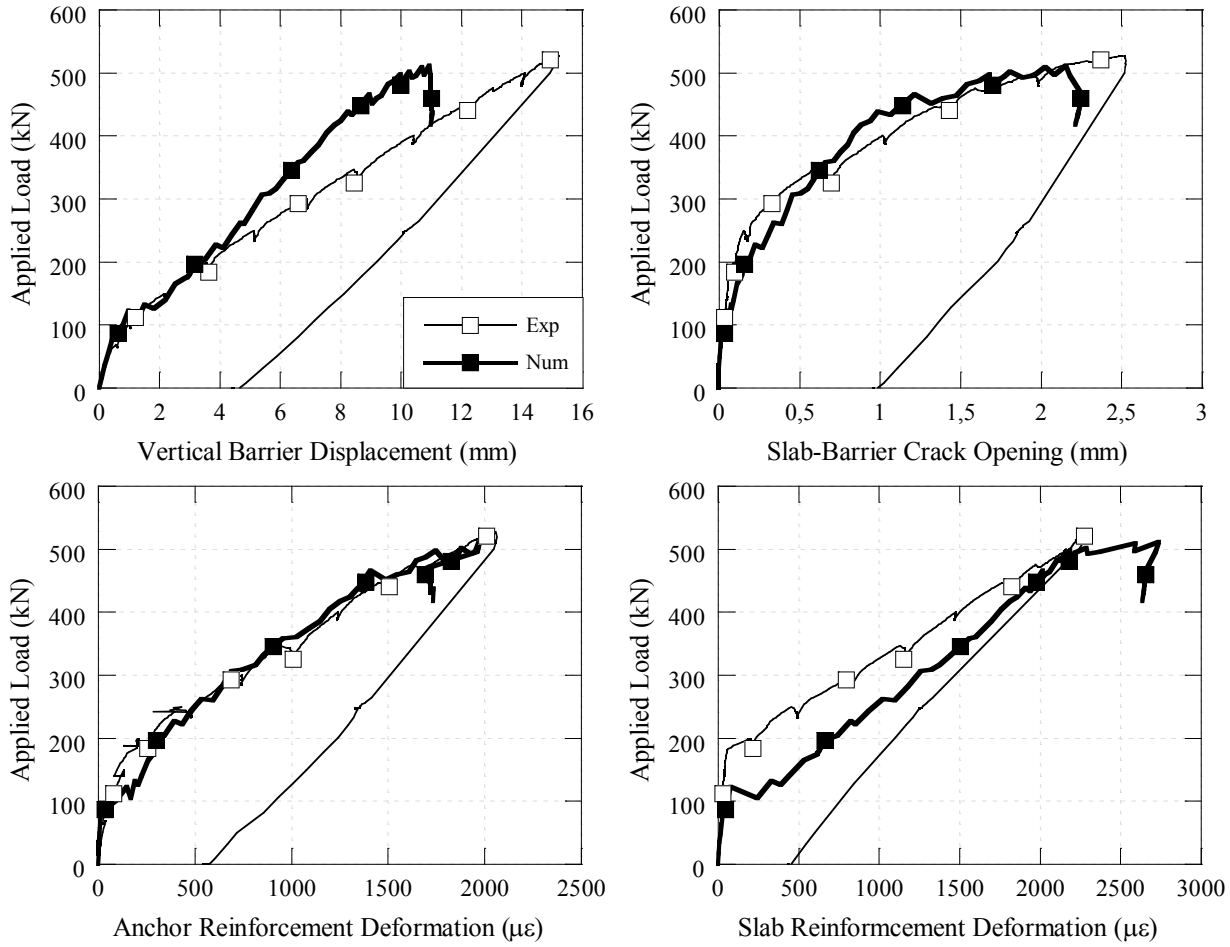

Figure 5-49: Test Configuration 1 Results

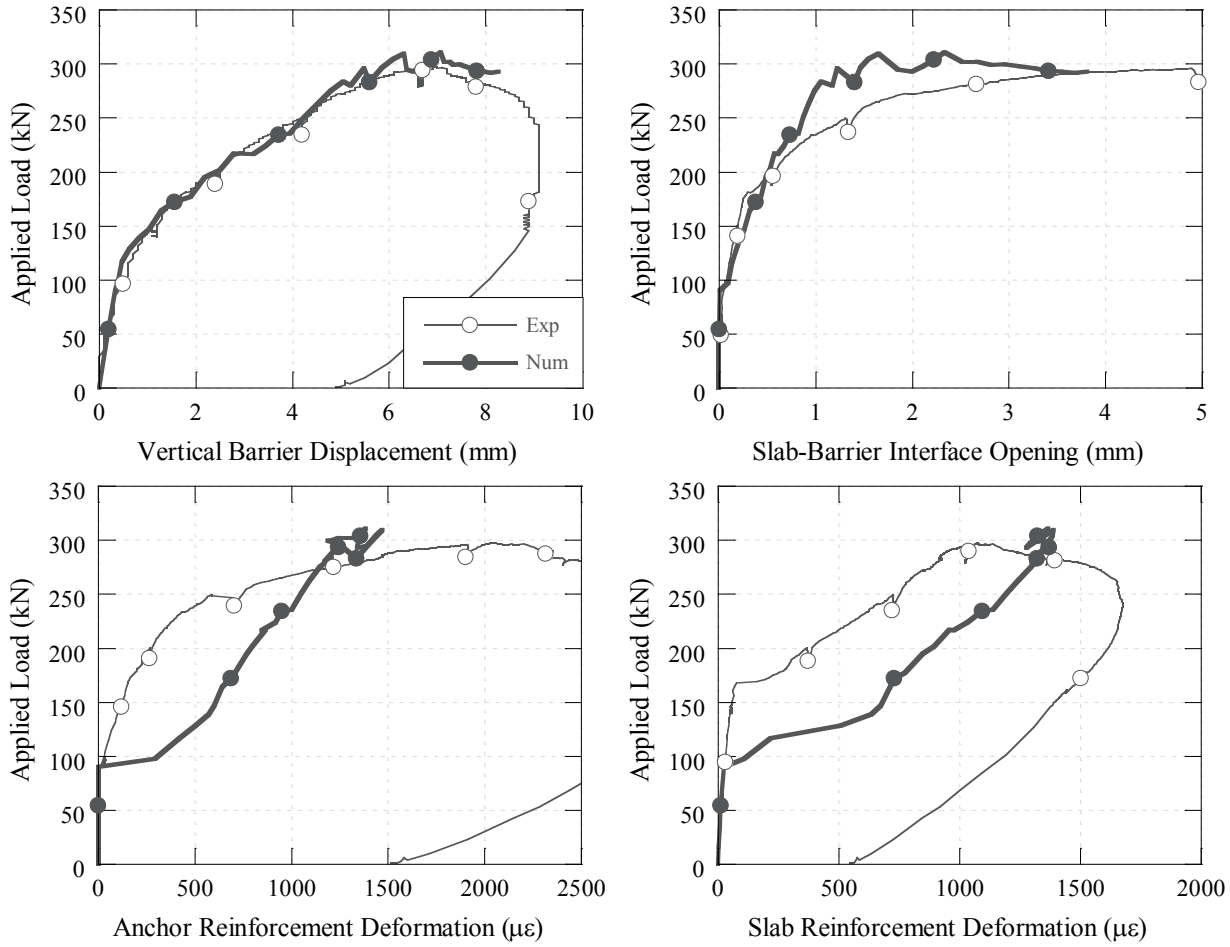

Figure 5-50: Test Configuration 2 Results

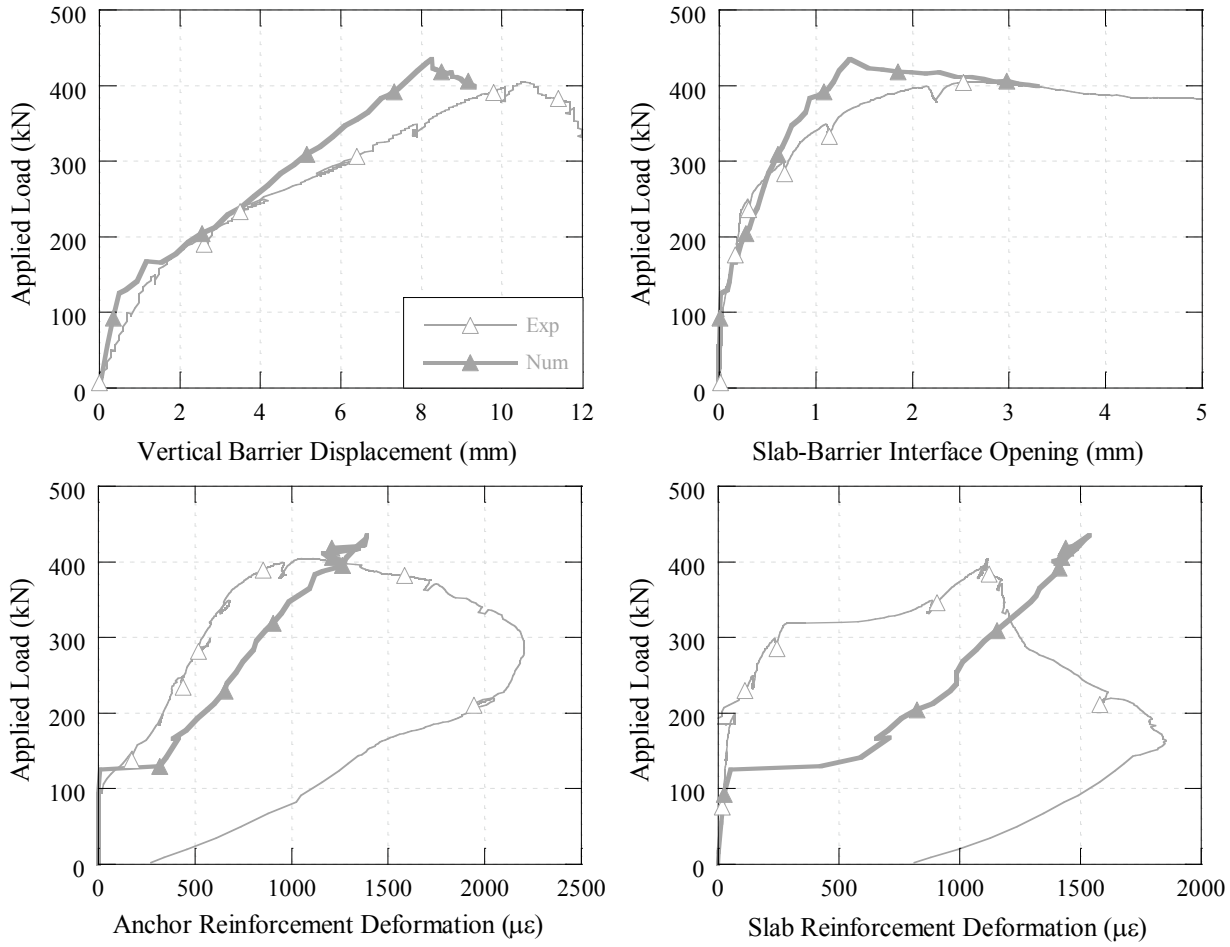

Figure 5-51: Test Configuration 3 Results

5.8 Complimentary Parametric Studies

The following parametric studies were also performed in addition to those already presented in Chapter 4.

5.8.1 Loading Effect

The surface used to apply the equivalent static load in the experimental tests was 350 x 700 mm. This surface was prescribed in the AASHTO Guide Specifications for Bridge Railings (1989) for PL-2 impact vehicles. The current bridge codes in the U.S. and Canada do not prescribe a loading surface but simply a 1.05 m load length applied 700 mm above finished slab grade. The Guide Specifications surface was used to maintain continuity between the projects of Niamba (2009), Duchesneau (2010), and Namy (2012) in the development of precast barriers at Polytechnique Montréal.

`

Numerical models were used to confirm that the difference between the loading surface used and the loading prescribed in the current bridge codes would not substantially alter the behaviour observed experimentally. A numerical simulation was done for each test configuration with the load applied to the barriers using a 150 x 1050 mm rigid steel beam.

The force-displacement relationships for the loading effect study are shown in Figure 5-52. The results show only a slight increase in ultimate strength for Test Configuration 1. The peak strength reaches 547 kN and represents a 7% strength increase from the numerical model with the actual loading configuration. This strength increase is logical since the load is applied over a longer length and more barrier stirrups resist the punching shear. The total perimeter of the modified load application is also increased from 2.1 m to 2.4 m and therefore the concrete shear resistance is also increased. The modified load effect increases the contribution of steel and concrete to shear resistance and is therefore slightly less critical to the punching failure.

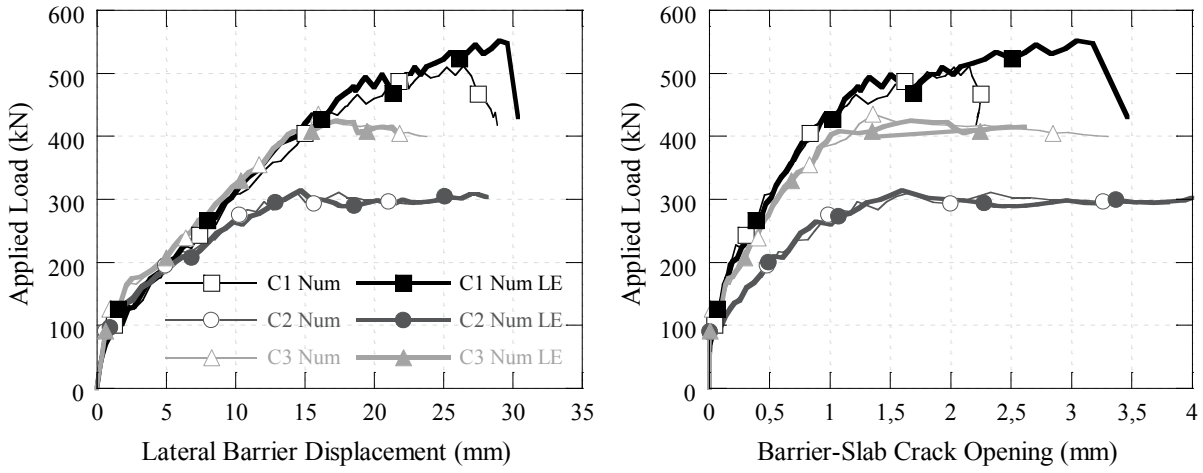

Figure 5-52: Load Effect Study, Test Configurations 1, 2, and 3

5.8.2 Modified Precast Barrier Reinforcement Detail

As mentioned previously, the behaviour of Test Configuration 3 only began diverging from the reference Test Configuration 1 when shear cracks grew in the exterior barriers at the connections. It is possible that an improved reinforcement detail could prevent the formation and growth of the shear cracks.

Numerical simulations were performed to investigate the proposed reinforcement modifications shown in Figure 5-53 for Test Configuration 3. The stirrups spacing was increased, the

`

longitudinal reinforcement was extended to the barrier edges, and standard 90° hooks were added to the top row of longitudinal bars. The modifications were meant to minimize any increase in steel quantity.

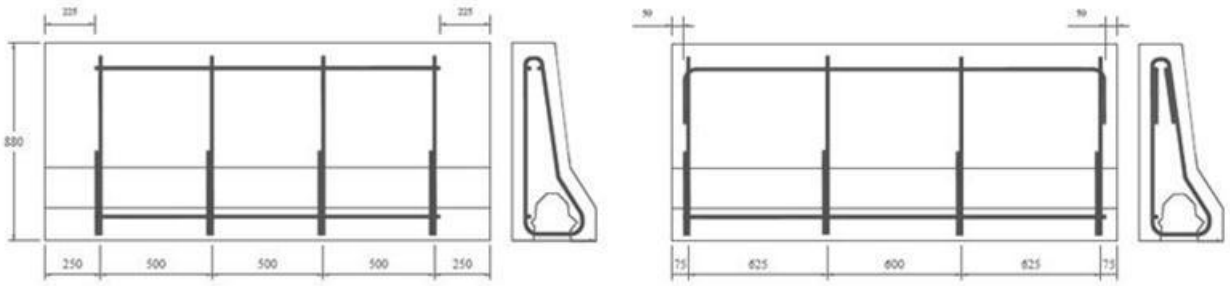

a) Original Barrier Reinforcement Detail b) Modified Barrier Reinforcement Detail

Figure 5-53: Barrier Reinforcement Detail

The results from the barrier reinforcement detail study are shown in Figure 5-54. The new models have slightly higher peak strength than the reference models (6% gain in peak strength); however the strength gain is not significant. The shear cracks seem to simply move around the reinforcement (Figure 5-54b). The change to the reinforcement detail only slightly increases the quantity of steel reinforcement, but the gains do not seem to justify the extra materials.

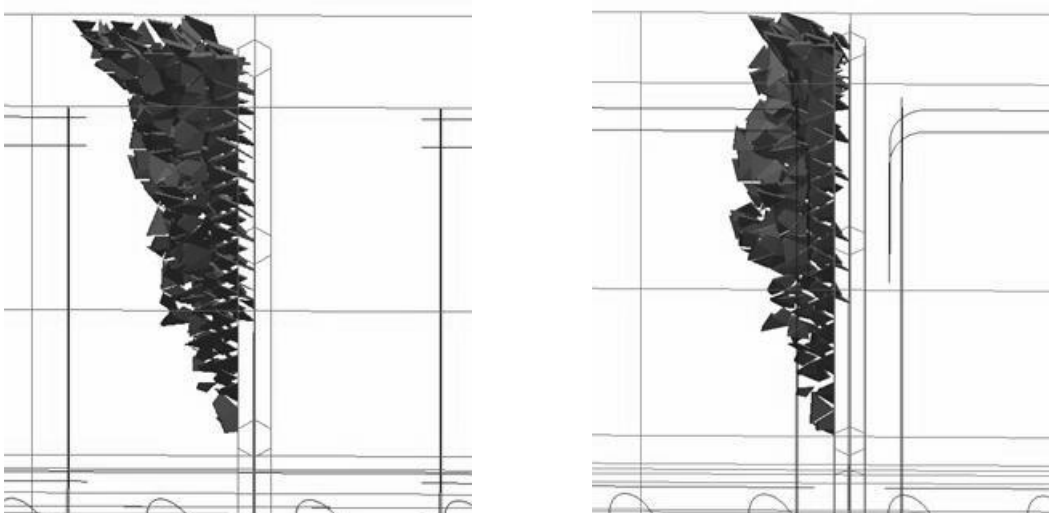

a) Shear Failure Original Reinforcement b) Shear Failure Modified Reinforcement

Figure 5-54: Barrier Reinforcement Study, Test Configuration 3

`

5.8.3 Modified Anchor Reinforcement Detail

Aminmansour (2004) used extensive strut-and-tie modeling to optimize the connection of the anchor reinforcement between barrier and slab overhang. Aminmansour (2004) recommended hooking both legs of the anchor bar back towards the slab overhang edge in order to resist compressive struts at end of the slab and increase the development of the tensile forces within the anchor (Figure 5-55a). This modification was also meant to decrease the opening of shear cracks in the slab beneath the barrier. The shear cracks were not quantified during the experimental tests; however, they are very substantial in the numerical simulations and have been noted within the literature as the cause of failure in the slab overhangs (Aminmansour 2004, Benmokrane et al. 2010 - Figure 5-55d). Moreover, the numerical models for Test Configurations 2 and 3 highlighted that the anchors are not adequately developed.

The anchors used in the Duchesneau (2010) precast barriers only have one leg directed back towards the slab overhang edge (Figure 5-55b), the leg less critical to the transfer of the tensile load. A numerical simulation was performed using Aminmansour's (2004) recommended anchor design (Figure 5-55c) to evaluate if angling both legs back toward the overhang edge would decrease shear cracking in the slab and improve the development of the anchors.

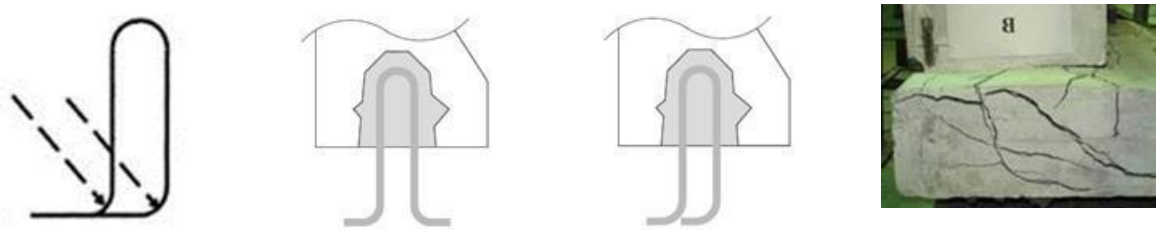

a) Anchor Detail (Aminmansour 2004) b) Duchesneau (2010) Anchors c) Anchor Modification d) Shear Failure (Benmokrane et al., 2010)

Figure 5-55: Anchor Design, Development, and Shear Cracking

The results of the anchor reinforcement detail study are described in Table 5-14. The anchor reinforcement modification did not significantly change the force-displacement relationships or peak strength (increase of 8% and 3% for Configurations 2 and 3 respectively). However, the results generally demonstrate an increased stress in the anchor bars at a given load, particularly near peak strength.

`

The anchor design modification does not conclusively demonstrate an improved performance. However, the higher anchor stresses recorded at peak load are indicative of an improved anchor development. It should also be noted that the new anchor design would not increase the material or fabrication costs associated with the precast barriers and therefore should be considered for future tests.

Table 5-14: Anchor Reinforcement Study, Slab Shear Cracking and Anchor Stress Development

Load kN	Measure	Configuration 2 Standard	Configuration 2 Anchor Change	Configuration 3 Standard	Configuration 3 Anchor Change
200 kN	Stress[1]	160 MPa	160 MPa	110 MPa	110 MPa
	Crack[2]	0.1 mm	0.1 mm	< 0.1 mm	< 0.1 mm
300 kN	Stress[1]	260 MPa	280 MPa	160 MPa	160 MPa
	Crack[2]	0.3 mm	0.3 mm	0.1 mm	0.1 mm
400 kN	Stress[1]	NA	NA	250 MPa	250 MPa
	Crack[2]			0.25 mm	0.2 mm
Peak Strength	Stress[1]	350 MPa	380 MPa	280 MPa	300 MPa
	Crack[2]	0.9 mm	0.7 mm	0.3 mm	0.3 mm
	Load	310 kN	336 kN	435 kN	449 kN
25 mm Disp.	Stress[1]	400 MPa	400 MPa	330 MPa	370 MPa
	Crack[2]	2.7 mm	2.5 mm	2.0 mm	2.0 mm
	Load	299 kN	306 kN	395 kN	432 kN

[1.]Max anchor stress on tensile leg [2.]Max shear crack width in slab

5.9 General Discussion

This Chapter has provided extensive background information to the articles submitted for publication in Chapter 3 and Chapter 4 on the experimental and numerical results obtained during this research project.

A detailed account of the preliminary FE evaluation to establish the design parameters of the experimental tests – bridge deck length, overhang length, and barrier configurations – was given in Section 5.2. This initial evaluation identified the importance of the barrier-slab load transfer length and barrier continuity. The length of load transfer was demonstrated to reach beyond 4 m, and therefore a 6.2 m slab length was selected for testing. A 1.0 m slab overhang length was established as a realistic testing length and a critical case for bridge deck overhangs.

`

The design considerations and fabrication methods of the test specimens are documented in Sections 5.2 and 5.3. The specimens were all designed to be representative of bridge deck specimens typically found in Canada (with the exception of the precast barriers). The specimen formulation and final properties are fully documented.

The design of the testing setup, loading procedure, and assembly are all detailed in Section 5.4. The experimental testing performed for this project was non-standard, and involved large-scale specimens, sophisticated laboratory testing equipment, and extensive instrumentation. The setup required a large attention to detail in order to ensure that the experimental tests were well executed and that a maximum of quantitative data could be derived from each test.

The assembly of the testing components was generally straightforward with the exception of the FRM injection to connect the barriers to the slab. In order to ensure an adequate injection, the FRM material was optimized, and a full-scale injection test was performed. The details of which are provided in Section 5.5 and APPENDIX E. This injection is critical to the performance of the precast barrier test configurations, and it is difficult to control the overall quality of the injection process since there can be no visual inspections. This highlights a weakness in the current precast barrier design. Small design modifications could simplify either the injection quality control, or the injection technique. Small vertical ducts could be cast from the top of the hollow recess to the outer face of the barrier at 1 m intervals. The tubes would only fill with the injected cementitious material once the entire section was filled and would provide a visual confirmation of the injection quality. Another option would be to cast large ducts into the top of the hollow recess that would be used for the injection itself. In fact, it would not really be an injection but a pour, and it would be sufficient to ensure that a self-leveling cementitious material is used for the pour. This concept is similar to the precast barrier design of Jeon et al. (2011).

In Section 5.6 complementary results and discussion are provided to the experimental data in Chapter 3. The complimentary data clearly distinguish the effect of barrier longitudinal continuity on the experimental results. The complimentary data draw out that the effect of the barrier longitudinal continuity (or lack thereof) is very evident in the experimental data. The cast-in-place barrier used in Configuration 1 is fully continuous which increases the barrier longitudinal strain and distributes the applied overturning moment over the length of the slab. The precast barriers used in Configuration 2 exhibited at first a small amount of barrier continuity due to a

`

certain friction between precast barriers. However, it quickly dissipated and the slab overhang was stressed more locally. This is apparent in the considerably higher slab compressive strain observed in line with the load rather compared to the 1 m offset section. As would be expected the precast barriers with shear connections used in Configuration 3 exhibit a mixed behaviour between these two extremes. Until the peak strength was reached the exterior barriers were displaced with the loaded barrier and the load-transfer length from barrier to slab was very similar to that of Configuration 1. After peak strength was reached the beneficial contribution of the shear keys dissipated and the loaded barrier began to move relatively to the exterior barriers. From this point the behaviour of Configuration 3 moved towards that of Configuration 2. A flexural failure was observed and the load transfer length was limited to 2 m. The compressive strain at the 1 m offset section does demonstrate that there was still some force transfer between precast barriers at the beginning of the softening regime. This likely explains the increased residual strength observed compared to Test Configurations 2.

The full details of the numerical validation models of each test configuration are disclosed in Section 5.6 along with more extensive numerical results. The element formulations used, precise mesh dimensions, and gap contact element properties are each described. The structural condition prior to the application of the displacement load was very important for the numerical models. This is because the concrete shrinkage and restraint conditions prestress the slab overhangs and, in the case of test Configuration 1, the barrier as well. The pre-displacement loading steps are detailed for each validation model. The description of the numerical models is sufficiently detailed that the numerical models and results can be simulated with an appropriate NLFE program.

The additional parametric studies on the loading application effect, barrier reinforcement detail, and barrier-slab anchor bar detail are performed and discussed in Section 5.8.

The loading application study investigated the loading surface used in the experimental tests. The loading surface used was based off recommendations from the AASHTO Guide Specification for Bridge Barriers (1989) and is different from the current load recommendations found in the CSA (2006) and AASHTO LRFD (2010). The numerical results showed that only the Test Configuration 1 was impacted by the load surface. The modified loading surface of 1050 x 150 mm (from the current codes) activates more steel shear reinforcement and more concrete surface

`

to resist the critical punching shear loads. This resulted in a 7% increase in ultimate strength. The structural stiffness and damage progression was not affected however.

The barrier reinforcement detail was investigated to improve the barrier resistance to shear at load transfer. The results demonstrated the shear cracks would simply move around the new reinforcement positioning, with only a modest strength gain (6%). The increased strength does not seem to justify the design changes which would slightly increase the steel quantity.

A new anchor reinforcement detail was based on design recommendations from Aminmansour (2004) on similarly designed precast barriers. The design modification did not increase material quantity or fabrication costs and was meant to improve the development of tensile forces in the anchor bars. The effects of the modification on the structural performance were not found to be significant, however the tensile leg of the anchor bars did seem to have a better stress development at a given load, particularly near peak strength and post-peak. The modification merits further investigation considering there are no extra costs.

`

CHAPTER 6 CONCLUSION AND RECOMENDATIONS

This master's thesis provides exhaustive documentation of the work performed during the research project on the behaviour of bridge barrier wall subjected to static transverse loads. The research objectives have been achieved, and valuable conclusions and recommendations have been found for the continued development, use, and improvement of precast bridge barriers on bridge deck overhangs.

6.1 Reminder of Research Objectives

The primary research objective for this research project was to develop an improved understanding of bridge barriers anchored to the deck overhang behaviour during transverse loading to evaluate the impact of using precast barriers on the strength of the bridge slab overhang and to optimize the precast barrier design for industrial use.

To achieve this objective, three large-scale experimental tests were performed on bridge deck overhangs with different barrier configurations. Test Configuration 1 used a traditional MTQ Type 201 cast-in-place barrier to establish a performance reference. Test Configuration 2 used three adjacent precast barriers developed by Duchesneau (2010). Test Configuration 3 added shear connections between the three adjacent precast barriers. An effective shear key compatible with the precast barriers had to be designed for Test Configuration 3. The findings of the experimental tests were broadened with the use of numerical parametric studies performed with validated NLFE models.

6.2 Conclusions

The analysis of the experimental and numerical results has led to the following conclusions for the use of the HPFRC precast bridge barriers:

- The precast barriers built to an appropriate 4 m length have an equivalent strength and structural stiffness as their cast-in-place counter-part (MTQ Type 201 F shaped barrier).
- The experimental testing configurations using 2 m precast barriers loaded in the structure centre represent a load case at least as critical as an eccentric edge load applied to 4 m precast barriers, with or without consideration of shear keys between barriers.

- The ultimate strength of the bridge deck overhangs built with HPFRC precast bridge barriers exceed the design criteria specified in the CSA 2006 and AASHTO 2010.
- Utilization of shear keys provided a greater load transfer length and increased peak strength.
- The shear keys added between precast barriers are necessary to satisfy loading demands prescribed by design codes, to limit relative barrier deflections during service loads, and to eliminate potential adverse effects during vehicle-barrier impacts.
- The results from this study indicate that the precast barriers with shear connections meet the necessary stipulations in the CSA (2006) Commentary for barrier modifications. The frontal geometry is unchanged, the HPFRC is a more durable concrete, adequate anchor strength has been demonstrated, and the structural stiffness is equivalent.

The HPFRC precast barriers have conclusively been shown to provide a more than adequate strength and stiffness to be used in industrial applications. The stipulations for modifying existing barrier design, the MTQ Type 201 cast-in-place barrier, have been met. The results in this study indicate that the precast barriers with shear keys would pass crash tests. Responsible jurisdictions in Canada may now consider using these barriers, or investing in crash test validation. Furthermore, the results from this study could be used to receive FHWA certification for this barrier design for barrier performance level 2 (test level 4).

6.3 Recommendations

The literary review, specimen fabrication, specimen installation, experimental results, and numerical studies all help provide several new research areas for the potential improvement of the HPFRC precast barriers used in this study.

Bridge slab overhangs are significantly reinforced, particularly to resist the transverse negative moment in the overhang. It would be helpful if the barrier anchor bars could be placed perpendicular to the slab edge, as this makes it much more difficult to follow the proper anchor spacing, and complicates the anchor bar assembly. The angle of anchor rotation may be maintained, but the legs of the anchors bars could both be angled backwards and parallel to the slab reinforcement. There is no reason to believe that this modification would adversely affect the

`

structural behaviour, and the results from the anchor modification parametric study indicate that the development of the anchor tensile stresses would be improved.

The injection quality of the hollow recess of the anchors is also questionable. During this project, extensive time and resources were dedicated to ensure that the FRM injection would be adequate. It is unlikely that industrial contractors will spend a similar amount of energy. Using industrial concrete pumps could significantly ease the injection process; however, the barriers would have to be properly fixed to the bridge slab, and sealed at all joints – a time consuming process. Furthermore, some sort of quality control mechanism would still need to be implemented in order to visually confirm the injection quality. Jeon (2011) boxed voids directly out of the barriers that fed into the top of the recess. This is perhaps the easiest fix because it provides visual access into the recess, and simplifies the injection process (which essentially becomes a pour and not injection). Another option would be to add air ducts from the top of the recess to the exterior face of the barrier at well-defined intervals. This would facilitate the quality control of the injection. More research should be performed on the recess injection method.

Adding a compressible material on the inside of the edges could also help fit the precast barriers against one another and improve the barrier-barrier seal before injecting the recess. A simple solution would be to place a soft rubber or neoprene on the sides of the precast barrier forms before casting. A cost-benefit analysis of this design modification should be considered before modifying the barrier design.

The performance of the HPFRC precast barrier Test Configurations was very good, especially when 4 m precast barrier lengths were considered. However, the numerical studies demonstrated that the fibre orientation was not optimized to resist the shear loads at the barrier-barrier connection. Investigation into other barrier fabrication techniques could potentially improve the fibre orientation in these areas. An improved fibre orientation would certainly be necessary to achieve a higher barrier performance level (test level). For a higher performance level, the anchor design used by Aminmansour (2004) should also be evaluated. Aminmansour (2004) installed hooped bars from both the slab and barrier into the recess and connected the two with a steel dowel. This essentially creates a mechanical connection between the steel components and should improve the strength and ductility of the recess. It would also add redundancy to the connection detail should the injection by faulty.

`

In all the experimental tests and numerical studies, the slab overhang cracked prior to the bridge barriers. This is a function of the barrier lever arm which is significantly larger than that of the slab. The slab overhang had visible cracks exceeding 0.1 mm opening widths by 150 kN and was substantially cracked by 250 kN for all three test configurations. A numerical study using a 50 MPa HPFRC in the slab with a 50% reduction in transversal steel reinforcement demonstrated that the crack opening widths would be substantially reduced during service loads compared to conventionally reinforced concrete design (less than 0.05 mm at 300 kN applied load) and that the structural stiffness would also be increased. The potential gains of using a HPFRC slab should be seriously evaluated because the reduction in costs of steel installation and placement could largely offset the increased costs of the HPFRC slab. Moreover, the increased deck overhang stiffness should reduce the risks of vehicle rollover observed when using safety shaped concrete barriers because the initial slope face of the barrier would not be significantly decreased due to the slab deflection (an decreased slope would generate more vehicle lift and create additional vehicle instability immediately following impact).

`

BIBLIOGRAPHY

AASHTO. 1989. Guide Specifications for Bridge Barriers. American Association of State Highway and Transportation Officials. Washington, D.C.

AASHTO. 2007. Bridge Design Specifications, SI Units, 4th Edition. American Association of State Highway and Transportation Officials. Washington, D.C.

ACI Committee 209. *Prediction of Creep, Shrinkage, and Temperature Effects in Concrete Structures,* ACI Manual of Concrete Practice. Detroit, Michigan, 1992, pp. 209R-1-209R-47.

Albin, R., Bullard, L., Abu-Odeh, A., Menges, W. Washington State Precast Barrier. Washington State Department of Transportation.

Alaywan, W. 2011. Design, Behaviour, and Performance of Precast Concrete Bridge Barriers. Ph.D. Thesis. Lousiana Tech University, LA.

Aminmansour, A. 2004. Performance Characteristics of Precast and Reinforced Concrete Bridge Barriers Subjected to Static and Impact Loads. Ph.D. Thesis. The Pennsylvania State University. PA.

ASTM Standard C1437, 2007, "Standard Test Method for Flow of Hydraulic Cement Mortar," ASTM International, West Conshohocken, PA, 2003, DOI: 10.1520/C1437-07, www.astm.org.

Beaurivage, F. (2009). Étude de l'influence des paramètres structuraux sur les lois de comportement des bétons fibrés pour la conception de structures. M.Sc. Thesis. Montréal: École Polytechnique de Montréal.

Benmokrane, B., Ahmed, E., Dulude, C., El-Gamal, S. (2010). Testing of full-scale bridge barriers reinforced with GFRP bars. Proceedings of 8th International Conference on Short and Medium Span Bridges. Niagara Falls, Canada 2010

Bissonette, B., Morin, R. 2000. Experimentation of a ternary cement for the rehabilitation of the highway overpass Notre-Dame/St-Augustin in Montréal. Conference on research progress on civil infrastructures in Québec, ACI, Montréal.

Bligh, R., Nauman, S. Menges W., Haug, R. (2005). Portable Concrete traffic barrier for maintenance operations. Final Report. Report No FHWA/TX-05/0-4692-1. Texas Transportation Institute.

Braike, S. 2007. Conception d'élément préfabriqués de ponts avec des bétons fibrés à hautes et ultra haute performance. M.Sc. Thesis. École Polytechnique de Montréal, Montréal.

Brara, A., Klepaczko, J. 2007. Fracture energy of concrete at high loading rates in tension. International Journal of Impact Engineering, 34, p. 424-435.

Bronstad, M.E., Michie, J.O., Mayer, Jr., J.D. 1987. Performance of Longitudinal Traffic Barriers. National Cooperative Highway Research Program Report 289, TRB, National Academy of Sciences.Washington, D.C.

Bullard, D.L., Sheikh, N.M., Bligh, R.P., Haug, R.R., Schutt, J.R., Storey, B.J. 2006. Aesthetic Concrete Barrier Design. National Cooperative Highway Research Program Report 554, TRB, National Academy of Sciences.Washington, D.C.

Buth, C.E., Hirsch, T.J., and McDevitt, C.F.1990. *Performance Level 2 Railings*.Transportation Research Record 1258, pp. 32-50

Charron, J-P., Niamba, E., Massicotte, B. (2011). Static and dynamic behaviour of high- and ultrahigh-performance fibre-reinforced concrete precast bridge parapets. ASCE Journal of Bridge Engineering, Vol 16, Issue 3, pp. 413-421.

CEB-FIB. 2000. Bond of reinforcement in concrete, State-of-art report. International Federation for Structural Concrete (FIB), Lausanne, Switzerland. Bulletin 10.

Conciatori, D. 2005. Effet du microclimat sur l'initiation de la corrosion des aciers d'armature dans les ouvrages en béton armé. Ph.D. Thesis. École Polytechnique Fédérale de Lausanne, Lausanne, Switzerland.

CSA-A23.3, 2004. Concrete Design Handbook (CDH). CSA International. Toronto, Canada.

CSA-S16-01, 2007. Limit States Design of Steel Structures. CSA International. Toronto, Canada.

CSA-S6-06. 2006. Canadian Highway Bridge Design Code (CHBDC). CSA International. Toronto, Canada.

Cervenka, V., Jendele, L., and Cervenka, J. 2011. ATENA Program documentation. Cervenka Consulting Ltd. Prague, Czech Republic.

`

Claude, J-F., Ahmed, E., Cusson, D., Benmokrane, B. (2011). Early-age cracking of steel and GRFP-reinforced concrete bridge barriers. CSCE Annual Conference, Ottawa, Canada, June 14-17, pp. 1-10.

Cusson, D., Repette, W. (2000). Early-Age Cracking in Reconstructed Concrete Bridge Barrier Walls. ACI Materials Journal, Vol 97, No 4, pp. 438-446.

De Borst, R. 1986. Non-linear analysis of frictional materials, Ph.D. Thesis, Delft University of Technology, 1986.

Delsol, S. 2012. Évaluation du coefficient d'orientation dans les bétons renforcés de fibres métalliques. M.Sc. Thesis. École Polytechnique de Montréal, Montréal.

Desmettre, C., Charron, J-P. (2012). Water permeability of reinforced concrete with and without fibre subjected to static and constant tensile loading. Cement and Concrete Research, Vol 42, Issue 7, pp. 945-952.

Duchesneau, F., Charron, J-P., Massicotte, B. (2011). Monolithic and hybrid precast bridge barriers in high and ultra-high performance fibre reinforced concretes. Canadian Journal of Civil Engineering, Vol 38, No 8, pp. 859-869.

Duchesneau, F. 2010. Conception de barrier préfabriqué Hybrides et Monolithiques en utilisant des bétons à haute et ultra-haute performance. M.Sc. Thesis. École Polytechnique de Montréal, Montréal.

FHWA. 1986. Memorandum. Federal Highway Administration, August 28, Washington, DC.

FHWA. 1996. Memorandum. Bridge Railing Design and Testing. Federal Highway Administration, August 28, Washington, DC.

FHWA. 2005. Bridge Rail Guide. Federal Highway Administration. Retrieved fromhttp://www.fhwa.dot.gov/bridge/bridgerail/

FHWA. 2009. Connection Details for Prefabricated Bridge Elements and Systems. Culmo, M. Federal Highway Administration. Report No. FHWA-IF-09-010

FHWA. 2009. Federal Highway Research Centre: Safetery and Design Team Presentation on M.A.S.H. Retrieved from http://fhwa.na3.acrobat.com/mashfinal

`

Haluk, A., Attanayaka, U. 2004. Causes and cures for cracking of concrete barriers, Michigan Department of Transportation, Lansing. Research Report RC-1448.

Hirsch, T. *Analystical evaluation of Texas Bridge Rails to Contain Buses and Trucks*. Research Report 230-2, Texas Transportation Institute, Texas A&M University, College Station, TX, 1978.

Hordijk, D.A. 1991. Local approach to fatigue of concrete. Ph.D. Thesis. Delft University of Technology, Delft, Netherlands.

Jeon, S-J., Choi, M-S., Kim, Y-J. 2011. Failure Mode and Ultimate Strength of Precast Concrete Barrier. ACI Structural Journal: January-Febuary 2011, Vol 108, No 1, pp. 99-107.

Jiang, T., Grzebieta, R.H., Zhaor, X.L. (2004). Predicting impact loads of a car crashing into a concrete roadside safety barrier. International Journal of Crashworthiness, Vol 9, No 1, pp. 45-63.

Khayat, Kamal Henri, Omran, Ahmed F., Pavate, Trimbak V. (2010). *Inclined Plane Test to Evaluate Structural Buildup at Rest of Self-Consolidating Concrete*. ACI Mateials Journal: Title no. 107-M59.

Kozel, S. 2004. *New Jersey Median Barrier History*. Retrieved April 1, 2012 from Roads to the Future Highway and Transportation Historic Website: www.roadstothefuture.com/main.html

Lessard, M.-C. (2009). Conception de pré-dalles en bétons innovants pour les ponts. Montréal: École Polytechnique de Montréal, mémoire de maîtrise.

MASH. 2009. Manual for Assessing Safety Hardware. American Association of State Highway and Transportation Officials. Washington, D.C.

MacDonald, D.J., Kirk, A.R. (2001) Precast Concrete Barrier Crash Testing, Final Report. Report No. FHWA-OR-RD-02-07. Oregon Department of Transportation.

Mak, K.K, Gripne, D.J., McDevitt, C.F., 1994. *Single-Slope Concrete Bridge Rail*.Transportation Research Record 1468. Pp. 25-33.

Mak, K.K., Sicking, D.L. 1990. *Rollovers Caused by Concrete Safety-shaped Barriers*. Transportation Research Record 1258, pp. 71-81.

McDevitt, C. 2000. *Basics of Concrete Barriers*. Public Roads Journal: Vol. 63, No. 5, March/April 2000.

`

Medina, J., Benekohal, R. 2006. High Tension Cable Median Barrier: A Scanning Tour Report No. FHWA-IL/UI-TOL-18. University of Illinoias at Urbana-Champaign. Urbana, IL.

Menétrey, Ph. Willam, K.J. (1995). Triaxial Failure Criterion for Concrete and its Gerneralization. ACI Structural Journal, V. 92, No. 3, pp. 311-318.

Michie, J.O. 1981. Recommended Procedures for the Safety Perfomance Evaluation of Highway Safety Appurtenances. National Cooperative Highway Research Program Report 230, TRB, National Academy of Sceinces, Washington, D.C.

Ministry of Transportation of Quebec (MTQ). 2010. Normes – Ouvrages d'Art Tome III. Ministère des Transport du Québec, Québec.

Ministry of Tranportation of Quebec (MTQ). 2004. Manuel de Conception des Structures – Volume I. Ministère des Transport du Québec, Québec.

Mitchell, G., Tolnai, M., Gokan, V., et al. 2006. Design of Retrofit Vehicular Barriers using Mechanical Anchors. Centre for Transportation Research Report 4823-1F. University of Texas at Austin, 2006.

Mitchell, G., Strahota, M.T., Gokani, V., Picòn, R., Yang, S., Klingner, R.-E. (2010). Performance of retrofit highway barriers with mechanical anchors. ACI Structural Journal, Vol 107, Issue 4, pp. 381-389.

Moffat, K. (2001). Analyse de dalles de pont avec armature réduite et béton de fibres métalliques. Montréal: École Polytechnique de Montréal, mémoire de maîtrise.

National Cooperative Highway Research Program Report 239. TRB, National Academy of Sciences.Washington, D.C.

Ngan, C. 2006. Experimental Investigations of Anchorage Capacity of Precast Concrete Bridge Barrier for Performance Level 2. M.Sc. Thesis. The University of British Columbia, Vancouver.

Niamba, É. 2009. Développement de barriers préfabriqués en bétons renforcés de fibres pour les ponts. M.Sc. Thesis. École Polytechnique de Montréal, Montréal.

Patel, G., Sennah, K., Kianoush, R. 2009. Developement of Precast Concrete Bridge Barrier Wall System to Accelerate Bridge Construction of Replacement. CSCE 2009 Annual General Conference. St. John`s, Newfoundland and Labrador: May 27-30, 2009.

`

PCI. 2010. Bridge Design Manual. Precast/Prestressed Concrete Institute. Chicago, IL.

Rossi, P., Acker, P., Malier, Y. (1987). Effect of steel fibres at two different stages: the material and the structure. Materials and Structures Journal: 20, pp. 436-439.

Ross, H.E., Sicking, D.L., Zimmer, R.a. 1993. Recommended Procedure for the Safety Performance Evaluation of Highway Features. National Cooperative Highway Research Program Report 350, TRB, National Academy of Sciences. Washington, D.C.

Sennah, K. (2011). Accelerated bridge construction research and development. Canadian Civil Engineer (L'Ingénieur Civil Canadien).

TAC ATC (2010). Guide to Bridge Traffic and Barriers. Transportation Association of Canada – Association des Transports du Canada, Ottawa.

WSDOT (2009). Cable Meian Barrier Reassessment and Recommendations report. Washington State Department of Transportation. Olympia, WA.

`

APPENDIX A DESIGN DRAWINGS, AS-BUILT DRAWINGS, AND REINFORCEMENT SCHEDULES

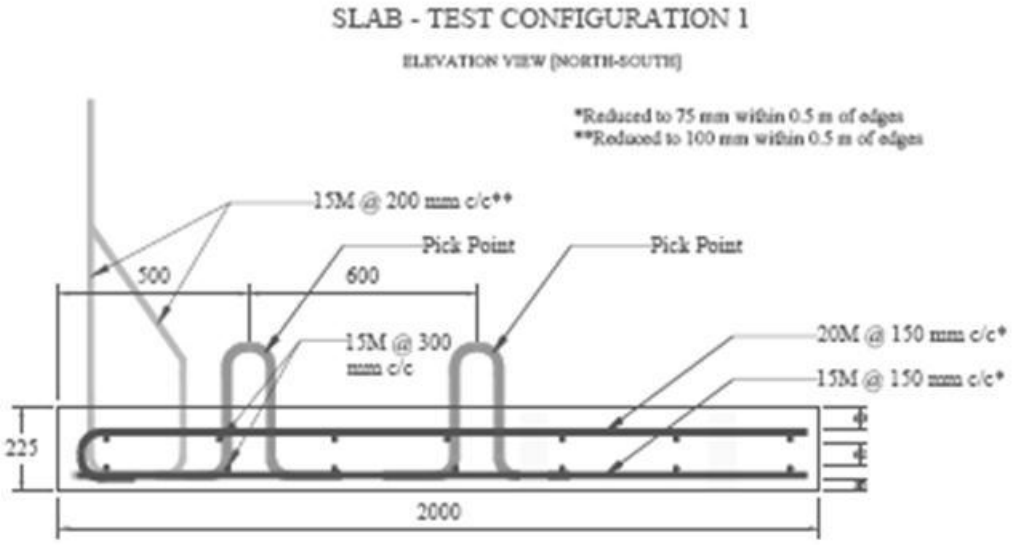

Appendix A Figure 1: Slab ~ Configuration 1: Design and As-Built, Elevation

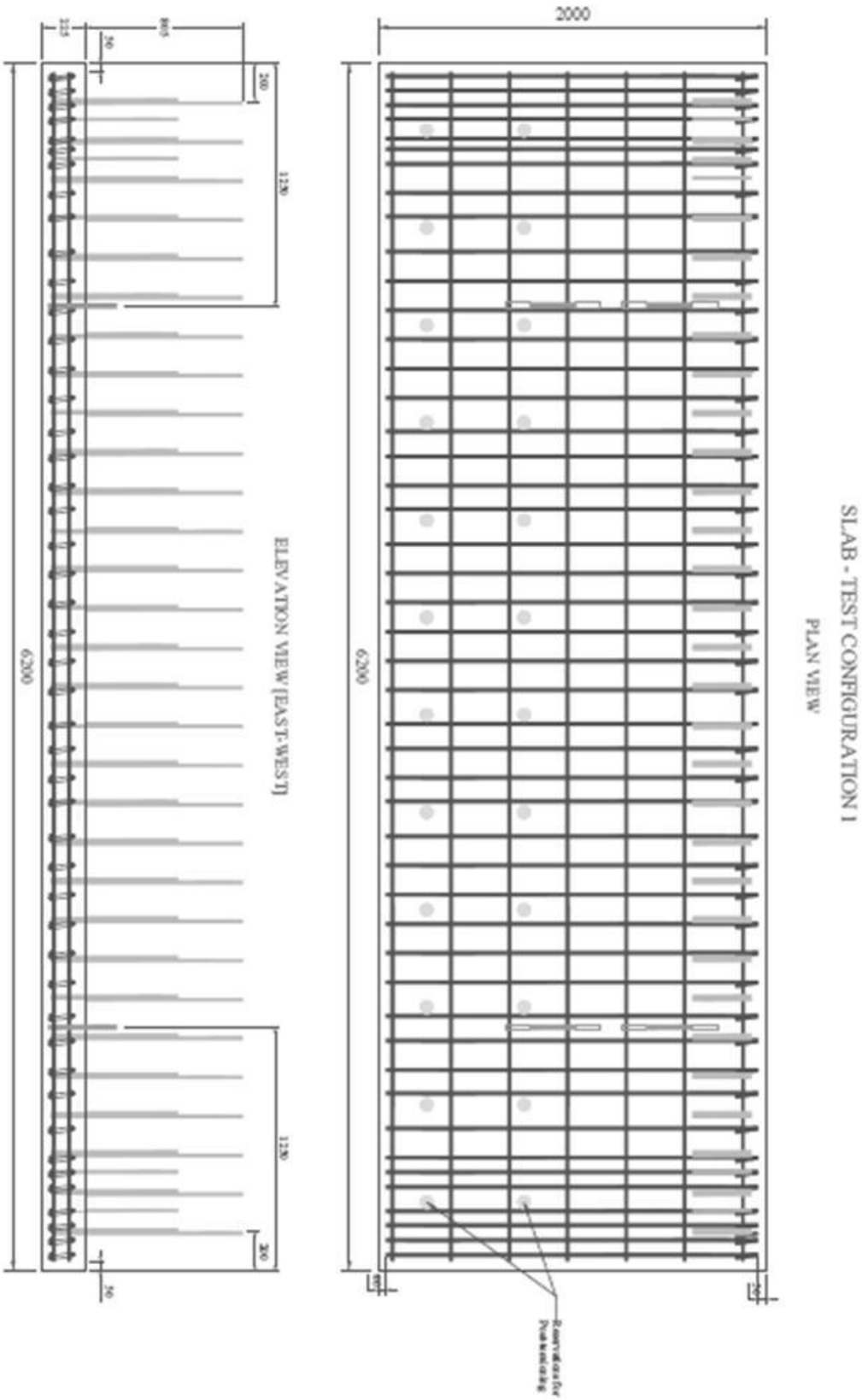

Appendix A Figure 2: Slab ~ Configuration 1: Design and As-Built, Plan and Elevation

`

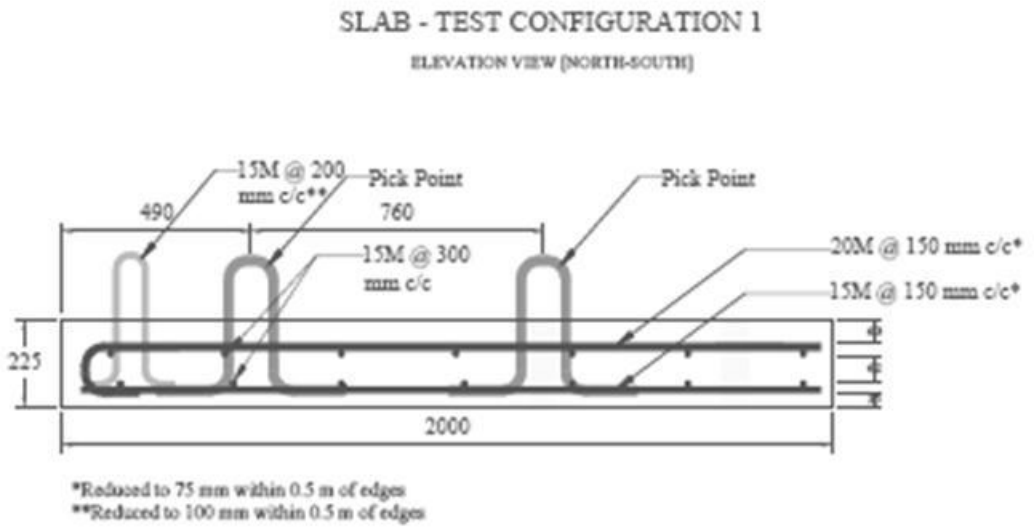

Appendix A Figure 3: Slab ~ Configurations 2 and 3: Design and As-Built, Elevation

`

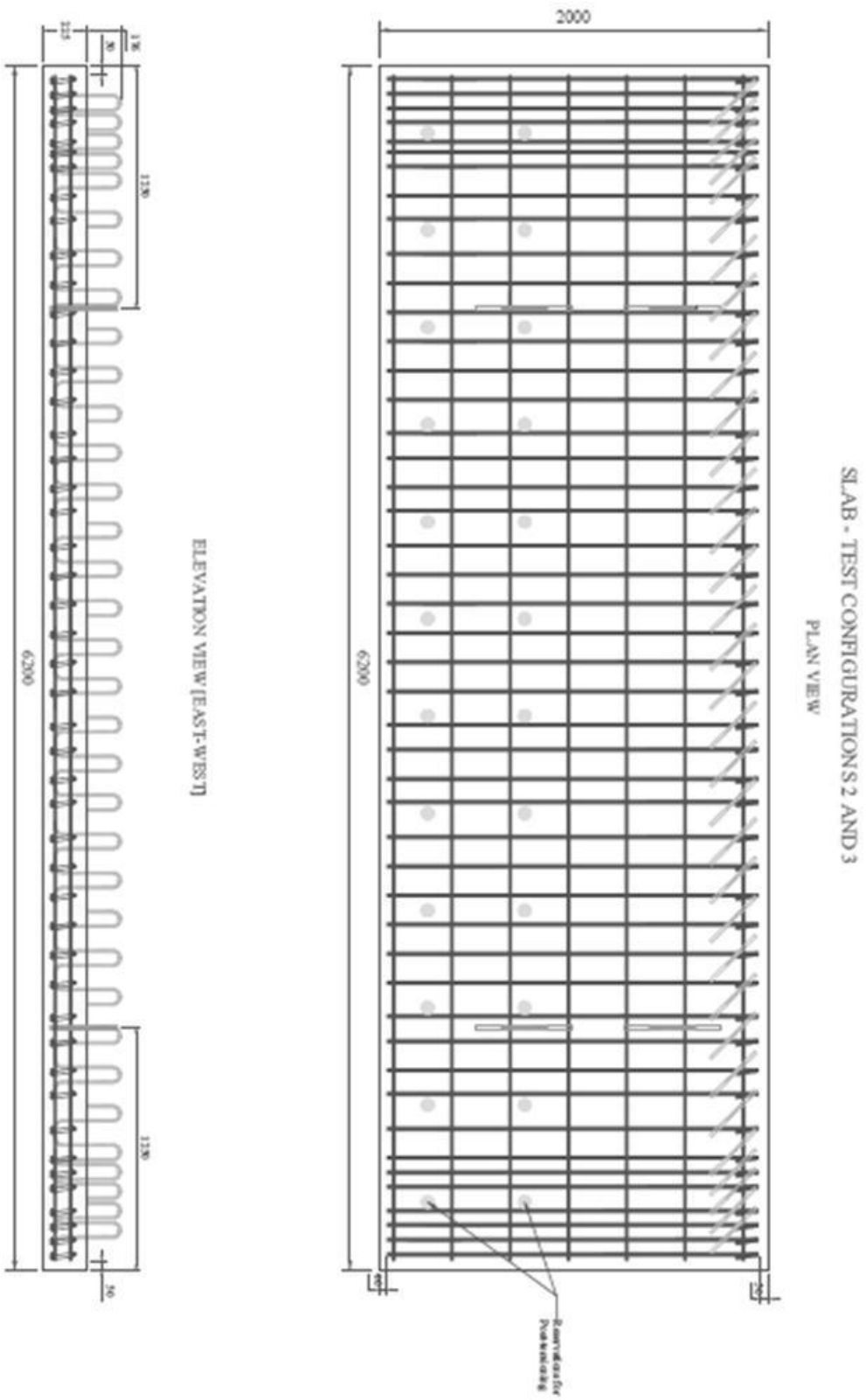

Appendix A Figure 4: Slab ~ Configurations 2 and 3: Design and As-Built, Plan and Elevation

`

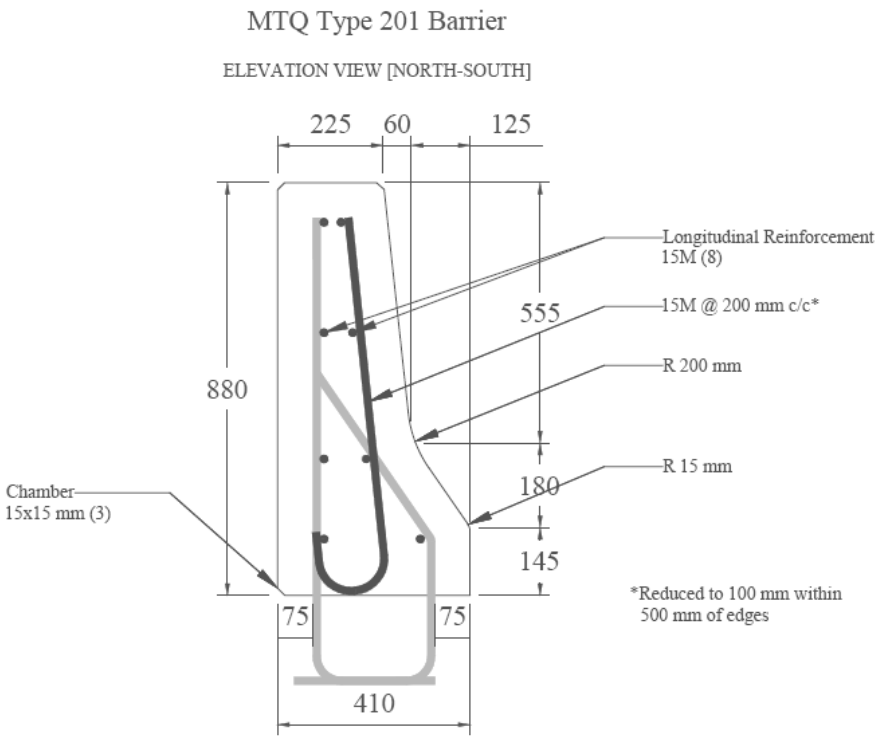

Appendix A Figure 5: MTQ Type 201 Barrier ~ Test Configuration 1: Design Only, Elevation

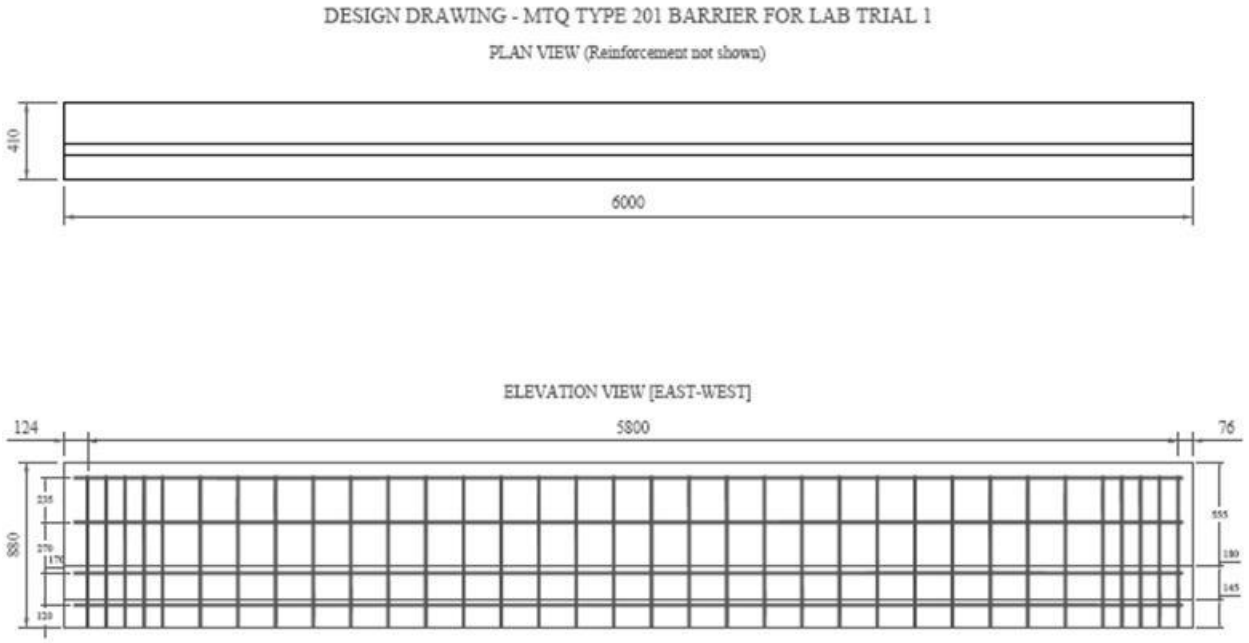

Appendix A Figure 6: MTQ Type 201 Barrier ~ Configuration 1: Design Only, Plan and Elevation

`

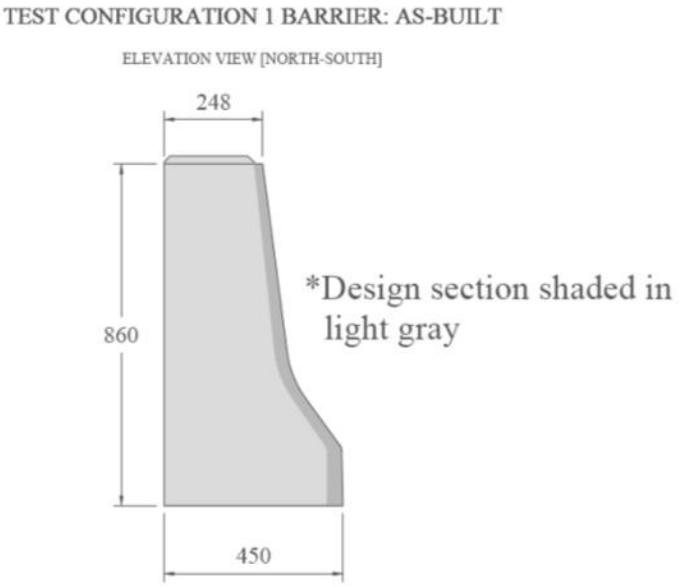

Appendix A Figure 7: Barrier ~ Test Configuration 1: As-Built Only, Elevation

`

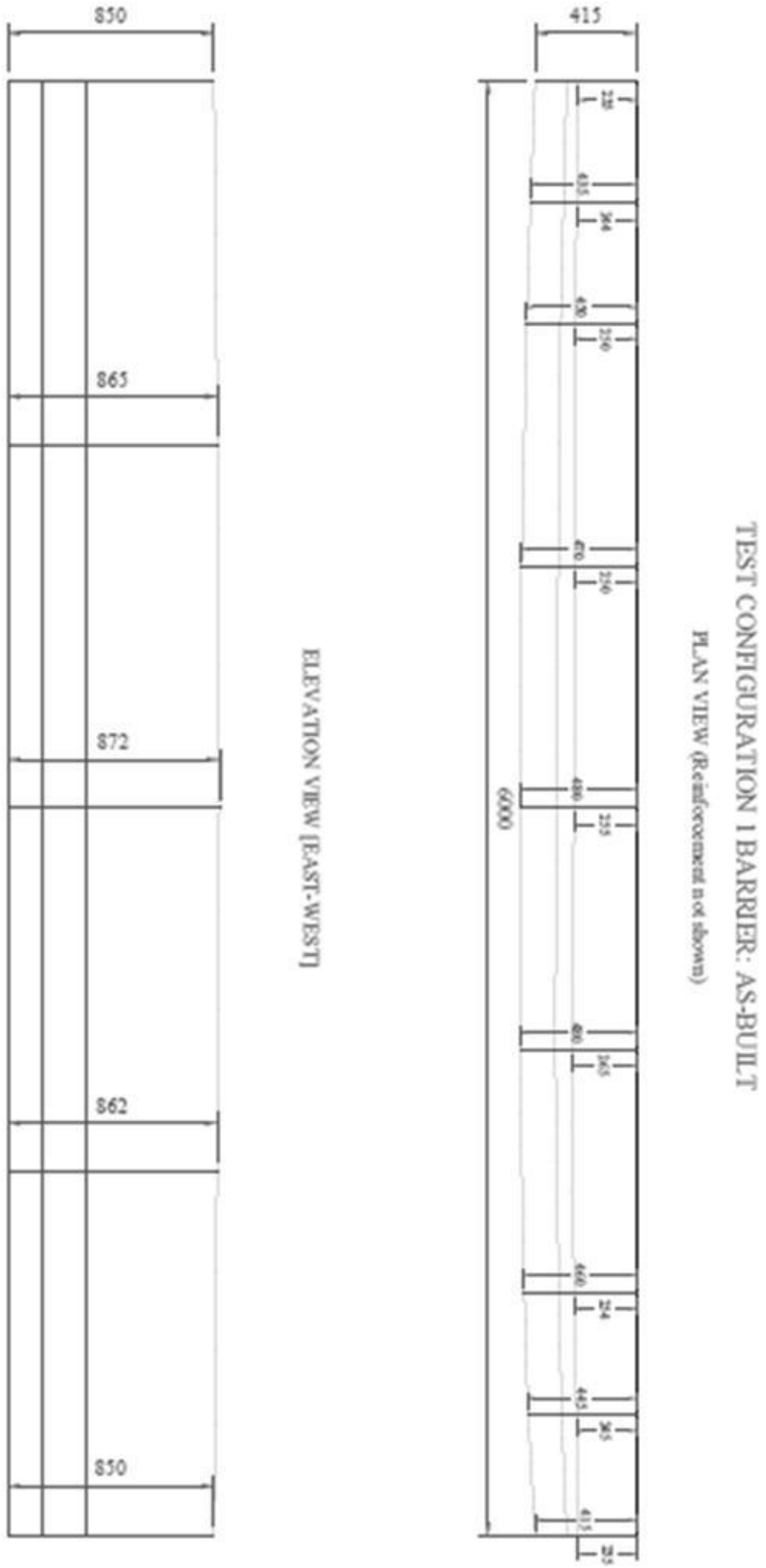

Appendix A Figure 8: Barrier ~ Test Configuration 1: As-Built Only, Plan and Elevation

`

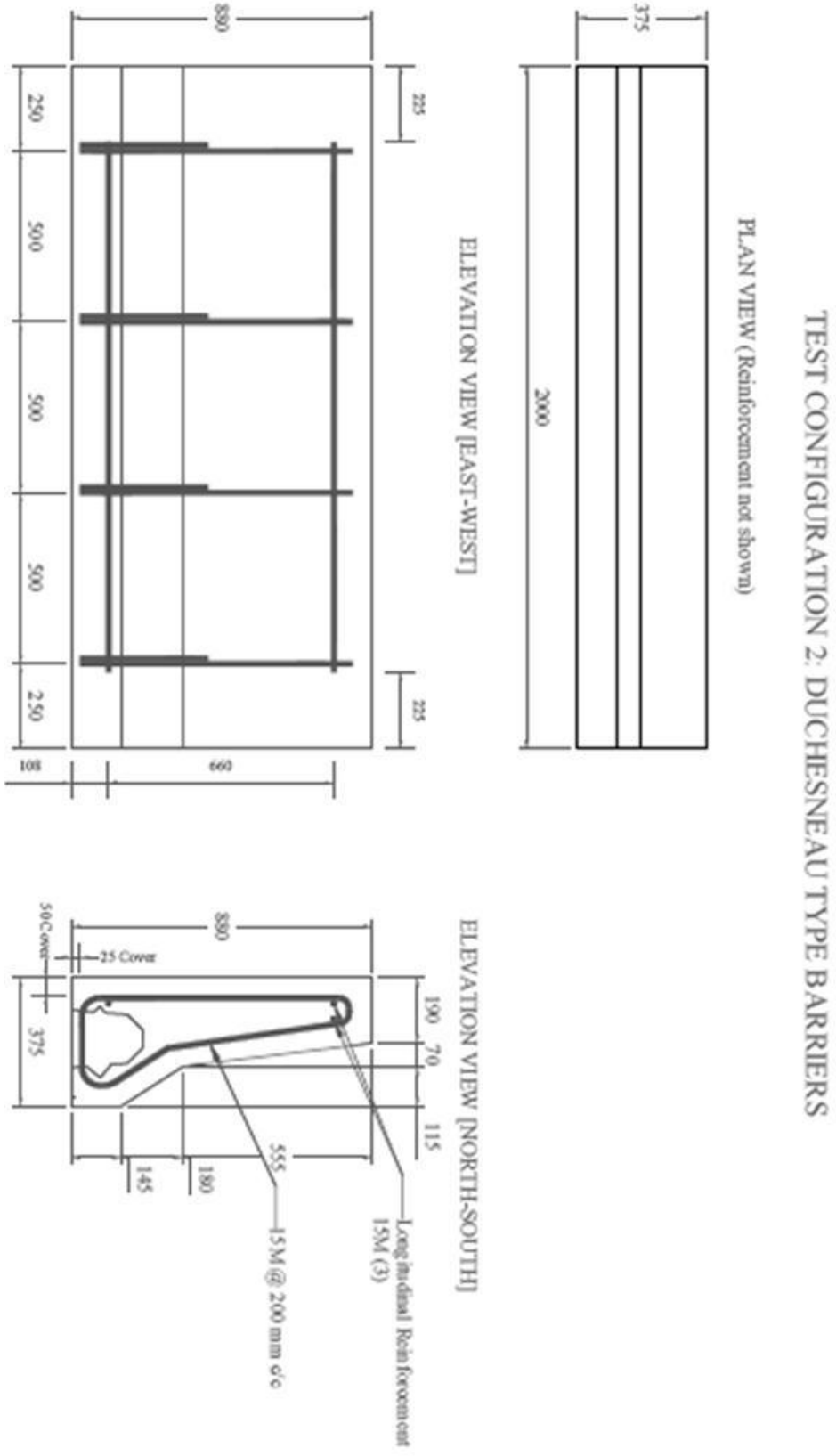

Appendix A Figure 9: Duchesneau Type Barrier ~ Test Configuration 2: Design and As-Built

`

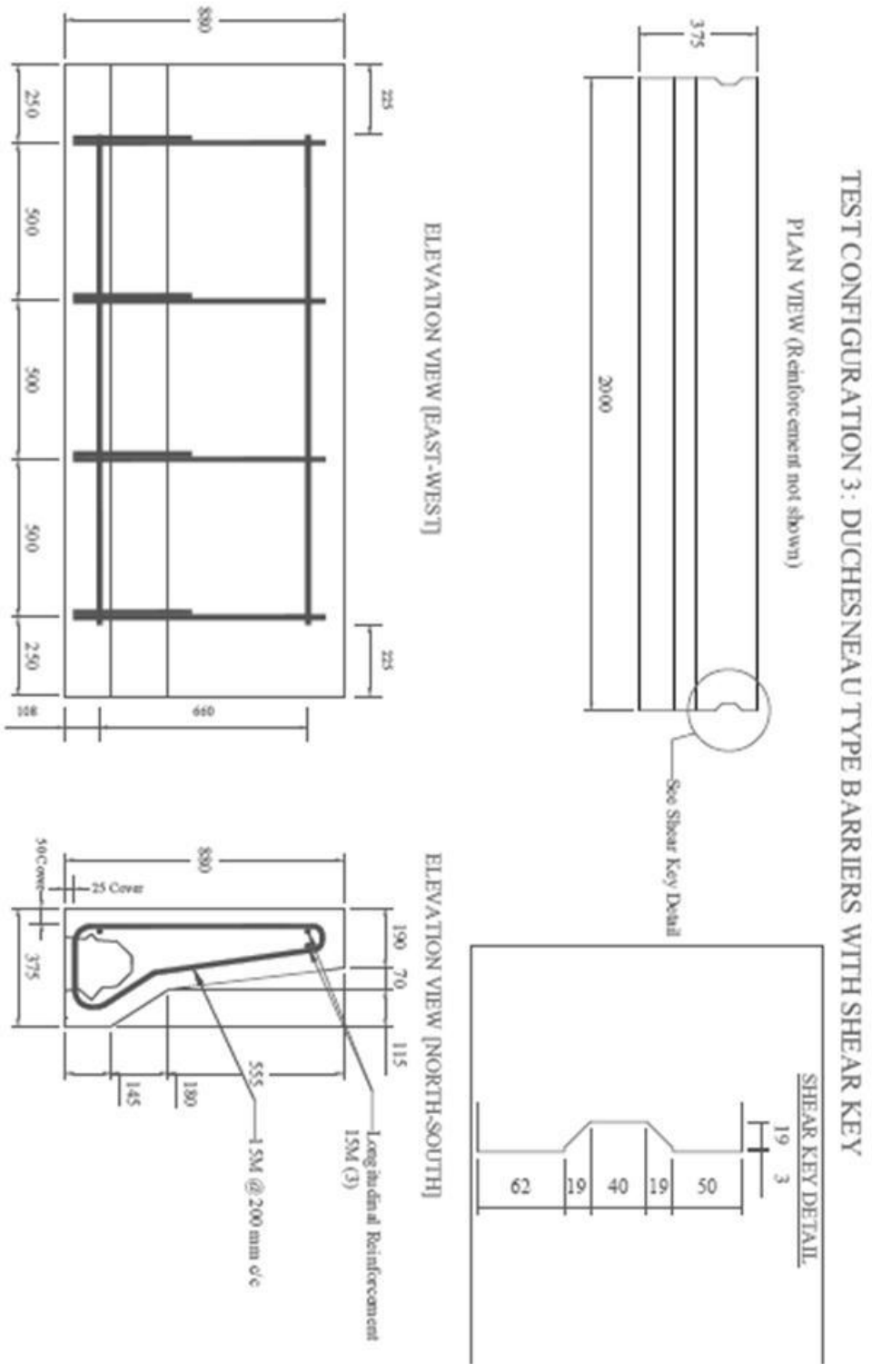

Appendix A Figure 10: Duchesneau Type Barrier with Shear Key ~ Test Configuration 3 : Design and As-Built

`

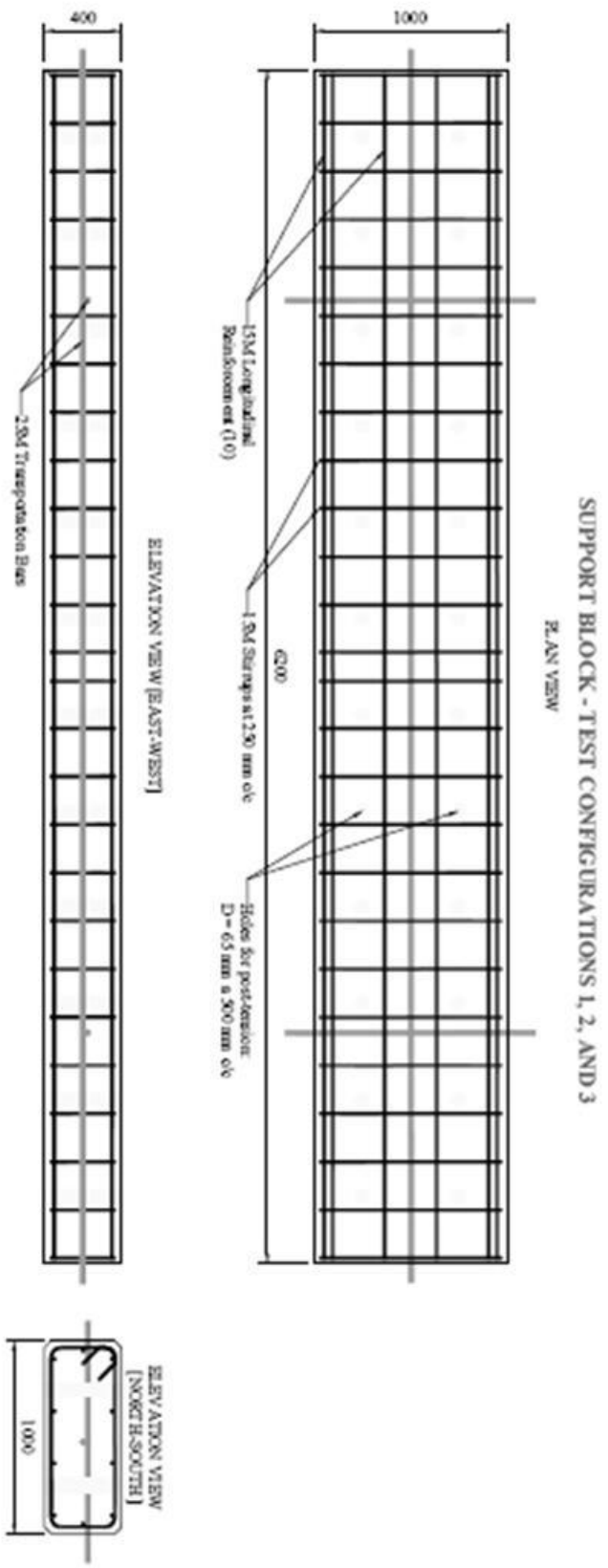

Appendix A Figure 11: Support Block ~ Test Configurations 1, 2, and 3 : Design and As-Built

`

APPENDIX B INSTRUMENTATION

The instrumentation plans for each laboratory test, with the corresponding schedules are detailed in this appendix. At the end of the appendix, two photos of the instrumentation used to measure the relative barrier displacements and also the separation of the injected mortar from the barrier.

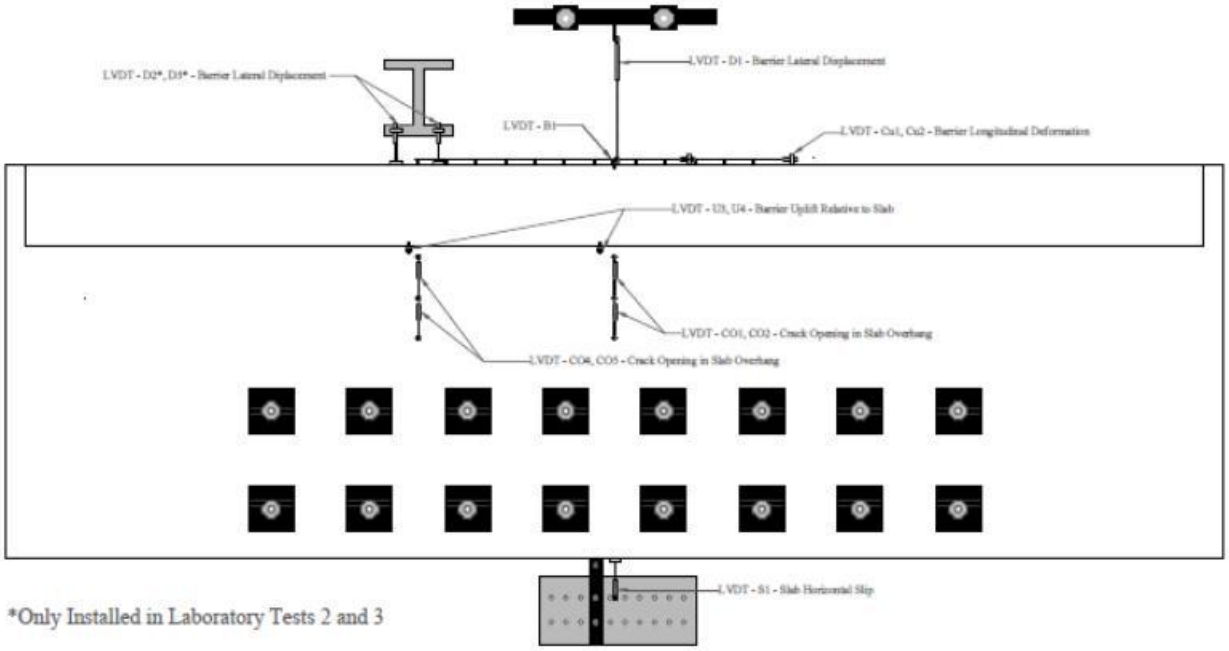

Appendix B Figure 1: Instrumentation Plan View

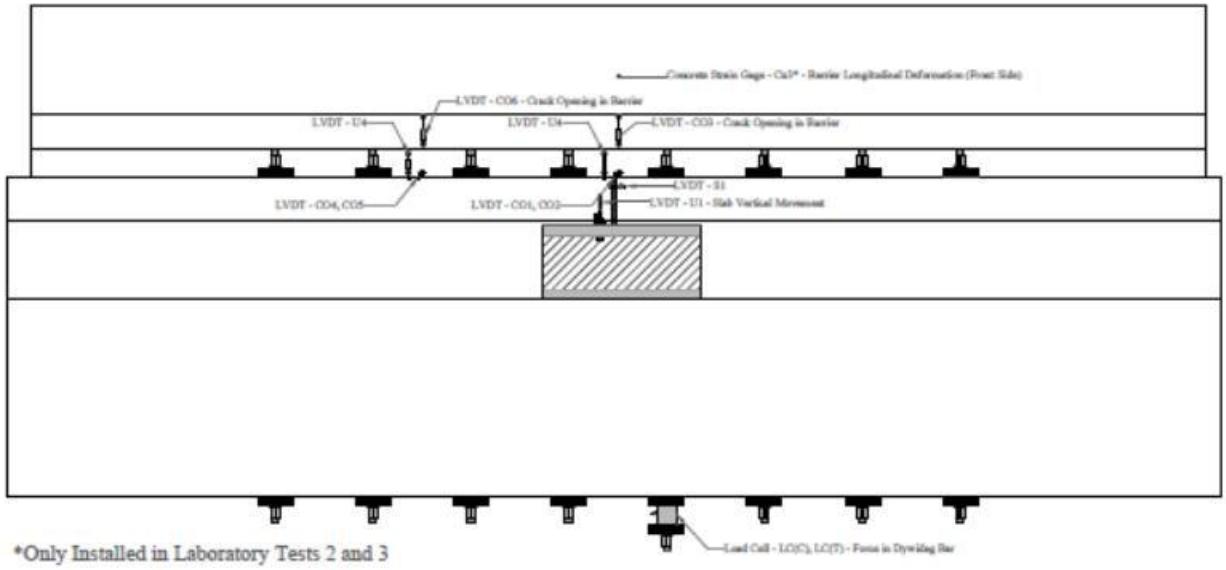

Appendix B Figure 2: Instrumentation Elevation View

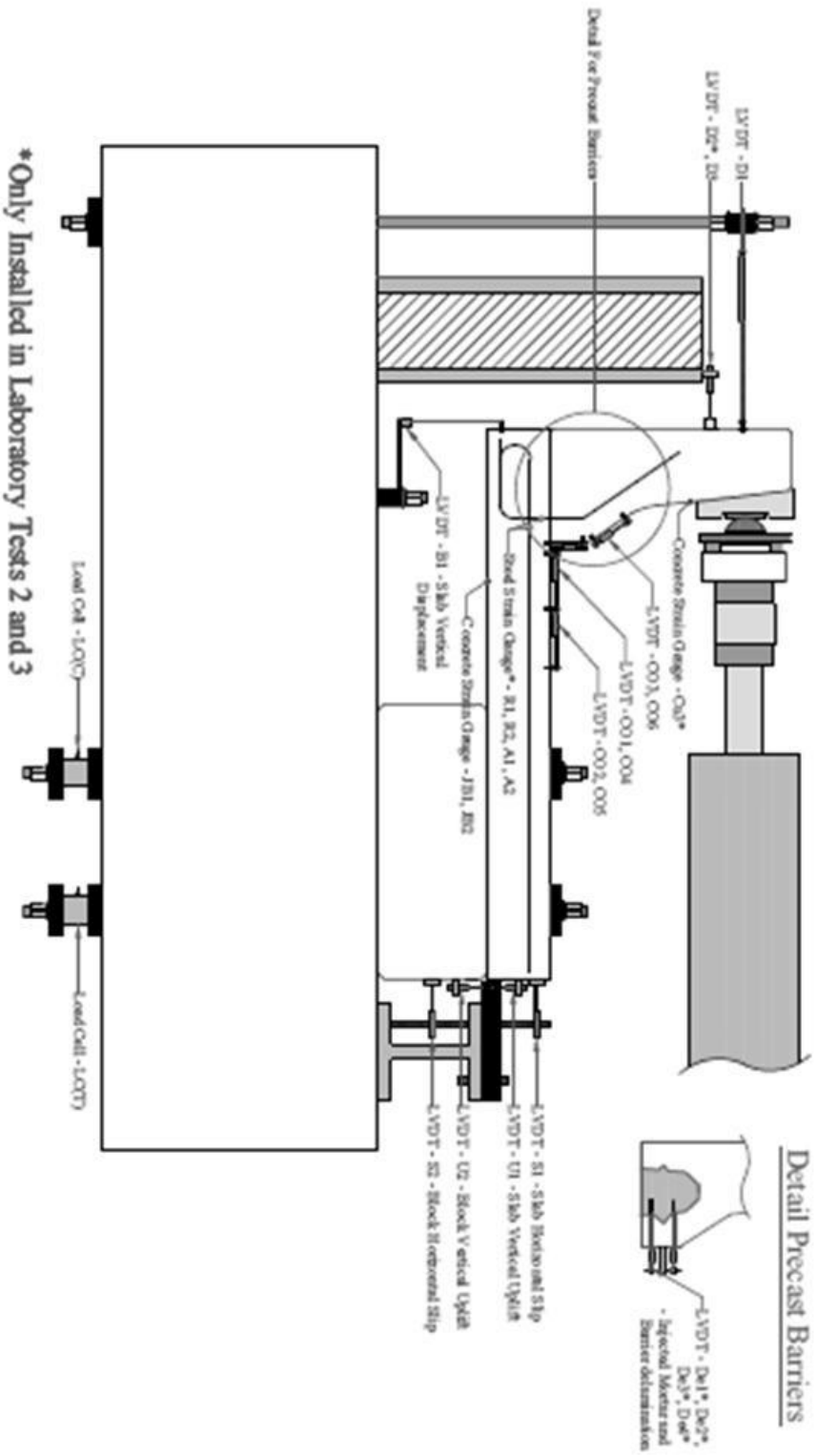

Appendix B Figure 3: Instrumentation Elevation View

Appendix B Table 1: Instrumentation Schedule Lab Test 1

Instrumentation Laboratory Test 1 - MTQ Type 201 Cast-in-Place Barrier				
Type	ID	Length (mm)	Offset (mm)	Notes
Linear Pot	D1	481	49	Lateral displacement barrier at load application
String Pot	B1	260	429	Vertical displacement slab
Linear Pot	CO1	263	28	Slab overhang crack opening in line with load
Linear Pot	CO2	268	27	Slab overhang crack opening in line with load
Linear Pot	CO3	180	27	Barrier crack opening in line with load
Linear Pot	CO4	260	27	Slab overhang crack opening offset 1 m from load
Linear Pot	CO5	269	27	Slab overhang crack opening offset 1 m from load
Linear Pot	CO6	176	30	Barrier crack opening offset 1 m from load
LVDT	S1	186	505	Horizontal slip slab
LVDT	S2	--	204	Horizontal slip beam
LVDT	U1	100	470	Vertical uplift slab
LVDT	U2	108	255	Vertical uplift beam
Linear Pot	U3	140	58	Relative barrier to slab uplift in line with load
Linear Pot	U4	132	56	Relative barrier to slab uplift offset 1 m from load
String Pot	U5	600	1805	Vertical displacement actuator
LVDT	Cu1	1860	29	Longitudinal extension barrier back face
LVDT	Cu2	780	27	Longitudinal extension barrier back face
Gage 350 Ω	R1	--	--	Strain in slab transversal reinforcement
Gage 350 Ω	R2	--	--	Strain in slab transversal reinforcement
Gage 350 Ω	A1	--	--	Strain in anchor bar
Gage 350 Ω	A2	--	--	Strain in anchor bar
Gage 120 Ω	JB1	--	--	Strain underside of slab overhang in line with load
Gage 120 Ω	JB2	--	--	Strain underside of slab overhang offset 1 m from load
Load Cell	LC(C)	--	--	Force in post-tension bar on compressed row, in line with load
Load Cell	LC(T)	--	--	Force in post-tension bar on extended row, in line with load

`

Appendix B Table 2: Instrumentation Schedule Lab Test 2

Instrumentation Laboratory Test 2 - Duchesneau Precast Barriers				
Type	ID	Length (mm)	Offset (mm)	Notes
Linear Pot	D1	519	68	Lateral displacement barrier at load application
LVDT	D2	134	1177	Lateral displacement loaded barrier at 70 mm from end
LVDT	D3	134	1177	Lateral displacement adjacent barrier at 70 mm from end
String Pot	B1	300	452	Vertical displacement slab
Linear Pot	CO1	285	26	Slab overhang crack opening in line with load
Linear Pot	CO2	317	27	Slab overhang crack opening in line with load
Linear Pot	CO3	206	24	Barrier crack opening in line with load
Linear Pot	CO4	285	25	Slab overhang crack opening offset 1 m from load
Linear Pot	CO5	316	24	Slab overhang crack opening offset 1 m from load
Linear Pot	CO6	192	23	Barrier crack opening offset 1 m from load
LVDT	S1	168	515	Horizontal slip slab
LVDT	S2	173	203	Horizontal slip beam
LVDT	U1	90	460	Vertical uplift slab
LVDT	U2	103	260	Vertical uplift beam
Linear Pot	U3	140	38	Relative barrier to slab uplift in line with load
Linear Pot	U4	155	33	Relative barrier to slab uplift offset 1 m from load
String Pot	U5	600	1805	Vertical displacement actuator
LVDT	Cu1	1915	29	Longitudinal extension barrier back face
LVDT	Cu2	790	27	Longitudinal extension barrier back face
Gage 120 Ω	Cu3	--	--	Longitudinal compressive strain barrier front face
Gage 350 Ω	R1	--	--	Strain in slab transversal reinforcement
Gage 350 Ω	R2	--	--	Strain in slab transversal reinforcement
Gage 350 Ω	A1	--	--	Strain in anchor bar
Gage 350 Ω	A2	--	--	Strain in anchor bar
Gage 120 Ω	JB1	--	--	Strain underside of slab overhang in line with load
Gage 120 Ω	JB2	--	--	Strain underside of slab overhang offset 1 m from load
Linear Pot	De1	55-h	80	Delamination barrier and injected mortar in line with load
Linear Pot	De2	125-h	80	Delamination barrier and injected mortar in line with load
Linear Pot	De3	55-h	85	Delamination barrier and injected mortar offset from load
Linear Pot	De4	125-h	85	Delamination barrier and injected mortar offset from load
Load Cell	LC(C)	--	--	Force in post-tension bar on compressed row, in line with load
Load Cell	LC(T)	--	--	Force in post-tension bar on extended row, in line with load

`

Appendix B Table 3: Instrumentation Schedule Lab Test 3

Instrumentation Laboratory Test 3 - Duchesneau Precast Barriers with Shear Connection				
Type	ID	Length (mm)	Offset (mm)	Notes
Linear Pot	D1	571	75	Lateral displacement barrier at load application
LVDT	D2	196	1178	Lateral displacement loaded barrier at 70 mm from end
LVDT	D3	200	1181	Lateral displacement adjacent barrier at 70 mm from end
String Pot	B1	276	440	Vertical displacement slab
Linear Pot	CO1	285	27	Slab overhang crack opening in line with load
Linear Pot	CO2	316	28	Slab overhang crack opening in line with load
Linear Pot	CO3	198	30	Barrier crack opening in line with load
Linear Pot	CO4	285	32	Slab overhang crack opening offset 1 m from load
Linear Pot	CO5	316	28	Slab overhang crack opening offset 1 m from load
Linear Pot	CO6	198	28	Barrier crack opening offset 1 m from load
LVDT	S1	168	515	Horizontal slip slab
LVDT	S2	173	203	Horizontal slip beam
LVDT	U1	90	460	Vertical uplift slab
LVDT	U2	103	260	Vertical uplift beam
Linear Pot	U3	138	31	Relative barrier to slab uplift in line with load
Linear Pot	U4	138	43	Relative barrier to slab uplift offset 1 m from load
String Pot	U5	600	1805	Vertical displacement actuator
LVDT	Cu1	1862	28	Longitudinal extension barrier back face
LVDT	Cu2	795	29	Longitudinal extension barrier back face
Gage 120 Ω	Cu3	--	--	Longitudinal compressive strain barrier front face
Gage 350 Ω	R1	--	--	Strain in slab transversal reinforcement
Gage 350 Ω	R2	--	--	Strain in slab transversal reinforcement
Gage 350 Ω	A1	--	--	Strain in anchor bar
Gage 350 Ω	A2	--	--	Strain in anchor bar
Gage 120 Ω	JB1	--	--	Strain underside of slab overhang in line with load
Gage 120 Ω	JB2	--	--	Strain underside of slab overhang offset 1 m from load
Linear Pot	De1	55-h	80	Delamination barrier and injected mortar in line with load
Linear Pot	De2	125-h	80	Delamination barrier and injected mortar in line with load
Linear Pot	De3	55-h	80	Delamination barrier and injected mortar offset from load
Linear Pot	De4	125-h	80	Delamination barrier and injected mortar offset from load
Load Cell	LC(C)	--	--	Force in post-tension bar on compressed row, in line with load
Load Cell	LC(T)	--	--	Force in post-tension bar on extended row, in line with load

`

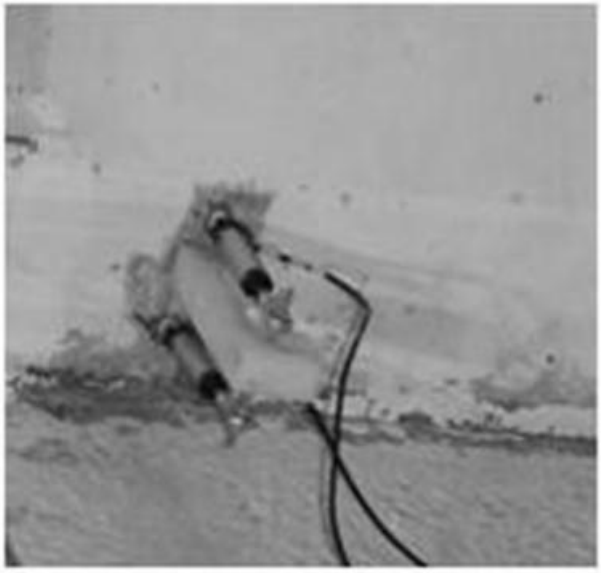

Appendix B Figure 4: Barrier and Injected Mortar Separation

Appendix B Figure 5: Displacement at End of Loaded Barrier and Adjacent Barrier

`

APPENDIX C SLAB OVERHANG DESIGN

Final Checks

Moment ULS Check Interior Portion of Slab Overhang

ULS 1 = 1.2DL + 1.7LL= 1.2*9.0 + 1.7*36.7 = 73.2 kN-m/m

ULS 8 = 1.2DL + 1.7H[3] = 1.2*9.0 + 38 = 48.8 kN-m/m

$\alpha M_{ULS,}$ 73.2 kN-m/m $<\phi M_{r,}$ 99.7 kN-m/m OK!

Moment ULS Check Exterior Portions of Slab Overhang

ULS 1 = 1.2DL + 1.7LL= 1.2*9.0 + 1.7*73.4 = 136.6 kN-m/m

ULS 8 = 1.2DL + 1.7H = 1.2*9.0 + 52 = 60.0 kN-m/m

$\alpha M_{ULS,}$ 136.6 kN-m/m $<\phi M_{r,}$ 177.1 kN-m/m OK!

Axial ULS Check Interior Portion of Slab Overhang

ULS 8 = 1.2DL + 1.7H = 1.2*0 + 100 = 100 kN/m

$\alpha P_{ULS,}$ 100 kN/m $<\phi P_{r,}$ 1200 kN/m OK!

Axial ULS Check Exterior Portion of Slab Overhang

ULS 8 = 1.2DL + 1.7H = 1.2*0 + 142 = 142 kN/m

$\alpha P_{ULS,}$ 142 kN/m $<\phi P_{r,}$ 1920 kN/m OK!

Flexure and Axial Load Check

$P_{ULS}/P_r + M_{ULS}/M_r < 1.0$

100/1200 + 73.2/99.7 = 0.82 OK!

142/1920 + 136.6/177.1 = 0.85 OK!

Shear Resistance at Slab Barrier Interface Check Interior Portion

---

[3]In CSA S6 2006 Commentary Clause 3.8.8.1 specifies to use a load factor of 1.7 for barrier loads and not 1.0 as written in Table 3.1 of the S6 2006 Code.

`

$V_{ULS,}$ 100 kN/m < $V_{r,}$ 278.8 kN/m OK!

Shear Resistance at Slab Barrier Interface Check Exterior Portion

$V_{ULS,}$ 142 kN/m < $V_{r,}$ 386.9 kN/m OK!

Transversal Resisting Moment of Slab

Given:

f'_c = 35 MPa, f_y = 400 MPa, E_c = 30000 MPa, E_s = 200000 MPa

ϕ_s = 0.9, ϕ_c = 0.75

α_1 = 0.7975, β_1 = 0.8825

Slab Height = 225 mm

Height to top reinforcement, d = 155.3 mm

Height to bottom reinforcement, d' = 43.0 mm

Interior Portion of Overhang:

$A_{s,top}$, A_s = 300*1000/150 = 2000 mm^2/m

$A_{s,bot}$, A'_s = 200*1000/150 = 1333 mm^2/m

Transversal Resisting Moment, $\phi M_{r,x}$ = 99.7 kN-m/m

Exterior Portion of Overhang within S_c[4] to slab edge:

$A_{s,top}$, A_s = 300*1000/75 = 5000 mm^2/m

Transversal Resisting Moment, $\phi M_{r,x}$ = 177.1 kN-m/m

Axial Resistance of Slab

Design Assumptions:

1. Only transversal steel reinforcement resists axial tension in slab

2. Both top and bottom rows of transversal reinforcement resist axial tension in slab

[4]Due to limited length of slab overhang of 6.2 m, S_c was reduced from 1.0 m to 0.5 m for slab design

`

Given:

A_s in slab interior portion = 3333 mm^2/m

A_s in slab exterior portion = 5333 mm^2/m

$\underline{\phi P_{r,int} = 1200 \text{ kN/m}}$

$\underline{\phi P_{r,int} = 1920 \text{ kN/m}}$

Shear Resistance of Slab at Barrier Interface

Given:

$f'_c = 35$ MPa, $f_y = 400$ MPa

$\phi_s = 0.9$, $\phi_c = 0.75$

Cohesion, c = 0.5 MPa, friction coefficient, $\mu = 0.6$

$A_{vf} = 1000\ mm^2/m$, $A_{cv} = 410000\ mm^2/m$

N = barrier weight = 6.69 kN/m

Interface shear resistance, $v_{r,int} = \phi_c*(c + \mu\sigma) < 0.25\phi_c f'_c = 9.3$ MPa &**6.5 MPa**

Where $\sigma = \rho_v f_y + N/A_{cv}$ and $\rho = A_{vf}/A_{cv}$

$\underline{\phi v_{r,int} = 0.68 \text{ MPa}, \phi V_{r,int} = 278.8 \text{ kN/m}}$

$\underline{\text{At exterior slab regions } A_{vf} = 2000\ mm^2/m \text{ and } \phi V_{r,int} = 386.9 \text{ kN/m}}$

Transversal Moment (M_y) due to CL-625 wheel loads

CL-625 transversal bending moment in slab overhang can be calculated with the below equation, CSA S6 2006 Clause 5.7.1.6.1.1.

$M_y = (2PA/\square) * 1/[1+(A-x)/(C-y)^2]^2$, where

P = Wheel load

A = Coefficient from figure 5.2 = 0.47

C = Transverse distance of load P from supported edge of slab

C = Overhang (1.0) - Barrier width (0.41) – Distance to wheel centre (0.3) = 0.29 m

`

x = Offset from point on slab being evaluated in longitudinal direction, depends on wheel load for CL-625 being analysed.

y = Offset in transversal direction, 0 in all cases (critical).

My must be found for critical CL-625 truck wheel load in the slab overhang, and the loads superimposed upon one another. The final value needs to be amplified by the proper DLA value, $M_y = (\Sigma My\ CL\text{-}625)*(1+DLA)$

M_y is critical when x = 0 for the 4th wheel of CL-625 truck, and DLA = 0.4 (only 4th axel of truck on bridge.

$M_{y,critical}$ CL-625 = 26.2 *(1.4) = 36.7 kN-m/m (not factored)

At distance within S_c of longitudinal slab edge M_y is doubled!

Transversal Moment (M_y) and Shear (V_y) due to Barrier Impact Loads

From Table C5.4 in CSA S6 2006 Commentary:

Factored M_y at barrier edge for PL-2 = 38 kN-m/m

Factored V_y at barrier edge for PL-2 = 100 kN/m

Factored M_y within S_c of slab longitudinal edge for PL-2 = 52 kN-m/m

Factored V_y within S_c of slab longitudinal edge for PL-2 = 142 kN/m

Vertical force for PL-2 railing is 30 kN applied over 5.5 m length at railing crest (225 mm)

Factored M_y due to vertical impact force = 30*1.7*(1-0.225)/5.5 = 7.2 kN-m/m

$M_{y,critical}$ Barrier Impact Loads = 45.2 kN-m/m (factored)

$M_{y,critical}$ Barrier Impact Loads within S_c of slab edge = 59.2 kN-m/m (factored)

Transversal Moment (M_y) due to dead loads

Barrier weight = 6.68 kN/m, Barrier C.G. = 0.84 m from support

Slab Overhang weight = 6.76 kN/m, Slab Overhang C.G. = 0.5 m from support

$M_{y\ Dead\ Loads}$ = 9.0 kN-m/m (not factored)

Check that Manipulation Stresses will not crack slab concrete, $\sigma_{max} < f_t$ concrete

`

Longitudinal Moment (Mx) due to Manipulation and Transportation of Slab

Slab anchors positioned at 0.21*Length of slab from each end in order to minimize bending moment with 4 anchors in total.

Slab weight per 1 m of slab width, w = 6.8 kN/m

Positive Moment = $w*(L-0.21*L)^2/8 – w*(0.21*L)^2/2 =$ 5.3 kN-m

Negative Moment = $w*(0.21*L)^2/2$ = -5.7 kN-m

Add maximum dynamic amplification factor of 2

$M_{x, critical}$ Slab Movement = 11.4 kN-m

Maximum tensile stresses due to M_x

$\sigma_{max} = M_x*y/I = 6M/bh^2 = 6*5.7E6$ N-mm/$(1000*225^2)$ = 0.68 MPa

σ_{max}< f't Concrete, slab should not crack during manipulation and transportation.

Negative Moment Reinforcement Development Length

Straight Bars:

$L_d = 1.15*[(k_1k_2k_3k_4)/(d_{cs} + K_{tr})]*f_y/f'^{0.5}_c*A_b$> 300 mm

$d_{cs} = 2.5d_b$ and $K_{tr} = 0$ for slabs

$k_1k_2k_3k_4$= 0.8

L_d = 382.8 mm

180° Hooked Bars:

$L_{hb} = 100d_b/f'^{0.5}_c$ * Reduction Factor, Reduction Factor = 0.7

L_{hb} = 230.7 mm

`

APPENDIX D SPECIMEN FABRICATION LOG

2010-11-23 Support Block, Test Configurations 1, 2, and 3– HPFRC 70 MPa

10h54 - Water and admixtures added to dry mix

11h14 - Temperature 20.1° C

- Slump Flow 820 mm

- Mix highly liquid but ok

11h15 - Fibres added to mix manually

11h30 - Air content 1%

- Density 2383 kg/m^3 (error with tare, value indicative only)

- Too much segregation and bleeding visible in the mix!

11h40 - Addition of 1.5 kg of CATEXOL Collaxim L7, viscosity modifying agent

11h53 - Temperature 20.7° C

- Slump flow 755 mm

- Slump flow 775 mm without rodding

- Improvement in concrete mix, but still too much segregation and bleeding

- Addition of 2 kg of CATEXOL Collaxim L7, viscosity modifying agent

12h00 - Temperature 20.7° C

- Air content 1.1%

- Density 2425 kg/m^3

- Slump flow 770 mm (no rodding)

- Mix much more stable, and has been deemed acceptable for casting.

12h20 - Pouring of concrete begins

- Concrete self-leveling and self-compacting

- Steel fibres and aggregate moves with flow, mix stability is satisfactory

`

- Casting of characterization specimens: 4 concrete coupons and 12 101.6 mm (4 in) cylinders

12h40 - Pouring of concrete finished

- Begin finishing of exposed surface

13h00 - End finishing of exposed surface

- Surface well finished but concrete very viscous and sticky, so not perfect

- Polyethylene plastic placed on top of support block.

Follow-up Directions

1. Attempt to refinish surface in 1-2 hours
2. At end of day shift, 17h00, begin steam curing and cover support block with insolated tarp to make sure specimen does not freeze over-night
3. Continue steam cure until support block has reached at least 45 MPa
4. Always keep characterization specimens in same conditions as support block

2010-12-06 Slab, Test Configuration 1 –MTQ 35 MPa Concrete

15h20 - Water and admixtures added to dry mix

- Temperature 19° C

- Slump flow 640 mm

- Air 7.2% (within specifications for air-entrained mix)

- Concrete ready for pour

16h00 - Pouring of slab begins

- Casting of characterization specimens: 12 101.6 mm (4 in) cylinders

16h20 - Pouring of slab finished

- Slab surfaced finished with trowel

Follow-up Directions

1. Progressively begin steam cure in starting at 17h00

`

2. Cover slab with insolated tarps
3. Steam cure until slab reaches 35 MPa
4. Cure gradually stopped to reduce thermal shock
5. Slab surface maintained humid until pour of cast-in-place barrier
6. Always keep characterization specimens in same conditions as slab

2010-12-16 Cast-in-place Barrier, Test Configuration 1 – MTQ 35 MPa Concrete

10h15 - Water and admixtures added to dry mix

10h40 - Problems taking air reading, eventually air content established at 6%

- Slump flow 550 mm, however this is the concrete at the end of the pump and is likely stiffer than fresher concrete.

- Concrete sample taken directly from cement truck much more workable

- Concrete ready for pour

10h50 - Pouring of barrier begins

- Several cracks heard during pouring and two sides of barrier forms begin to separate. Clamps placed and tightened on top of formwork to restrict movement of two sides of forms.

- Due to deflections of forms and cracks that were heard, the concrete is just poured to cover the reinforcement and not all the way to the design height.

- Casting of characterization specimens: 4 concrete coupons and12 101.6 mm (4 in) cylinders

<u>Follow-up Directions</u>

1. Progressively begin steam cure in starting at 16h00
2. Cover barrier with insolated tarps
3. Steam cure until barrier reaches 35 MPa
4. Cure gradually stopped to reduce thermal shock

`

5. Always keep characterization specimens in same conditions as slab

2011-01-13 Duchesneau Type Precast Barriers (x3), Test Configuration 2 – HPFRC 70 MPa

10h50 - Cement loaded into concrete truck with two big bags (1000 kg each)

11h10 - Water and admixtures added to dry mix

11h30 - Air content 3.5%

- Slump flow 597.5 mm

11h32 - 18 bags of steel fibres, Dramix ZP-305, added to concrete truck by hand

11h42 - Fibres all added

11h50 - 8 L of super-plasticizer, Eucon 37, added to the mix to improve workability

12h00 - Slump flow 365 mm

- Air 12%, too high for casting!

12h05 - Another 12 L of super-plasticizer added to mix (20 L total)

- Air still at 10.5%, concrete mix wasted

Notes

1. Air content only became problematic after introduction of fibres and extra super-plasticizer, and jumped from 3.5% to 12%.
2. When the cement was added to the dry mix in the concrete truck via big bag, one of the bags interior plastic lining fell into the mix. It was later removed after mixing, but lots of cement was caught in it and it was not good for the mix homogeneity. In future pours more attention must be paid to make sure the plastic lining does not fall into the concrete truck.

2011-02-07 Slab, Test Configuration 2 – MTQ 35 MPa Mix

13h30 - Water and admixtures added to dry mix

13h55 - Air content 5.5%

- Slump flow 540 mm, too stiff for the pour

`

14h05 - 2.84 L of super-plasticizer added to mix

14h15 - Air content 6%

- Slump Flow 610 mm

- Concrete ready for pour

14h20 - Pouring of slab begins

- Casting of characterization specimens: 12 101.6 mm (4 in) diametre cylinders

14h40 - Pouring of slab finished.

- Slab surface finished with trowel

14h45 - Surface retarder sprayed over slab at portion to be in contact with precast barriers

Follow-up Directions

1. Progressively begin steam cure in starting at 16h00
2. Cover slab with insolated tarps
3. After 24 hours of curing temporarily stop steam cure and spray slab with high pressure water hose at portion to be in contact with precast barriers
4. Steam cure until slab reaches strength of 50 MPa (to match strength of previous slab)
5. Cure gradually stopped to reduce thermal shock
6. Always keep characterization specimens in same conditions as slab

2011-02-08 Duchesneau Type Precast Barriers (x3),Test Configuration 2 – HPFRC 70 MPa

13h50 - Cement truck loaded with aggregate

14h10 - Cement loaded into concrete truck with two big bags (1000 kg each)

14h30 - Water and admixtures added to dry mix

- 20 L of super-plasticizer, Eucon 37, added at this time (50% of total dosage)

14h50 - Air content 1.2%

- Slump flow 440 mm

`

- Temperature 15.3° C

14h55 - 18.5 bags of steel fibres, Dramix ZP-305, added to concrete truck by hand

15h01 - All fibres added

15h05 - 6 L of super-plasticizer, Eucon 37, added to the mix to improve workability

15h20 - Air content 7.2%

- Slump flow 430 mm

- Temperature 17.7° C

- Concrete is deemed ok for barrier pour. No more super-plasticizer is added to the mix for fear of introducing more air.

15h25 - Pouring of barrier begins

- Concrete generally looks good, however some unmixed balls of cement found in mix.

- External vibrator and trowels used to push concrete and improve compaction

15h40 - Casting of characterization specimens: 4 concrete coupons, 4 small slabs, and 12 101.6 mm (4 in) cylinders

15h50 - Pouring of barrier finished

- Finishing of barriers by trowel

16h15 - Barriers sealed off with plastic to maintain finish

Follow-up Directions

1. Begin steam cure at half-power at 17h00
2. Beginning of morning shift following day increase steam cure to full power
3. Begin breaking cylinders after 24hours of steam curing every 24 hours
4. Once concrete compressive strength has reached 25 MPa, strip molds and then continue steam cure
5. Continue steam cure until barriers have reached 70 MPa or 7 days have passed

`

7. Always keep characterization specimens in same conditions as slab

2011-03-17 Slab, Test Configuration 3 – MTQ 35 MPa

9h45 - Water and admixtures added to dry mix

10h30 - Air content 5.0%

- Slump flow 610 mm

- Temperature 21.3° C

- Concrete ready for pouring

10h38 - Pouring of slab begins.

- Casting of characterization specimens: 12 101.6 mm (4 in) diametre cylinders

10h55 - Pouring of slab finished.

- Slab surface finished with trowel

11h20 - Surface retarder sprayed over slab at portion to be in contact with precast barriers

Follow-up Directions

1. Progressively begin steam cure in afternoon
2. Cover slab with insolated tarps
3. After 24 hours of curing temporarily stop steam cure and spray slab with high pressure water hose at portion to be in contact with precast barriers
4. Steam cure until slab reaches strength of 50 MPa (to match strength of previous slabs)
5. Cure gradually stopped to reduce thermal shock
6. Always keep characterization specimens in same conditions as slab

2011-04-12 Precast Barriers with Shear Connections (x3), Test Configuration 3 – HPFRC 70 MPa

9h50 - Cement truck loaded with aggregate

10h10 - Cement loaded into concrete truck with two big bags (1000 kg each)

`

10h30 - Water and admixtures added to dry mix

- 20 L of super-plasticizer, Eucon 37, added at this time (50% of total dosage)

10h40 - Air content 2.0%

- Slump flow 380 mm

- Slump 220 mm

- Temperature 19.7° C

10h45 - 374.4 kg of steel fibres, Dramix ZP-305, added to concrete truck by hand

10h50 - All fibres added

11h00 - Air content 2.8%

- Slump flow NA, concrete too stiff

- Slump 70 mm

- Temperature 20.6° C

11h05 - 8 L of super-plasticizer, Eucon 37, added

11h20 - 12 L of super-plasticizer, Eucon 37, added

11h12 - Air content 12.0%

- Slump flow 325 mm

- Temperature 24.8° C

- Density 2149 kg/m^3

11h25 - 200 mL of Eucon Air Out added

11h35 - Air content 5.0%

- Temperature 25.0° C

- Density 2386 kg/m^3

- Concrete deemed ok for pour

11h40 - Pouring of barrier begins

`

- Concrete generally looks good, however a little stiff due to long delay between water cement contact and pour

- External vibrator and trowels used to push concrete and improve compaction

11h50 - Casting of characterization specimens: 4 concrete coupons and 12 101.6 mm (4 in) cylinders

12h20 - Pouring of barrier finished

- Finishing of barriers by trowel

12h25 - Barriers sealed off with plastic to maintain finish

Notes

1. The increase in air content after the addition of the fibres and super-plasticizer highlighted the synergetic effect between the fibres and super-plasticizer on the air content within the concrete mix
2. The Eucon Air Out proved to be a very effective means of stopping the problem, only 200 mL were needed for nearly a 3.5 m^3 concrete pour!

Follow-up Directions

1. Begin steam cure following morning after removing plastic
2. Begin breaking cylinders after 24hours of steam curing every 24 hours
3. Once concrete compressive strength has reached 25 MPa, strip molds and then continue steam cure
4. Continue steam cure until barriers have reached 70 MPa or 7 days have passed
5. Always keep characterization specimens in same conditions as slab

`

APPENDIX E FRM OPTIMIZATION STUDIES

The main studies that guided the optimization of the FRM mix are detailed in this appendix. It is important to note that certain inconsistencies were found between the mortar shipments, as one shipment in particular may have been expired. The shipment used for the study is always noted and the conclusions drawn are relative to the shipment.

Study 1 – 22nd December 2010 – Water Content

EHFG Shipment from November 2010

Appendix E Table 1: Mortar Optimization Study 1, Water Content

Component	Reference	Mix 1	Mix 2	Mix 3	Unit
EHFG[5]	22.7	22.7	22.7	22.7	kg
Conex	0.330	0.330	0.330	0.330	kg
Fibres	1.014	1.014	1.014	1.014	kg
Water	2.625	**3.044**	**3.526**	**3.989**	kg
Ice	0.865	0.865	0.865	0.865	kg
Eucon727	17.5	17.5	17.5	17.5	g

Tests and Results

Mini cone, small cone, and temperature were taken for each mix immediately after mixing.

Appendix E Table 2: Study 1 Results

Mix	Temp, °C	Mini Cone (mm)	Small Cone (mm)
Reference	NA	170	237.5
Mix 1 - 3L	22.9	180	260
Mix 2 - 3.5L	23.4	220	290
Mix 3 - 4.0L	22.7	220	NA

Commentary

The influence of water content on the mini cone and small cone slump flow is clearly established as expected. The higher the water content, the higher the slump flow.

[5]The mix quantities have been normalized to one bag of EHFG for comparative purposes, since the quantity of EHFG was not always identical. Typically the formulations for these tests only used 10 or 11 kg of EHFG and the mortar components were adjusted accordingly.

`

After this study it was still necessary to evaluate the loss of slump flow over time, as well as to establish the necessary/acceptable increase in water content.

Study 2 – 11, and 18th January 2011 –Eucon 727 and Water Content

EHFG Shipment from January 2011

Appendix E Table 3: Mortar Optimization Study 2

Component	Reference	Mix 1	Mix 2	Unit
EHFG	22.7	22.7	22.7	kg
Conex	0.330	0.330	0.330	kg
Fibres	1.014	1.014	1.014	kg
Water	2.625	2.625	**3.008**	kg
Ice	0.865	0.865	**0.992**	kg
Eucon727	0.0	**12.0**	12.0	g

Tests and Results

Inclined plane tests were taken immediately following mixing and in 20 minute intervals for 60 minutes. Mini cone, small cone, and temperature were taken 15 and 60 minutes after mixing.

Appendix E Table 4: Study 2 Inclined Plane Results

Rest Time (minutes)	Static Yield Stress, τ_0 (MPa)		
	Reference	Mix 1[a]	Mix 2[a]
0	113.4	39.4	33.9
20	179.4[a]	46.3[a]	39.2
40	--	49.5[a]	61.4[a]
60	--	113.0[a]	--

a. Indicates static yield stress only achieved after shaking inclined plane
-- Static yield stress not attained

Appendix E Table 5: Study 2 Results, Temperature and Flow

Mix	Delay (min)	Temp, °C	Mini Cone (mm)	Small Cone (mm)
Reference	15	20.4	190.0	285.0
	60	21	117.5	147.5
Mix 1[a]	15	14.8	270.0	377.5
	60	15.1	197.5	372.5
Mix 2[a]	15	11.3	327.5	435.0
	60	12.6	192.5	270.0

a. Ambient temperature in laboratory only 13-14 °C due to external circumstances

`

Commentary

The addition of the Eucon 727 decreased the static yield stress, increased the initial flow, and reduced the structural buildup over the 60 minutes period. The same effect was more pronounced in Mix 2 with both Eucon 727 and increased water content.

It should be noted that the differences between the reference mix and the modified mixes were quite drastic. It is likely that the lower laboratory temperature – 6°C colder than usual because the windows had to be opened due to dust problems – had an effect on the fluidity of the mixes. This assumption is supported by the results of Study 3.

Study 3 – 10th February 2011 – Mix Component Isolation

EHFG Shipment from February 2011

Appendix E Table 6: Mortar Optimization Study 3

Component	Reference	Mix 1	Mix 2	Mix 3	Mix 4	Units
EHFG	22.7	22.7	22.7	22.7	22.7	kg
Conex	0	**0.33**	0	0	0	kg
Fibres	0	0	0	**1.014**	0	kg
Water	3.5	3.5	**2.625**	3.5	3.5	kg
Ice	0	0	**0.875**	0	0	kg
Eucon727	0	0	0	0	**17.4**	g

Tests and Results

Inclined plane tests were taken immediately following mixing and in 20 minute intervals for 60 minutes. Mini cone, small cone, and temperature were taken 15 and 60 minutes after mixing.

Appendix E Table 7: Study 3 Inclined Plane Results

Rest Time (minutes)	Static Yield Stress, τ_0 (MPa)				
	Reference	Mix 1	Mix 2	Mix 3	Mix 4
0	239.5	77.0	36.9	80.3	43.9
20	281.9[a]	--	119.9[a]	315.4[a]	187.9[a]
40	--	--	--	387.0[a]	230.0[a]
60	--	--	--	--	--

a. Indicates static yield stress only achieved after shaking inclined plane
-- Indicates static yield stress was not attained

`

Appendix E Table 8: Study 3 Results, Temperature and Flow

Mix	Delay (min)	Temp, °C	Mini Cone (mm)	Small Cone (mm)
Reference	15	25.5	130.0	180.0
	60	21.8	100.0	115.0
Mix 1	15	21.7	157.5	210.0
	60	21.8	100.0	120.0
Mix 2	15	17.3	227.5	297.5
	60	20.3	135.0	185.0
Mix 3	15	21.7	167.5	205.0
	60	21.0	100.0	125.0
Mix 4	15	20.8	205.0	280.5
	60	20.0	125.0	160.0

Commentary

The results from this study were generally logical, unfortunately it did seem as though the reference mix was slightly less workable/fluid than normal. The following conclusions could still be drawn however.

- Conex, the shrinkage reducing admixture, did not improve the initial flow rate, and increased structural buildup.
- Substituting ice for water improved the initial flow rate and decreased structural buildup. This supports the observation from Study 2 that the colder room temperature improved the FRM flow properties.
- Steel fibres did not improve the initial flow rate, and increased structural buildup.
- Eucon 727, water reducing admixture, improved the initial flow rate and decreased structural buildup.

An optimized mix will include the Eucon 727 and a higher proportion of ice with respect to water.

`

Study 4 – 21, 34th February 2011 – Final FRM Mix Design

EHFG Shipment from February 2011

Appendix E Table 9: Mortar Optimization Study 4

Component	Reference	Mix 1	Mix 2	Mix 3	Mix 4	Units
EHFG	22.7	22.7	22.7	22.7	22.7	kg
Conex	0.33	0.33	0.33	0.33	0.33	kg
Fibres	1.014	1.014	1.014	1.014	1.014	kg
Water	2.625	**2.450**	**2.275**	**2.190**	**2.250**	kg
Ice	0.875	**1.050**	**1.225**	**1.460**	**1.500**	kg
Total Water	3.50	3.50	3.50	**3.65**	**3.75**	kg
Ice/Water Ratio	25	**30**	**35**	**40**	40	%
Eucon727	17.5	17.5	17.5	17.5	**0.0**[b]	g

[a] Mix 3 selected for injection
[b] Eucon 727 left out of mix erroneously.

Tests and Results

Inclined plane tests were taken immediately following mixing and in 20 minute intervals for 60 minutes. Mini cone, small cone, and temperature were taken 15 and 60 minutes after mixing.

Appendix E Table 10: Study 4 Inclined Plane Results

Rest Time (minutes)	Static Yield Stress, τ_0 (MPa)				
	Reference	Mix 1	Mix 2	Mix 3	Mix 4
0	57.4	28.8	34.6	20.5	14.9
20	119.7[a]	54.5	69.3	17.8	17.7
40	--	--	--	37.4	52.3
60	--	--	--	--	--

a. Indicates static yield stress only achieved after shaking inclined plane
-- Indicates static yield stress was not attained

`

Appendix E Table 11: Study 4 Results, Temperature and Flow

Mix	Delay (min)	Temp, °C	Mini Cone (mm)	Small Cone (mm)
Reference	15	20.8	192.5	272.5
	60	21.6	130	162.5
Mix 1	15	16.6	227.5	310
	60	19.4	152.5	217.5
Mix 2	15	16.8	240	300
	60	20.2	140	175
Mix 3	15	15.5	260	362.5
	60	19.3	170	237.5
Mix 4	15	13.6	262.5	355
	60	18.1	172.5	242.5

Commentary

This last optimization study confirmed the effect of the ice to water ratio. The following observations were evident.

- The lower the mortar temperature, the higher the initial flow rate and the slower the structural buildup.
- An ice to water ratio of 40% presented no mixing problems. After the standard 5 minutes of mixing, the mortar was homogenous.
- An increased ice to water ratio did not produce any noticeable effects on the mortar segregation or bleeding.
- A significant improvement in the mortar behaviour can be deduced from the above studies, and Mix 3 had very adequate properties for the injection.
- Mix 3 was selected as the optimal mix, shown in Appendix E Table 12

Appendix E Table 12: FRM Mix and Properties

Mortar Final Mix		Fresh and Hardened State Properties		
EHFG	22.7 kg		Lab Test 2	Lab Test 3
Conex	0.33 kg	Slump Flow	845 mm	775 mm
Fibres	1.014 kg	Temperature	18.3 C	17.4 C
Water	2.19 kg	f'_c	40.0 MPa	60.4 MPa
Ice	1.46 kg	f_t	3.3 MPa	3.2 MPa
Eucon727	0.017 kg	E_c	19400 MPa	26090 MPa

`